AN ABSTRACT OF A THESIS

DYNAMICS AND CONTROL OF A BATTERY INVERTER SINGLE-PHASE INDUCTION GENERATOR SYSTEM

Obasohan I. Omozusi

Master of Science in Electrical Engineering

The operation of a single-phase induction generator with a PWM inverter as a source of excitation was tested and analyzed. The battery included in the system was found to be an excellent configuration for a source or sink of real power depending on the given load of the single-phase induction generator. The system modeling was done considering the effect of saturation of magnetizing inductance. Experimental results were recorded for different impedance and motor loads for a one horse power single-phase induction generator.

The steady-state model for the system was developed for impedance and motor loads using the harmonic balance technique. Experimental results for different impedance and motor loads compare favorably with the steady-state model calculation.

The simulation of the single-phase induction generator, battery, and PWM inverter was done using device model. Matlab/Simulink was found to be a great tool in modeling the PWM inverter and the single-phase induction generator. Simulation results of the different impedance and motor loads compare favorably with the experimental waveforms for the single-phase induction generator system.

The battery inverter single-phase induction generator system can be used as a source of regulated voltage and frequency for isolated applications such as in commercial and industrial uses especially in situations where engine-driven single-phase synchronous generators are presently being used. The system can be used as power sources for isolated systems and for utility interface to single-phase power system grids. The system will find application for battery charging purpose and controllable single-phase ac voltage source, i.e. traction power systems.

VITA

Mr. Obasohan Omozusi was born in Benin-City, Nigeria. He attended Edo College, Benin-City, Nigeria, and graduated in June 1986. He received his B.Sc. in Electronic and Electrical Engineering from Obafemi Awolowo University, Ife-Ile, Nigeria, in 1992. He entered Tennessee Technological University in August 1996 and received a Master of Science degree in Electrical Engineering in December 1998.

DYNAMICS AND CONTROL OF A BATTERY INVERTER SINGLE-PHASE INDUCTION GENERATOR SYSTEM

A Thesis

Presented to

the Faculty of the Graduate School

Tennessee Technological University

by

Obasohan I. Omozusi

In Partial Fulfillment

of the Requirements for the Degree

MASTER OF SCIENCE

Electrical Engineering

December 1998

CERTIFICATE OF APPROVAL OF THESIS

DYNAMICS AND CONTROL OF A BATTERY INVERTER SINGLE-PHASE INDUCTION GENERATOR SYSTEM

by

Obasohan I. Omozusi

Graduate Advisory Committee:

_____ _____
Chairperson date

_____ _____
Member date

_____ _____
Member date

Approved for the Faculty:

_____
Dean of Graduate Studies

_____
Date

STATEMENT OF PERMISSION TO USE

In presenting this thesis in partial fulfillment of the requirements for a Master of Science degree at Tennessee Technological University, I agree that the University Library shall make it available to borrowers under rules of the Library. Brief quotations from this thesis are allowable without special permission, provided that accurate acknowledgment of the source is made.

Permission for extensive quotation from or reproduction of thesis may be granted by my major professor when the proposed use of the material is for scholarly purposes. Any copying or use of the material in this thesis for financial gain shall not be allowed without my written permission.

Signature _____

Date _____

DEDICATION

This thesis is dedicated to my parents

Ebenezer and Elizabeth

and brothers

Osayande and Ogieriahki

ACKNOWLEDGMENTS

I would like to express my appreciation to Dr. Olorunfemi Ojo, my major professor and chairman of the advisory committee, for his valuable direction and assistance. I would also like to thank Dr. Charles Hickman a member of my advisory committee for his assistance during this work. I also want to thank Dr. Prit Chowdhuri a member of my advisory committee for assistance.

I express my gratitude to Dr. Esther Ososanya and Dr. Ghadir Radman for their assistance. I am grateful to Dr. P. K. Rajan, Dr. Ken Purdy, Dr. M. O. Omoigui, Dr. Jeffrey R. Austen, Prof. Eusebisu J. Doedel, Antonio Ginart, Zhiqing Wu, Sandy Garrison, Helen Knott, Keith Jones, Conard F. Murray, L. V. Randolph, Patricia A. Roberts, and Joel Seber for their assistance. I acknowledge the financial support of the Center for Electric Power at Tennessee Technological University for this research.

TABLE OF CONTENTS

.....

.....Page

LIST OF TABLES .....

.....x

LIST OF FIGURES.....

..... xi

Chapter

1. Introduction .....

.....1

1.1. Introduction.....

.....1

1.2. Review of Previous Work.....

.....2

1.3. Scope of Present Research .....

.....7

2. Single-Phase Pulse Width Modulation Inverter

2.1. Introduction 12

2.2. Control Scheme Method for Single-Phase PWM Inverter.....

.....13

2.2.1. Single-Phase PWM Inverter.....

.....13

2.2.2. Single-Phase Inverters .....

.....16

2.2.2.1. PWM with bipolar voltage switching.....

.....16

2.2.2.2. PWM with unipolar voltage switching.....
.....24
2.2.2.3. Modified PWM bipolar voltage switching scheme .....
.....26
2.3. Design, Implementation, and Operation of Bipolar Voltage Switching Scheme for Single-Phase Inverter .....
.....35
3. Model of a Single-Phase Induction Motor 39
3.1. Introduction .....
.....39
3.2. Derivation of Single-Phase Induction Motor Equation .....
.....39
3.2.1. Reference Frame Transformation and Turn Transformations.....
.....43

Chapter Page

3.2.2. Torque Equation Derivation.....
.....48
3.3. Harmonic Balance Technique .....
.....50
3.3.1. Phasors and Sinusoidal Solutions.....
.....51
3.3.2. Basic Theorems .....
.....52
3.4. Steady State Analysis of Single-Phase Induction Motor .....
.....54
3.5. Evaluation of Machine Parameters.....
.....59
3.5.1. Determination of the Main Winding Rotor Resistance 60
3.5.2. Determination of the Auxiliary Winding Rotor Resistance 62

3.5.3. Determination of the Main Winding Parameters 63

3.5.4. Determination of the Auxiliary Winding Parameters 65

4. Analysis of Battery Inverter Single-phase Induction Generator System with Impedance Load..... 70

4.1. Introduction .....

.....70

4.2. Mathematical Model of System.....

.....71

4.3. Comparison of Simulation and Experiment Waveforms for the System Feeding a Resistive Load .....
.....75

4.3.1. Battery Inverter Generator System (Linear Modulation Region) 75

4.3.2. Battery Inverter Generator System (Overmodulation Region) 79

4.4 Steady State Calculation and Experiment .....

.....82

4.4.1. Experiment and Predicted Performance Results 87

4.4.2. Experiment Performance Results for Variable Resistive Load 92

4.4.3. Experiment Performance Results for Variables Generator Rotor Speed 97

4.4.4. Experiment Performance Results for Regulated Load Voltage 103

Chapter Page

4.5 Parametric Studies for the Battery Inverter Single-Phase Induction Generator with Impedance Load .....
.....106

4.6. Transient and Dynamic Performance for the System Feeding an Impedance Load 113

4.6.1. Start-up Process 114

4.6.2. System Dynamics due to Changes in Load 117

4.6.3 System Dynamics due to Changes in Generator Rotor Speed 121

5. Analysis of Battery Inverter Single-Phase Induction Generator System with Single-Phase Induction Motor Load..... 126

5.1. Introduction .....

.....126

5.2. Mathematical Model of System.....

.....127

5.3. Comparison of Simulation and Experiment Waveforms for the System Feeding SPIM Load .....

.....132

5.3.1. Battery Inverter SPIG System Feeding SPIM Load (Linear Region) 132

5.3.2. Battery Inverter SPIG System Feeding SPIM Load (Overmodulation Region) 136

5.4 Steady State Calculation and Experiment .....

.....140

5.4.1. Experiment and Predicted Performance Results 141

5.4.2. Predicted Performance Results 144

5.5 Parametric Studies for the Battery Inverter Single-Phase Induction Generator with SPIM Load .....

.....147

5.6. Transient and Dynamic Performance for the System feeding a SPIM Load 149

5.6.1. Start-up Process 149

5.6.2. System Dynamics due to Changes in Load Torque 156

5.6.3 System Dynamics due to Changes in Generator Rotor Speed..... 161

Chapter Page

5.6.4 System Voltage Collapse..... 167

6. Analysis of Capacitor Inverter Single-Phase Induction Generator System with Impedance Load..... 173

6.1. Introduction .....
.....173
6.2. Mathematical Model of System.....
.....174
6.3. Condition for Self Excitation.....
.....177
6.4. Results .....
.....181
7. Conclusions and Suggestion for Further Work.....
.....185
7.1. Conclusions.....
.....185
7.2. Suggestion for Further Work .....
.....186
REFERENCES.....
.....187
APPENDIX .....
.....191
VITA .....
.....194

LIST OF TABLES

Table Page

2.1. Switching state of the unipolar PWM and the corresponding voltage levels 26

2.2. Switching state of the modified bipolar PWM and the corresponding voltage levels 28

3.1. Stand-still test 60

3.2. Synchronous test 61

LIST OF FIGURES

Figure Page

1.1. Block diagram of the proposed system 8

2.1. Schematic diagram for inverter system 13

2.2. Half-bridge PWM Inverter Waveforms 14

2.3. Schematic diagram for Half-bridge PWM Inverter 15

2.4. Single-phase full-bridge inverter 16

2.5. PWM with bipolar voltage switching 17

2.6. Phase relationship of output voltage to modulating carrier signals for bipolar voltage scheme. Condition, $0 \le \omega_m t + \phi < \pi$ 18

2.7. Phase relationship of output voltage to modulating carrier signals for bipolar voltage scheme. Condition, $\pi \le \omega_m t + \phi < 2\pi$ 19

2.8. Single-phase PWM with unipolar voltage switching 25

2.9. PWM with modified bipolar voltage switching 27

2.10. Phase relationship of output voltage to modulating carrier signals for modified bipolar voltage scheme. Condition, $0 \le \omega_m t + \phi < \pi$ 29

2.11. Phase relationship of output voltage to modulating carrier signals for modified bipolar voltage scheme. Condition, $\pi \le \omega_m t + \phi < 2\pi$ 30

2.12. Inverter comparator 36

2.13. Block diagram of ECG 858M (dual op-amp).....36

2.14. Inverting comparator circuit.....37

2.15. Non-inverting comparator circuit.....37

3.1. Cross-sectional view of a single-phase induction machine 40

3.2. Equivalent circuit of single-phase induction machine 57

3.3. Equivalent circuit of single-phase induction machine with core loss 57

Figure Page

3.4. Equivalent circuit of single-phase induction machine with $I_{ds} = 0$, and $\omega_r = 0$ 61

3.5. Equivalent circuit of single-phase induction machine with $I_{qs} = 0$, and $\omega_r = 0$ 63

3.6. Equivalent circuit of single-phase induction machine with $I_{ds} = 0$, and $\omega_r = \omega_e$.....64

3.7. Equivalent circuit of single-phase induction machine with $I_{qs} = 0$, and $\omega_r = \omega_e$.....66

3.8. Experimental values q-d magnetizing inductances vs peak input voltage 68

3.9. Experimental values of q-d core loss resistance vs peak input voltage.....69

3.10. Experimental values sum of q-d axis leakage inductances vs peak input

voltage....69

4.1. Block diagram of the proposed system 70

4.2. Schematic diagram of the single-phase induction generator with a battery-PWM inverter system 72

4.3. The q-d equivalent circuit of the battery-PWM inverter generator system 72

4.4. Load voltage steady-state waveforms. Modulation Index = 0.75, load impedance = 40.9 Ohms, rotor speed = 1825 rpm. 76

4.5. Main winding current steady-state waveforms. Modulation Index = 0.75, load impedance = 40.9 Ohms, rotor speed = 1825 rpm. 77

4.6. Auxiliary winding voltage steady-state waveforms. Modulation Index = 0.75, load impedance = 40.9 Ohms, rotor speed = 1825 rpm. 77

4.7. Auxiliary winding current steady-state waveforms. Modulation Index = 0.75, load impedance = 40.9 Ohms, rotor speed = 1825 rpm. 78

4.8. Load current steady-state waveforms. Modulation Index = 0.75, load impedance = 40.9 Ohms, rotor speed = 1825 rpm. 78

4.9. Load voltage steady-state waveforms. Modulation Index = 1.13, load impedance = 40.9 Ohms, rotor speed = 1830 rpm. 79

4.10. Main winding current steady-state waveforms. Modulation Index = 1.13, load impedance = 40.9 Ohms, rotor speed = 1830 rpm. 80

Figure Page

4.11. Auxiliary winding voltage steady-state waveforms. Modulation Index = 1.13, load impedance = 40.9 Ohms, rotor speed = 1830 rpm. 80

4.12. Auxiliary winding current steady-state waveforms. Modulation Index = 1.13, load impedance = 40.9 Ohms, rotor speed = 1830 rpm. 81

4.13. Load current steady-state waveforms. Modulation Index = 1.13, load impedance = 40.9 Ohms, rotor speed = 1830 rpm. 82

4.14. Measured and calculated main winding voltage as a function of modulation index. Constant rotor speed = 1830 rpm. 87

4.15. Measured and calculated main winding current as a function of modulation index. Constant rotor speed = 1830 rpm. 88

4.16. Measured and calculated load current as a function of modulation index. Constant rotor speed = 1830 rpm. 89

4.17. Measured and calculated load power as a function of modulation index. Constant rotor speed = 1830 rpm. 89

4.18. Measured and calculated auxiliary winding voltage as a function of modulation index. Constant rotor speed = 1830 rpm. 90

4.19. Measured and calculated auxiliary winding current as a function of modulation index. Constant rotor speed = 1830 rpm. 91

4.20. Measured and calculated battery current as a function of modulation index. Constant rotor speed = 1830 rpm. 91

4.21. Measured load voltage as a function of modulation index. Constant rotor speed = 1840 rpm. 93

4.22. Measured main winding current as a function of modulation index. Constant rotor speed = 1840 rpm. 93

4.23. Measured output power as a function of modulation index. Constant rotor speed = 1840 rpm. 94

4.24. Measured load current as a function of modulation index. Constant rotor speed = 1840 rpm. 95

4.25. Measured auxiliary winding voltage as a function of modulation index. Constant rotor speed = 1840 rpm. 95

Figure Page

4.26. Measured auxiliary winding current as a function of modulation index. Constant rotor speed = 1840 rpm. 96

4.27. Measured battery current as a function of modulation index.

Constant rotor speed = 1840 rpm. 97

4.28. Measured load voltage as a function of modulation index.
Constant load impedance = 20.8 Ohms..... 98

4.29. Measured main winding current as a function of modulation index.
Constant load impedance = 20.8 Ohms..... 99

4.30. Measured output power as a function of modulation index.
Constant load impedance = 20.8 Ohms..... 100

4.31. Measured load current as a function of modulation index.
Constant load impedance = 20.8 Ohms..... 100

4.32. Measured auxiliary winding voltage as a function of modulation index.
Constant load impedance = 20.8 Ohms..... 101

4.33. Measured auxiliary winding current as a function of modulation index.
Constant load impedance = 20.8 Ohms..... 102

4.34. Measured battery current as a function of modulation index.
Constant load impedance = 20.8 Ohms..... 102

4.35. Measured auxiliary winding voltage as a function of slip.
Constant load impedance = 41.1 Ohms..... 103

4.36. Measured auxiliary winding current as a function of slip.
Constant load impedance = 41.1 Ohms..... 104

4.37. Measured modulation index as a function of slip. Constant load
impedance = 41.1 Ohms. 105

4.38. Measured battery current as a function of slip. Constant load
impedance = 41.1 Ohms. 105

4.39. Contour plot of load voltage, [V] as a variation of generator rotor
speed (per unit) and load capacitor C_q. 107

4.40. Contour plot of main winding current, [A] as a variation of generator rotor
speed (per unit) and load capacitor C_q. 107

Figure Page

4.41. Contour plot of load current, [A] as a variation of generator rotor speed (per unit) and load capacitor C_q. 108

4.42. Contour plot of load power, [W] as a variation of generator rotor speed (per unit) and load capacitor C_q. 108

4.43. Contour plot of auxiliary winding voltage, [V] as a variation of generator rotor speed (per unit) and load capacitor C_q. 109

4.44. Contour plot of auxiliary winding current, [A] as a variation of generator rotor speed (per unit) and load capacitor C_q. 110

4.45. Contour plot of efficiency as a variation of generator rotor speed (per unit) and load capacitor C_q. 110

4.46. Contour plot of battery current, [A] as a variation of generator rotor speed (per unit) and load capacitor C_q. 111

4.47. Contour plot of load voltage, [V] as a variation of generator rotor speed (per unit) and load capacitor C_q. 111

4.48. Contour plot of efficiency as a variation of generator rotor speed (per unit) and load capacitor C_q. 112

4.49. Contour plot of battery current, [A] as a variation of generator rotor speed (per unit) and load capacitor C_q. 113

4.50. Load voltage start-up waveform. Modulation index = 0.8, load impedance = 20 Ohms, rotor speed = 1860 rpm. 115

4.51. Main winding current start-up waveform. Modulation index = 0.8, load impedance = 20 Ohms, rotor speed = 1860 rpm. 115

4.52. Auxiliary winding current start-up waveform. Modulation index = 0.8, load impedance = 20 Ohms, rotor speed = 1860 rpm. 116

4.53. Battery current start-up waveform. Modulation index = 0.8, load impedance = 20 Ohms, rotor speed = 1860 rpm. 116

4.54. Generator torque start-up waveform. Modulation index = 0.8, load impedance = 20 Ohms, rotor speed = 1860 rpm. 117

4.55. Changes in the values of the load impedance. Modulation index = 0.8, and rotor speed = 1840 rpm. 118

Figure Page

4.56. Load voltage waveform response to changes in load. Modulation index = 0.8, and rotor speed = 1840 rpm. 118

4.57. Main winding current waveform response to changes in load. Modulation index = 0.8, and rotor speed = 1840 rpm. 119

4.58. Auxiliary winding current waveform response to changes in load. Modulation index = 0.8, and rotor speed = 1840 rpm. 119

4.59. Battery current waveform response to changes in load. Modulation index = 0.8, and rotor speed = 1840 rpm. 120

4.60. Generator torque waveform response to changes in load. Modulation index = 0.8, and rotor speed = 1840 rpm. 121

4.61. Changes in the values of generator rotor speeds. Modulation index = 0.8, and load resistance = 40 Ohms. 122

4.62. Load voltage waveform response to changes in generator rotor speed. Modulation index = 0.8, and load resistance = 40 Ohms. 122

4.63. Main winding current waveform response to changes in generator rotor speed. Modulation index = 0.8, and load resistance = 40 Ohms. 123

4.64. Auxiliary winding current waveform response to changes in generator rotor speed. Modulation index = 0.8, and load resistance = 40 Ohms. 123

4.65. Battery current waveform response to changes in generator rotor speed. Modulation index = 0.8, and load resistance = 40 Ohms. 124

4.66. Generator torque waveform response to change in generator rotor speed. Modulation index = 0.8, and load resistance = 40 Ohms. 125

5.1. Block diagram of the system 126

5.2. Schematic diagram of the system with induction motor load 128

5.3. The q-d equivalent circuit of the battery-PWM inverter generator system with single-phase induction motor load 129

5.4. Induction motor input voltage steady-state waveforms. Modulation index = 0.875, rotor speed = 1840 rpm 133

Figure Page

5.5. Induction generator main winding current steady-state waveforms. Modulation index = 0.875, rotor speed = 1840 rpm 133

5.6. Generator auxiliary winding voltage steady-state waveforms. Modulation index = 0.875, rotor speed = 1840 rpm 134

5.7. Generator auxiliary winding current steady-state waveforms. Modulation index = 0.875, rotor speed = 1840 rpm 134

5.8. Induction motor main winding current steady-state waveforms. Modulation index = 0.875, rotor speed = 1840 rpm 135

5.9. System battery current steady-state waveforms. Modulation index = 0.875, rotor speed = 1840 rpm 136

5.10. Induction motor input voltage steady-state waveforms. Modulation index = 1.375, rotor speed = 1840 rpm 137

5.11. Induction generator main winding current steady-state waveforms. Modulation index = 1.375, rotor speed = 1840 rpm 137

5.12. Generator auxiliary winding voltage steady-state waveforms. Modulation index = 1.375, rotor speed = 1840 rpm 138

5.13. Generator auxiliary winding current steady-state waveforms. Modulation index = 1.375, rotor speed = 1840 rpm 138

5.14. Induction motor main winding current steady-state waveforms. Modulation index = 1.375, rotor speed = 1840 rpm 139

5.15. System battery current steady-state waveforms. Modulation index = 1.375, rotor speed = 1840 rpm 139

5.16. Measured and calculated motor input voltage as a function of motor

speed. Constant generator rotor speed = 1840 rpm 141

5.17. Measured and calculated motor torque as a function of motor speed. Constant generator rotor speed = 1840 rpm 142

5.18. Measured and calculated motor input voltage as a function of motor speed. Constant generator rotor speed = 1840 rpm 143

5.19. Measured and calculated generator winding current as a function of motor speed. Constant generator rotor speed = 1840 rpm 143

Figure Page

5.20. Measured and calculated battery current as a function of motor speed. Constant generator rotor speed = 1840 rpm 144

5.21. Predicted motor voltage as a function of motor torque. Constant generator rotor speed = 1840 rpm 145

5.22. Predicted motor voltage as a function of motor input power. Constant generator rotor speed = 1840 rpm 146

5.23. Predicted motor torque as a function of motor rotor speed. Constant generator rotor speed = 1840 rpm 146

5.24. Contour plot of torque, [Nm] as a variation of generator rotor speed (per unit) and motor rotor speed (per unit) 150

5.25. Contour plot of motor voltage, [V] as a variation of generator rotor speed (per unit) and motor rotor speed (per unit) 150

5.26. Contour plot of output power, [W] as a variation of generator rotor speed (per unit) and motor rotor speed (per unit) 151

5.27. Contour plot of battery current, [A] as a variation of generator rotor speed (per unit) and motor rotor speed (per unit) 151

5.28. Motor voltage start-up waveform. Modulation index = 0.8, and generator rotor speed = 1840 rpm 152

5.29. Motor main winding current start-up waveform. Modulation index = 0.8, and generator rotor speed = 1840 rpm 152

5.30. Motor rotor speed start-up waveform. Modulation index = 0.8, and generator rotor speed = 1840 rpm 153

5.31. Motor torque start-up waveform. Modulation index = 0.8, and generator rotor speed = 1840 rpm 153

5.32. Generator main winding current start-up waveform. Modulation index = 0.8, and generator rotor speed = 1840 rpm 154

5.33. Generator auxiliary winding current start-up waveform. Modulation index = 0.8, and generator rotor speed = 1840 rpm 155

5.34. Battery current start-up waveform. Modulation index = 0.8, and generator rotor speed = 1840 rpm 155

Figure Page

5.35. Generator torque start-up waveform. Modulation index = 0.8, and generator rotor speed = 1840 rpm 156

5.36. Changes in the values of the load torque. Modulation index = 2.0 and rotor generator speed = 1840 rpm 157

5.37. Motor input voltage waveform response to changes in load torque. Modulation index = 2.0 and rotor generator speed = 1840 rpm 157

5.38. Motor rotor speed waveform response to changes in load torque. Modulation index = 2.0 and rotor generator speed = 1840 rpm 158

5.39. Motor torque waveform response to changes in load torque. Modulation index = 2.0 and rotor generator speed = 1840 rpm 158

5.40. Generator main winding current waveform response to changes in load torque. Modulation index = 2.0 and rotor generator speed = 1840 rpm 159

5.41. Generator auxiliary winding current waveform response to changes in load torque. Modulation index = 2.0 and rotor generator speed = 1840 rpm 159

5.42. Battery current waveform response to changes in load torque. Modulation index = 2.0 and rotor generator speed = 1840 rpm 160

5.43. Generator torque waveform response to changes in load torque. Modulation index = 2.0 and rotor generator speed = 1840 rpm 160

5.44. Changes in the values of generator rotor speeds. Modulation index = 2.0 and Load Torque = 0.25 Nm 162

5.45. Motor input voltage waveform response to changes in generator rotor speed. Modulation index = 2.0 and Load Torque = 0.25 Nm 162

5.46. Motor main winding current waveform response to changes in generator rotor speed. Modulation index = 2.0 and Load Torque = 0.25 Nm..... 163

5.47. Motor rotor speed waveform response to changes in generator rotor speed. Modulation index = 2.0 and Load Torque = 0.25 Nm 164

5.48. Motor torque waveform response to changes in generator rotor speed. Modulation index = 2.0 and Load Torque = 0.25 Nm 164

5.49. Generator main winding current waveform response to changes in generator rotor speed. Modulation index = 2.0 and Load Torque = 0.25 Nm..... 165

Figure Page

5.50. Generator auxiliary winding current waveform response to changes in generator rotor speed. Modulation index = 2.0 and Load Torque = 0.25 Nm..... 166

5.51. Battery current waveform response to changes in generator rotor speed. Modulation index = 2.0 and Load Torque = 0.25 Nm 166

5.52. Generator torque waveform response to changes in generator rotor speed. Modulation index = 2.0 and Load Torque = 0.25 Nm 167

5.53. Changes in the values of the load torque. Modulation index = 1.2 and rotor generator speed = 1840 rpm 168

5.54. Motor input voltage waveform. Modulation index = 1.2 and rotor generator speed = 1840 rpm..... 168

5.55. Motor main winding current waveform. Modulation index = 1.2 and rotor generator speed = 1840 rpm 169

5.56. Motor speed waveform. Modulation index = 1.2 and rotor generator speed = 1840 rpm..... 169

5.57. Motor torque waveform. Modulation index = 1.2 and rotor generator

speed = 1840 rpm.....170

5.58. Generator main winding current waveform. Modulation index = 1.2 and rotor generator speed = 1840 rpm.....170

5.59. Generator auxiliary winding current waveform. Modulation index = 1.2 and rotor generator speed = 1840 rpm.....171

5.60. Battery current waveform. Modulation index = 1.2 and rotor generator speed = 1840 rpm.....172

5.61. Generator torque waveform. Modulation index = 1.2 and rotor generator speed = 1840 rpm.....172

6.1. Block diagram of the system.....173

6.2. Schematic diagram of the system.....174

6.3. The q-d equivalent circuit of the capacitor-PWM inverter generator system with impedance load.....175

Figure Page

6.4. Self-excitation for the system without battery. Calculated load resistance vs generator rotor speed.....182

6.5. Self-excitation for the system without battery. Contour plot of load resistance, [Ω] as a variation of generator rotor speed and load capacitor.....183

6.6. Self-excitation for the system without battery. Contour plot of load resistance, [Ω] as a variation of M_d and M_q.....184

CHAPTER 1

INTRODUCTION

1.1 Introduction

Basically there are two broad categories of ac generators; they are the synchronous generators and the induction generators. Synchronous generators use synchronous machines that generate output voltage; the frequency of the output voltage is proportional to the rotational speed of the rotating parts. Induction generators are primarily induction motors (machines) that are driven above their synchronous speed. They cannot generate power on their own without some form of reactive power for excitation which has to be provided through the stator winding. When the induction machine is driven by an external prime mover, the flux in the rotor induces a small voltage in the stator windings. The stator-winding voltage has a leading current if a suitable source of reactive power is connected to the terminal. The source of reactive power could be a synchronous generator, a bank of capacitors, or an inverter. The induced voltages and currents would continue to rise, but the magnetic saturation in the machine limits them. This results in a steady-state operating condition of the induction generator. The steady-state voltage is dependent on speed, capacitance, machine parameters, and load.

The induction generator has the advantage of simplicity as it is the same as a squirrel-cage motor of the same output, needing neither field windings, exciter nor

automatic regulator. It has the disadvantages of needing supply to obtain the magnetizing current and it generates at a leading power factor, requiring its magnetizing current to be supplied by other synchronous generators or from the mains. This limitation can be overcome by using the capacitor-excited or static versions of the machine.

Induction generator applications in power systems have been studied [1]. The use of single-phase self-excited induction generator in rural electrification projects is finding wide application in isolated areas [22].

1.2 Review of Previous Work

The two methods for application of induction generator include:

(i) connecting the induction generator to a grid and

(ii) using a self-excited stand-alone induction generator.

In the grid-connected application of the induction generator the reactive power for excitation is supplied by the synchronous machine in the system while for a stand-alone case the reactive power may be provided by a static VAR source such as capacitors or an inverter.

The induction machine can be operated as a generator by capacitor self-excitation. Capacitor self-excitation in an induction machine occurs when an appropriate capacitor bank is connected across an externally driven induction machine; this results in an electromotive force being induced in the machine windings. The induced voltages and currents would continue to rise, but for the magnetic saturation in the machine that results in an equilibrium state being reached.

A capacitor self-excited induction generator offers certain advantages over a conventional synchronous generator as a source of isolated power supply. It has reduced unit cost, brushless rotor (squirrel cage construction), absence of a separate dc source, and ease of maintenance. The disadvantage of a capacitor self-excited induction generator is its inability to control the supplied voltage and frequency under varying load conditions.

A wind energy conversion scheme using an induction machine driven by a variable speed wind turbine is discussed in [2]. Excitation control was obtained by employing a capacitor and a thyristor-controlled inductor. The wind speed cube law was used in loading the induction machine for maximizing energy conversion. Performance characteristic of the generation scheme was evaluated over a wide speed range. The harmonic analysis of the scheme shows that the harmonics generated by the converters are extremely small.

A variable-speed generating system was discussed in [3] using a 3-phase squirrel-cage induction machine with self-excited capacitors. The self-excited induction generator with controlled rectifier allows wide changes in wind-turbine speed with optimum generating power set at all speeds by rectifier delay-angle control. A constant output dc voltage can be maintained and the generator always operates in the low slip region.

The analysis of self-excited induction generators was reported in [4]. The Newton-Raphson method was used to predict the steady-state behavior of capacitor self-excited induction generators. The values of the saturated magnetizing reactance and ouput frequency of the given capacitance, speed, and load were also identified.

Capacitance requirements for an isolated self-excited induction generator have been examined in [5]. An analytical method was proposed to find the minimum capacitance value required for self-excitation of isolated induction generator under no load conditions. The calculated values of the capacitance were compared with the experimental results for some test machines. The influence of the load impedance, load power factor, and machine speed on the value of minimum capacitor were also discussed.

The steady-state performance of an isolated self-excited single-phase induction generator when the excitation capacitor is connected to one winding and the load is connected to the other is examined in [6]. A nonlinear analytical equation in terms of the magnetization reactance and the operating frequency was developed. The resulting equation was solved using Newton-Raphson numerical technique for the airgap voltage and other performance indices. The predicted performance of the system is validated with experimental results.

A single-phase induction generator was investigated [7,8]. The work describes a newly developed single-phase capacitor self-excited induction generator with self-regulating features. The generator was designed with two uniquely designed stator windings in quadrature, connected externally to a shunt and a series capacitor, respectively. It employs a standard die-cast squirrel cage rotor. The features, advantages, and theoretical concepts of the system were highlighted and a detailed experimental result was presented.

The modeling and steady-state performance of a single-phase induction generator based on the principles of harmonic balance were examined in [9]. The effects of saturation of the magnetizing flux linkages and core loss of the generator were included

in the model of the single-phase induction generator. Experimental results were corroborated with steady-state calculation of the system.

The steady-state analysis of a single-phase, self-excited induction generator, which supplies an isolated resistive load, was reported in [10]. The equivalent circuit model was developed neglecting the magnetizing reactance in the negative sequence circuits. Experimental results verified the equivalent circuit model and the assumptions used in the analysis.

The transient performance of a single-phase induction generator with series or parallel connected load was discussed in [11]. The dependency of the load impedance on the generator self-excitation was explored using the determinant of the generator steady-state equation. It was concluded that for self excitation, a minimum amount of airgap flux linkages is required. Maximum load impedance was specified for rotor speed and excitation capacitors when load is connected in series with the main winding. If the load connected in parallel with the capacitor, a minimum load impedance was required for self-excitation.

Reference [12] examines the influence of different excitation topologies, shunt, short-shunt, and long-shunt, on the steady-state and dynamic performance of the single-phase, self-excited induction generator. It was concluded that a long-shunt generator delivers lower output power at reduced output voltage while the short-shunt generator system has load voltage characteristics and output power profile that can outperform the same generator with the shunt excitation connection. Also the small-signal analysis showed that the generator with either short-shunt or long-shunt excitation connections had a good overload capability; there was no generator de-excitation at moderate

overload. Also, a generator with either of these excitations quickly recovers when overload is relieved.

The capacitor self-excited induction generator has limited applications due to its inability to control the load voltage and frequency under varying load conditions. To cope with the varying load and/or speed variation of the induction generator, the voltage can be controlled by using adjustable reactive power generators, such as inverters, connected to the terminals of the induction machine.

Self-excitation in inverter-driven induction machines was investigated in [13]. A theoretical treatment was discussed based on a first harmonic approximation of inverter performance. The system performance was shown to depend on the magnetization characteristic and the stator and rotor resistances of the machines. Experimental results were then used to confirm the validity of the analysis.

A simple exciter scheme based on using a static reactive power generator implemented with fixed capacitors and thyristor-controlled inductors is discussed in [14]. The feasibility of the proposed scheme with naturally commutated thyristors was verified by measurements on a test setup employing a standard 15-hp induction motor.

Reference [15] describes self-excited induction-generator/controlled-rectifier units, which eliminate the problems of voltage and frequency variations inherent in self-excited induction generator machines. Theoretical and experimental results are provided showing that the self-excited induction generator can operate in the linear region of the magnetization curve while feeding a variable dc load at constant voltage. It was also shown that the unit could be used to feed controllable power into an existing a.c network through a dc transmission link.

The steady-state modelling of regeneration and self-excitation in induction machines was discussed in [16]. Six modes of source-connected and self-excited induction generator operation including both voltage and current inverter systems were reviewed and compared. The equivalent circuit for each mode was presented and its use to model steady-state performance was shown. The properties of regeneration and self-excitation were derived to illustrate the similarities and differences between the various modes. The experimental results were supported by the validity of the models used in the study.

The limitations of self-excited induction generator discussed thus far are:

i. Its inability to control the supplied voltage and frequency under varying load condition
ii. Operation below the synchronous speed will cease generation.

The present research proposes an alternate design to eliminate the limitations of the previous research.

1.3 Scope of Present Research

The main objective of this research is to present the dynamic and steady-state performance characteristics of a stand-alone single-phase induction generator system, which can be driven by wind or diesel engine. The proposed scheme, shown in Figure 1.1, has the advantage of ensuring a constant and regulated load voltage. In addition the mathematical model developed for the single-phase induction generator scheme with battery-PWM inverter will be useful in the prediction of the transient, dynamic, and steady-state performance. The load voltage and frequency of the isolated single-phase

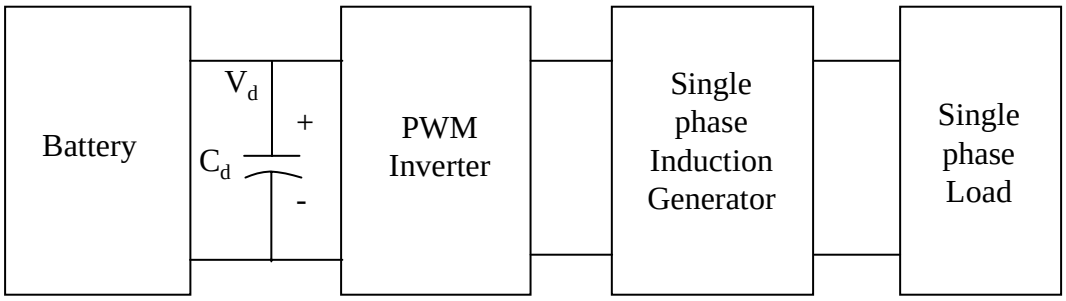

Figure 1.1. Block diagram of the proposed system.

induction generator is controlled or regulated using a single-phase, full bridge, pulse-width modulated (PWM) dc/ac inverter. A battery feeding the single-phase inverter provides real power to the load when the generator output is less than the real power required by the load. If the generator delivers more real power than what is required by the load, the battery through the bi-directional single-phase PWM inverter absorbs the excess real power. The inverter augmented with a shunt capacitor connected across the load effectively meets the reactive power requirement of the load.

The proposed system will find application in the following areas:

i. Provide regulated voltage and frequency for isolated applications such as in commercial and industrial uses especially in situations where engine-driven single-phase synchronous generators are presently being used.

ii. As power sources (hybrid power generation) for isolated systems and for utility interface to single-phase power system grids.

iii. As a source of regulated dc voltage by rectifying the generated voltage at the main winding.

iv. For battery charging purpose and controllable single-phase ac voltage source, i.e., traction power systems.

A series-compensated three-phase induction generator-battery supply topology, which provides a constant voltage and frequency at the terminals, was investigated in [17,32]. The system shows an induction generator to generate electric power and to filter the current harmonics; a PWM inverter to provide the excitation and set the desired frequency and an energy storage dc battery to allow a bi-directional power flow. The proposed system is similar to single-phase induction generator with battery-PWM inverter discussed in this thesis.

Due to the series connection topology configuration of the system proposed in [17,32], the inverter induces current and voltage harmonics that are directly transferred to the load. Unlike the system proposed in [17,32] the scheme presented here does not require an additional filter to remove current and voltage harmonics since the auxiliary winding which is connected to the inverter is only magnetically connected to the main winding acts as a filter. The mathematical model developed in this present research work accurately predicts the experimental results unlike the model system proposed in [17,32].

The single-phase induction machine used for this work is rated at 1 h.p. The operation of the system with battery, PWM (pulse width modulation) inverter, and impedance load was studied.

Experiments were performed with the generator system feeding impedance and motor loads. The condition for self-excitation of the system without battery was also studied.

Simulation of the system with impedance and motor loads was carried out including the influence of variation of load and generator speed. MATLAB/Simulink [18]

was found to be an excellent tool in simulating the dynamic mathematical model developed.

The steady-state model of the system was developed using harmonic balance technique [19]. The computation was carried out using MATHCAD [20], MATLAB, and MATHEMATICAL [21].

Chapter 2 discusses the theory behind the single-phase pulse width modulation inverter topologies. In addition, it explains the design, implementation, and operation of the bipolar PWM inverter used for this work.

The parameter determination of a single-phase induction motor is described in detail in chapter 3. The various steps in arriving at the parameters of the single-phase induction motor are highlighted and experimental results are discussed.

Chapter 4 analyzes the battery inverter single-phase induction generator system with an impedance load. The mathematical steps taken to arrive at the mathematical model of the system are discussed. The dynamic mathematical model is simulated and corroborated by experimental results. The steady-state calculations and experiment results are also discussed in this chapter. The dynamic performance and the influence of changing operating conditions are also examined

The analysis of a battery inverter single-phase induction generator system with a single-phase induction motor load is set forth in chapter 5. The mathematical model development is shown. The steady-state analysis, experiments, and calculations with results are explained. The dynamic mathematical model of the generator system connected to a single-phase induction motor (SPIM) load is simulated and the results are

corroborated experimental results. The influence of varying operating conditions and dynamic performance of the generator system feeding SPIM are discussed.

The condition for self-excitation of the single-phase induction generator system without battery is the subject of discussion in chapter 6. The steps involved at arriving at the condition of self-excitation are shown. The results of the numerical computation are also discussed.

Chapter 7 includes conclusions and suggestions for further work on the system.

CHAPTER 2

SINGLE-PHASE PULSE WIDTH MODULATION INVERTER

2.1 Introduction

The dc-ac converter, also known as inverter, basically converts dc power to ac power. Inverters can be grouped either as voltage-source or current-source inverters. A stiff dc voltage such as a battery or a rectifier feeds the voltage-source inverter. The filter capacitor across the inverter input terminals provide a constant dc link voltage. The inverter is, therefore, an adjustable-frequency voltage source. The current-source inverter is supplied with a controlled current from a dc source of high impedance. Normally, a phase-controlled thyristor feeds the inverter with a regulated current through a large series inductor. Hence, the load current rather than load voltage is controlled.

A standard single-phase voltage or current inverter can be half-bridge, full-bridge or H-bridge, and push-pull transformer center tap configurations. The single-phase unit can be joined to have three-phase or other multiphase topologies. Typically, inverter applications are used in ac machine drives, regulated-voltage and frequency power supplies, uninterruptible power supplies (UPS), induction heating, and static var generators.

In this chapter, different control schemes for single-phase PWM inverter will be reviewed. The design, implementation, and operation of the bipolar voltage-switching scheme for single-phase PWM inverter will be considered.

2.2 Control Scheme Method for Single-Phase PWM Inverter

The PWM inverters have constant input dc voltage that is essentially constant in magnitude, such as in the scheme in Figure 2.1. The battery or rectifier provides the dc supply to the inverter. The inverter is used to control the fundamental voltage magnitude and the frequency of the ac output voltages. This can be achieved by pulse-width modulation of the inverter switches. Hence such inverters are called PWM inverters.

2.2.1 Single-Phase PWM Inverter

The sinusoidal PWM (SPWM) method, also known as the triangulation, subharmonic, or suboscillation method, is very popular in industrial applications and is extensively reviewed in the literature [23-25]. The SPWM principle for a half-bridge inverter is illustrated in Figure 2.2. In order to produce a sinusoidal output voltage waveform at a desired frequency, a sine-modulating wave is compared with a triangular carrier wave. The point of intersection determines the switching points of the inverter power devices. The inverter switching frequency is determined by the frequency of the triangular waveform. The inverter switching frequency and amplitude are normally kept

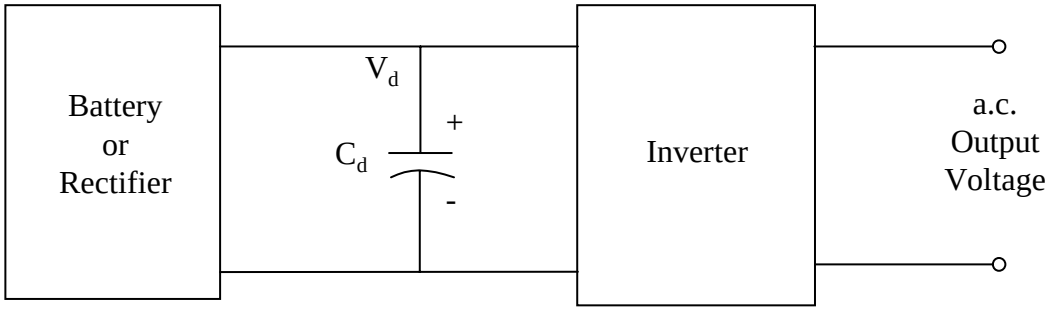

Figure 2.1. Schematic diagram for inverter system.

constant. The triangular waveform, v_t, is at a switching or carrier frequency f_t, which determines the frequency with which the inverter switches are switched. The modulating or control signal v_m is used to modulate the switch duty ratio and has a frequency f_m, which is the desired fundamental frequency of the inverter voltage output. The amplitude modulation ratio m_a is defined as

$$m_a = \frac{\hat{V}_m}{\hat{V}_t} \tag{2.1}$$

where $\hat{V}_m$ is the peak amplitude of the control signal. The amplitude $\hat{V}_t$ of the triangular signal is generally kept constant.

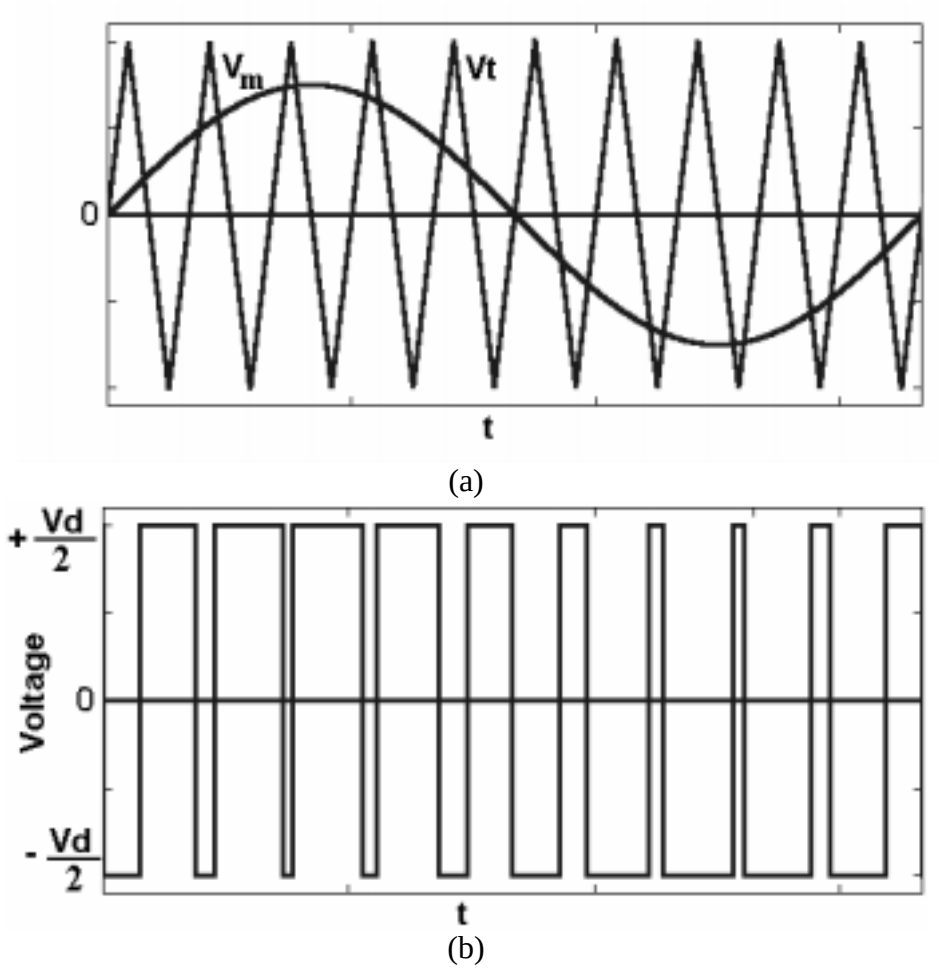

Figure 2.2. Half-bridge PWM Inverter Waveforms. (a) Generation Method, (b) inverter output voltage.

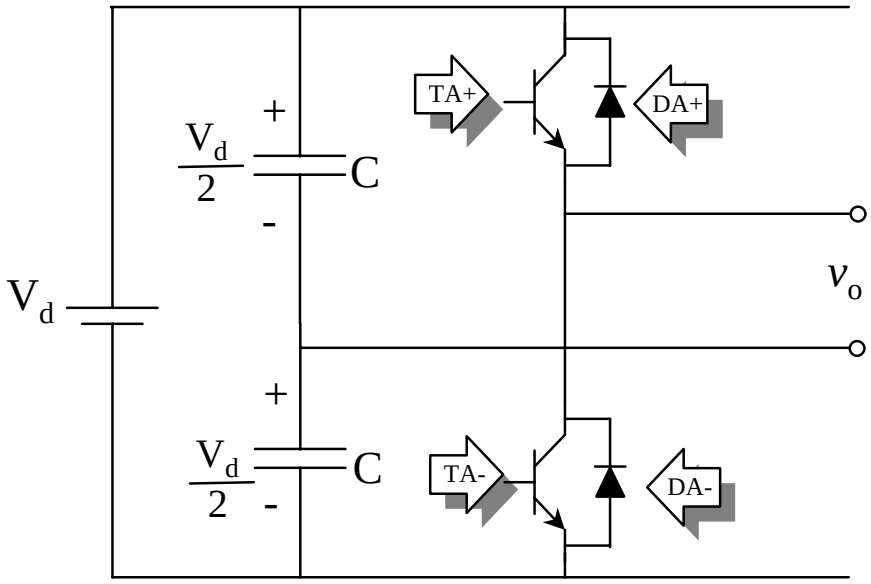

Figure 2.3. Schematic diagram for Half-bridge PWM inverter.

The frequency-modulation ratio m_f is defined as

$$m_f = \frac{f_t}{f_m} \quad . \tag{2.2}$$

In the inverter of Figure 2.3, the switches T_{A+} and T_{A-} are controlled based on the comparison of control signal, v_m and triangular signal, v_t, and the following output voltage results, independent of the direction of output current:

$$v_m > v_t, \qquad T_{A+} \quad \text{is on,} \qquad v_o = \frac{V_d}{2} \tag{2.3}$$

and

$$v_m < v_t, \qquad T_{A-} \quad \text{is on,} \qquad v_o = -\frac{V_d}{2} \quad . \tag{2.4}$$

The switches on the same leg are protected against turning on at the same time. This enables the output voltage, v_o, to fluctuate between $V_d/2$ and - $V_d/2$. v_o is shown in Figure 2.2 b.

2.2.2 Single-Phase Inverters

A single-phase inverter is shown in Figure 2.4. This inverter, also known as the H-bridge or full-bridge inverter, consists of two half-bridge inverters shown in Figure 2.3. The full-bridge inverter can produce an output power twice that of the half-bridge inverter with the same input voltage. Different PWM switching schemes will now be discussed.

2.2.2.1 PWM with bipolar voltage switching. In this scheme the diagonally opposite transistors (T_{A+}, T_{B-}) and (T_{A-}, T_{B+}) form the two legs in Figure 2.4 and are switched as switch-pairs 1 and 2, respectively. The output of leg A is equal and opposite to the output of leg B. The output voltage is determined by comparing the control signal, v_m, and the triangular signal, v_t. This is illustrated in Figure 2.5a.

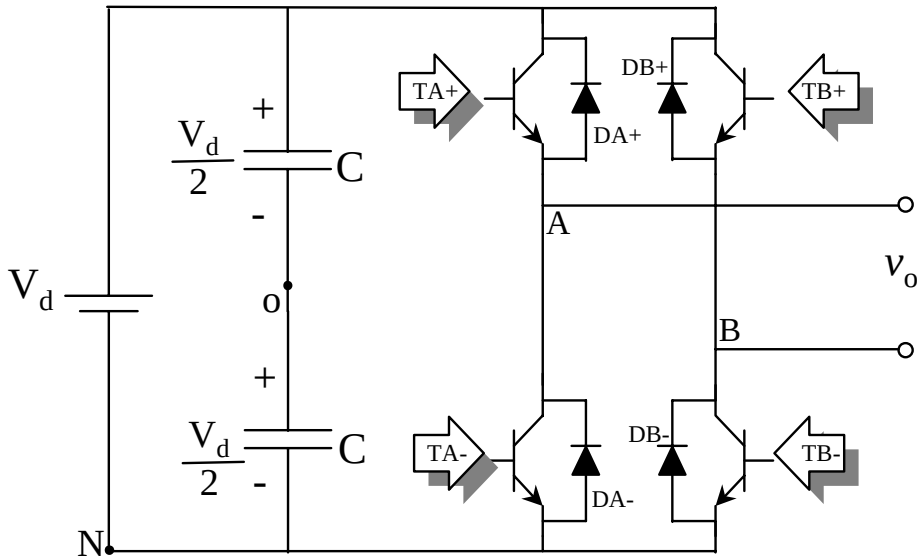

Figure 2.4. Single-phase full-bridge inverter.

The switching pattern is as follows

$$v_m > v_t, \quad T_{A+} \text{ is on } \Rightarrow \; v_{Ao} = \frac{V_d}{2} \quad \text{and} \quad T_{B-} \text{ is on } \Rightarrow v_{Bo} = -\frac{V_d}{2}; \tag{2.5a}$$

$$v_m < v_t, \quad T_{A-} \text{ is on } \Rightarrow \; v_{Ao} = -\frac{V_d}{2} \quad \text{and} \quad T_{B+} \text{ is on } \Rightarrow v_{Bo} = \frac{V_d}{2}; \tag{2.5b}$$

hence

$$v_{Bo}(t) = -v_{Ao}(t) \; . \tag{2.6}$$

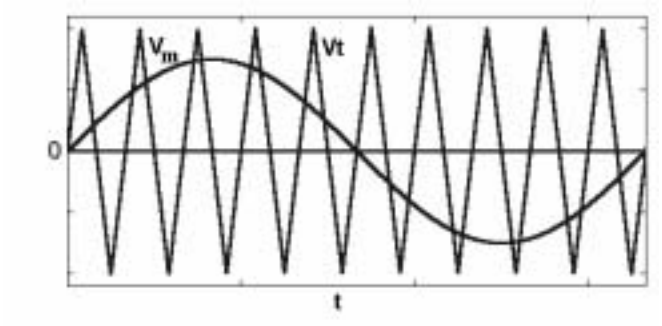

(a)

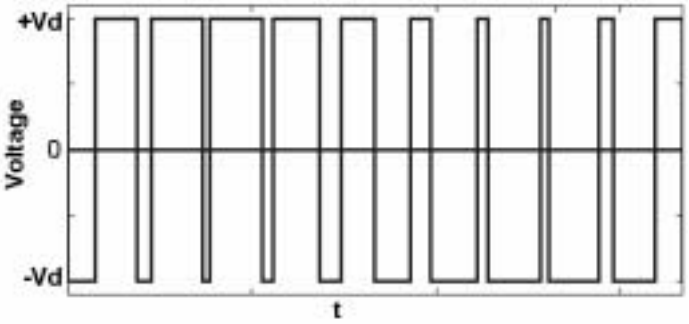

(b)

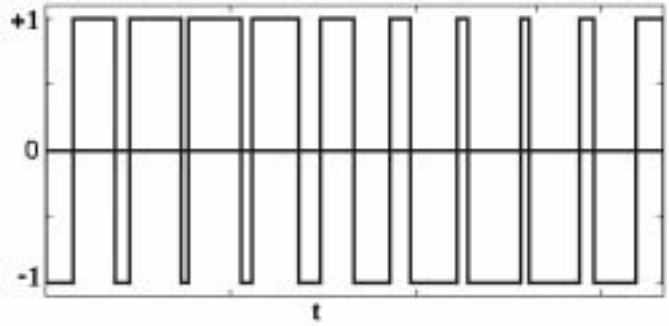

(c)

Figure 2.5. PWM with bipolar voltage switching. (a) Generation Method, (b) inverter output voltage, (c) inverter switching function.

The output voltage can then be expressed as shown in Equation 2.7 with a waveform shown in Figure 2.5b.

$$v_o(t) = v_{Ao}(t) - v_{Bo}(t) = 2v_{Ao}(t) \tag{2.7}$$

The inverter switching function, which is similar to the inverter output voltage is shown in Figure 2.5c.

In Figure 2.5, the output voltage v_o produced by the modulating signal, v_m and the carrier signal, v_t can be expressed by a complex double Fourier series. The output voltage in Figure 2.5 is determined using the phase relationship between the modulating and carrier signal shown in Figure 2.6 and 2.7. The peak value and angular frequency of the

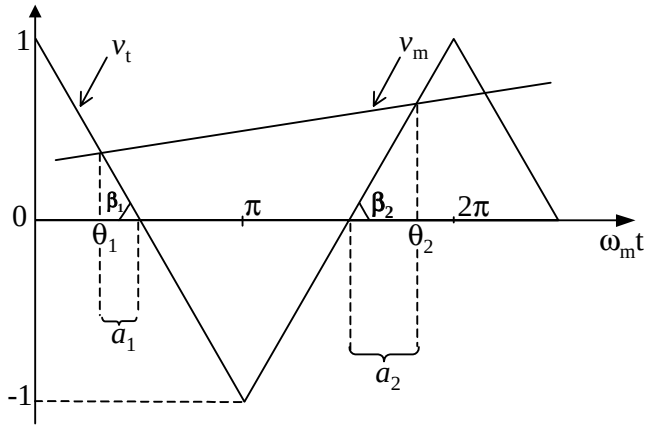

(a) Modulating and carrier signal waveforms, $0 \le \omega_m t + \phi < \pi$.

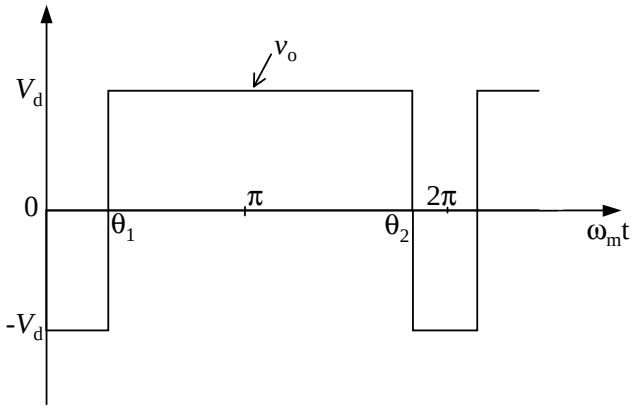

(b) Inverter output voltage, $0 \le \omega_m t + \phi < \pi$.

Figure 2.6. Phase relationship of output voltage to modulating and carrier signals for bipolar voltage scheme. Condition, $0 \le \omega_m t + \phi < \pi$.

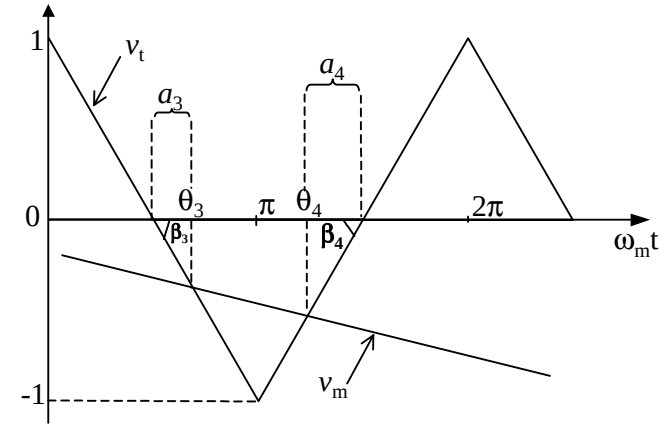

(a) Modulating and carrier signal waveforms, $\pi \le \omega_m t + \phi < 2\pi$.

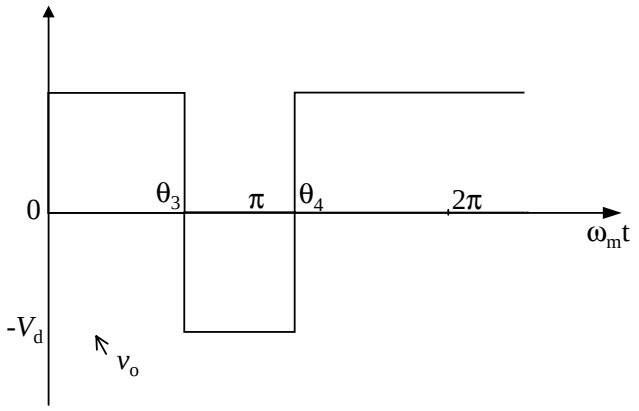

(b) Inverter output voltage, $\pi \le \omega_m t + \phi < 2\pi$.

Figure 2.7. Phase relationship of output voltage to modulating and carrier signals for bipolar voltage scheme. Condition, $\pi \le \omega_m t + \phi < 2\pi$.

carrier signal are 1 and ω_t, respectively. The modulating signal is expressed as $v_o = m_a \sin(\omega_m t + \phi)$, where ω_m is the angular frequency of the modulating signal.

The output voltage of Figure 2.5 can be expressed by complex double Fourier series as follow [33, 34]:

$$v_o = \sum_{k=-\infty}^{\infty} \sum_{n=-\infty}^{\infty} K_{kn} \exp\left(j\{kx + ny\}\right) \tag{2.8}$$

where $x = \omega_m t + \phi$ and $y = \omega_t t$. Equation 2.8 expressing the frequency spectrum of the PWM waveform comprises the angular frequencies of n (integer) times ω_t and the

sideband waves arranged at intervals of the angular frequencies of k (integer) times ω_m in frequencies and sidebands.

The complex Fourier coefficient K_{kn} can be expressed as follows:

$$K_{kn} = \frac{V_d}{4\pi^2}\left\{\begin{array}{l} \int_0^{\pi} e^{-jkx}\left(-\int_0^{\theta_1} e^{-jny}dy + \int_{\theta_1}^{\theta_2} e^{-jny}dy - \int_{\theta 2}^{2\pi} e^{-jny}dy\right)dx \\ + \int_{\pi}^{2\pi} e^{-jkx}\left(\int_0^{\theta_3} e^{-jny}dy - \int_{\theta_3}^{\theta 4} e^{-jny}dy + \int_{\theta_4}^{2\pi} e^{-jny}dy\right)dx \end{array}\right\} \qquad (2.9)$$

where , $k = 0, \pm 1, \pm 2, \ldots$ and $n = 0, \pm 1, \pm 2, \ldots$.

Angles θ_1 and θ_2 are the intersection points of v_m and v_t when modulating signal $v_m = m_a \sin(\omega_m t + \phi)$ is greater than zero; and angles θ_3 and θ_4 are similar intersection points of v_m and v_t when the modulating signal $v_m = m_a \sin(\omega_m t + \phi)$ is less than zero. The angle θ_1 is determined as

$$\theta_1 + a_1 = \frac{\pi}{2}, \qquad \Rightarrow \theta_1 = \frac{\pi}{2} - a_1$$

$$\tan\beta_1 = \frac{1}{\pi/2}, \qquad \text{also} \quad \tan\beta_1 = \frac{m_a \sin x}{a_1}$$

$$\therefore \quad \frac{m_a \sin x}{a_1} = \frac{1}{\pi/2}, \qquad \Rightarrow a_1 = \frac{\pi}{2} m_a \sin x$$

Hence

$$\theta_1 = \frac{\pi}{2}\left(1 - m_a \sin x\right). \qquad (2.10a)$$

Similarly, θ_2, θ_3, and θ_4 are determined; their values are given as:

$$\theta_2 = \frac{\pi}{2}\left(3 + m_a \sin x\right)$$

$$\theta_3 = \frac{\pi}{2}\left(1 - m_a \sin x\right) \qquad (2.10b)$$

$$\theta_4 = \frac{\pi}{2}\left(3 + m_a \sin x\right)$$

Equation 2.8 will now be separated into its respective frequency components.

(i) dc component. The dc component is determined by setting k = n = 0 in Equations 2.8 and 2.9, this result in

$$v_{00} = \frac{2V_d}{\pi} m_a \qquad \text{and} \qquad K_{00} = \frac{2V_d}{\pi} m_a$$

(ii) n = 0 components. From Equation 2.8, K_{k0} is determined by letting n = 0:

$$K_{k0} = \frac{V_d}{4\pi^2}\left\{\int_0^{\pi} e^{-jkx}\left(2\theta_2 - 2\theta_1 - 2\pi\right)dx + \int_{\pi}^{2\pi} e^{-jkx}\left(2\theta_3 + 2\pi - 2\theta_4\right)dx\right\}. \quad (2.11)$$

But

$$2\theta_2 - 2\theta_1 - 2\pi = 2\pi m_a \sin x \quad (2.12a)$$

$$2\theta_3 + 2\pi - 2\theta_4 = -2\pi m_a \sin x \quad (2.12b)$$

from Equations 2.10a and 2.10b, then Equation 2.11 becomes

$$K_{k0} = \frac{V_d}{4\pi}\left\{\int_0^{\pi} e^{-jkx}\left(2m_a \sin x\right)dx + \int_{\pi}^{2\pi} e^{-jkx}\left(-2m_a \sin x\right)dx\right\} \quad (2.13)$$

where

$$K_{ko} = \begin{cases} -\dfrac{V_d m_a}{\pi}\left(\dfrac{2}{k^2 - 1}\right) & (k = 2, 4, 6, \cdots) \\ 0 & (k : \text{odd number}) \end{cases} \quad (2.14)$$

The output voltage for the harmonic components, v_{ko} is obtained by substituting Equation 2.13 into Equation 2.8. The output voltage by performing real Fourier Expansion is given as (Appendix C)

$$v_{ko} = K_{k0}\exp\left(j\{kx + 0\}\right)$$

$$v_{ko} = \begin{cases} \left(\dfrac{(-1)^{\frac{(k+2)}{2}}}{k^2 - 1} \right) \dfrac{4m_a V_d}{\pi} \sin x & (k = 2, 4, 6, \cdots) \\ 0 & (k : \text{odd number}) \end{cases} \tag{2.15}$$

In Equation 2.15, the fundamental component of the signal is zero and the components of k = 2, 4, 6, … express the second, the fourth and sixth harmonic components, and so on.

(iii) k, n components. Rearranging Equation 2.9 yields

$$K_{kn} = \frac{V_d}{4\pi^2} \left\{ \int_0^{2\pi} e^{-jkx} \left(- \int_0^{\theta_1} e^{-jny} dy + \int_{\theta_1}^{\theta_2} e^{-jny} dy - \int_{\theta_2}^{2\pi} e^{-jny} dy \right) dx \right\}$$

$$K_{kn} = \frac{V_d}{j4\pi^2 n} \left\{ \int_0^{2\pi} e^{-jkx} \left(2e^{-jn\theta_1} - 2e^{-jn\theta_2} + e^{-j2n\pi} - 1 \right) dx \right\} \tag{2.16}$$

Substituting Equations 2.10a and 2.10b into Equation 2.16, result in

$$K_{kn} = \frac{V_d}{j4\pi^2 n} \left\{ \int_0^{2\pi} e^{-jkx} \left(\begin{array}{l} 2e^{-\frac{1}{2}jn\pi} e^{\frac{1}{2}jn\pi m_a \sin x} - 2e^{-\frac{3}{2}jn\pi} e^{-\frac{1}{2}jn\pi m_a \sin x} \\ + e^{-j2n\pi} - 1 \end{array} \right) dx \right\} \tag{2.17}$$

The value of K_{kn} from Equation 2.17 when n is an even number is given as

$$K_{kn} = (-1)^{\frac{n}{2}} \frac{2V_d}{j4\pi^2 n} \left\{ \int_0^{2\pi} e^{-jkx} \left(e^{\frac{1}{2}jn\pi m_a \sin x} - e^{-\frac{1}{2}jn\pi m_a \sin x} - 1 \right) dx \right\} \tag{2.18}$$

$$K_{kn} = \begin{cases} (-1)^{\frac{n}{2}} \dfrac{2V_d}{j\pi n} J_k \left(\dfrac{m_a n\pi}{2} \right) & (k : \text{odd number}) \\ 0 & (k : \text{even number}) \end{cases} \tag{2.19}$$

where

$$J_k \left(\frac{m_a n\pi}{2} \right) = \frac{1}{\pi} \int_0^{\pi} \sin kx \sin \left(\frac{m_a n\pi}{2} \sin x \right) dx$$

The J_k is the kth-order Bessel function of the first kind. $J_k\left(\frac{m_a n\pi}{2}\right)$ is a function whose value will become small as k increases.

The value of K_{kn} from Equation 2.17 when n is an odd number is given as:

$$K_{kn} = (-1)^{\frac{(n+1)}{2}} \frac{2V_d}{4\pi^2 n}\left\{ \int_0^{2\pi} e^{-jkx}\left(e^{\frac{1}{2}jn\pi m_a \sin x} + e^{-\frac{1}{2}jn\pi m_a \sin x}\right) dx\right\} \tag{2.20}$$

$$K_{kn} = \begin{cases} (-1)^{\frac{(n+1)}{2}} \frac{2V_d}{\pi n} J_k\left(\frac{m_a n\pi}{2}\right) & (k : \text{odd number}) \\ 0 & (k : \text{even number}) \end{cases} \tag{2.21}$$

where

$$J_k\left(\frac{m_a n\pi}{2}\right) = \frac{1}{\pi}\int_0^{\pi} \cos kx \cos\left(\frac{m_a n\pi}{2}\sin x\right) dx$$

The output voltage, v_o in Equation 2.8 is expressed as

$$\begin{aligned} v_o = {} & \frac{2V_d}{\pi} m_a \; + \sum_{k=2,4\cdots}^{\infty} (-1)^{\frac{(k+1)}{2}} \left(\frac{4m_a V_d}{(k^2-1)\pi}\right) \sin(k\omega_m t + k\phi) \\ & + \sum_{n=1,3\cdots}^{\infty} (-1)^{\frac{(n+1)}{2}} \left(\frac{4V_d}{n\pi}\right) \left[\begin{array}{l} J_o\left(\frac{m_a n\pi}{2}\right)\cos n\omega_t t + \sum_{k=2,4}^{\infty} J_k\left(\frac{m_a n\pi}{2}\right) \\ \times\left[\cos((n\omega_t + k\omega_m)t + k\phi) + \cos((n\omega_t - k\omega_m)t + k\phi)\right] \end{array} \right] \\ & + \sum_{n=2,4\cdots}^{\infty} (-1)^{\frac{n}{2}} \left(\frac{4V_d}{n\pi}\right) \sum_{k=1,3}^{\infty} J_k\left(\frac{m_a n\pi}{2}\right) \left[\sin((n\omega_t + k\omega_m)t + k\phi) - \sin((n\omega_t - k\omega_m)t + k\phi) \right] \end{aligned} \tag{2.22}$$

The first term in Equation 2.22 is the dc component of the output voltage. The second expresses the harmonic components of even terms of the signal. The third and fourth terms give the sideband components when n is an odd number and an even number, respectively.

The relationship between fundamental input and output voltage in the overmodulating region is given as [25]

$$V_o = MV_d \tag{2.23}$$

where

$$M = \frac{2m_a}{\pi}\left(\sin^{-1}\alpha + \alpha\sqrt{1-\alpha^2}\right) \quad , \; m_a > 1$$

$$\alpha = 1/m_a \; .$$

2.2.2.2 PWM with unipolar voltage switching. In this scheme, the diagonally opposite transistors (T_{A+}, T_{B-}) and (T_{A-}, T_{B+}) form the two legs of the full-bridge inverter Figure 2.4 and are not switched simultaneously. The legs A and B of the full-bridge are controlled by comparing triangular signal, $v_{t.}$ with control signal, v_m and -v_m, respectively. This is illustrated in Figure 2.8.

The comparison of v_m and v_t provides logic signals to control the switches in leg A:

$$v_m > v_t : T_{A+} \; on \quad and \quad v_{AN} = V_d$$

and (2.24)

$$v_m < v_t : T_{A-} \; on \quad and \quad v_{AN} = 0 \; .$$

The output of the inverter leg A and leg B with respect to the negative dc bus N is shown in Figures 2.8b and 2.8c respectively. For controlling the leg B transistors, (-v_m) is compared with the same triangular waveform, yielding the following:

$$-v_m > v_t : T_{B+} \; on \quad and \quad v_{BN} = V_d$$

and (2.25)

$$v_m < v_t : T_{B-} \; on \quad and \quad v_{BN} = 0 \; .$$

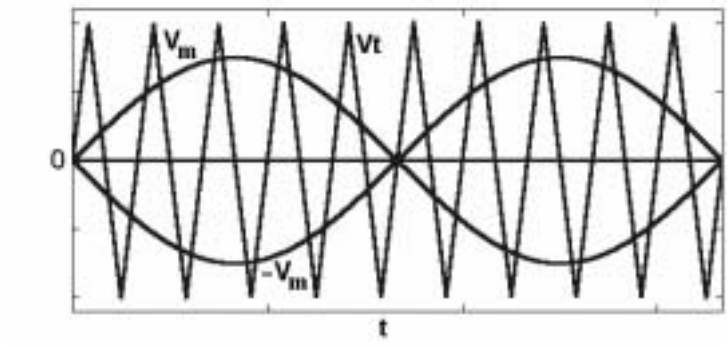

(a)

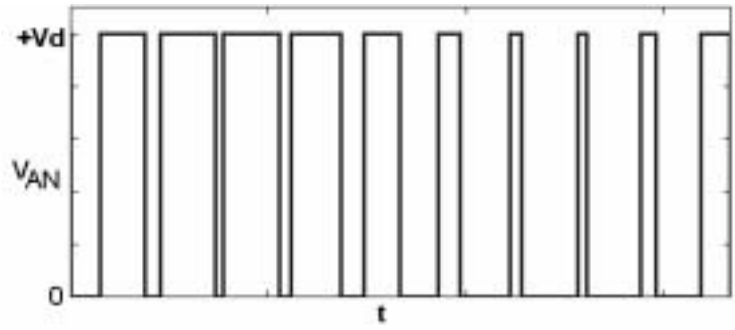

(b)

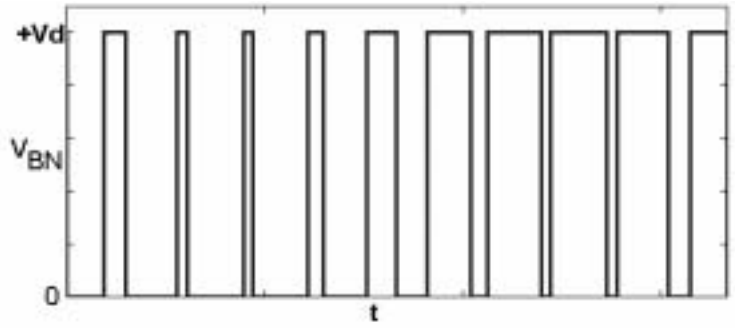

(c)

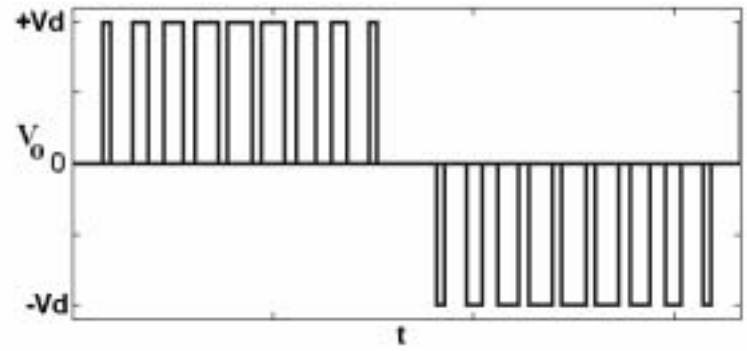

(d)

Figure 2.8. Single-Phase PWM with unipolar voltage switching. (a) Generation Method, (b) leg A output voltage, (c) leg B output voltage, (d) inverter output voltage.

Table 2.1. Switching state of the unipolar PWM and the corresponding voltage levels.

T_{A+}	T_{A-}	T_{B+}	T_{B-}	v_{AN}	v_{BN}	V_o
ON	-	-	ON	V_d	0	V_d
-	ON	ON	-	0	V_d	$-V_d$
ON	-	ON	-	V_d	V_d	0
-	ON	-	ON	0	0	0

Table 2.1 shows the switching state of the unipolar PWM and the corresponding voltage levels. It should be noticed that when both the upper switches are on, the output voltage is zero. The output current circulates in a loop through (T_{A+} and D_{B+}) or (D_{A+} and T_{B+}) depending on the direction of inverter output current, i_o. During this interval, the inverter input current i_d is zero. A similar condition occurs when both bottom switches T_{A-} and T_{B-} are on.

In this type of PWM scheme, when a switching occurs, the output voltage changes between 0 and $+V_d$ or between 0 and $-V_d$ voltage levels. For this reason, this type of PWM scheme is called the pulse width modulation with a unipolar voltage switching, as opposed to the PWM with bipolar (between $+V_d$ and $-V_d$). This scheme has the advantage of "effectively" doubling the switching frequency as far as the output harmonics are concerned, compared to the bipolar-voltage switching scheme. Also the voltage jumps in the output at each switching are reduced to V_d, as compared to $2V_d$ in the bipolar scheme.

2.2.2.3 Modified PWM bipolar voltage switching scheme. In this scheme, the diagonally opposite transistors (T_{A+}, T_{B-}) and (T_{A-}, T_{B+}) form the two legs of the full

bridge inverter Figure 2.4 and are not switched simultaneously. The output voltage is determined by comparing the control signal, v_m, and the triangular signal, v_t. This is illustrated in Figure 2.9a. The switching pattern for positive values of modulating signal, v_m is as follows

$$v_m > v_t, \quad T_{A+} \text{ is on } \Rightarrow \quad v_{AN} = V_d$$

$$\text{and} \quad v_m < v_t, \quad T_{A-} \text{ is on } \Rightarrow \quad v_{AN} = 0. \tag{2.26}$$

The switching pattern for negative values of modulating signal, v_m is given as

$$v_m < v_t, \quad T_{B+} \text{ is on } \Rightarrow \quad v_{BN} = V_d$$

$$\text{and} \quad v_m > v_t, \quad T_{B-} \text{ is on } \Rightarrow \quad v_{BN} = 0. \tag{2.27}$$

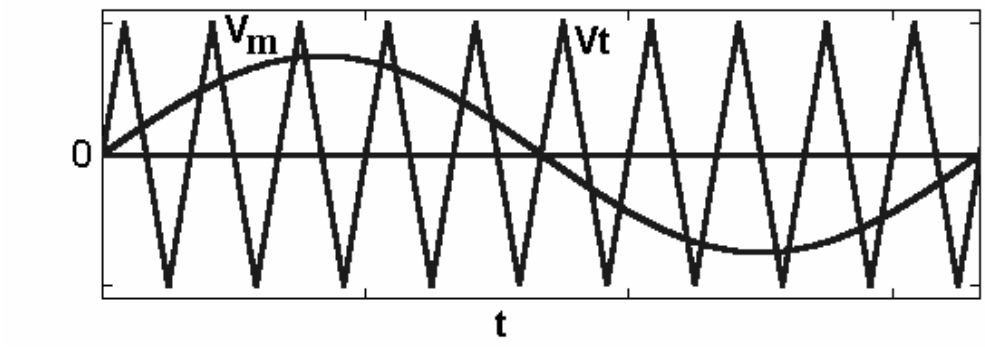

(a)

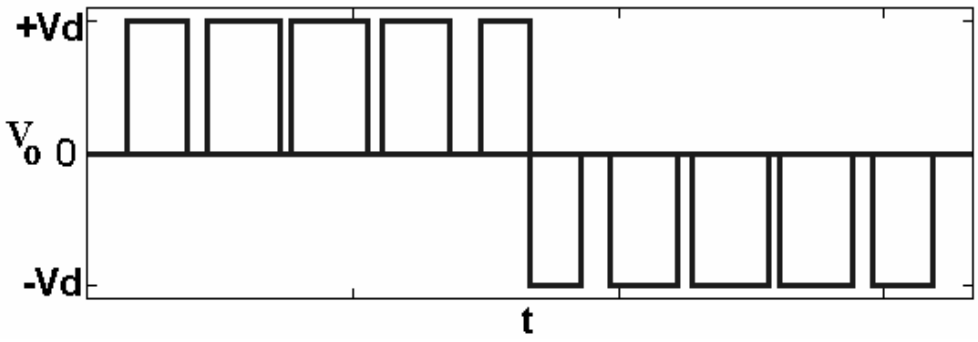

(b)

Figure 2.9. PWM with modified bipolar voltage switching. (a) Generation Method, (b) inverter output voltage.

The output voltage can then be expressed as shown in Equation 2.28 with a waveform shown in Figure 2.9b.

$$v_o(t) = v_{AN}(t) - v_{BN}(t) \tag{2.28}$$

Table 2.2 shows the switching state of the modified bipolar PWM and the corresponding voltage levels. It should be noticed that when both the upper switches are on, the output voltage is zero. The output current circulates in a loop through (T_{A+} and D_{B+}) or (D_{A+} and T_{B+}) depending on the direction of inverter output current, i_o. During this interval, the inverter input current i_d is zero. A similar condition occurs when both bottom switches T_{A-} and T_{B-} are on. In the modified bipolar PWM scheme, when a switching occurs, the output voltage changes between 0 and $+V_d$ or between 0 and $-V_d$ voltage levels.

Table 2.2. Switching state of the modified bipolar PWM and the corresponding voltage levels.

T_{A+}	T_{A-}	T_{B+}	T_{B-}	v_{AN}	v_{BN}	V_o
ON	-	-	ON	V_d	0	V_d
-	ON	ON	-	0	V_d	$-V_d$
ON	-	ON	-	V_d	V_d	0
-	ON	-	ON	0	0	0

In Figure 2.9, the output voltage v_o produced by the modulating signal, v_m and the carrier signal, v_t can be expressed by a complex double Fourier series. The output voltage in Figure 2.9 is determined using the phase relationship between the modulating and carrier signal shown in Figure 2.10 and 2.11. The peak value and angular frequency of

the carrier signal are 1 and ω_t, respectively. The modulating signal is expressed as $v_o = m_a \sin(\omega_m t + \phi)$, where ω_m is the angular frequency of the modulating signal.

The output voltage of Figure 2.9 can be expressed by complex double Fourier series as follow [33, 34]:

$$v_o = \sum_{k=-\infty}^{\infty} \sum_{n=-\infty}^{\infty} K_{kn} \exp\left(j\{kx + ny\}\right) \tag{2.29}$$

where $x = \omega_m t + \phi$ and $y = \omega_t t$. Equation 2.29 expressing the frequency spectrum of the PWM waveform comprises the angular frequencies of n (integer) times ω_t and the sideband waves arranged at intervals of the angular frequencies of k (integer) times ω_m in frequencies above and below them in high frequencies.

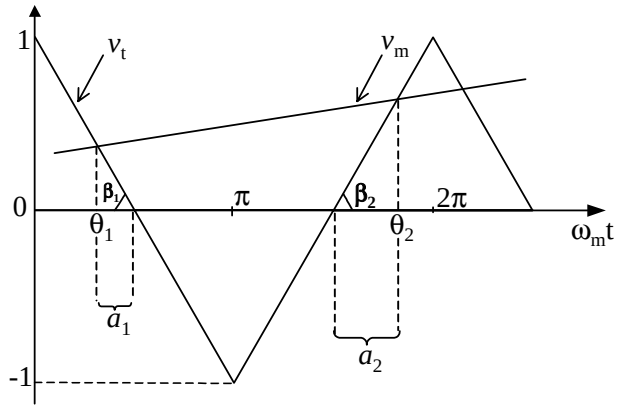

(a) Modulating and carrier signal waveforms, $0 \le \omega_m t + \phi < \pi$.

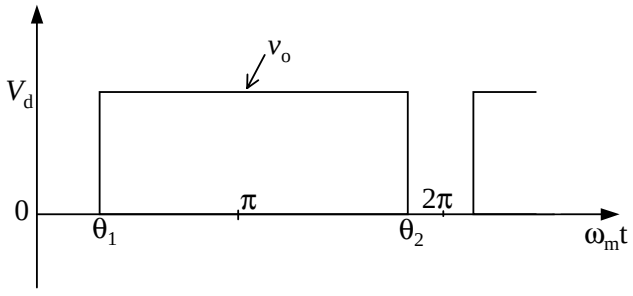

(b) Inverter output voltage, $0 \le \omega_m t + \phi < \pi$.

Figure 2.10. Phase relationship of output voltage to modulating and carrier signals for modified bipolar voltage scheme. Condition, $0 \le \omega_m t + \phi < \pi$.

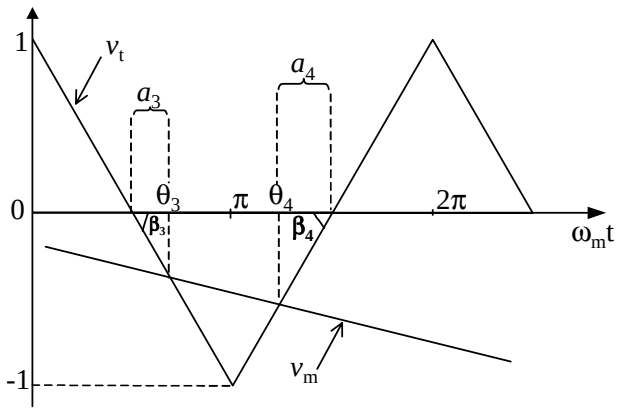

(a) Modulating and carrier signal waveforms, $\pi \le \omega_m t + \phi < 2\pi$.

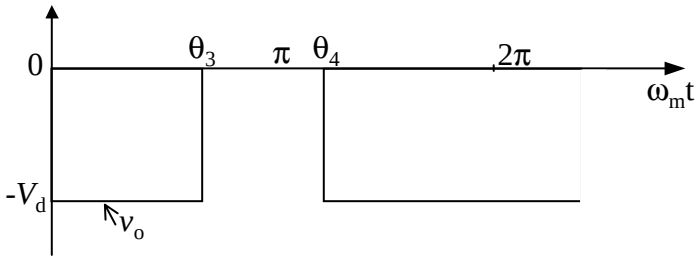

(b) Inverter output voltage, $\pi \le \omega_m t + \phi < 2\pi$.

Figure 2.11. Phase relationship of output voltage to modulating and carrier signals for modified bipolar voltage scheme. Condition, $\pi \le \omega_m t + \phi < 2\pi$.

The complex Fourier coefficient K_{kn} can be expressed as follows:

$$K_{kn} = \frac{V_d}{4\pi^2}\left\{\int_0^{\pi} e^{-jkx}\left(\int_{\theta_1}^{\theta_2} e^{-jny}dy\right)dx - \int_{\pi}^{2\pi} e^{-jkx}\left(\int_0^{\theta_3} e^{-jny}dy + \int_{\theta_4}^{2\pi} e^{-jny}dy\right)dx\right\} \qquad (2.30)$$

where , $k = 0, \pm 1, \pm 2, \ldots$ and $n = 0, \pm 1, \pm 2, \ldots$.

Angles θ_1 and θ_2 are the intersection points of v_m and v_t when the modulating signal $v_m = m_a \sin(\omega_m t + \phi)$ is greater than zero; and angles θ_3 and θ_4 are the intersection points of v_m and v_t when modulating signal $v_m = m_a \sin(\omega_m t + \phi)$ is less than zero. The angle θ_1 can be determined as

$$\theta_1 + a_1 = \frac{\pi}{2}, \qquad \Rightarrow \theta_1 = \frac{\pi}{2} - a_1$$

$$\tan\beta_1 = \frac{1}{\pi/2}, \qquad \text{also} \quad \tan\beta_1 = \frac{m_a \sin x}{a_1}$$

$$\therefore \quad \frac{m_a \sin x}{a_1} = \frac{1}{\pi/2}, \qquad \Rightarrow a_1 = \frac{\pi}{2} m_a \sin x$$

Hence

$$\theta_1 = \frac{\pi}{2}\left(1 - m_a \sin x\right). \tag{2.31a}$$

Similarly, θ_2, θ_3, and θ_4 are determined; their values are given as

$$\theta_2 = \frac{\pi}{2}\left(3 + m_a \sin x\right)$$

$$\theta_3 = \frac{\pi}{2}\left(1 - m_a \sin x\right) \tag{2.31b}$$

$$\theta_4 = \frac{\pi}{2}\left(3 + m_a \sin x\right)$$

Equation 2.29 will now be separated into its respective frequency components.

(i) dc component. The dc component is determined by setting k = n = 0 in Equation 2.29. This result in $K_{00} = 0$ from Equation 2.30.

(ii) n = 0 components. From Equation 2.29, K_{k0} is determined by letting n = 0:

$$K_{k0} = \frac{V_d}{4\pi^2}\left\{\int_0^{\pi} e^{-jkx}\left(\theta_2 - \theta_1\right)dx - \int_{\pi}^{2\pi} e^{-jkx}\left(\theta_3 + 2\pi - \theta_4\right)dx\right\} \tag{2.32}$$

But

$$\theta_2 - \theta_1 = \pi\left(1 + m_a \sin x\right) \tag{2.33a}$$

$$\theta_3 + 2\pi - \theta_4 = \pi\left(1 - m_a \sin x\right) \tag{2.33b}$$

from Equations 2.31a and 231b, then Equation 2.32 becomes

$$K_{k0} = \frac{V_d}{4\pi^2}\left\{\int_0^{\pi} e^{-jkx}\left(\pi(1+m_a\ sin\ x)\right)dx - \int_{\pi}^{2\pi} e^{-jkx}\left(\pi(1-m_a\ sin\ x)\right)dx\right\} \qquad (2.34)$$

where

$$\int_0^{2\pi} e^{-jkx}\left(m_a\ sin\ x\right)dx = \begin{cases} -\ jm_a\pi & (k=1) \\ 0 & (k\neq 1) \end{cases} \qquad (2.35a)$$

$$\int_0^{\pi} e^{-jkx}\ dx - \int_{\pi}^{2\pi} e^{-jkx}dx = \begin{cases} -\ j\dfrac{4}{k} & (k:\text{odd number}) \\ 0 & (k:\text{even number}) \end{cases} \qquad (2.35b)$$

$$K_{ko} = \begin{cases} -\ jV_d\left(\dfrac{1}{\pi}+\dfrac{m_a}{4}\right) & (k=1) \\ -\ j\left(\dfrac{V_d}{\pi k}\right) & (k:\text{odd number}) \\ 0 & (k:\text{even number}) \end{cases} \qquad (2.36)$$

The output voltage for the harmonic component, v_{ko} can be obtained by substituting Equation 2.34 into Equation 2.29. The output voltage by performing real Fourier Expansion is given as (Appendix C)

$$v_{ko} = K_{k0}\exp\left(j\{kx+0\}\right)$$

$$v_{ko} = \begin{cases} MV_d\ sin\ x & (k=1) \\ \dfrac{2V_d}{k\pi}\ sin\ kx & (k=3,5,7\cdots) \end{cases} \qquad (2.37)$$

where

$$M = \left(\frac{2}{\pi}+\frac{m_a}{2}\right)$$

In Equation 2.37, the components of k = 1, 3, 5, … express the fundamental signal and the third and fifth harmonic components, and so on.

(iii) k, n components. Rearranging Equation 2.30 yields

$$K_{kn} = \frac{V_d}{4\pi^2}\left\{\int_0^{2\pi} e^{-jkx}\left(\int_{\theta_1}^{\theta_2} e^{-jny}dy\right)dx\right\}$$

$$K_{kn} = \frac{V_d}{j4\pi^2 n}\left\{\int_0^{2\pi} e^{-jkx}\left(e^{-jn\theta_1} - e^{-jn\theta_2}\right)dx\right\} \tag{2.38}$$

Substituting Equations 2.31a and 2.31b, into Equation 2.38, result in

$$K_{kn} = \frac{V_d}{j4\pi^2 n}\left\{\int_0^{2\pi} e^{-jkx}\left(e^{-\frac{1}{2}jn\pi} e^{\frac{1}{2}jn\pi m_a \sin x} - e^{-\frac{3}{2}jn\pi} e^{-\frac{1}{2}jn\pi m_a \sin x}\right)dx\right\} \tag{2.39}$$

The value of K_{kn} from Equation 2.39 when n is an even number is given as

$$K_{kn} = (-1)^{\frac{n}{2}} \frac{V_d}{j4\pi^2 n}\left\{\int_0^{2\pi} e^{-jkx}\left(e^{\frac{1}{2}jn\pi m_a \sin x} - e^{-\frac{1}{2}jn\pi m_a \sin x}\right)dx\right\} \tag{2.40}$$

$$K_{kn} = \begin{cases} (-1)^{\frac{n}{2}} \dfrac{V_d}{j\pi n} J_k\left(\dfrac{m_a n\pi}{2}\right) & (k : \text{odd number}) \\ 0 & (k : \text{even number}) \end{cases} \tag{2.41}$$

where

$$J_k\left(\frac{m_a n\pi}{2}\right) = \frac{1}{\pi}\int_0^{\pi} \sin kx \sin\left(\frac{m_a n\pi}{2}\sin x\right)dx$$

The J_k is the kth-order Bessel function of the first kind. $J_k\left(\dfrac{m_a n\pi}{2}\right)$ is a function whose value will become small as k increases.

The value of K_{kn} from Equation 2.39 when n is an odd number is given as

$$K_{kn} = (-1)^{\frac{(n+1)}{2}} \frac{V_d}{4\pi^2 n}\left\{\int_0^{2\pi} e^{-jkx}\left(e^{\frac{1}{2}jn\pi m_a \sin x} + e^{-\frac{1}{2}jn\pi m_a \sin x}\right)dx\right\} \tag{2.42}$$

$$K_{kn} = \begin{cases} (-1)^{\frac{(n+1)}{2}} \dfrac{V_d}{\pi n} J_k\left(\dfrac{m_a n\pi}{2}\right) & (k : \text{odd number}) \\ 0 & (k : \text{even number}) \end{cases} \tag{2.43}$$

where

$$J_k\left(\frac{m_a n\pi}{2}\right) = \frac{1}{\pi}\int_0^{\pi} \cos kx \cos\left(\frac{m_a n\pi}{2} \sin x\right) dx$$

The output voltage, v_o in Equation 2.29 can be expressed as

$$\begin{aligned} v_o = {} & MV_d \sin(\omega_m t + \phi) + \sum_{k=3,5\cdots}^{\infty} \left(\frac{2V_d}{k\pi}\right) \sin(k\omega_m t + k\phi) \\ & + \sum_{n=1,3\cdots}^{\infty} (-1)^{\frac{(n+1)}{2}} \left(\frac{2V_d}{n\pi}\right) \left[\begin{array}{l} J_o\left(\dfrac{m_a n\pi}{2}\right) \cos n\omega_t t + \sum\limits_{k=2,4}^{\infty} J_k\left(\dfrac{m_a n\pi}{2}\right) \\ \times \left[\cos((n\omega_t + k\omega_m)t + k\phi) + \cos((n\omega_t - k\omega_m)t + k\phi)\right] \end{array} \right] \\ & + \sum_{n=2,4\cdots}^{\infty} (-1)^{\frac{n}{2}} \left(\frac{2V_d}{n\pi}\right) \sum_{k=1,3}^{\infty} J_k\left(\frac{m_a n\pi}{2}\right) \left[\sin((n\omega_t + k\omega_m)t + k\phi) - \sin((n\omega_t - k\omega_m)t + k\phi) \right] \end{aligned} \tag{2.44}$$

The first term in Equation 2.44 is the fundamental component of the output voltage. The second term expresses the harmonic components of odd term of the fundamental signal and is a term not related to the modulation index. The third and fourth terms give the sideband components when n is an odd number and an even number, respectively.

The relationship between fundamental input and output voltage given as

$$V_o = MV_d \tag{2.45}$$

where

$$M = 0.5 \times \left(m_a + \frac{4}{\pi}\right) \qquad , m_a \le 1.$$

2.3 Design, Implementation, and Operation of Bipolar Voltage Switching Scheme for Single-Phase PWM Inverter

The single-phase PWM inverter can be switched with different voltage switching schemes as discussed. Basically, the transistor used in the single-phase inverter has to be driven into the saturation region to act as a switch. The base signal used in driving the transistor is obtained from SEMIKRON, SEMIDRIVER SKHI 60 (Medium Power Six IGBT and MOSFET Driver). The base driver has the following features [26]: CMOS compatible inputs, interlock circuit, short circuit monitoring and switch off, supply undervoltage monitoring Vs < 13 V, isolation of primary from secondary by pulse transformer, error latch and monitoring output signal, and internal isolated power supply.

The supply to base drive board is +15 V. The input into the base driver (4 of 6) is obtained with operational amplifier and resistors. The pulse width modulation is obtained, as mentioned earlier by comparing a carrier signal with a modulating signal. The PWM can be obtained by using op amp (operational amplifier). The pulse modulating signal is achieved by driving the op amp in the saturated region.

From the theory in section 2.2.2.1, the PWM bipolar-voltage switching method is explained. The PWM with bipolar voltage switch scheme is obtained with operational amplifier. The operational amplifier was configured as a comparator as shown in Figure 2.12. The comparator circuit compares a signal voltage on one input of an op amp with known voltage called reference voltage on the other input. Its output may be (+) or (-) saturation voltage, depending on which input is larger. Figure 2.13 shows the dual low noise JFET input op-amp used (ECG 858M). In achieving the bipolar voltage switching

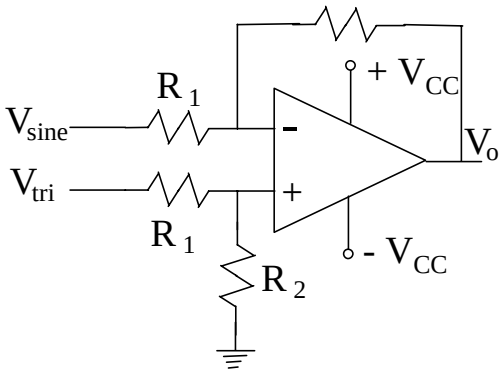

Figure 2.12. Inverting comparator.

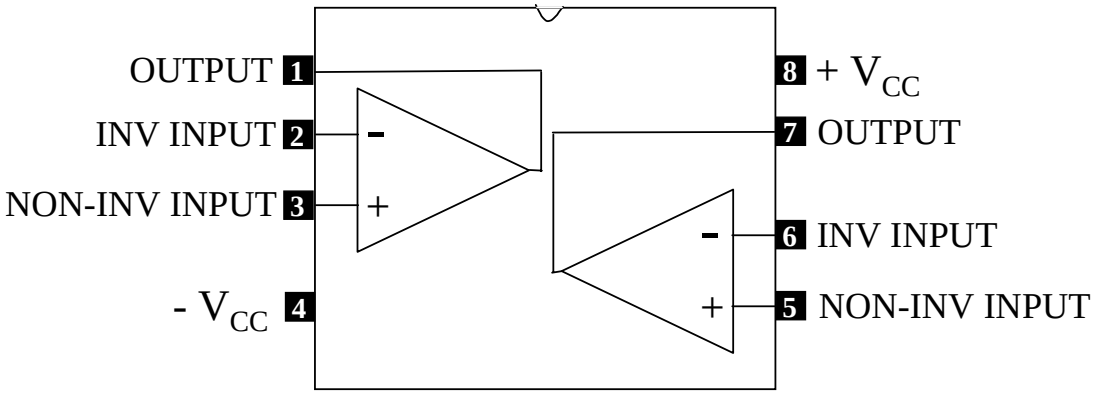

Figure 2.13. Block diagram of ECG 858M (dual op-amp).

scheme, the transistors T_{A+} (TOP 1) and T_{B-} (BOT 2) are turned on from the output of Figure 2.14.

The fixed reference voltage (triangular waveform) of 8 V peak to peak is applied to the (+) input, and the modulating signal (sinusoidal waveform, 0V - 20V) is applied to the (-) input. The circuit arrangement of Figure 2.14 is called the inverting comparator. When V_{sine} is greater than V_{tri}, the output voltage V_o is at -15V because the voltage at the (+) input is lesser than that at the (-) input. On the other hand, when V_{sine} is less than V_{tri}, the (-) input becomes negative with respect to the (+) input, and V_o goes to +15V. Hence V_o changes from one saturation level to another whenever $V_{sine} > V_{tri}$ or $V_{sine} < V_{tri}$.

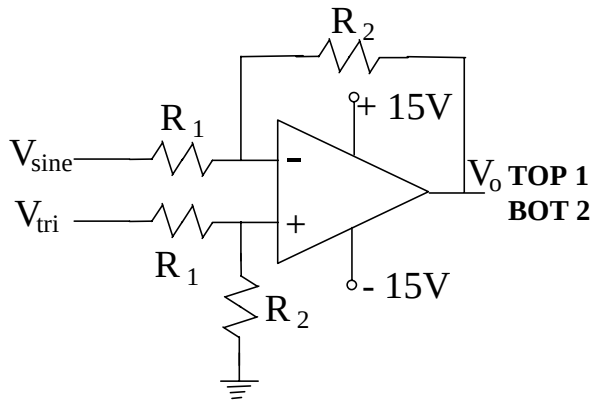

Figure 2.14. Inverting comparator circuit.

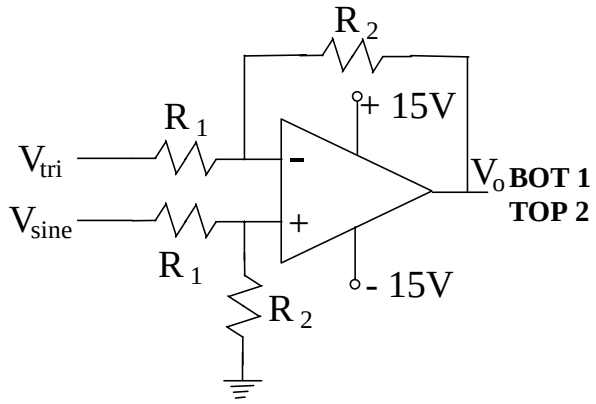

Figure 2.15. Non-inverting comparator circuit.

The other set of transistors T_{A-} (BOT 1) and T_{B+} (TOP 2) are switched using Figure 2.15. This is done using the bipolar voltage-switching scheme also. The fixed reference voltage (triangular waveform) of 8 V peak to peak is applied to the (-) input, and the modulating signal (sinusoidal waveform, 0V - 20V) is applied to the (+) input. When V_{sine} is less than V_{tri}, the output voltage V_o is at -15V because the voltage at the (-) input is higher than that at the (+) input. Conversely, when V_{sine} is greater than V_{tri}, the (+) input becomes positive with respect to the (-) input, and V_o goes to +15V. Hence V_o changes from one saturation level to another whenever $V_{sine} > V_{tri}$ or $V_{sine} < V_{tri}$.

The H-bridge inverter shown in Figure 2.4 is implemented using two sets of insulated gate bipolar transistor (IGBT). Each set of the international rectifiers (IRGTI050U06) is a half-bridge that consists of two transistors. The choice of IGBT for this power application was based on the facts that it has the following features [5]: rugged design, simple gate-drive, ultra-fast operation up to 25KHz hard switching or 100KHz resonant, and switching-loss rating. The outputs from the base drive were connected appropriately to the collector, emitter, and gate of the IGBT. The interlock circuit on the base driver ensures the IGBTs from the same leg do not turn on simultaneously.

CHAPTER 3

MODEL OF A SINGLE-PHASE INDUCTION MOTOR

3.1 Introduction

In this chapter, the development of the model of a single-phase induction motor is examined. First, the derivation of the single-phase induction motor (SPIM) equation is carried out. In simplifying the SPIM state-variables equations, two sets of transformation are used: the stationary reference frame and the turn ratio transformation. Next, a brief discussion of the theory of harmonic balance technique is set forth.

The harmonic balance technique is then used to develop a steady-state model for the SPIM. The parameters of the SPIM are determined with the resulting steady-state equation.

3.2 Derivation of Single-Phase Induction Motor Equation

A schematic cross section of a single-phase induction machine model is shown in Figure 3.1. The stator or main windings are nonidentical sinusoidally distributed windings arranged in space quadrature. The *as* winding is assumed to have N_q equivalent turns with resistance r_a. The auxiliary *bs* winding has N_d equivalent turns with resistance r_b. The rotor windings may be considered as two identical sinusoidally distributed windings

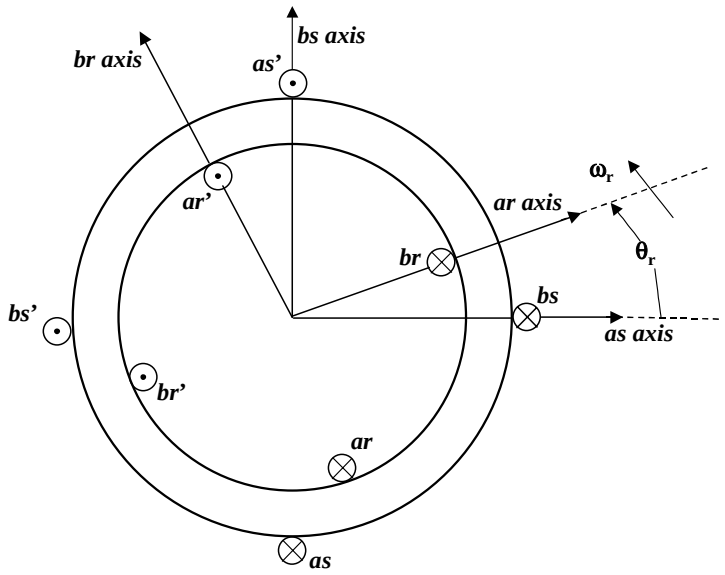

Figure 3.1. Cross-sectional view of a single-phase induction machine.

arranged in space quadrature. Each rotor winding has N_r equivalent turns with resistance r_r.

The stator and rotor voltage Equations of SPIM are given as

$$v_{as} = r_a i_{as} + p\lambda_{as} \tag{3.1}$$

$$v_{bs} = r_b i_{bs} + p\lambda_{bs} \tag{3.2}$$

$$v_{ar} = r_r i_{ar} + p\lambda_{ar} \tag{3.3}$$

$$v_{br} = r_r i_{br} + p\lambda_{br} \tag{3.4}$$

where r_a, r_b, and r_r are the resistances of the a-phase stator winding, b-phase stator winding, and rotor winding, respectively. The p denotes differentiation with respect to time. The stator and rotor flux linkage equations are

$$\begin{bmatrix} \lambda_{abs} \\ \lambda_{abr} \end{bmatrix} = \begin{bmatrix} L_s & L_{sr} \\ (L_{sr})^T & L_r \end{bmatrix} \begin{bmatrix} i_{abs} \\ i_{abr} \end{bmatrix} \tag{3.5}$$

where

$$\mathrm{L}_s = \begin{bmatrix} L_{asas} & L_{asbs} \\ L_{bsas} & L_{bsbs} \end{bmatrix} + \begin{bmatrix} L_{las} & 0 \\ 0 & L_{lbs} \end{bmatrix} \tag{3.6}$$

$$\mathrm{L}_r = \begin{bmatrix} L_{arar} & L_{arbr} \\ L_{brar} & L_{brbr} \end{bmatrix} + \begin{bmatrix} L_{lr} & 0 \\ 0 & L_{lr} \end{bmatrix} \tag{3.7}$$

$$\mathrm{L}_{sr} = \begin{bmatrix} L_{asar} & L_{asbr} \\ L_{bsar} & L_{bsbr} \end{bmatrix} \tag{3.8}$$

where L_s is the self-inductance for the stator winding, L_r is the self-inductance for the rotor, and L_{sr} is the mutual inductance.

Winding function principles [28] can be used in determining the self- and mutual inductance matrix in Equations 3.6 - 3.8. The inductance between any windings “i” and “j” in any machine is expressed as

$$L_{ij} = \frac{\mu_o r l}{g} \int_0^{2\pi} N_i(\phi) N_j(\phi) d\phi \ . \tag{3.9}$$

The average air-gap radius is r, the effective motor stack length is l, and the gap length is represented by g. The angle ϕ defines the angular position along the stator inner diameter, while the angular position of the rotor with respect to the stator reference frame is ϕ_r. The winding functions of windings “i” and “j” are given, respectively, as N_i (ϕ) and N_j (ϕ). In order to obtain closed-form inductance equations, the winding functions are represented by their respective fundamental components despite that the winding functions contain significant space harmonic components.

The fundamental component of the winding functions for the stator windings are given in Equation 3.10. The fundamental component of the winding functions for the rotor windings is given in Equation 3.11.

$$N_{as} = N_A \cos(\phi), \qquad N_{bs} = N_B \sin(\phi) \tag{3.10}$$

$$N_{ar} = N_r \cos(\phi - \phi_r), \qquad N_{br} = N_r \sin(\phi - \phi_r) \tag{3.11}$$

The self- and mutual inductances can be found using Equation 3.9-3.11. This results in the following inductances.

$$L_{asas} = \frac{\mu_o r l}{g} \int_0^{2\pi} (N_A \cos(\phi))^2 d\phi = \frac{\mu_o r l}{g} \pi N_A^2 \tag{3.12}$$

$$L_{asbs} = \frac{\mu_o r l}{g} \int_0^{2\pi} N_A \cos(\phi) \times N_B \sin(\phi) d\phi = 0 \tag{3.13}$$

$$L_{bsas} = \frac{\mu_o r l}{g} \int_0^{2\pi} N_B \sin(\phi) \times N_A \cos(\phi) d\phi = 0 \tag{3.14}$$

$$L_{bsbs} = \frac{\mu_o r l}{g} \int_0^{2\pi} (N_B \sin(\phi))^2 d\phi = \frac{\mu_o r l}{g} \pi N_B^2 \tag{3.15}$$

$$L_{arar} = \frac{\mu_o r l}{g} \int_0^{2\pi} (N_r \cos(\phi - \phi_r))^2 d\phi = \frac{\mu_o r l}{g} \pi N_r^2 \tag{3.16}$$

$$L_{arbr} = \frac{\mu_o r l}{g} \int_0^{2\pi} N_r \cos(\phi - \phi_r) \times N_r \sin(\phi - \phi_r) d\phi = 0 \tag{3.17}$$

$$L_{brar} = \frac{\mu_o r l}{g} \int_0^{2\pi} N_r \sin(\phi - \phi_r) \times N_r \cos(\phi - \phi_r) d\phi = 0 \tag{3.18}$$

$$L_{brbr} = \frac{\mu_o r l}{g} \int_0^{2\pi} (N_r \sin(\phi - \phi_r))^2 d\phi = \frac{\mu_o r l}{g} \pi N_r^2 \tag{3.19}$$

$$L_{asar} = \frac{\mu_o r l}{g} \int_0^{2\pi} N_A \cos(\phi) \times N_r \cos(\phi - \phi_r) d\phi = \frac{\mu_o r l}{g} \pi N_A N_r \cos(\phi_r) \tag{3.20}$$

$$L_{asbr} = \frac{\mu_o r l}{g} \int_0^{2\pi} N_A \cos(\phi) \times N_r \sin(\phi - \phi_r) d\phi = -\frac{\mu_o r l}{g} \pi N_A N_r \sin(\phi_r) \tag{3.21}$$

$$L_{bsar} = \frac{\mu_o r l}{g} \int_0^{2\pi} N_B \sin(\phi) \times N_r \cos(\phi - \phi_r) d\phi = \frac{\mu_o r l}{g} \pi N_B N_r \sin(\phi_r) \tag{3.22}$$

$$L_{bsbr} = \frac{\mu_o rl}{g}\int_0^{2\pi} N_B\, sin(\phi) \times N_r\, sin(\phi - \phi_r)d\phi = \frac{\mu_o rl}{g}\pi N_B N_r\, cos(\phi_r) \qquad (3.23)$$

Equations 3.6 - 3.8 become

$$\mathrm{L}_s = \begin{bmatrix} L_{las} + L_{ma} & 0 \\ 0 & L_{lbs} + L_{mb} \end{bmatrix} = \mathrm{k} \times \begin{bmatrix} N_A^2 & 0 \\ 0 & N_B^2 \end{bmatrix} + \begin{bmatrix} L_{las} & 0 \\ 0 & L_{lbs} \end{bmatrix} \qquad (3.24)$$

$$\mathrm{L}_r = \begin{bmatrix} L_{lr} + L_{mr} & 0 \\ 0 & L_{lr} + L_{mr} \end{bmatrix} = \mathrm{k} \times \begin{bmatrix} N_r^2 & 0 \\ 0 & N_r^2 \end{bmatrix} + \begin{bmatrix} L_{lr} & 0 \\ 0 & L_{lr} \end{bmatrix} \qquad (3.25)$$

$$\mathrm{L}_{sr} = \begin{bmatrix} L_{asar} & L_{asbr} \\ L_{bsar} & L_{bsbr} \end{bmatrix} = \mathrm{k} \times \begin{bmatrix} N_A N_r\, cos(\phi_r) & -N_A N_r\, sin(\phi_r) \\ N_B N_r\, sin(\phi_r) & N_B N_r\, cos(\phi_r) \end{bmatrix} \qquad (3.26)$$

where $\mathrm{k} = \frac{\mu_o rl}{g}\pi$.

In Equations 3.24 and 3.25, the leakage inductances of the a-phase and b-phase stator windings are L_{las} and $L_{lbs,}$ respectively, while those of the rotor windings is L_{lr}.

3.2.1 Reference Frame Transformations and Turn Transformations

The transformation of stator variables to the arbitrary reference frame, the transformation of stator variables between reference frames, and the transformation of rotor variables to the arbitrary reference frame are necessary in simplifying the SPIM voltage equation. In vector notation, the stator variables are represented as

$$\mathrm{f}_{abs} = \begin{bmatrix} \mathrm{f}_{as} \\ \mathrm{f}_{bs} \end{bmatrix} \qquad (3.27)$$

where f may be a voltage (v), current (i), or flux linkages (λ). If θ is the angular position of an arbitrary reference frame then the transformation of the stator variables to arbitrary reference frame is [29,30]

$$f_{qds} = K_{2s} f_{abs}, \qquad f_{abs} = (K_{2s})^{-1} f_{qds} \tag{3.28}$$

where

$$f_{qds} = \begin{bmatrix} f_{qs} \\ f_{ds} \end{bmatrix} \tag{3.29}$$

and

$$K_{2s} = \begin{bmatrix} cos\theta & sin\theta \\ sin\theta & -cos\theta \end{bmatrix}, \qquad (K_{2s})^{-1} = \begin{bmatrix} cos\theta & sin\theta \\ sin\theta & -cos\theta \end{bmatrix}. \tag{3.30}$$

Applying Equation 3.28 and 3.30 to Equation 3.1 and 3.2,

$$K_{2s} V_{abs} = K_{2s} r_{ab} I_{abs} + K_{2s} p\lambda_{abs} \tag{3.31}$$

where $r_{ab} = \begin{bmatrix} r_a & 0 \\ 0 & r_b \end{bmatrix}$

$$K_{2s} V_{abs} = K_{2s} r_{ab} (K_{2s})^{-1} I_{qds} + K_{2s} p(K_{2s})^{-1} \lambda_{qds} \quad . \tag{3.32}$$

Simplifying Equation 3.32,

$$\begin{bmatrix} v_{qs} \\ v_{ds} \end{bmatrix} = \begin{bmatrix} \frac{r_a + r_b}{2} + \frac{r_a - r_b}{2} cos 2\theta & \frac{r_a - r_b}{2} sin 2\theta \\ \frac{r_a - r_b}{2} sin 2\theta & \frac{r_a + r_b}{2} + \frac{r_b - r_a}{2} cos 2\theta \end{bmatrix} \begin{bmatrix} i_{qs} \\ i_{ds} \end{bmatrix} + \omega \begin{bmatrix} \lambda_{ds} \\ -\lambda_{qs} \end{bmatrix} + p \begin{bmatrix} \lambda_{qs} \\ -\lambda_{ds} \end{bmatrix} \tag{3.33}$$

where ω = pθ.

The stator voltage equation (3.33) is time-varying in view of the time-varying resistance. The equation can be simplified using the stationary reference frame, ω = 0 (θ = 0). With this transformation we can obtain constant parameters as

$$\begin{bmatrix} v_{qs} \\ v_{ds} \end{bmatrix} = \begin{bmatrix} r_a & 0 \\ 0 & r_b \end{bmatrix} \begin{bmatrix} i_{qs} \\ i_{ds} \end{bmatrix} + p \begin{bmatrix} \lambda_{qs} \\ -\lambda_{ds} \end{bmatrix} . \tag{3.34}$$

The rotor variables can be expressed in vector notation as

$$f_{abr} = \begin{bmatrix} f_{ar} \\ f_{br} \end{bmatrix}. \tag{3.35}$$

The transformation of rotor quantities to the arbitrary reference frame is

$$f_{qdr} = K_{2r} f_{abr}, \qquad f_{abr} = (K_{2r})^{-1} f_{qdr} \tag{3.36}$$

where

$$f_{qdr} = \begin{bmatrix} f_{qr} \\ f_{dr} \end{bmatrix} \tag{3.37}$$

and

$$K_{2r} = \begin{bmatrix} cos(\theta - \theta_r) & sin(\theta - \theta_r) \\ sin(\theta - \theta_r) & -cos(\theta - \theta_r) \end{bmatrix}, \qquad (K_{2r})^{-1} = \begin{bmatrix} cos(\theta - \theta_r) & sin(\theta - \theta_r) \\ sin(\theta - \theta_r) & -cos(\theta - \theta_r) \end{bmatrix}. \tag{3.38}$$

Applying Equations 3.28 and 3.30 to Equations 3.3 and 3.4,

$$K_{2r} V_{abr} = K_{2r} r_r I_{abr} + K_{2r} p \lambda_{abr} \tag{3.39}$$

$$K_{2r} V_{abr} = K_{2r} r_r (K_{2r})^{-1} I_{qdr} + K_{2r} p (K_{2r})^{-1} \lambda_{qdr} . \tag{3.40}$$

Simplifying Equation 3.40,

$$\begin{bmatrix} v_{qr} \\ v_{dr} \end{bmatrix} = r_r \begin{bmatrix} i_{qr} \\ i_{dr} \end{bmatrix} + (\omega - \omega_r) \begin{bmatrix} \lambda_{dr} \\ -\lambda_{qr} \end{bmatrix} + p \begin{bmatrix} \lambda_{qr} \\ -\lambda_{dr} \end{bmatrix} \tag{3.41}$$

where $\omega = p\theta$.

The rotor voltage Equation 3.41 using stationary reference frame, $\omega = 0$ becomes

$$\begin{bmatrix} v_{qr} \\ v_{dr} \end{bmatrix} = r_r \begin{bmatrix} i_{qr} \\ i_{dr} \end{bmatrix} - \omega_r \begin{bmatrix} \lambda_{dr} \\ -\lambda_{qr} \end{bmatrix} + p \begin{bmatrix} \lambda_{qr} \\ -\lambda_{dr} \end{bmatrix} . \tag{3.42}$$

The flux linkage Equation 3.5 is transformed to the stationary reference frame as follows

$$\begin{bmatrix}\lambda_{qds}\\ \lambda_{qdr}\end{bmatrix}=\begin{bmatrix}\mathrm{K}_{2s}\mathrm{L}_{s}(\mathrm{K}_{2s})^{-1} & \mathrm{K}_{2s}\mathrm{L}_{sr}(\mathrm{K}_{2r})^{-1}\\ \mathrm{K}_{2r}(\mathrm{L}_{sr})^{T}(\mathrm{K}_{2s})^{-1} & \mathrm{K}_{2r}\mathrm{L}_{r}(\mathrm{K}_{2r})^{-1}\end{bmatrix}\begin{bmatrix}\mathrm{i}_{abs}\\ \mathrm{i}_{abr}\end{bmatrix} \tag{3.43}$$

with θ(0) set equal to zero

$$\mathrm{K}_{2\mathrm{s}}=\begin{bmatrix}1 & 0\\ 0 & -1\end{bmatrix},\quad (\mathrm{K}_{2\mathrm{s}})^{-1}=\begin{bmatrix}1 & 0\\ 0 & -1\end{bmatrix}, \tag{3.44a}$$

$$\mathrm{K}_{2\mathrm{r}}=\begin{bmatrix}cos(-\theta_r) & sin(-\theta_r)\\ sin(-\theta_r) & -cos(-\theta_r)\end{bmatrix},\quad (\mathrm{K}_{2\mathrm{r}})^{-1}=\begin{bmatrix}cos(-\theta_r) & sin(-\theta_r)\\ sin(-\theta_r) & -cos(-\theta_r)\end{bmatrix}. \tag{3.44b}$$

Therefore,

$$\mathrm{K}_{2s}\mathrm{L}_{s}(\mathrm{K}_{2s})^{-1}=\mathrm{L}_{s} \tag{3.45}$$

$$\mathrm{K}_{2r}\mathrm{L}_{r}(\mathrm{K}_{2r})^{-1}=\mathrm{L}_{r} \tag{3.46}$$

$$\mathrm{K}_{2s}\mathrm{L}_{sr}(\mathrm{K}_{2r})^{-1}=\mathrm{K}_{2r}(\mathrm{L}_{sr})^{T}(\mathrm{K}_{2s})^{-1}=\mathrm{k}\times\begin{bmatrix}\mathrm{N}_{A}\mathrm{N}_{r} & 0\\ 0 & \mathrm{N}_{B}\mathrm{N}_{r}\end{bmatrix}. \tag{3.47}$$

Equation 3.43 reduces to

$$\begin{bmatrix}\lambda_{qds}\\ \lambda_{qdr}\end{bmatrix}=\begin{bmatrix}\mathrm{L}_{s} & \mathrm{L}_{12}\\ \mathrm{L}_{12} & \mathrm{L}_{r}\end{bmatrix}\begin{bmatrix}\mathrm{i}_{qds}\\ \mathrm{i}_{qdr}\end{bmatrix} \tag{3.48}$$

where

$$\mathrm{L}_{s}=\mathrm{k}\times\begin{bmatrix}N_{A}^{2} & 0\\ 0 & N_{B}^{2}\end{bmatrix}+\begin{bmatrix}L_{las} & 0\\ 0 & L_{lbs}\end{bmatrix}=\begin{bmatrix}L_{lqs}+L_{mq} & 0\\ 0 & L_{lds}+L_{md}\end{bmatrix} \tag{3.49a}$$

$$\mathrm{L}_{r}=\mathrm{k}\times\begin{bmatrix}N_{r}^{2} & 0\\ 0 & N_{r}^{2}\end{bmatrix}+\begin{bmatrix}L_{lr} & 0\\ 0 & L_{lr}\end{bmatrix}=\begin{bmatrix}L_{lqr}+L_{mr} & 0\\ 0 & L_{ldr}+L_{mr}\end{bmatrix} \tag{3.49b}$$

$$\mathrm{L}_{12}=\mathrm{k}\times\begin{bmatrix}\mathrm{N}_{A}\mathrm{N}_{r} & 0\\ 0 & \mathrm{N}_{B}\mathrm{N}_{r}\end{bmatrix}=\begin{bmatrix}L_{qr} & 0\\ 0 & L_{dr}\end{bmatrix}. \tag{3.49c}$$

In Equations 3.49a - 3.49b, the leakage inductances of the stator main and auxiliary windings are L_{lqs} and $L_{lds,}$ respectively, while those of the effective two mutually perpendicular rotor windings are L_{lqr} and L_{ldr}.

It is convenient to refer all *q* variables to the *as* winding with N_q effective turns and all d variables to the *bs* winding with N_d effective turns. If all the *q* variables are referred to the winding with N_q effective turns (*as* winding) and all *d* variables are referred to the winding with N_d effective turns (*bs* winding), the voltage equation becomes

$$v_{qs} = r_{qs} i_{qs} + p\lambda_{qs} \tag{3.50}$$

$$v_{ds} = r_{ds} i_{ds} + p\lambda_{ds} \tag{3.51}$$

$$v'_{qr} = r'_{qr} i'_{qr} - \frac{N_q}{N_d}\omega_r \lambda'_{dr} + p\lambda'_{qr} \tag{3.52}$$

$$v'_{dr} = r'_{dr} i'_{dr} + \frac{N_d}{N_q}\omega_r \lambda'_{qr} + p\lambda'_{dr} \tag{3.53}$$

where

$$\lambda_{qs} = L_{qs} i_{qs} + L_{mq} i_{qr} \tag{3.54}$$

$$\lambda_{ds} = L_{ds} i_{ds} + L_{md} i_{dr} \tag{3.55}$$

$$\lambda'_{qr} = L_{qr} i'_{qr} + L_{mq} i_{qs} \tag{3.56}$$

$$\lambda'_{dr} = L_{dr} i'_{dr} + L_{md} i_{ds} \tag{3.57}$$

where $L_{qs} = L_{lqs} + L_{mq}$, $L_{ds} = L_{lds} + L_{md}$, $L_{qr} = L_{lqr} + L_{mq}$ and $L_{dr} = L_{ldr} + L_{md}$. In which $v'_{qr} = \frac{N_q}{N_r} v_{qr}$, $i'_{qr} = \frac{N_r}{N_q} i_{qr}$, $v'_{dr} = \frac{N_d}{N_r} v_{dr}$, $i'_{dr} = \frac{N_r}{N_d} i_{dr}$, $r'_{qr} = \left(\frac{N_q}{N_r}\right)^2 r_r$,

$$L'_{lqr} = \left(\frac{N_q}{N_r}\right)^2 L_{lqr}\,,\ \ r'_{dr} = \left(\frac{N_d}{N_r}\right)^2 r_r\,,\ \ L'_{ldr} = \left(\frac{N_d}{N_r}\right)^2 L_{ldr}\,,\ \ L_{mq} = \frac{N_q}{N_r} L_{qsr}\,, L_{md} = \frac{N_d}{N_r} L_{dsr}\,.$$

Since the source voltages in the rotor circuit are zero, the SPIM voltage equation in the q-d stationary reference frame becomes

$$v_{qs} = r_{qs} i_{qs} + p\lambda_{qs} \tag{3.58}$$

$$v_{ds} = r_{ds} i_{ds} + p\lambda_{ds} \tag{3.59}$$

$$0 = r'_{qr} i'_{qr} - N_{qd}\omega_r \lambda'_{dr} + p\lambda'_{qr} \tag{3.60}$$

$$0 = r'_{dr} i'_{dr} + N_{dq}\omega_r \lambda'_{qr} + p\lambda'_{dr} \tag{3.61}$$

where,

$$N_{qd} = \frac{N_q}{N_d} \text{ and } N_{dq} = \frac{N_d}{N_q}\,.$$

3.2.2 Torque Equation Derivation

The energy of the SPIM can be written as [29]

$$W_f = \frac{1}{2}\left(i_{abs}\right)^T \left(L_s - L_{labs}\mathrm{I}\right) i_{abs} + \left(i_{abs}\right)^T \left(L_{sr}\right) i_{abr} + \frac{1}{2}\left(i_{abr}\right)^T \left(L_r - L_{labr}\mathrm{I}\right) i_{abr} \tag{3.62}$$

where I is an identity matrix. The change of mechanical energy in a rotational system with one mechanical input may be written as

$$dW_m = -T_e d\theta_{rm} \tag{3.63}$$

where T_e is the electromagnetic torque positive for motor action (torque output) and θ_{rm} is the actual angular displacement of the rotor. The flux linkages, currents, and W_f are all expressed as functions of the electrical angular displacement θ_r. Since

$$\theta_r = \left(\frac{P}{2}\right)\theta_{rm} \tag{3.64}$$

where P is the number of poles in the machine, then Equation (3.63) becomes

$$dW_m = -T_e\left(\frac{2}{P}\right)d\theta_r \ . \tag{3.65}$$

The electromagnetic torque can be evaluated from

$$T_e\left(i_j, \theta_r\right) = \left(\frac{P}{2}\right)\frac{\partial W_f\left(i_j, \theta_r\right)}{\partial \theta_r} \ . \tag{3.66}$$

Since L_s and L_r are not functions of θ_r, substituting W_f from Equation 3.62 in Equation 3.66 the electromagnetic torque in Newton meters (Nm) is given as

$$T_e = \left(\frac{P}{2}\right)\left(i_{abs}\right)^T \frac{\partial}{\partial \theta_r}\left[L_{sr}\right] i_{abr} \ . \tag{3.67}$$

Expanding Equation 3.67 results in

$$T_e = \left(\frac{P}{2}\right)\left[L_{qr} i_{as}\left(-i_{ar}\, sin\theta_r - i_{br}\, cos\theta_r\right) + L_{dr} i_{bs}\left(i_{ar}\, cos\theta_r - i_{br}\, sin\theta_r\right)\right] \ . \tag{3.68}$$

The torque and rotor speed are related by

$$T_e = J\left(\frac{2}{P}\right)p\omega_r + T_L \tag{3.69}$$

where J is the inertia of the rotor and the connected load. The load torque is T_L; it is positive for motor action.

The expression for the electromagnetic torque in terms of stationary reference frame variables may be obtained by substituting the equations of transformation into Equation 3.67. Thus,

$$T_e = \left(\frac{P}{2}\right)\left[\left(\mathrm{K}_s\right)^{-1} i_{qds}\right]^T \frac{\partial}{\partial \theta_r}\left[L_{sr}\right]\left[\left(\mathrm{K}_r\right)^{-1} i_{qdr}\right] \tag{3.70c}$$

$$T_e = \left(\frac{P}{2}\right)\left[\begin{bmatrix} cos(\theta) & sin(\theta) \\ sin(\theta) & -cos(\theta) \end{bmatrix}\begin{bmatrix} i_{qs} \\ i_{ds} \end{bmatrix}\right]^T \frac{\partial}{\partial\theta_r}\begin{bmatrix} L_{qr}\, cos(\theta_r) & -L_{qr}\, sin(\theta_r) \\ L_{dr}\, sin(\theta_r) & L_{dr}\, cos(\theta_r) \end{bmatrix}\cdots \times\begin{bmatrix} cos(\theta-\theta_r) & sin(\theta-\theta_r) \\ sin(\theta-\theta_r) & -cos(\theta-\theta_r) \end{bmatrix}\begin{bmatrix} i_{qr} \\ i_{dr} \end{bmatrix}. \quad (3.71)$$

Simplifying Equation 3.71 results in

$$T_e = \frac{P}{2}\left(L_{qr} i_{qs} i_{dr} - L_{dr} i_{ds} i_{qr}\right) . \quad (3.72)$$

In terms of referred, substitute variables the expression for the torque becomes

$$T_e = \frac{P}{2}\left(N_{dq}\lambda'_{qr} i'_{dr} - N_{qd}\lambda'_{dr} i_{qr}\right) . \quad (3.73)$$

3.3 Harmonic Balance Technique

Harmonic balance technique is a very important tool in engineering for three reasons:

(a) Many circuits generally operate in the sinusoidal steady state.

(b) The technique is very efficient, hence it is used in power systems, electric circuits, control systems, etc.

(c) If the response of a linear time-invariant circuit to a sinusoidal input of any frequency is known, then effectively its response to any signal can be calculated.

3.3.1 Phasors and Sinusoidal Solutions

A sinusoidal of angular frequency ω (rad/s) is defined as

$$A_m\cos(\omega t+\phi) \tag{3.74a}$$

where the amplitude A_m, the frequency ω, and the phase ϕ are real constants. The amplitude or the peak is assumed positive. The frequency ω is measured in radians per second. The period is T = 2π/ω in seconds. The sinusoidal function is of the form

$$A_m\cos(2\pi ft+\phi) \tag{3.74b}$$

when the frequency, f is hertz and T = 1/f.

The sinusoidal function can be rewritten in complex form as

$$A = A_m e^{j\phi} \tag{3.75}$$

where A is the complex number called the phasor. If the frequency ω is known, then the phasor A is related to the sinusoid by the equation

$$\mathrm{Re}\left[Ae^{j\omega t}\right] = \mathrm{Re}\left[A_m e^{j(\omega t+\phi)}\right] = A_m\cos(\omega t+\phi) \tag{3.76}$$

The relationship between sinusoids (at frequency ω) and phasor can be given as

Sinusoid $$A_m\cos(\omega t+\phi) = (A_m\cos\phi)\cos(\omega t) + (-A_m\sin\phi)\sin(\omega t) \tag{3.77a}$$

Phasor $$A = A_m e^{j\phi} = A_m\cos\phi + j(A_m\sin\phi)\ . \tag{3.77b}$$

The following can be concluded from Equations 3.77a and 3.77b

$$A_m\cos(\omega t+\phi) = \mathrm{Re}[A]\cos(\omega t) - \mathrm{Im}[A]\sin(\omega t)\ . \tag{3.78}$$

3.3.2 Basic Theorems

The use of harmonic balance technique in the analysis of linear time-invariant circuits in sinusoidal steady state are based on the following theorems [19].

Theorem 1 (Uniqueness). Two sinusoids are equal if and only if they are represented by the same phasor; symbolically, for all t,

$$\mathrm{Re}\left[Ae^{j\omega t}\right]=\mathrm{Re}\left[Be^{j\omega t}\right]\Leftrightarrow A=B. \tag{3.79}$$

Proof: By assumption let A = B. Then for all values of t,

$$Ae^{j\omega t}=Be^{j\omega t} \qquad \text{and} \qquad \mathrm{Re}\left[Ae^{j\omega t}\right]=\mathrm{Re}\left[Be^{j\omega t}\right].$$

By assumption for all values of t,

$$\mathrm{Re}\left[Ae^{j\omega t}\right]=\mathrm{Re}\left[Be^{j\omega t}\right]. \tag{3.80}$$

Specifically, when t = 0, Equation (3.80) becomes

$$\mathrm{Re}[A]=\mathrm{Re}[B]. \tag{3.81}$$

Similarly, for $t_o = \pi/2\omega$, $\exp j\omega t_o = \exp j(\pi/2) = j$ and Re[Aj] = - Im[A]; hence Equation (3.80) becomes

$$\mathrm{Im}[A]=\mathrm{Im}[B]. \tag{3.82}$$

Hence from 3.81 and 3.82, successively

$$A=\mathrm{Re}[A]+j\,\mathrm{Im}[B]=\mathrm{Re}[A]+j\,\mathrm{Im}[B]=B.$$

Theorem 2 (Linearity). The phasor represented a linear combination of sinusoids (with real coefficients) and is equal to the same linear combination of the phasors representing the individual sinusoids.

Symbolically, let the sinusoids be

$$x_1(t) = \mathrm{Re}\left[A_1 e^{j\omega t}\right] \qquad \text{and} \qquad x_2(t) = \mathrm{Re}\left[A_2 e^{j\omega t}\right].$$

Thus the phasor A_1 represents the sinusoid $x_1(t)$ and the phasor A_2 represents $x_2(t)$.

Let a_1 and a_2 be any two real numbers; then the sinusoid $a_1\, x_1(t) + a_2\, x_2(t)$ is represented by the phasor $a_1 A_1 + a_2 A_2$.

PROOF: Confirmation of the assertion by computation:

$$a_1\, x_1(t) + a_2\, x_2(t) = a_1\, \mathrm{Re}\left[A_1 e^{j\omega t}\right] + a_2\, \mathrm{Re}\left[A_2 e^{j\omega t}\right]. \tag{3.83}$$

Now a_1 and a_2 are real numbers, hence for any complex numbers z_1 and z_2,

$$a_i \mathrm{Re}[z_i] = \mathrm{Re}[a_i z_i] \qquad i = 1,2 \tag{3.84a}$$

and

$$a_1 \mathrm{Re}[z_1] + a_2 \mathrm{Re}[z_2] = \mathrm{Re}[a_1 z_1 + a_2 z_2]. \tag{3.84b}$$

Applying Equation 3.84b to Equation 3.83

$$a_1\, \mathrm{Re}\left[A_1 e^{j\omega t}\right] + a_2\, \mathrm{Re}\left[A_2 e^{j\omega t}\right] = \mathrm{Re}\left[(a_1 A_1 + a_2 A_2) e^{j\omega t}\right] \tag{3.85}$$

From Equation 3.83 and 3.85

$$a_1\, x_1(t) + a_2\, x_2(t) = \mathrm{Re}\left[(a_1 A_1 + a_2 A_2) e^{j\omega t}\right]. \tag{3.86}$$

that is, the sinusoid $a_1\, x_1(t) + a_2\, x_2(t)$ is represented by the phasor $a_1\, \mathrm{A}_1 + a_2\, \mathrm{A}_2$.

Theorem 3 (Differentiation rule). A is the phasor of a given sinusoid $A_m \cos(\omega t + \angle \mathrm{A})$ if and only if $j\omega A$ is the phasor of its derivative, $\frac{d}{dt}\left[A_m \cos(\omega t + \angle \mathrm{A})\right]$.

Symbolically,

$$\mathrm{Re}\left[j\omega A e^{j\omega t}\right] = \frac{d}{dt}\left(\mathrm{Re}\left[A e^{j\omega t}\right]\right). \tag{3.87}$$

Equation 3.87 indicates that the linear operators Re and $\frac{d}{dt}$ commute:

$$\mathrm{Re}\left[\frac{d}{dt}\left(A\mathrm{e}^{\mathrm{j}\omega t}\right)\right]=\mathrm{Re}\left[\mathrm{j}\omega A\mathrm{e}^{\mathrm{j}\omega t}\right]=\frac{d}{dt}\left[\mathrm{Re}\left(A\mathrm{e}^{\mathrm{j}\omega t}\right)\right].$$

PROOF: By calculation. $A=A_m\exp(j\angle\mathrm{A})$.

$$\frac{d}{dt}[\mathrm{Re}(A\exp(j\omega t))]$$

$$=\frac{d}{dt}[\mathrm{Re}(A_m\exp\ j(\omega t+\angle\mathrm{A}))] \qquad \text{where } \mathrm{A_m} \text{ is real}$$

$$=\frac{d}{dt}[A_m\cos(\omega t+\angle\mathrm{A})] \qquad \text{since } \exp\ jx=\cos x+j\sin x$$

$$=-A_m\omega\sin(\omega t+\angle\mathrm{A})$$

$$=\mathrm{Re}[j\omega\ A_m\exp\ j(\omega t+\angle\mathrm{A})]$$

$$=\mathrm{Re}[j\omega\ A\exp\ j\omega t].$$

It is worth noting some basic complex number identities

$$\mathrm{Re}[A]\times\mathrm{Re}[B]=\frac{1}{2}\left(\mathrm{Re}[AB]+\mathrm{Re}\left[AB^*\right]\right) \tag{3.88}$$

$$\mathrm{Re}[A]\times\mathrm{Re}[B]=\frac{1}{2}\left(\mathrm{Re}\left[A^*B\right]+\mathrm{Re}[AB]\right) \tag{3.89}$$

where A^* and B^* are complex conjugates of complex numbers *A* and *B*, respectively.

3.4 Steady State Analysis of Single-Phase Induction Motor

The state variables are approximated as

$$V_{qs}=\mathrm{Re}\left[V_{qss}e^{j\omega_e t}\right],\ V_{ds}=\mathrm{Re}\left[V_{dss}e^{j\omega_e t}\right],\ \lambda_{qs}=\mathrm{Re}\left[\lambda_{qss}e^{j\omega_e t}\right],\ \lambda_{ds}=\mathrm{Re}\left[\lambda_{dss}e^{j\omega_e t}\right],$$

$\lambda'_{qr} = \mathrm{Re}\left[\lambda'_{qrr}e^{j\omega_e t}\right]$, $\lambda'_{dr} = \mathrm{Re}\left[\lambda'_{drr}e^{j\omega_e t}\right]$, $I_{qs} = \mathrm{Re}\left[I_{qss}e^{j\omega_e t}\right]$, $I_{ds} = \mathrm{Re}\left[I_{dss}e^{j\omega_e t}\right]$, $I'_{qr} = \mathrm{Re}\left[I'_{qrr}e^{j\omega_e t}\right]$ and $I'_{dr} = \mathrm{Re}\left[I'_{drr}e^{j\omega_e t}\right]$.

where V_{dss}, V_{qss}, λ_{dss}, λ_{qss}, λ'_{qrr}, λ'_{drr}, I_{qss}, I_{dss}, I'_{qrr}, and I'_{drr} are complex peak quantities. At steady state the coefficients of the state variables in Equations 3.58-3.61 are time varying. Using the harmonic balance technique theorems in section 3.3

$$\mathrm{Re}\left[V_{dss}e^{j\omega_e t}\right] = r_{ds}\mathrm{Re}\left[I_{dss}e^{j\omega_e t}\right] + \mathrm{p}\left\{\mathrm{Re}\left[\lambda_{dss}e^{j\omega_e t}\right]\right\}; \tag{3.90a}$$

by comparing terms Equation 3.90a becomes

$$V_{dss} = r_{ds}I_{dss} + \mathrm{j}\omega_e\lambda_{dss} + p\lambda_{dss}\ . \tag{3.90b}$$

Similarly

$$\mathrm{Re}\left[V_{qss}e^{j\omega_e t}\right] = r_{qs}\mathrm{Re}\left[I_{qss}e^{j\omega_e t}\right] + \mathrm{p}\left\{\mathrm{Re}\left[\lambda_{qss}e^{j\omega_e t}\right]\right\} \tag{3.91a}$$

$$V_{qss} = r_{qs}I_{qss} + \mathrm{j}\omega_e\lambda_{qss} + p\lambda_{qss} \tag{3.91b}$$

$$0 = r'_{qr}\mathrm{Re}\left[I'_{qrr}e^{j\omega_e t}\right] - N_{qd}\omega_r\mathrm{Re}\left[\lambda'_{drr}e^{j\omega_e t}\right] + \mathrm{p}\left\{\mathrm{Re}\left[\lambda'_{qrr}e^{j\omega_e t}\right]\right\} \tag{3.92a}$$

$$0 = r'_{qr}I'_{qrr} - N_{qd}\omega_r\lambda'_{drr} + \mathrm{j}\omega_e\lambda'_{qrr} + p\lambda'_{qrr} \tag{3.92b}$$

$$0 = r'_{dr}\mathrm{Re}\left[I'_{drr}e^{j\omega_e t}\right] + N_{dq}\omega_r\mathrm{Re}\left[\lambda'_{qrr}e^{j\omega_e t}\right] + \mathrm{p}\left\{\mathrm{Re}\left[\lambda'_{drr}e^{j\omega_e t}\right]\right\} \tag{3.93a}$$

$$0 = r'_{dr}I'_{drr} + N_{dq}\omega_r\lambda'_{qrr} + \mathrm{j}\omega_e\lambda'_{drr} + p\lambda'_{drr}\ . \tag{3.93b}$$

Applying similarly harmonic balance technique to the flux linkages equation

$$\lambda_{qss} = L_{qs}I_{qss} + L_{mq}I'_{qrr} \tag{3.94}$$

$$\lambda_{dss} = L_{ds}I_{dss} + L_{md}I'_{drr} \tag{3.95}$$

$$\lambda'_{qrr} = L'_{qr}I'_{qrr} + L_{mq}I_{qss} \tag{3.96}$$

$$\lambda'_{drr} = L'_{dr}I'_{drr} + L_{md}I_{dss}\ . \tag{3.97}$$

The steady state electromagnetic torque can be approximated as

$$T_e = \mathrm{Re}\left[T_{e1} + T_{e2}e^{j2\omega_e t}\right]. \tag{3.98}$$

Using harmonic balance technique the steady state electromagnetic torque can be found as follows. Substituting the state variables in Equation (3.73)

$$\begin{aligned}&\mathrm{Re}\left[T_{e1} + T_{e2}e^{j2\omega_e t}\right]\\ &\quad= \frac{P}{2}\left\{N_{dq}\mathrm{Re}\left[\lambda'_{qrr}e^{j\omega_e t}\right]\mathrm{Re}\left[I'_{drr}e^{j\omega_e t}\right] - N_{qd}\mathrm{Re}\left[\lambda'_{drr}e^{j\omega_e t}\right]\mathrm{Re}\left[I'_{qrr}e^{j\omega_e t}\right]\right\}\end{aligned} \tag{3.99}$$

using the identity in Equation 3.88

$$\begin{aligned}&\mathrm{Re}\left[T_{e1} + T_{e2}e^{j2\omega_e t}\right]\\ &= \frac{P}{2}\left\{\frac{N_{dq}}{2}\left(\mathrm{Re}\left[\lambda'_{qrr}I'^{*}_{drr}\right] + \mathrm{Re}\left[\lambda'_{qrr}I'_{drr}e^{j2\omega_e t}\right]\right) - \frac{N_{qd}}{2}\left(\mathrm{Re}\left[\lambda'_{drr}I'^{*}_{qrr}\right] + \mathrm{Re}\left[\lambda'_{drr}I'_{qrr}e^{j2\omega_e t}\right]\right)\right\}.\end{aligned} \tag{3.100}$$

From section 3.3.2 Equation (3.100) can be further reduced to

$$T_{e1} = \frac{P}{4}\left(N_{dq}\lambda'_{qrr}I'^{*}_{drr} - N_{qd}\lambda'_{drr}I'^{*}_{qrr}\right) \tag{3.101}$$

$$T_{e2} = \frac{P}{4}\left(N_{dq}\lambda'_{qrr}I'_{drr} - N_{qd}\lambda'_{drr}I'_{qrr}\right) \tag{3.102}$$

where T_{e1} and T_{e2} are the average and pulsating electromagnetic torque, respectively.

The equivalent circuit for the system using voltage equations (3.90b-3.93b) is shown in Figure 3.2.

Core loss resistances R_{mq} and R_{md} are added to the equivalent circuit in Figure 3.2 to account for core loss. The new equivalent circuit including core resistance is shown in Figure 3.3. The steady-state equation the for new equivalent circuit is given in Equation2 3.103-3.110

$$0 = V_{dss} - r_{ds}I_{dss} - \mathrm{j}\omega_e\lambda_{dss} \tag{3.103}$$

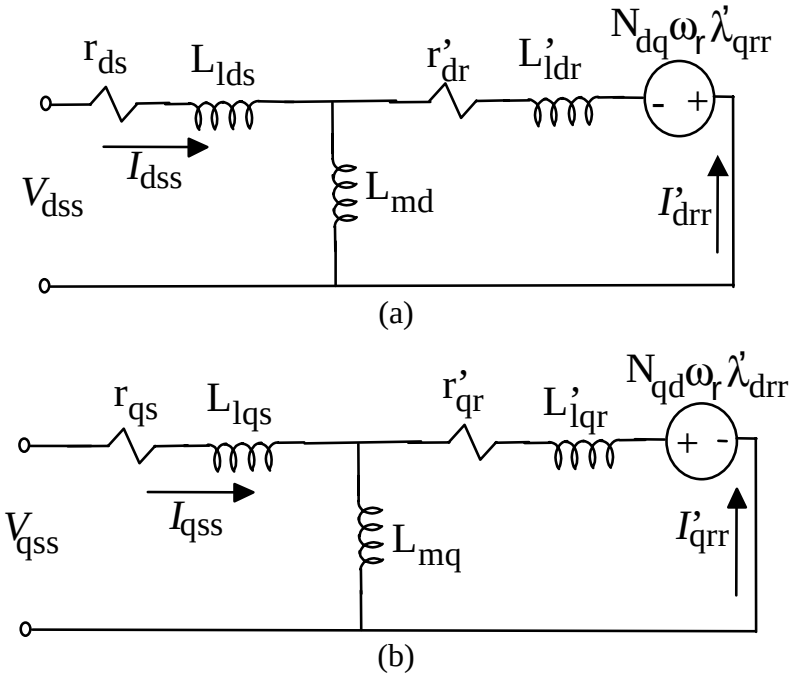

Figure 3.2. Equivalent circuit of single-phase induction machine (a) d-axis, (b) q-axis.

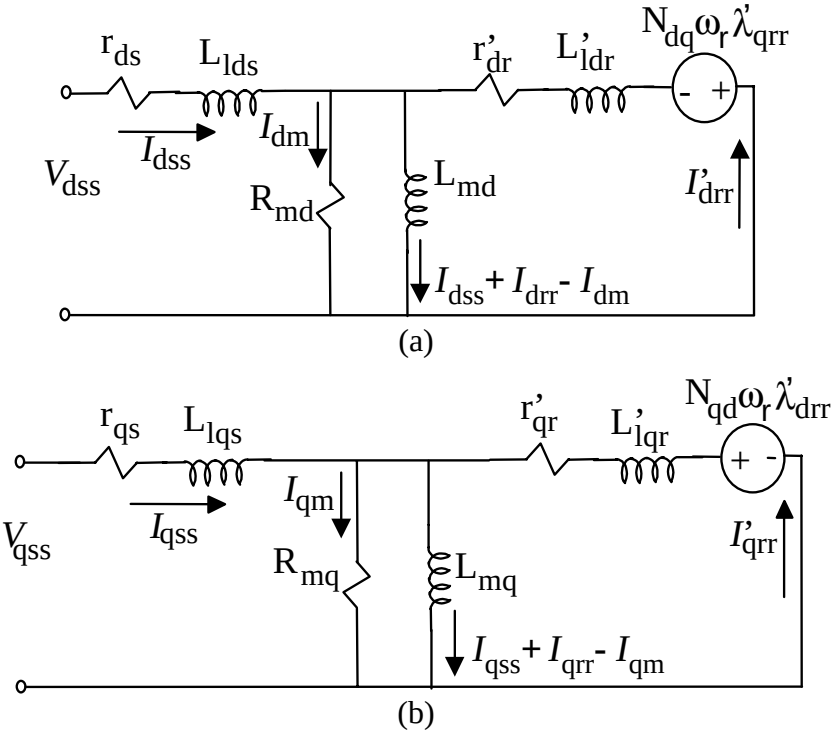

Figure 3.3. Equivalent circuit of single-phase induction machine with core loss (a) d-axis, (b) q-axis.

$$0 = V_{qss} - r_{qs} I_{qss} - \mathrm{j}\omega_e \lambda_{qss} \tag{3.104}$$

$$0 = N_{qd} \omega_r \lambda'_{drr} - r'_{qr} I'_{qrr} - \mathrm{j}\omega_e \lambda'_{qrr} \tag{3.105}$$

$$0 = -N_{dq} \omega_r \lambda'_{qrr} - r'_{dr} I'_{drr} - \mathrm{j}\omega_e \lambda'_{drr} \tag{3.106}$$

where the q-d flux linkages are defined in terms of the steady state q-d currents as

$$\lambda_{qss} = L_{lqs} I_{qss} + L_{mq} \left(I_{qss} + I'_{qrr} - I_{qm} \right) \tag{3.107}$$

$$\lambda_{dss} = L_{lds} I_{dss} + L_{md} \left(I_{dss} + I'_{drr} - I_{dm} \right) \tag{3.108}$$

$$\lambda'_{qrr} = L'_{lqr} I'_{qrr} + L_{mq} \left(I'_{qrr} + I_{qss} - I_{qm} \right) \tag{3.109}$$

$$\lambda'_{drr} = L'_{ldr} I'_{drr} + L_{md} \left(I'_{drr} + I_{dss} - I_{dm} \right) . \tag{3.110}$$

The q-d flux linkages (3.107-3.110) are then substituted in the voltage equations (3.103-3.106). The following equations result.

$$V_{dss} = r_{ds} I_{dss} + \mathrm{j}\omega_e L_{lds} I_{dss} + \mathrm{j}\omega_e L_{md} R_{md} \frac{\left(I_{dss} + I'_{drr} \right)}{\left(R_{md} + \mathrm{j}\omega_e L_{md} \right)} \tag{3.111}$$

$$V_{qss} = r_{qs} I_{qss} + \mathrm{j}\omega_e L_{lqs} I_{qss} + \mathrm{j}\omega_e L_{mq} R_{mq} \frac{\left(I_{qss} + I'_{qrr} \right)}{\left(R_{mq} + \mathrm{j}\omega_e L_{mq} \right)} \tag{3.112}$$

$$\begin{aligned} 0 = r'_{qr} I'_{qrr} - N_{qd} \omega_r \left\{ L_{ldr} I'_{drr} + L_{md} R_{md} \frac{\left(I_{dss} + I'_{drr} \right)}{\left(R_{md} + \mathrm{j}\omega_e L_{md} \right)} \right\} + \mathrm{j}\omega_e L'_{lqr} I'_{qrr} \cdots \\ + \mathrm{j}\omega_e L_{mq} R_{mq} \frac{\left(I_{qss} + I'_{qrr} \right)}{\left(R_{mq} + \mathrm{j}\omega_e L_{mq} \right)} \end{aligned} \tag{3.113}$$

$$\begin{aligned} 0 = r'_{dr} I'_{drr} + N_{dq} \omega_r \left\{ L_{lqr} I'_{qrr} + L_{mq} R_{mq} \frac{\left(I_{qss} + I'_{qrr} \right)}{\left(R_{mq} + \mathrm{j}\omega_e L_{mq} \right)} \right\} + \mathrm{j}\omega_e L'_{ldr} I'_{drr} \cdots \\ + \mathrm{j}\omega_e L_{md} R_{md} \frac{\left(I_{dss} + I'_{drr} \right)}{\left(R_{md} + \mathrm{j}\omega_e L_{md} \right)} . \end{aligned} \tag{3.114}$$

3.5 Evaluation of Machine Parameters

The main and auxiliary winding resistances were found by applying a dc voltage across the terminals of the main and auxiliary windings. The values are main winding resistance, r_{qs}=1.1 Ω and auxiliary winding resistance, r_{ds}=4.3 Ω.

The other parameters are estimated using the stand-still and synchronous-speed tests. The stand-still test is carried out by holding the rotor down and by applying a single-phase voltage across the auxiliary winding with the main winding opened. As the voltage across the auxiliary winding is increased gradually, the auxiliary winding input power, phase voltage, and current are measured along with the voltage across the main winding. Also, the voltage source is applied across the main winding with the auxiliary winding open. Main winding input power, phase voltage, and current, as well as the voltage at the terminals of the auxiliary winding, are then measured as the main voltage is increased.

The synchronous test is performed in addition to the stand-still test. This test is accomplished by running the rotor at the synchronous speed. Then all other steps of the test are carried out as was described in the stand-still test. The measured experimental results are shown in Tables 3.1 - 3.2.

Table 3.1: Stand-still test: voltage applied to (a) the auxiliary winding and (b) the main winding.

(a)

V1A [V]	I1A [A]	P1A [W]	V2M [V]
3.162	0.1662	0.264	0.192
6.346	0.32	0.9672	0.539
8.843	0.5438	2.474	0.685
11.98	0.8693	5.957	0.627
16.28	1.3409	13.77	0.597
20.6	1.8034	24.92	0.498
24.27	2.2	37.22	0.434
27.31	2.53	49.29	0.373

(b)

V1M [V]	I1M [A]	P1M [W]	V2A [V]
3.79	0.331	0.585	0.025
5.049	0.555	1.076	0.032
7.23	1.052	3.188	0.044
10.16	1.765	8.374	0.082
13.71	2.687	19.07	0.12
17.33	3.672	36.01	0.156
19.58	4.224	46.92	0.182
25.24	5.67	84.9	0.256

Notes: where V1A is the auxiliary winding voltage with voltage applied to the auxiliary winding, I1A is the auxiliary winding current with voltage applied to the auxiliary winding, P1A is the power to auxiliary winding power with voltage applied to the auxiliary winding, V2M is the main winding voltage with voltage applied to the auxiliary winding, V1M is the main winding voltage with voltage applied to the main winding, I1M is the main winding current with voltage applied to the main winding, P1M is the power to the main winding power with voltage applied to the main winding, and V2A is the auxiliary winding voltage with voltage applied to the main winding,

Use of the stationary reference frame transformation results in the following relationship V1M= V_{qs}, I1M= I_{qs}, V1A= V_{ds}, and I1A= I_{ds}.

3.5.1 Determination of the Main Winding Rotor Resistance

From the data in Table 3.1b, the main winding rotor resistance, r_{qr} can be found. When $I_{ds} = 0$, and $\omega_r = 0$ the equivalent circuit is shown in Figure 3.4.

Table 3.2: Synchronous test: voltage applied to (a) the auxiliary winding and (b) the main winding.

(a)

V1A [V]	I1A [A]	P1A [W]	V2M [V]
10.18	0.2655	1.1	2.386
20.33	0.4835	3.252	6.31
30.18	0.6845	5.781	11.83
40.25	0.8989	9.135	17.69
50.31	1.114	13.209	23.61
60.22	1.3276	17.852	29.57
70.37	1.5553	23.55	35.5
80.4	1.7814	30	41.5
90.13	1.9985	36.59	47.4
100.1	2.24	45.29	53.3
110.5	2.499	55.3	59.7
120.8	2.772	66.6	65.8
130.3	3.051	79.62	71.5
140.6	3.386	96.06	77.8
150.9	3.764	114.75	84
161	4.222	141.32	89.8

(b)

V1M [V]	I1M [A]	P1M [W]	V2A [V]
10.16	0.511	1.271	5.95
20.91	1.014	4.208	17.41
32.04	1.518	8.716	31.08
39.14	1.813	12.01	39.9
50.73	2.374	19.61	54.3
60.25	2.831	26.9	66.2
70.12	3.328	36.19	78.7
80.13	3.867	47.87	91.6
90.17	4.435	61.67	104.1
100.4	5.11	79.51	116.8
110.2	5.935	101.8	128.9
120.3	7.139	137.9	140.9
131	8.945	201.9	152.4
139.9	10.89	280	160.7

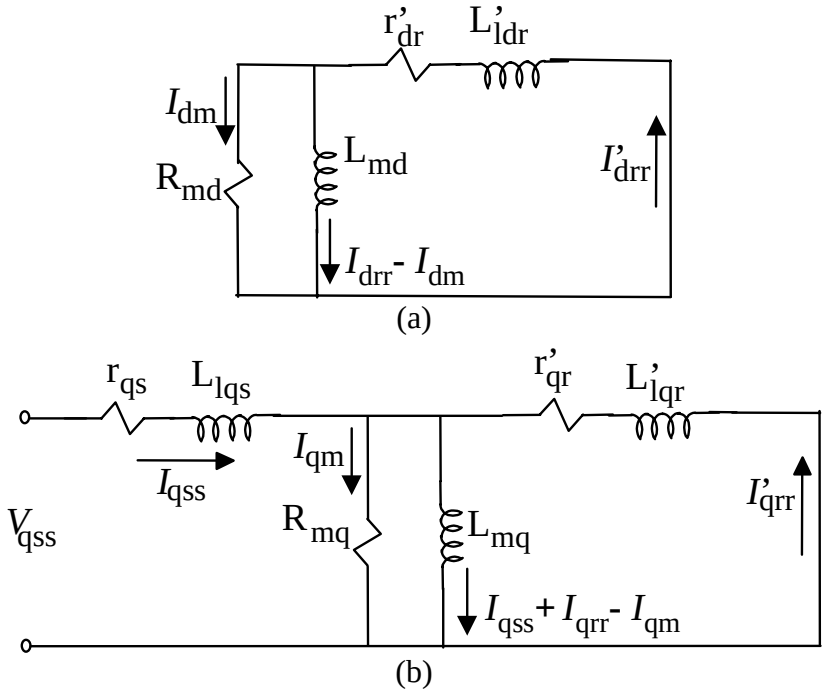

Figure 3.4. Equivalent circuit of single-phase induction machine with $I_{ds} = 0$, and $\omega_r = 0$ (a) d-axis, (b) q-axis.

From equivalent circuit the following equation results.

$$\frac{V_{qss}}{I_{qss}} = Z_{qsc} = R_{qsc} + \mathrm{j}X_{qsc} \approx \left(r_{qs} + r'_{qr}\right) + \mathrm{j}\left(\omega_e L_{lqs} + \omega_e L'_{lqr}\right) \tag{3.115}$$

From the stationary test result in Table 3.1b and given r_{qs}, r_{qr} can be calculated using the following procedure.

$$\left|Z_{qsc}\right| = \frac{V_{1M}}{I_{1M}} = {R_{qsc}}^2 + {X_{qsc}}^2 \tag{3.116}$$

$$R_{qsc} = \frac{P_{1M}}{{I_{1M}}^2} \tag{3.117}$$

$$X_{qsc} = \sqrt{{Z_{qsc}}^2 - {R_{qsc}}^2} \tag{3.118}$$

$$r_{qr} = R_{qsc} - r_{qs} \tag{3.119}$$

3.5.2 Determination of the Auxiliary Winding Rotor Resistance

From the data in Table 3.1a, the auxiliary winding rotor resistance, r_{dr}, can be found. When $I_{qs} = 0$, and $\omega_r = 0$ the equivalent circuit is shown in Figure 3.5.

From equivalent circuit the following equation results.

$$\frac{V_{dss}}{I_{dss}} = Z_{dsc} = R_{dsc} + \mathrm{j}X_{dsc} \approx \left(r_{ds} + r'_{dr}\right) + \mathrm{j}\omega_e\left(L_{lqs} + L'_{lqr}\right) \tag{3.120}$$

From the stationary test result in Table 3.1a and given r_{ds}, r_{dr} can be calculated using the following procedure.

$$\left|Z_{dsc}\right| = \frac{V_{1A}}{I_{1A}} = {R_{dsc}}^2 + {X_{dsc}}^2 \tag{3.121}$$

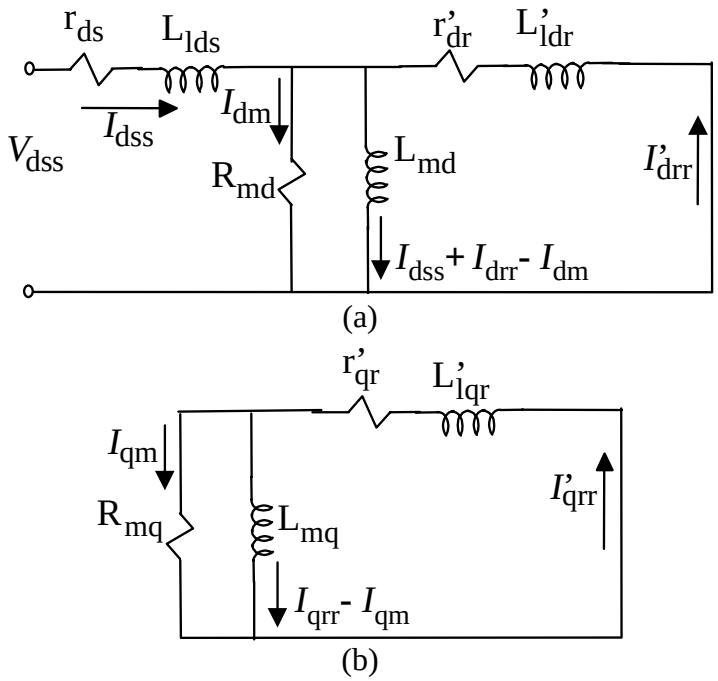

Figure 3.5. Equivalent circuit of single-phase induction machine with $I_{qs} = 0$, and $\omega_r = 0$ (a) d-axis, (b) q-axis.

$$R_{dsc} = \frac{P_{1A}}{I_{1A}^{\ 2}} \tag{3.122}$$

$$X_{dsc} = \sqrt{Z_{dsc}^{\ 2} - R_{dsc}^{\ 2}} \tag{3.123}$$

$$r_{dr} = R_{dsc} - r_{ds} \tag{3.124}$$

The turn ratio, N_{dq}, can be found be using the following relationship,

$N_{dq} = \sqrt{\frac{X_{dsc}}{X_{qsc}}}$ with N_{qd} is the inverse of N_{dq} as $N_{qd} = \frac{1}{N_{dq}}$.

3.5.3 Determination of the Main Winding Parameters

From the data in Table 3.2b, the main winding parameter can be found.

When $I_{ds} = 0$, and $\omega_r = \omega_e$ the equivalent circuit is shown in Figure 3.6.

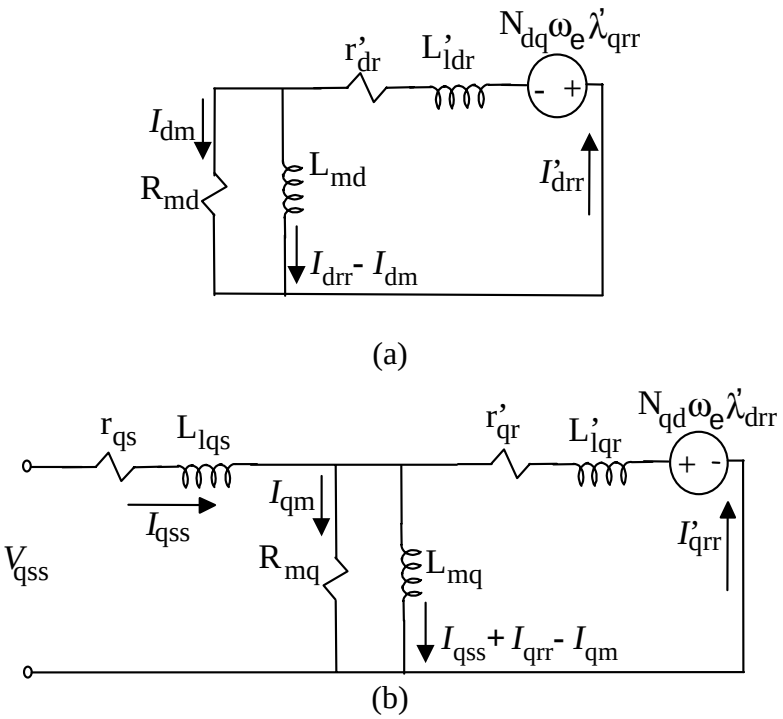

Figure 3.6. Equivalent circuit of single-phase induction machine with $I_{ds} = 0$, and $\omega_r = \omega_e$ (a) d-axis, (b) q-axis.

From equivalent circuit in Figure 3.6 the following equation results.

$$Z_{dq} = \frac{N_{dq} R_{mq}^2 X_{mq}^2}{\left[\sqrt{\left(4R_{mq}^2 + r_{qr}^2 + 4r_{qr}R_{mq} + 4X_{lqr}^2\right)\times X_{mq}^2 \cdots + \left(8X_{lqr}X_{mq} + 4X_{lqr}^2 + r_{qr}^2\right)\times R_{mq}^2} \times \sqrt{R_{mq}^2 + X_{mq}^2}\right]} \tag{3.125}$$

$$R_{qss} = r_{qs} + X_{mq}^2 \frac{R_{mq}}{R_{mq}^2 + X_{mq}^2} + J_{q1}\frac{V_{q1}}{V_{q1}^2 + V_{q2}^2} + J_{q2}\frac{V_{q2}}{V_{q1}^2 + V_{q2}^2} \tag{3.126}$$

$$X_{qss} = X_{lqs} + X_{mq}\frac{R_{mq}^2}{R_{mq}^2 + X_{mq}^2} + J_{q2}\frac{V_{q1}}{V_{q1}^2 + V_{q2}^2} - J_{q1}\frac{V_{q2}}{V_{q1}^2 + V_{q2}^2} \tag{3.127}$$

$$J_{q1} = X_{mq}^2 R_{mq}^3 r_{qr} \tag{3.128}$$

$$J_{q2} = X_{mq}^3 R_{mq}^2 r_{qr} \tag{3.129}$$

$$V_{q1} = \begin{pmatrix} 2X_{mq}^{2}X_{lqr} - X_{mq}^{2}r_{qr} - 2X_{mq}^{2}R_{mq} - 4X_{mq}X_{lqr}R_{mq} - 2X_{mq}R_{mq}^{2}\cdots \\ -2X_{mq}r_{qr}R_{mq} + r_{qr}R_{mq}^{2} - 2X_{lqr}R_{mq}^{2} \end{pmatrix} r_{qr}X_{mq} \quad (3.130)$$

$$V_{q2} = \begin{pmatrix} 2X_{mq}^{2}R_{mq} + X_{mq}^{2}r_{qr} + 2X_{mq}^{2}X_{lqr} - 2X_{mq}r_{qr}R_{mq} - 2X_{mq}R_{mq}^{2}\cdots \\ +4X_{mq}X_{lqr}R_{mq} - r_{qr}R_{mq}^{2} - 2X_{lqr}R_{mq}^{2} \end{pmatrix} r_{qr}X_{mq} \quad (3.131)$$

From the synchronous test result in Table 3.2b the following Z_{dq}, Z_{qss}, R_{qss}, and X_{qss} can be found using the relationship

$$\left|Z_{dq}\right| = \frac{V_{2Aa}}{I_{1Ma}} \quad (3.132)$$

$$\left|Z_{qss}\right| = \frac{V_{1Ma}}{I_{1Ma}} \quad (3.133)$$

$$R_{qss} = \frac{P_{1Ma}}{I_{1Ma}^{2}} \quad (3.134)$$

$$X_{qss} = \sqrt{Z_{qss}^{2} - R_{qss}^{2}} \ . \quad (3.135)$$

Given the constant values in Equations 3.132-3.135 the following unknowns L_{mq}, R_{mq}, L_{lqr}, and L_{lqs} can be determined. The nonlinear Equations 3.125-3.131 are solved using matlab-fsolve program for these unknown parameters.

3.5.4 Determination of the Auxiliary Winding Parameters

From the data in Table 3.2a, the auxiliary winding parameter can be found. When $I_{qs} = 0$, and $\omega_r = \omega_e$ the equivalent circuit is shown in Figure 3.7.

From equivalent circuit in Figure 3.5 the following Equation results.

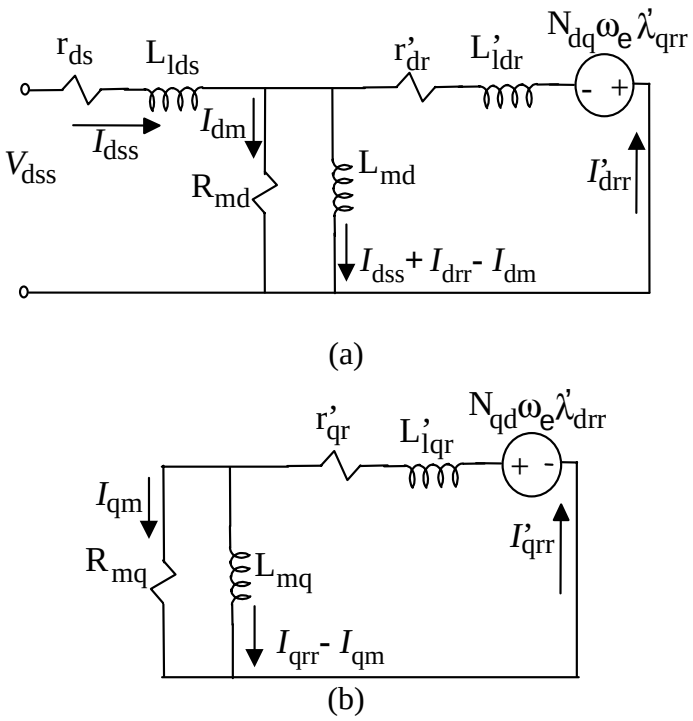

Figure 3.7. Equivalent circuit of single-phase induction machine with $I_{qs} = 0$, and $\omega_r = \omega_e$ (a) d-axis, (b) q-axis.

$$Z_{qd} = \frac{N_{qd} R_{md}^2 X_{md}^2}{\left[\sqrt{\begin{array}{l}\left(4R_{md}^2 + r_{dr}^2 + 4r_{dr}R_{md} + 4X_{ldr}^2\right) * X_{md}^4 + \left(8R_{md}^2 X_{ldr} X_{md}^3\right)\ldots \\ + \left(4R_{md}^4 + 4R_{md}^3 r_{dr} + \left(8X_{ldr}^2 + 2r_{dr}^2\right) * R_{md}^2\right) * X_{md}^2 \ldots \\ + 8R_{md}^4 X_{md} X_{ldr} + \left(r_{dr}^2 + 4X_{ldr}^2\right) * R_{md}^4\end{array}}\right]} \tag{3.136}$$

$$R_{dss} = r_{ds} + X_{md}^2 \frac{R_{md}}{R_{md}^2 + X_{md}^2} + J_{d1} \frac{V_{d1}}{V_{d1}^2 + V_{d2}^2} + J_{d2} \frac{V_{d2}}{V_{d1}^2 + V_{d2}^2} \tag{3.137}$$

$$X_{dss} = X_{lds} + X_{md} \frac{R_{md}^2}{R_{md}^2 + X_{md}^2} + J_{d2} \frac{V_{d1}}{V_{d1}^2 + V_{d2}^2} - J_{d1} \frac{V_{d2}}{V_{d1}^2 + V_{d2}^2} \tag{3.138}$$

$$J_{d1} = -r_{dr} X_{md}^2 R_{md}^3 \tag{3.139}$$

$$J_{d2} = -r_{dr} X_{md}^3 R_{md}^2 \tag{3.140}$$

$$V_{d1} = -\left(2X_{md}^3 X_{ldr} - 3r_{dr} X_{md}^2 R_{md} - 4X_{md}^2 R_{md}^2 - 6X_{ldr} R_{md}^2 X_{md} + r_{dr} R_{md}^3\right) \times r_{dr} \tag{3.141}$$

$$V_{d2} = \begin{pmatrix} r_{dr} X_{md}^3 + 2X_{md}^3 R_{md} + 6X_{ldr} X_{md}^2 R_{md} - 3r_{dr} R_{md}^2 X_{md} - 2X_{md} R_{md}^3 \cdots \\ -2X_{ldr} R_{md}^3 \end{pmatrix} \times r_{dr} \quad (3.142)$$

From the synchronous test result in Table 3.2a the following Z_{qd}, Z_{dss}, R_{dss}, and X_{dss} can be found using the relationship

$$\left|Z_{qd}\right| = \frac{V_{2Ma}}{I_{1Aa}} \quad (3.143)$$

$$\left|Z_{dss}\right| = \frac{V_{1Aa}}{I_{1Aa}} \quad (3.144)$$

$$R_{dss} = \frac{P_{1Aa}}{I_{1Aa}^2} \quad (3.145)$$

$$X_{dss} = \sqrt{Z_{dss}^2 - R_{dss}^2}\ . \quad (3.146)$$

Given the constant values in Equations 3.143-3.146 the following unknown L_{md}, R_{md}, L_{ldr}, and L_{lds} can be determined. The nonlinear Equations 3.136-3.142 are solved using matlab-fsolve program for these unknown parameters.

The single-phase induction motor used was rated at 0.5 hp, 115 V, 7.8 A, and 1725 rpm. The q-d magnetizing inductances of the SPIM as a function of input voltage are shown in Figure 3.8. The q-d magnetizing inductance increases steadily with increase in input voltage then falls steadily with additional input voltage as the machine goes into saturation.

Figure 3.9 shows the q-d core loss resistances also as a function of the input voltage for the SPIM. It can be noticed from the graph the variation of the core loss resistances with the input voltage. The value increases then decreases as the machine goes into saturation.

The sum of q-d axis stator and rotor leakage inductances is shown in Figure 3.10 as a function input voltage. The value decreases with increase of terminal voltage due to redistribution of flux linkage.

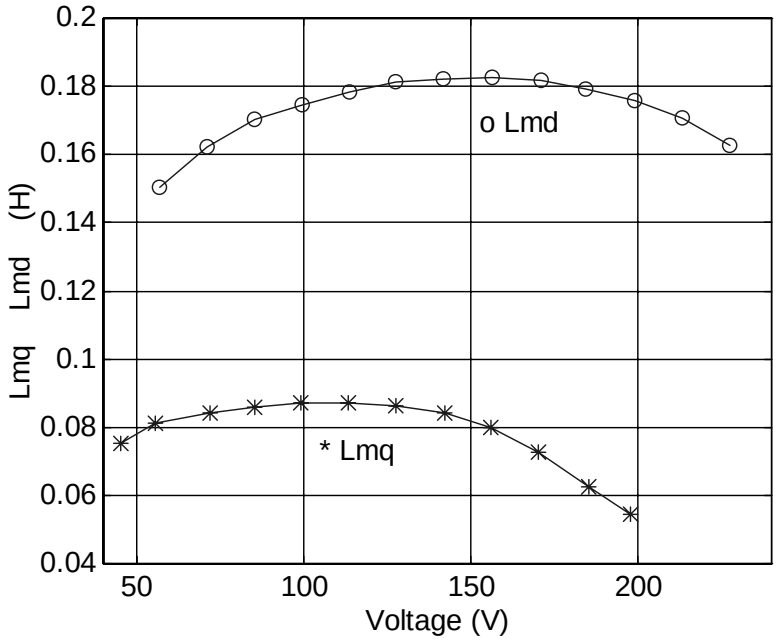

Figure 3.8. Experimental values q -d magnetizing inductances vs peak input voltage.

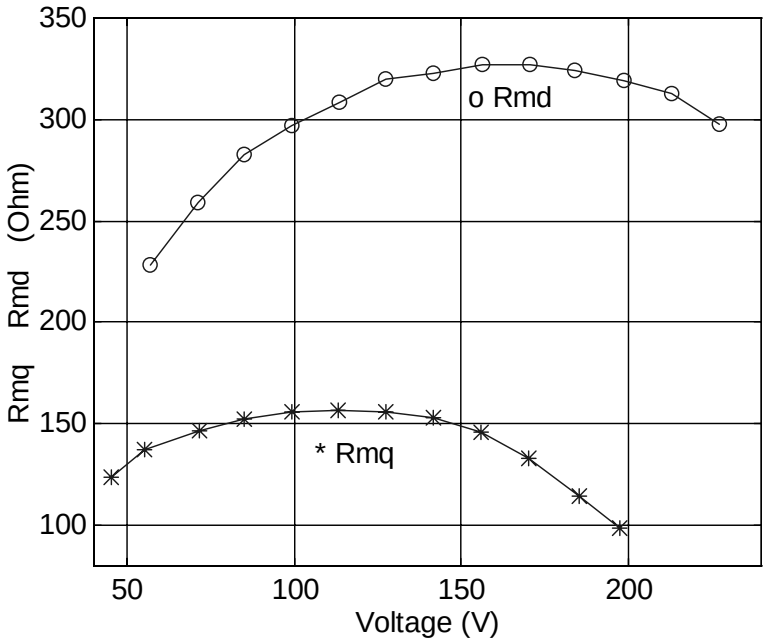

Figure 3.9. Experimental values of q-d core loss resistances vs peak input voltage.

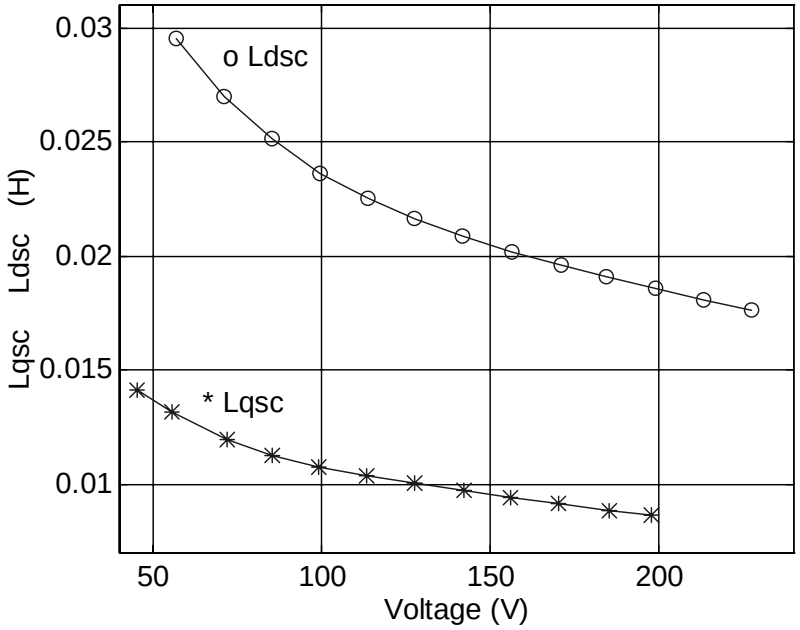

Figure 3.10. Experimental values sum of q -d axis leakage inductances vs peak input voltage.

CHAPTER 4

ANALYSIS OF BATTERY INVERTER SINGLE-PHASE INDUCTION GENERATOR SYSTEM WITH IMPEDANCE LOAD

4.1 Introduction

In this chapter, the steady-state analysis and simulation of the battery inverter single-phase induction generator system feeding an impedance load will be presented. A block diagram describing the proposed battery-PWM inverter single-phase induction generator (SPIG) is shown in Figure 4.1.

The battery inverter single-phase induction generator system with impedance load will find applications in isolated areas. The generator system can be used as a source of heating and it can also be used for lighting load.

This chapter gives a description of the generator system, dynamic and steady-state models, steady-state characteristics and simulation results.

The first part of this chapter deals with generator system description and the development of the mathematical model for the generator system feeding an impedance

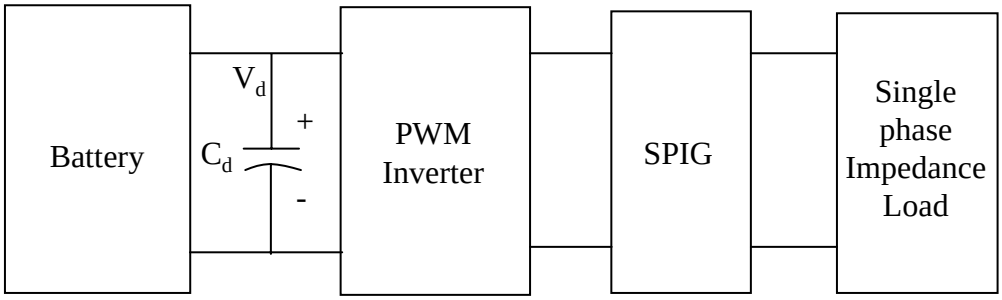

Figure 4.1. Block diagram of the proposed system.

load using q-d stationary reference frame transformation. Next, the dynamic mathematical model developed is used for the simulation of the generator system with an impedance load. The simulation results are then discussed with the experimental results.

The generator system steady-state mathematical model is developed. This model is then used to predict the steady-state variables of the generator system with an impedance load. The comparison between experimental results and predicted results of the generator system with impedance load will be examined. The measured state variables at different loads and speeds are also presented.

4.2 Mathematical Model of System

The generator system is comprised of battery, PWM inverter, and single-phase generator. The generator system schematic is shown in Figure 4.2. The bipolar voltage switching scheme is used in the switching of the bridge IGBT transistors. The full-bridge bipolar PWM inverter is fed with a battery connected through a capacitor C_d to the auxiliary winding. The single-phase induction generator is excited by adjusting the modulation index of the full-bridge bipolar PWM inverter. In addition to providing excitation for the single-phase induction generator, the inverter also supplies reactive power to the load [13, 16]. With the single-phase induction generator excited, it supplies real power to the load. The battery acts as a source or sink of real power depending on the real power requirement of the load and generator. When the real power supplied by the generator exceeds the load power requirement and losses, the excess power charges the battery through the bi-directional PWM inverter. The battery supplies real power when

the load power demand exceeds that provided by the generator to the load. One advantage of this system topology is that controlling the modulation index of the inverter the load voltage can be easily regulated.

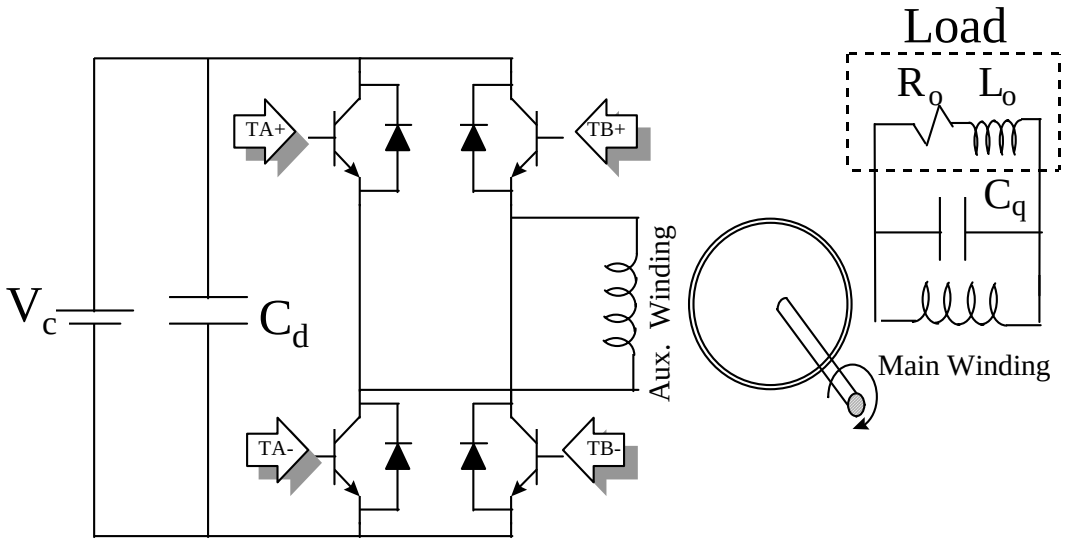

Figure 4.2. Schematic diagram of the single-phase induction generator with a battery-PWM inverter system.

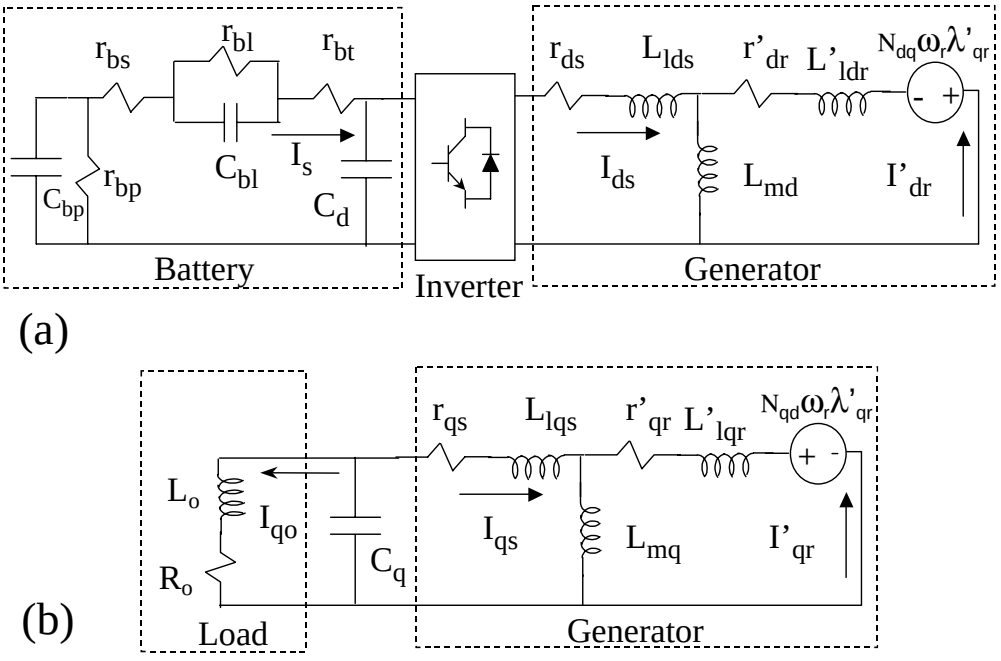

Figure 4.3. The q-d equivalent circuit of the battery-PWM inverter generator system. (a) d-axis circuit, (b) q-axis circuit.

The q-d equivalent circuit for the generator system is shown in Figure 4.3 with equivalent circuit of the battery, PWM inverter, and the load.

The dynamic equations of the lead-acid battery are given as [31]

$$C_{bp}\,pV_{bp} = I_s - \frac{V_{bp}}{r_{bp}} \tag{4.1}$$

$$C_{b1}\,pV_{b1} = I_s - \frac{V_{b1}}{r_{b1}} \tag{4.2}$$

$$V_d = V_{bp} - V_{b1} - I_s\left(r_{bs} + r_{bt}\right) \tag{4.3}$$

The output battery voltage and open circuit battery voltage are V_d and V_{bpo}, respectively. The current flowing out of the battery is I_s, while r_{bt} is the equivalent resistance of the parallel/series battery connection. The parallel circuit of C_{b1} and r_{b1} is used to describe the energy and voltage during charging or discharging. C_{bp} is connected in parallel with r_{bp} to simulate the self-discharging of the battery. The battery output voltage is V_d. The derivative of the state with respect to time is denoted as p. The equations combining the state variables of the battery, PWM inverter and the auxiliary winding are

$$pV_d = \frac{1}{C_d}\left(I_s - I_{ds}S_a\right) \tag{4.4}$$

$$V_{ds} = S_a V_d \tag{4.5}$$

where S_a is the inverter switching function and C_d is the input filtering capacitance of the inverter. The auxiliary windings input voltage and current are V_{ds} and I_{ds}, respectively. The q-d equations of the single-phase induction generator and the impedance load in the stationary reference frame are as follows from Figure 4.3:

$$p\lambda_{ds} = V_{ds} - r_{ds}I_{ds} \tag{4.6}$$

$$p\lambda_{qs} = V_{qs} - r_{qs} I_{qs} \tag{4.7}$$

$$p\lambda'_{qr} = N_{qd}\omega_r \lambda'_{dr} - r'_{qr} I'_{qr} \tag{4.8}$$

$$p\lambda'_{dr} = -N_{dq}\omega_r \lambda'_{qr} - r'_{dr} I'_{dr} \tag{4.9}$$

$$pV_{qs} = -\frac{1}{C_q}\left(I_{qs} + I_{qo}\right) \tag{4.10}$$

$$pI_{qo} = \frac{1}{L_o}\left(V_{qs} - R_o I_{qo}\right). \tag{4.11}$$

The main winding voltage is V_{qs}, while the q-axis and load currents are I_{qs} and I_{qo}, respectively. The ratio of the number of turns of the q-axis winding and the d-axis winding is denoted as N_{qd}. The inverse of is N_{qd} is denoted as N_{dq}. The stator q and d axes currents are I_{qs} and I_{ds}, respectively, while those of the rotor referred circuits are I'_{qr} and I'_{dr}, respectively. The stator q and d axes flux linkages are λ_{qs} and λ_{ds}, respectively, while those of the rotor referred circuits are λ'_{qr} and λ'_{dr}, respectively. The q-d flux linkages are defined in terms of the q-d currents as

$$\lambda_{qs} = L_{qs} I_{qs} + L_{mq} I'_{qr} \tag{4.12}$$

$$\lambda_{ds} = L_{ds} I_{ds} + L_{md} I'_{dr} \tag{4.13}$$

$$\lambda'_{qr} = L'_{qr} I'_{qr} + L_{mq} I_{qs} \tag{4.14}$$

$$\lambda'_{dr} = L'_{dr} I'_{dr} + L_{md} I_{ds} \tag{4.15}$$

where $L_{qs} = L_{lqs} + L_{mq}$, $L_{ds} = L_{lds} + L_{md}$, $L_{qr} = L'_{lqr} + L_{mq}$, and $L_{dr} = L'_{ldr} + L_{md}$. The referred rotor q-d leakage inductance are L'_{lqr} and L'_{ldr}, respectively. The referred rotor q-d resistance are r'_{qr} and r'_{dr}, respectively. The referred stator q-d leakage inductances are L'_{lqs} and L'_{lds}, respectively, with the q-d magnetizing inductances given, respectively, as

L_{mq} and L_{md}. The stator per-phase resistance for the q-winding and the corresponding value for the d-axis winding are r_{qs} and r_{ds}, respectively. The load resistor and inductor are denoted as R_o and L_o, respectively. The electrical angular speed is ω_r.

The dynamics of the turbine is approximated by the following mechanical equation:

$$p\omega_r = \frac{P}{2J}(T_o - T_e) \tag{4.16}$$

$$T_e = \frac{P}{2}\left(N_{dq}\lambda'_{qr}I'_{dr} - N_{qd}\lambda'_{dr}I'_{qr}\right). \tag{4.17}$$

The moment of inertia and the number of poles of the generator are J and P, respectively, while the driving and generated electromagnetic torques are T_o and T_e, respectively.

4.3. Comparison of Simulation and Experiment Waveforms for the System Feeding a Resistive Load

This section includes the comparison between simulation and measured waveforms for battery inverter single-phase induction generator feeding a resistive load. MATLAB/Simulink was used in the simulation of the dynamic Equations in 4.1 to 4.15. Two different simulation and experimental conditions are examined. The first condition considers the generator system in the linear modulation region ($0 \le M_a \le 1$) while the second condition considers the generator system in the overmodulation region ($M_a \ge 1$).

4.3.1 Battery Inverter Generator System (Linear Modulation Region)

This section examines the simulation and experimental waveforms of the battery inverter generator system feeding a resistive load in the linear modulation region. The

generator system parameters are shown in appendix A. The experiment and simulation were carried out with a generator rotor speed of 1825 rpm and a load of resistance of 40.9 ohms. The modulation index was set at a value of 0.75 with a carrier frequency of 2 kHz and modulating frequency of 60 Hz. The battery voltage and load capacitor is 144 V and 180 μF, respectively.

Figure 4.4 shows the simulated and measured steady-state waveforms for the load voltage. A comparison the simulated and measured steady-state load voltage waveforms shows the load frequency and magnitude are quite close. The results indicate that the model used in the simulation predicted fairly well the laboratory experimental setup.

The steady-state waveform for the generator main winding current is shown in Figure 4.5. As we can observe from Figure 4.5, the main winding current is free of PWM inverter induced harmonics, which makes this scheme good, and does not need additional filtering. The result also indicates that the experiment differs a little in magnitude from the simulation result.

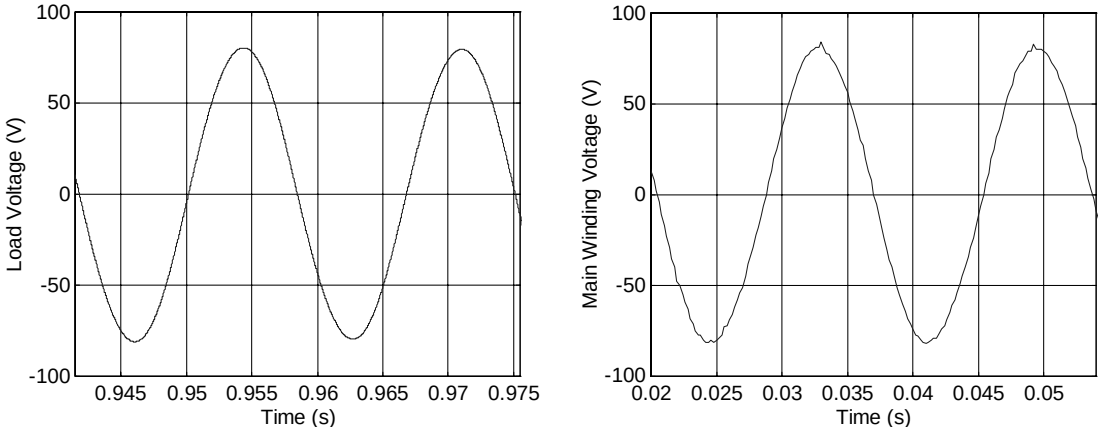

I. Simulation II. Experiment

Figure 4.4. Load voltage steady-state waveforms. Modulation index = 0.75, load impedance = 40.9 ohms, rotor speed = 1825 rpm

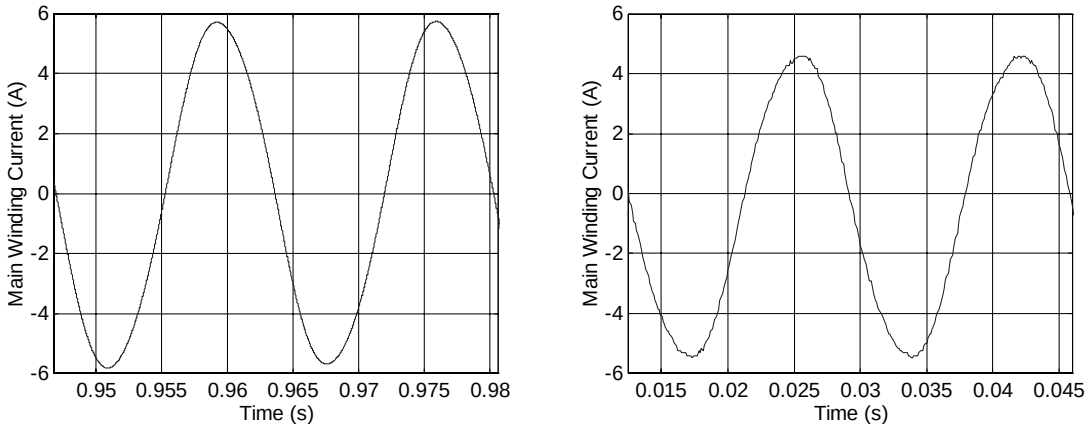

I. Simulation II. Experiment

Figure 4.5. Main winding current steady-state waveforms. Modulation index = 0.75, load impedance = 40.9 ohms, rotor speed = 1825 rpm.

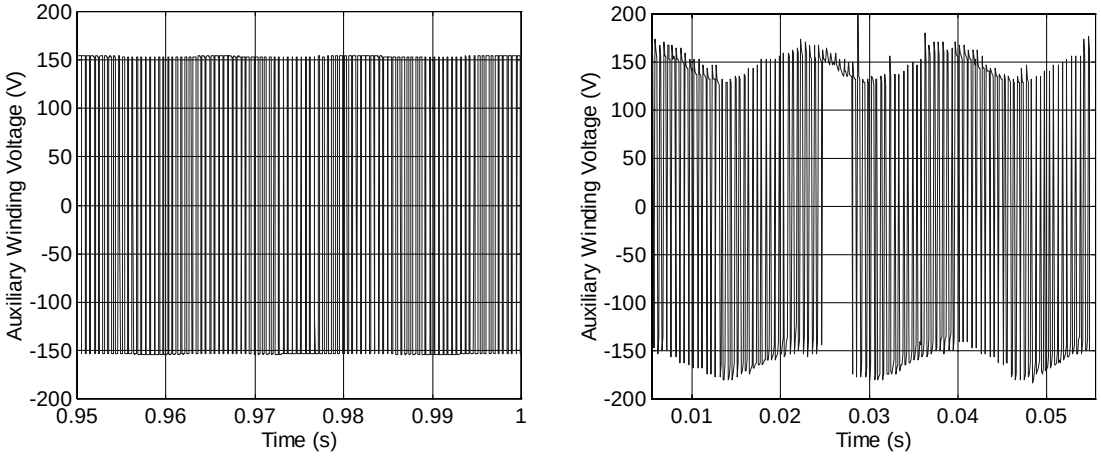

I. Simulation II. Experiment

Figure 4.6. Auxiliary winding voltage steady-state waveforms. Modulation index = 0.75, load impedance = 40.9 ohms, rotor speed = 1825 rpm.

The simulation and experimental waveforms of the auxiliary winding voltage of the single-phase induction generator are shown in Figure 4.6. The experimental result shows an envelope, which is due to the charging of the battery.

The simulated and experimental steady-state auxiliary current waveforms are in shown Figure 4.7. As expected, this current is not free from the PWM inverter induced harmonic.

The simulated and experimental current flowing through the load are shown in Figure 4.8; as in Figure 4.5 it is free from the harmonic produced by the PWM inverter. It can also be seen in Figures 4.4 and 4.6 that Figure 4.8 has the same frequency of the modulating signal of the inverter (60 Hz). This result clearly shows that the load frequency can be regulated by adjusting the modulating signal frequency appropriately.

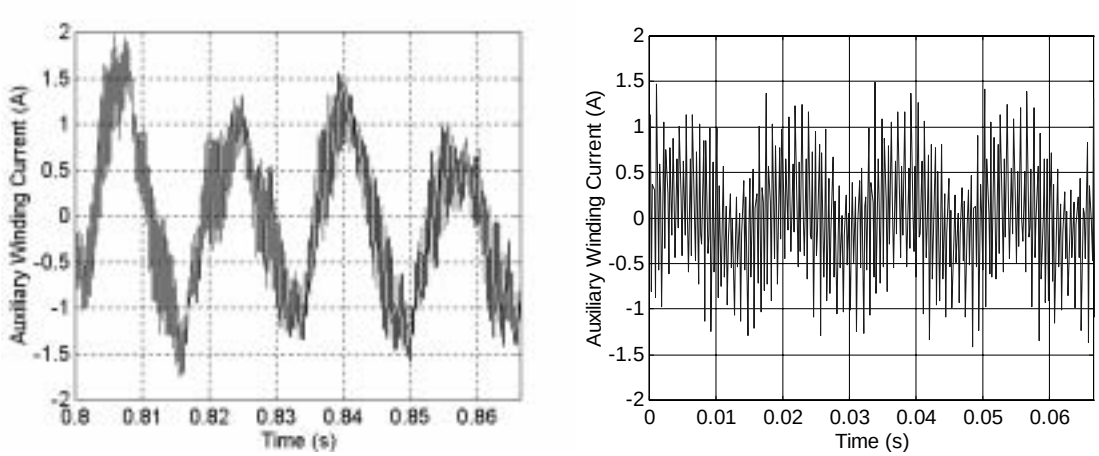

I. Simulation II. Experiment

Figure 4.7. Auxiliary winding current steady-state waveforms. Modulation index = 0.75, load impedance = 40.9 ohms, rotor speed = 1825 rpm.

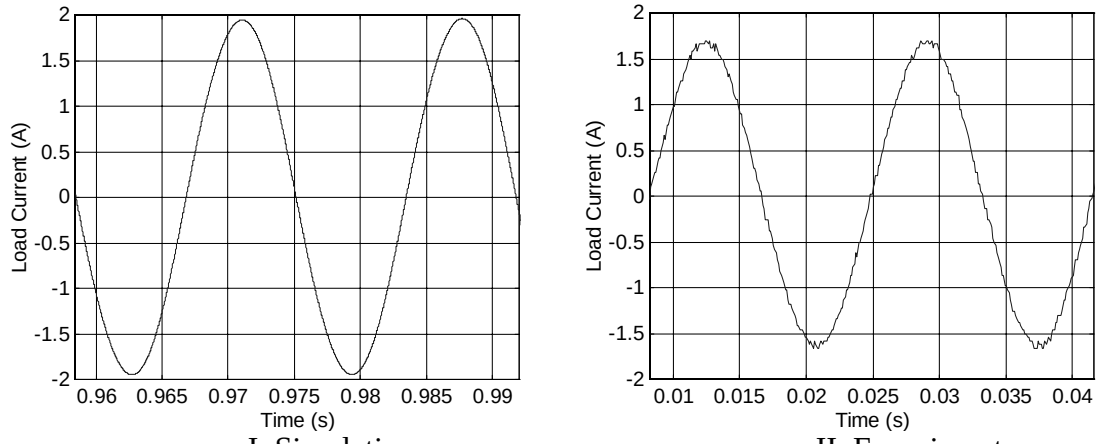

I. Simulation II. Experiment

Figure 4.8. Load current steady-state waveforms. Modulation index = 0.75, load impedance = 40.9 ohms, rotor speed = 1825 rpm.

4.3.2 Battery Inverter Generator System (Overmodulation Region)

This section examines the simulation and experimental waveform of the battery inverter generator system feeding a resistive load in the overmodulation region. The overmodulation region is when modulation index (M_a) is greater than one (M_a>1). The generator system parameters are shown in appendix A. The experiment and simulation were carried out with modulation index of 1.13, a load resistance of 41.2 ohms, and a generator rotor speed of 1830 rpm. The triangular wave signal frequency (carrier frequency) was set at 2 kHz and sinusoidal wave signal frequency (modulating frequency) was set at 60 Hz. The battery voltage and load capacitor are 144 V and 180 μF, respectively.

Experimental and simulation results of the load voltage under the overmodulation range are shown in Figure 4.9. The simulation result compares favorably with the experimental one. Again, the load voltage is uncontaminated by inverter harmonics.

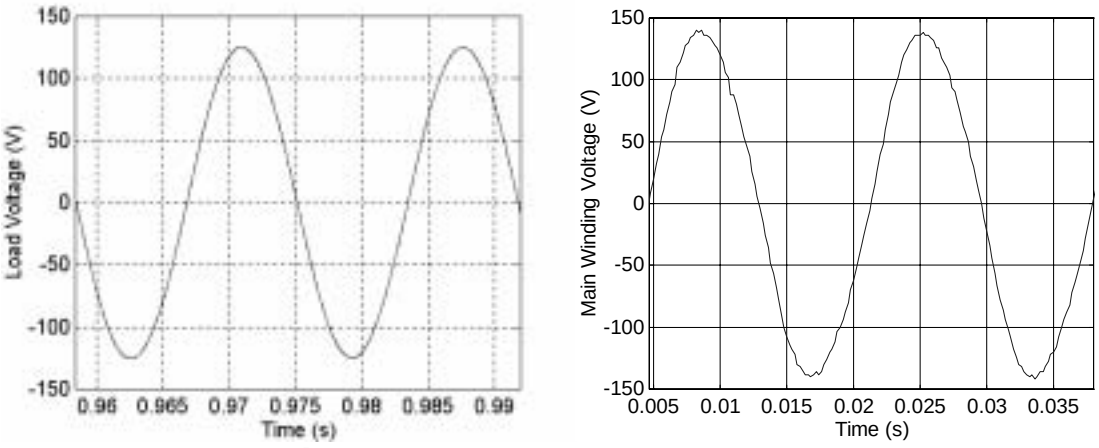

I. Simulation II. Experiment

Figure 4.9. Load voltage steady-state waveforms. Modulation index =1.13, load impedance = 40.9 ohms, rotor speed = 1830 rpm.

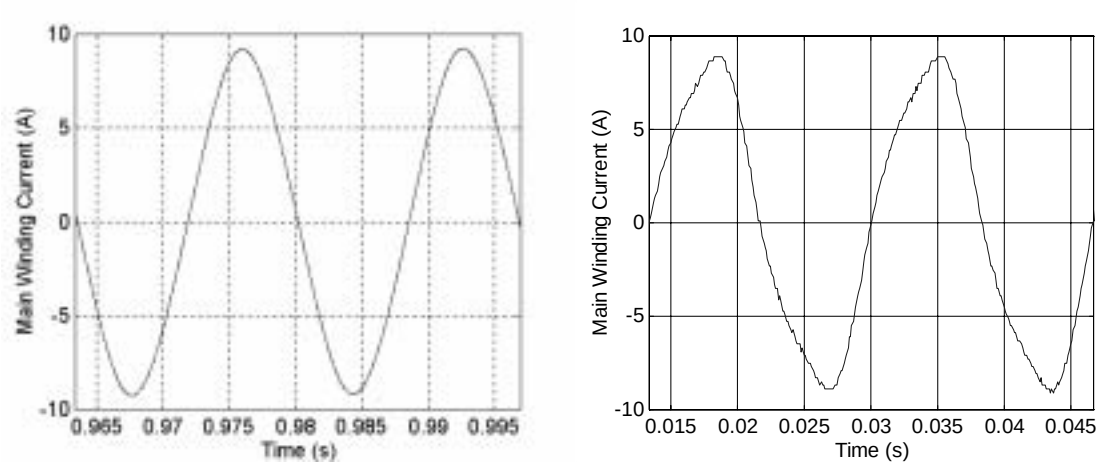

I. Simulation II. Experiment

Figure 4.10. Main winding current steady-state waveforms. Modulation index =1.13, load impedance = 40.9 ohms, rotor speed = 1830 rpm.

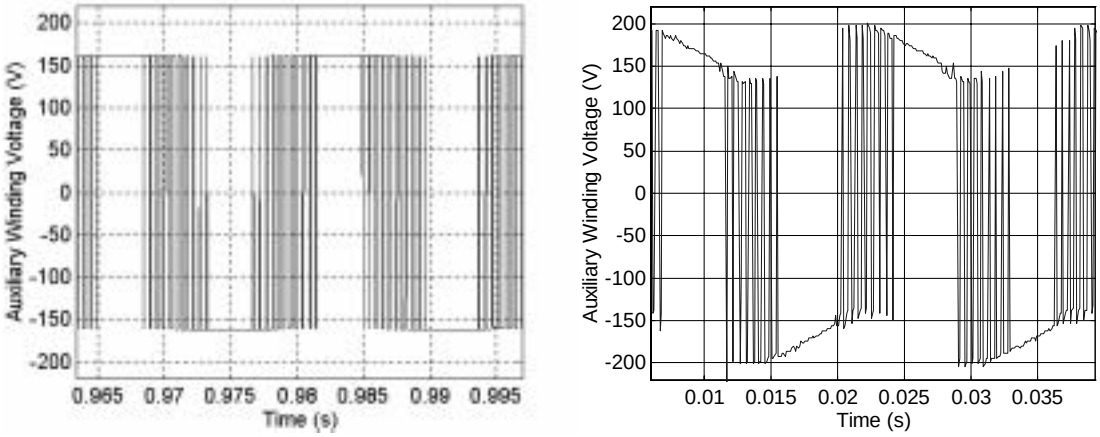

I. Simulation II. Experiment

Figure 4.11. Auxiliary winding voltage steady-state waveforms. Modulation index =1.13, load impedance = 40.9 ohms, rotor speed = 1830 rpm.

The simulated and experimental main winding currents are shown in Figure 4.10. As expected, the inverter induced harmonic are not present. The simulated and experimental results are quiet close with a frequency of 60 Hz, the modulating signal frequency.

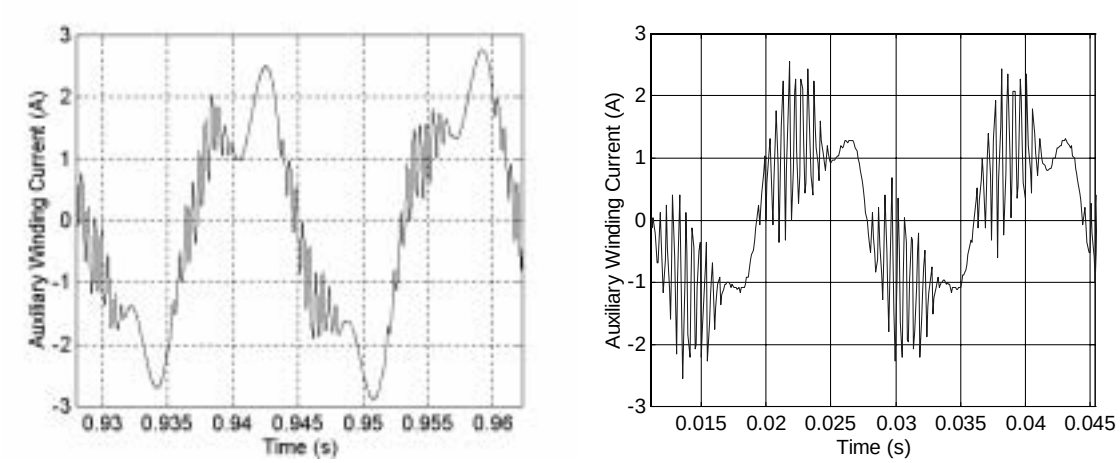

I. Simulation II. Experiment

Figure 4.12. Auxiliary winding current steady-state waveforms. Modulation index =1.13, load impedance = 40.9 ohms, rotor speed = 1830 rpm

The simulated and experimental auxiliary winding voltages are shown in Figure 4.11. The results indicate clearly that the PWM inverter is operating in the overmodulation range. The measured waveform of the auxiliary winding voltage peak is not constant due to the charging of the battery.

Figure 4.12 illustrates the simulated and experimental auxiliary winding current waveforms in the overmodulation range. The PWM inverter switching can be observed from the waveform.

The generator system load current is shown in Figure 4.13 for overmodulation range. The simulated and experimental load currents are seen to be free from the PWM inverter induced harmonics and its frequency 60 Hz the same as the modulating signal frequency. It also indicated that the simulated waveform compares well with the experimental waveform.

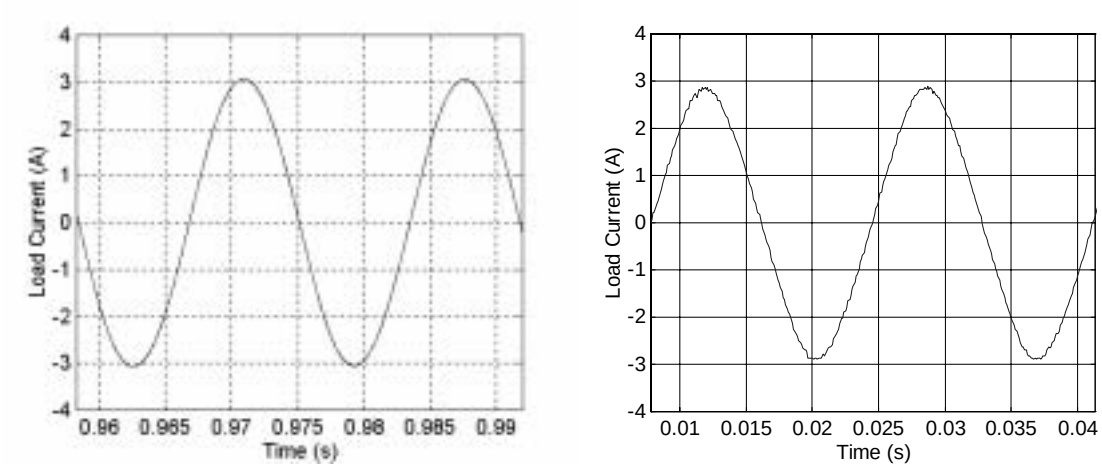

I. Simulation II. Experiment

Figure 4.13. Load current steady-state waveforms. Modulation index =1.13, load impedance = 40.9 ohms, rotor speed = 1830 rpm.

4.4 Steady State Calculation and Experiment

The single-phase induction generator - inverter battery system steady-state equations were derived by using harmonic balance technique. In order to reduce the complexity of the derivation of the generator system steady-state equation the following assumptions were made:

(i) Fundamental component of the state variable is used.

(ii) The battery current, I_s and inverter input voltage V_d, have second harmonic content riding on the constant d.c. component.

(iii) The flux linkages are sinusoidal.

(iv) The leakage inductances are constant.

(v) Core resistances are ignored.

Hence the state variables in steady state are given as

$$\lambda_{qs} = \mathrm{Re}\left(\lambda_{qss} e^{j\omega_e t} \right) \tag{4.18}$$

$$\lambda_{ds} = \mathrm{Re}\left(\lambda_{dss} e^{j\omega_e t}\right) \tag{4.19}$$

$$\lambda'_{qr} = \mathrm{Re}\left(\lambda'_{qrr} e^{j\omega_e t}\right) \tag{4.20}$$

$$\lambda'_{dr} = \mathrm{Re}\left(\lambda'_{drr} e^{j\omega_e t}\right) \tag{4.21}$$

$$V_{qs} = \mathrm{Re}\left(V_{qss} e^{j\omega_e t}\right) \tag{4.22}$$

$$V_{ds} = \mathrm{Re}\left(V_{dss} e^{j\omega_e t}\right) \tag{4.23}$$

$$I_{qo} = \mathrm{Re}\left(I_{qqo} e^{j\omega_e t}\right) \tag{4.24}$$

$$S_a = \mathrm{Re}\left(Me^{j\omega_e t}\right) \tag{4.25}$$

$$I_{ds} = \mathrm{Re}\left(I_{dss} e^{j\omega_e t}\right) \tag{4.26}$$

$$V_d = \mathrm{Re}\left(V_{do} + V_{d1} e^{j2\omega_e t}\right) \tag{4.27}$$

$$I_s = \mathrm{Re}\left(I_{so} + I_{s1} e^{j2\omega_e t}\right) \tag{4.28}$$

$$I_{qs} = \mathrm{Re}\left(I_{qss} e^{j\omega_e t}\right) \tag{4.29}$$

$$I'_{qr} = \mathrm{Re}\left(I_{qrr} e^{j\omega_e t}\right) \tag{4.30}$$

$$I'_{dr} = \mathrm{Re}\left(I_{drr} e^{j\omega_e t}\right) \tag{4.31}$$

where V_{dss}, V_{qss}, λ_{dss}, λ_{qss}, λ'_{qrr}, λ'_{drr}, I_{qqo}, I_{qss}, I_{dss}, I'_{qrr}, and I'_{drr} are complex peak quantities.

Substituting Equations 4.25 and 4.27 into Equation 4.5

$$V_{ds} = \mathrm{Re}\left[V_{do}\right] * \mathrm{Re}\left[Me^{j\omega_e t}\right] + \mathrm{Re}\left[Me^{j\omega_e t}\right] * \mathrm{Re}\left[V_{d1} e^{j2\omega_e t}\right]; \tag{4.32}$$

using the identity in Equation 3.88 and comparing terms Equation 4.32 becomes

$$\mathrm{Re}\left[V_{dss}e^{j\omega_e t}\right]=\mathrm{Re}\left[MV_{do}e^{j\omega_e t}\right]+\frac{1}{2}\left(\mathrm{Re}\left[M^{*}V_{d1}e^{j\omega_e t}\right]+\mathrm{Re}\left[MV_{d1}e^{j3\omega_e t}\right]\right). \tag{4.33}$$

Since the third harmonic content is assumed to be small it can be ignored resulting in

$$V_{dss}=MV_{do}+\frac{MV_{d1}}{2}. \tag{4.34}$$

Note that the magnitude of the left-hand side is equal to the right-hand side.

The differential of Equation 4.27 results in

$$\mathrm{p}V_d=\mathrm{Re}[\mathrm{p}V_{do}]+\mathrm{Re}\left[\mathrm{p}V_{d1}e^{j2\omega_e t}\right]+\mathrm{Re}\left[j2\omega_e V_{d1}e^{j2\omega_e t}\right]. \tag{4.35}$$

Substituting Equations 4.28, 4.25, and 4.26 into Equation 4.4

$$\mathrm{p}V_d=\frac{1}{C_d}\left[\mathrm{Re}[I_{so}]+\mathrm{Re}\left[I_{s1}e^{j2\omega_e t}\right]-\frac{1}{2}\left\{\mathrm{Re}\left[M^{*}I_{dss}\right]+\mathrm{Re}\left[MI_{dss}e^{j2\omega_e t}\right]\right\}\right]. \tag{4.36}$$

Comparing the terms in Equations 4.35 and 4.36 results in

$$\mathrm{p}V_{do}=\frac{1}{C_d}\left[I_{so}-\frac{\mathrm{Re}[MI_{dss}]}{2}\right] \tag{4.37}$$

$$\mathrm{p}V_{d1}+j2\omega_e V_{d1}=\frac{1}{C_d}\left[I_{s1}-\frac{MI_{dss}}{2}\right]. \tag{4.38}$$

Applying harmonic balance technique to the other voltage equation results in

$$p\lambda_{dss}=V_{dss}-r_{ds}I_{dss}-j\omega_e\lambda_{dss} \tag{4.39}$$

$$p\lambda_{qss}=V_{qss}-r_{qs}I_{qss}-j\omega_e\lambda_{qss} \tag{4.40}$$

$$p\lambda'_{qrr}=N_{qd}\omega_r\lambda'_{drr}-r'_{qr}I'_{qrr}-j\omega_e\lambda'_{qrr} \tag{4.41}$$

$$p\lambda'_{drr}=-N_{dq}\omega_r\lambda'_{qrr}-r'_{dr}I'_{drr}-j\omega_e\lambda'_{drr} \tag{4.42}$$

$$pV_{qss} = -\frac{1}{C_q}\left(I_{qss} + I_{qqo}\right) - j\omega_e V_{qss} \tag{4.43}$$

$$pI_{qqo} = \frac{1}{L_o}\left(V_{qss} - R_o I_{qqo}\right) - j\omega_e I_{qqo} \ . \tag{4.44}$$

Under steady-state operating conditions, the state variables are constant, making the derivatives in Equations 4.35- 4.44 above to be equal to zero. Then Equations 4.37 and 4.38 becomes

$$I_{so} = \mathrm{Re}\left[\frac{MI_{dss}}{2}\right] \tag{4.45}$$

$$I_{s1} = \frac{MI_{dss}}{2} + j2\omega_e C_d V_{d1}. \tag{4.46}$$

From Equations 4.1, 4.2, and 4.3

$$V_d = I_s R_d \tag{4.47}$$

where $R_d = r_{bp} + \left(r_{b1} + r_{bs} + r_{bt}\right)$.

Using Equations 4.47, 4.27, and 4.28

$$V_{do} = I_{so} R_d \tag{4.48}$$

$$V_{d1} = I_{s1} R_d \ . \tag{4.49}$$

From Equations 4.46 and 4.49, V_{d1} can be expressed as

$$V_{d1} = \frac{MR_d I_{dss}}{2\left(1 - j2\omega_e C_d R_d\right)} \ . \tag{4.50}$$

Then Equation 4.37 becomes

$$V_{dss} = MV_{do} + \frac{M^2 R_d I_{dss}}{4\left(1 - j2\omega_e C_d R_d\right)} \ . \tag{4.51}$$

The d-axis voltage equation can now be expressed as

$$MV_{do} + \frac{M^2 R_d I_{dss}}{4(1 - j2\omega_e C_d R_d)} - r_{ds} I_{dss} - j\omega_e \left(L_{ds} I_{dss} + L_{md} I'_{drr}\right) = 0 \ . \tag{4.52}$$

The other voltage equation is expressed as

$$V_{qss} - r_{qs} I_{qss} - j\omega_e \left(L_{qs} I_{qss} + L_{mq} I'_{qrr}\right) = 0 \tag{4.53}$$

$$N_{qd}\omega_r \left(L'_{dr} I'_{drr} + L_{md} I_{dss}\right) - r'_{qr} I'_{qrr} - j\omega_e \left(L'_{qr} I'_{qrr} + L_{mq} I_{qss}\right) = 0 \tag{4.54}$$

$$-N_{dq}\omega_r \left(L'_{qr} I'_{qrr} + L_{mq} I_{qss}\right) - r'_{dr} I'_{drr} - j\omega_e \left(L'_{dr} I'_{drr} + L_{md} I_{dss}\right) = 0 \tag{4.55}$$

$$\frac{1}{C_q}\left(I_{qss} + I_{qqo}\right) + j\omega_e V_{qss} = 0 \tag{4.56}$$

$$\frac{1}{L_o}\left(V_{qss} - R_o I_{qqo}\right) - j\omega_e I_{qqo} = 0 \, . \tag{4.57}$$

The saturation of the magnetizing inductance is accounted for by fitting an equation relating the magnetizing airgap flux to the magnetizing inductance L_{mq} and L_{md}. For the 1 h.p. generator, L_{mq} and L_{md} are related to the airgap flux linkages by [10]

$$\lambda_m = \left[\lambda_{qm}^2 + \lambda_{dm}^2\right]^{1/2} \tag{4.58}$$

$$\frac{1}{L_{mq}} - \left(15.177 - 17.62|\lambda_m| + 22.67\lambda_m^2\right) = 0 \tag{4.59}$$

$$\frac{1}{L_{md}} - \left(6.29 - 3.28|\lambda_m| + 3.042\lambda_m^2\right) = 0 \, . \tag{4.60}$$

The average electromagnetic torque is given as

$$T_{e1} = \frac{P}{4}\left(N_{dq}\lambda'_{qrr} I'^{*}_{drr} - N_{qd}\lambda'_{drr} I'^{*}_{qrr}\right) \, . \tag{4.61}$$

The nonlinear Equations 4.52-4.61 are solved for the state variables using MATLAB.

4.4.1 Experiment and Predicted Performance Results

The constant parameters for the generator system are shown in appendix A. The experiment was carried out with generator rotor speed of 1830 rpm and load resistances of 10.2 and 55.6 ohms. The battery voltage and load capacitor are 144 V and 210 μF, respectively.

Figure 4.14 shows how measured and calculated main winding voltages of the single-phase induction generator vary as a function of the modulation index. The result shows that in the linear region (M_a<1) the main winding voltage increases linearly by but in the over modulation region the main winding voltage becomes fairly constant. Hence in applications that require higher load voltages such as heating, the modulation index could be increased appropriately to give a higher voltage which leads to more energy.

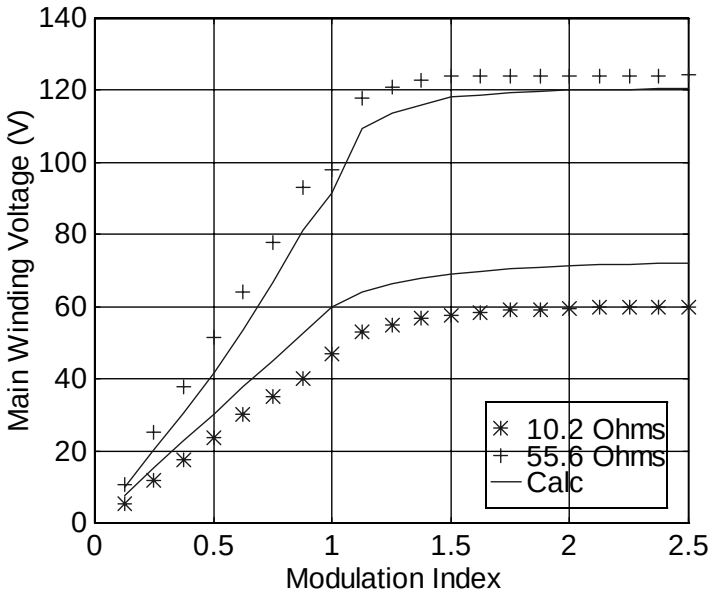

Figure 4.14: Measured and calculated main winding voltage as a function of modulation index. Constant rotor speed = 1830 rpm.

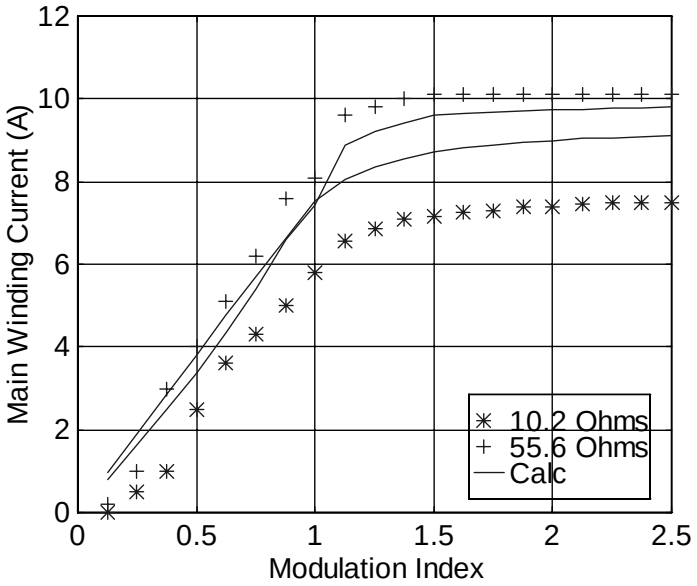

Figure 4.15: Measured and calculated main winding current as a function of modulation index. Constant rotor speed = 1830 rpm.

Figure 4.15 shows the variation of the measured and calculated main winding currents of the single-phase induction generator as a function of the modulation index. The current increases linearly in the linear region and becomes relatively constant then in the overmodulation region.

The measure and calculated rms load currents as a function of the modulation are shown in Figure 4.16. The result indicates that the steady state model predicts the load current more accurately at higher resistor value. This is attributed to the fact an inverter loss, which is not accounted for in the model, increases with increasing load/inverter output current.

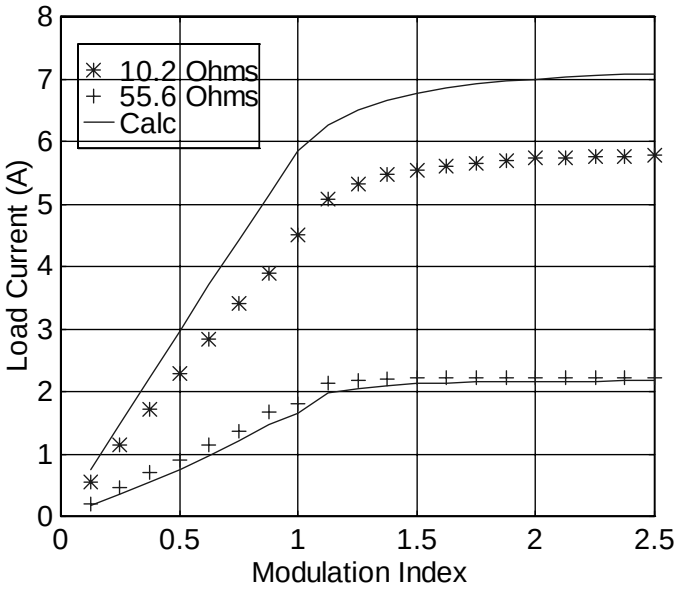

Figure 4.16: Measured and calculated load current as a function of modulation index. Constant rotor speed = 1830 rpm.

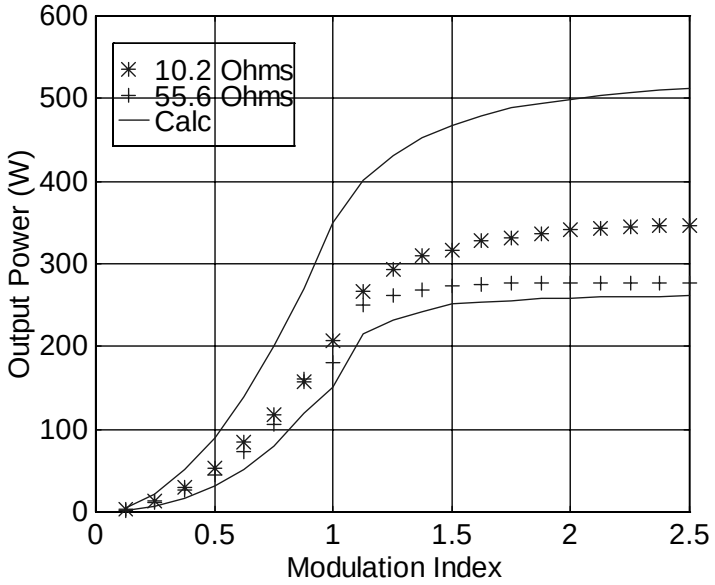

Figure 4.17: Measured and calculated load power as a function of modulation index. Constant rotor speed = 1830 rpm.

Figure 4.17 shows the variation of the measured and calculated load powers as a function of the modulation index. The result indicates that the steady state model predicts the load power more accurately at higher resistor value. This is attributed to the fact that

inverter loss, which is not accounted for in the model, increases with increasing load current.

Figures 4.18 and 4.19 show the variation of the measured and calculated auxiliary winding voltages and currents as a function of the modulation index, respectively. The calculated value at 10.2 ohms is relatively different from the measurement due to inverter switching and inverter losses that are not taken into account in the model. This difference is higher at a small value of load impedance (large load current). The result indicates that the steady state model predicts the load power more accurately at higher resistor value. This is attributed to the fact that losses are small at lower values of load currents.

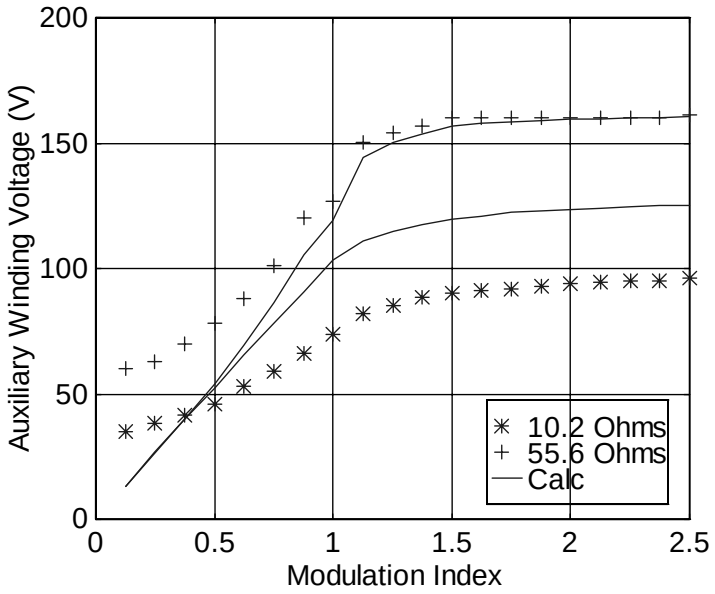

Figure 4.18: Measured and calculated auxiliary winding voltage as a function of modulation index. Constant rotor speed = 1830 rpm.

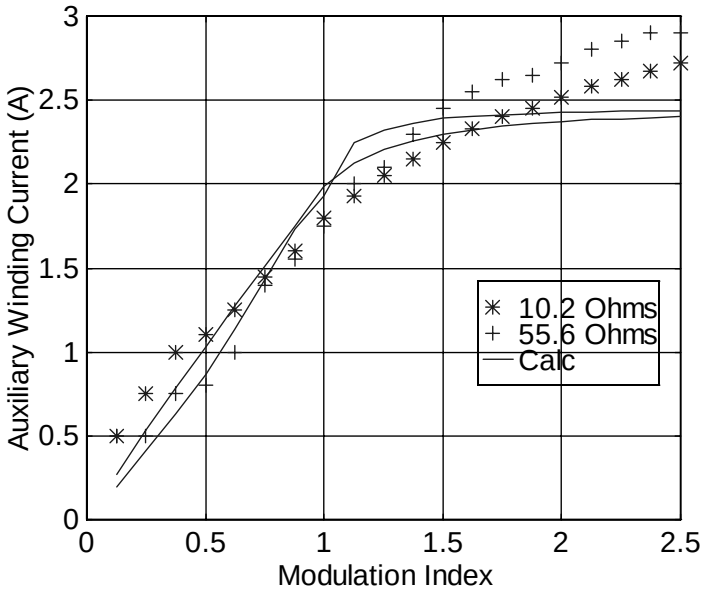

Figure 4.19: Measured and calculated auxiliary winding current as a function of modulation index. Constant rotor speed = 1830 rpm.

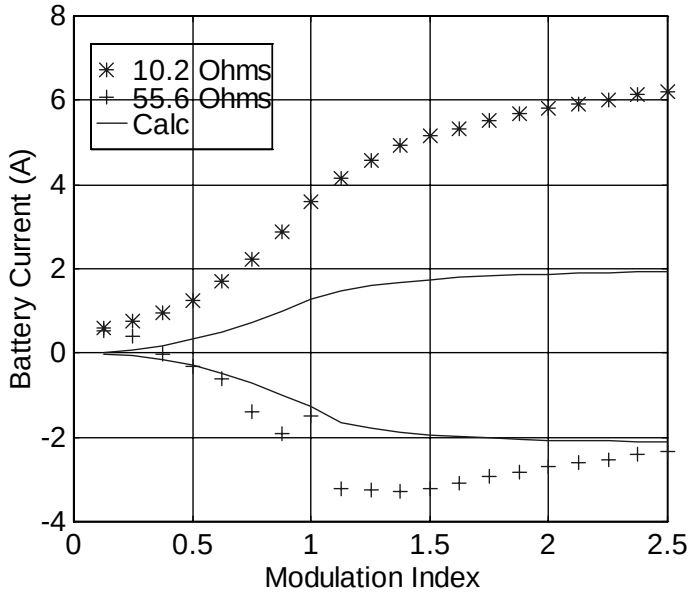

Figure 4.20: Measured and calculated battery current as a function of modulation index. Constant rotor speed = 1830 rpm.

The measured and calculated battery currents as a function of the modulation index are shown in Figure 4.20. The result indicates that the steady state model predicts the load power more accurately at higher resistor value. This is attributed to the fact that

losses are small at lower value of load current. The negative battery current (55.6 Ω) indicates the condition during which the generator system absorbs real power while the positive battery current (10.2 Ω) shows that the generator system supplies real power to the load.

4.4.2 Experiment Performance Results for Variable Resistive Load

This section discusses the measured steady state performance of the battery inverter generator system feeding a resistive load. The experiment setup is carried under two different load resistances of 41.2 and 20.8 ohms. The generator rotor speed and triangular wave signal frequency was kept at 1840 rpm and 2 kHz, respectively. The sinusoidal wave signal frequency was set at 60 Hz. The battery voltage and load capacitor are 96 V and 180 μF, respectively.

The variation of the generator system load voltage as a function of modulation index is shown in Figure 4.21. The load voltage increases with increase in the load resistance. The system increases linearly in the linear region then become non-linear in the over modulation region.

Figure 4.22 shows the single-phase induction generator main winding current as a function of the modulation index. The current gradually increases in the linear region then becomes relatively constant in the over modulation region.

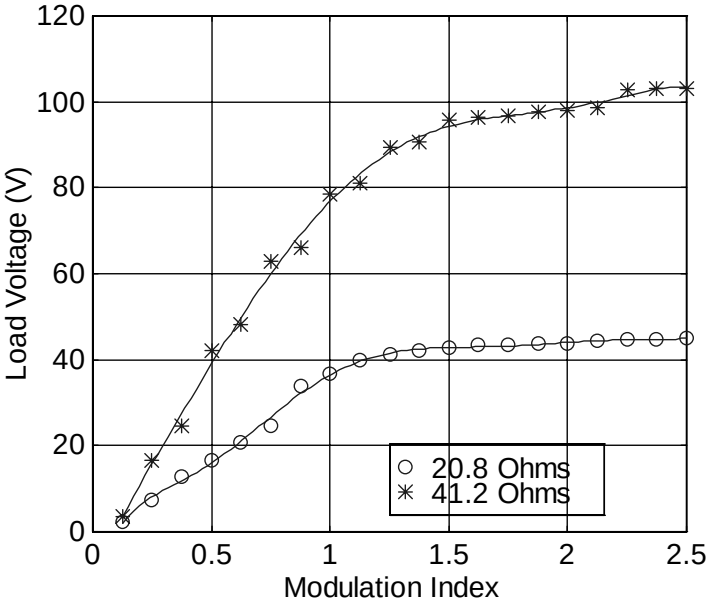

Figure 4.21: Measured load voltage as a function of modulation index. Constant rotor speed = 1840 rpm.

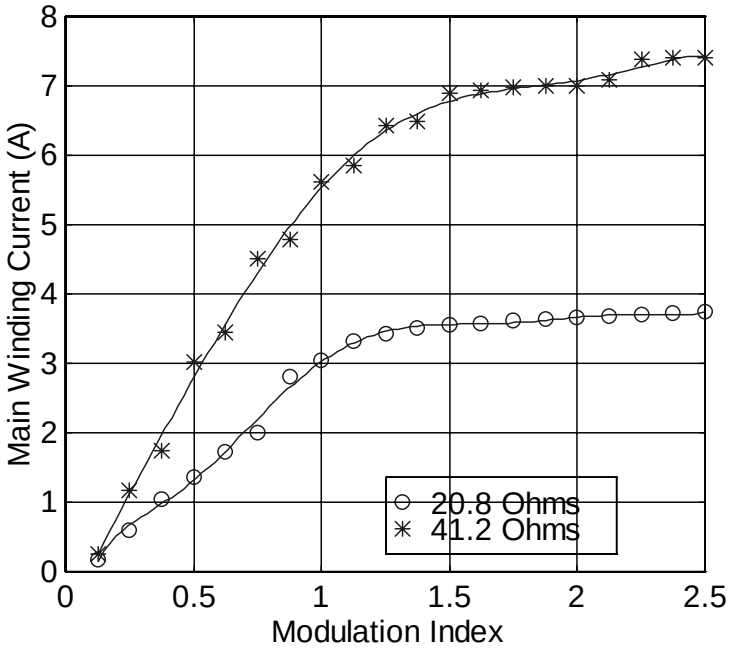

Figure 4.22: Measured main winding current as a function of modulation index. Constant rotor speed = 1840 rpm.

The output power from the generator system is shown in Figure 4.23 as a variation of modulation index. The power increases linearly for each resistance value in the linear region and it becomes fairly constant in the over modulation region.

The generator system measured steady-state characteristic for the load current as a function of modulation index for different load values, as shown in Figure 4.24. The load current is relatively constant in the over modulation region while it increases linearly in the linear region.

Figure 4.25 shows the single-phase induction generator measured auxiliary winding voltage as a variation of the modulation index. The load resistor value of 41.2 ohms has more voltage in the auxiliary winding voltage compared with the load resistor value of 20.8 ohms. The voltage across the auxiliary winding is fairly constant in the over modulation region while in the linear region it increases linearly.

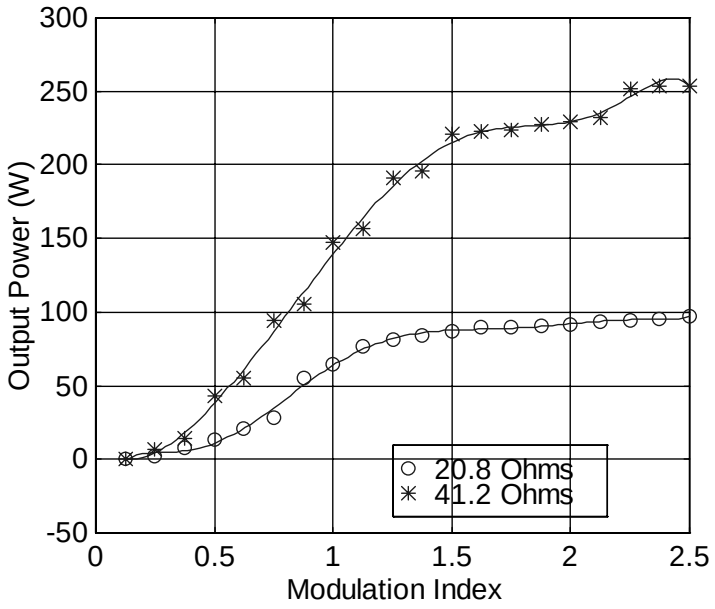

Figure 4.23: Measured Output Power as a function of modulation index. Constant rotor speed = 1840 rpm.

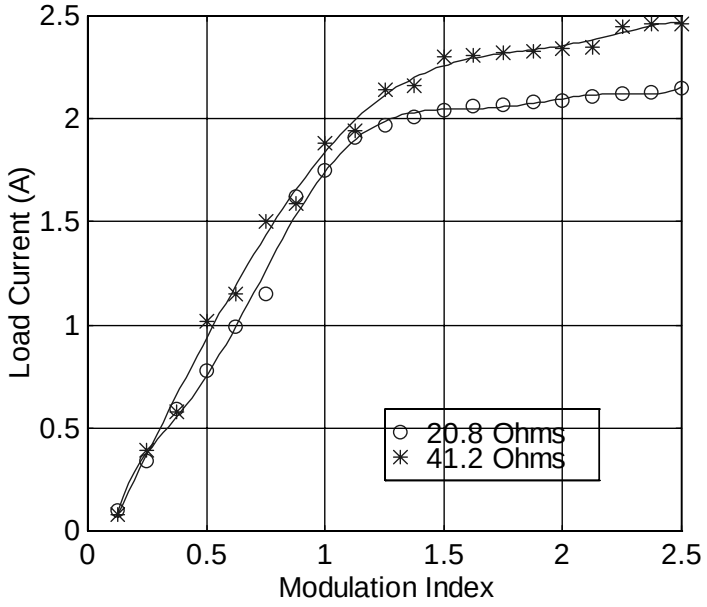

Figure 4.24: Measured Load Current as a function of modulation index. Constant rotor speed = 1840 rpm.

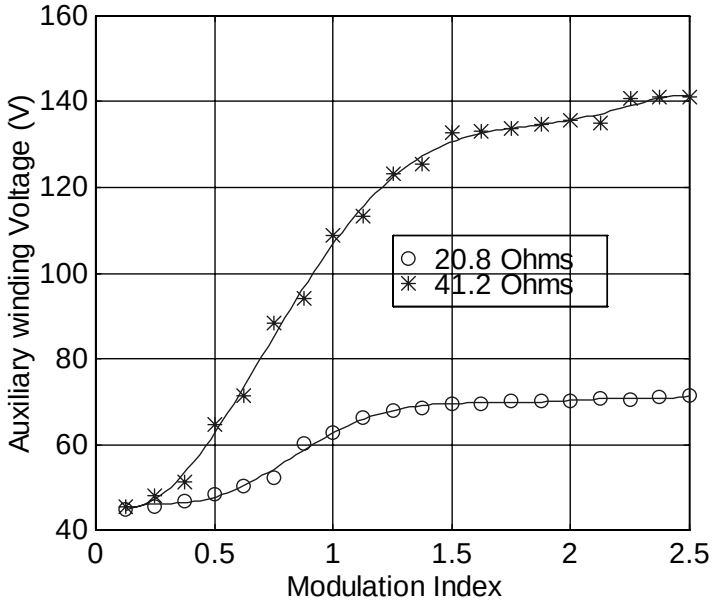

Figure 4.25: Measured auxiliary winding voltage as a function of modulation index. Constant rotor speed = 1840 rpm.

The single-phase induction generator measured auxiliary winding current as a function of the modulation index is shown in Figure 4.26. The current flow through the

auxiliary winding is increasing over the range of modulation index. This is due to the presence of higher harmonic in the auxiliary winding current as shown in the dynamic waveforms in Figures 4.7 and 4.12.

The generator system battery current for both resistor values as a function of modulation index in shown in Figure 4.27. At load resistance of 41.2 ohms the battery current is negative. This is due to the fact that the battery absorbs the excess power produced by the single-phase induction generator not required by the load. On the other hand, when the load resistance is 20.8 ohms, the battery current is positive. Under this condition the single-phase induction generator gives reduced power required by the load, hence the battery augments the power of the induction generator by providing extra power.

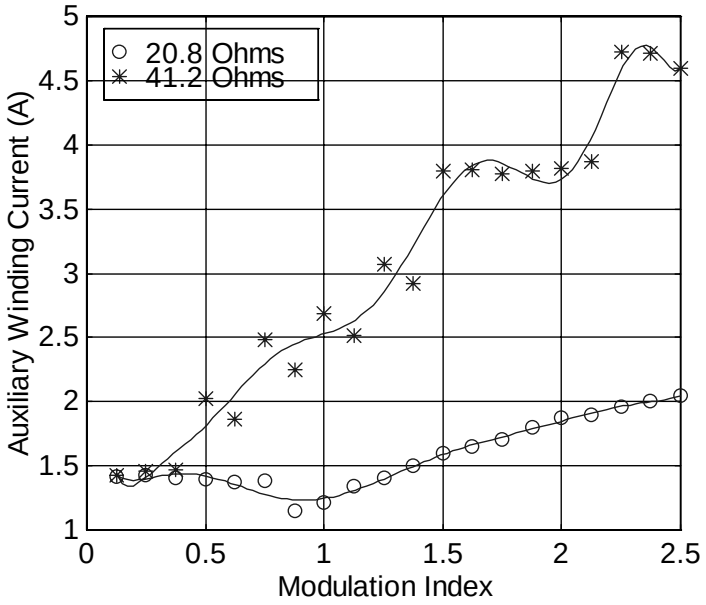

Figure 4.26: Measured auxiliary winding current as a function of modulation index. Constant rotor speed = 1840 rpm.

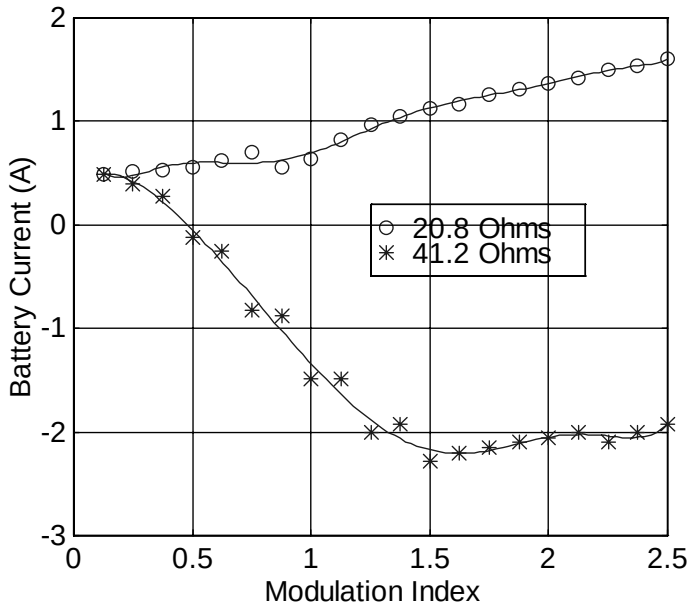

Figure 4.27: Measured battery current as a function of modulation index. Constant rotor speed = 1840 rpm.

4.4.3 Experiment Performance Results for Variable Generator Rotor Speed

This section discusses the measured steady state performance of the battery inverter generator system feeding a resistive load under variable generator rotor speed. The experiment is carried out with load resistance of 20.8 ohms and generator rotor speed of 1840 and 1850 rpm; the triangular wave signal frequency (carrier frequency) was set at 2 kHz and sinusoidal wave signal frequency (modulating frequency) was set at 60 Hz. The battery voltage and load capacitor are 96 V and 180 μF, respectively. The parameters of the test generator are given in the appendix A.

The generator system load voltage as a function of the modulation index is shown in Figure 4.28. The graph shows that with 10 rpm increase in the single-phase induction generator speed the load voltage is almost doubled. Also the load voltage is relatively

constant in the overmodulation region while in the linear region the load voltage increases linearly with the modulation index. Hence, the generator system load voltage can be increased either by increasing the modulation index or increasing the induction generator rotor speed.

Figure 4.29 shows the variation of the main winding current of the induction generator as a function of the modulation index. The main winding current at 1850 rpm is about twice the induction generator rotor speed at 1840 rpm. The main winding current increases linearly in the linear region then gradually becomes constant in the over modulation region.

The generator system output power as a function of the modulation index is shown in Figure 4.30. It is observed that at higher rotor speed there is more output power. In addition, more output power could be obtained by increasing the modulation index.

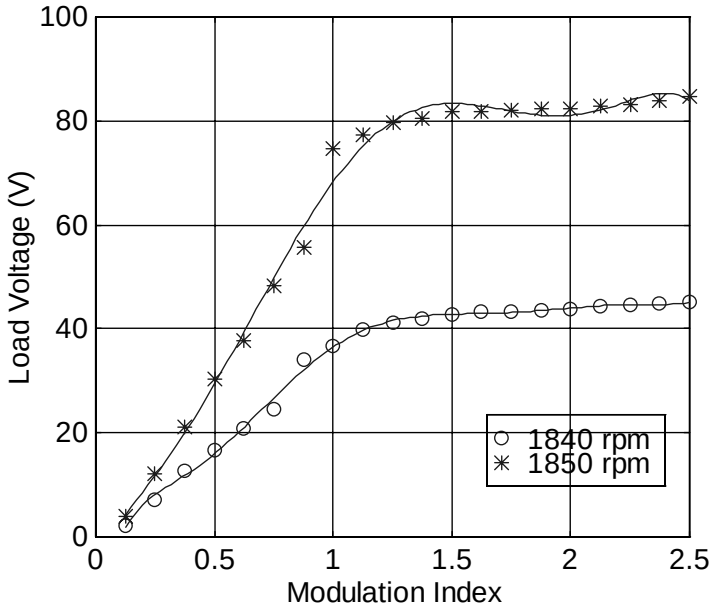

Figure 4.28: Measured load voltage as a function of modulation index. Constant load impedance = 20.8 ohms.

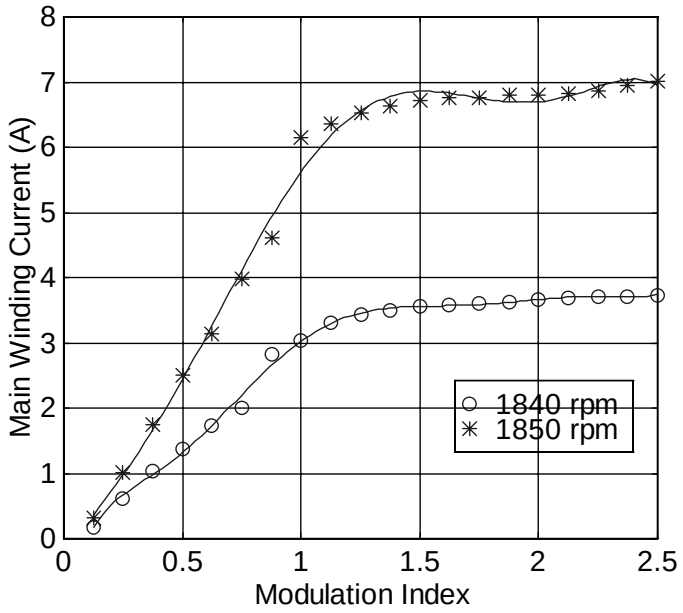

Figure 4.29: Measured main winding current as a function of modulation index. Constant load impedance = 20.8 ohms.

The generator system load current as a function of the modulation index is shown in Figure 4.31. The load current is higher for generator rotor speed of 1850 rpm as compared to 1840 rpm (Figure 4.31). Also, a higher load current can be achieved in the over modulation region.

Figure 4.32 shows the variation of the induction generator measured auxiliary winding voltage as a function of modulation index. The voltage across the auxiliary winding voltage is increased with increase in the rotor speed of the generator. A higher auxiliary winding voltage can be obtained by increasing the modulation index.

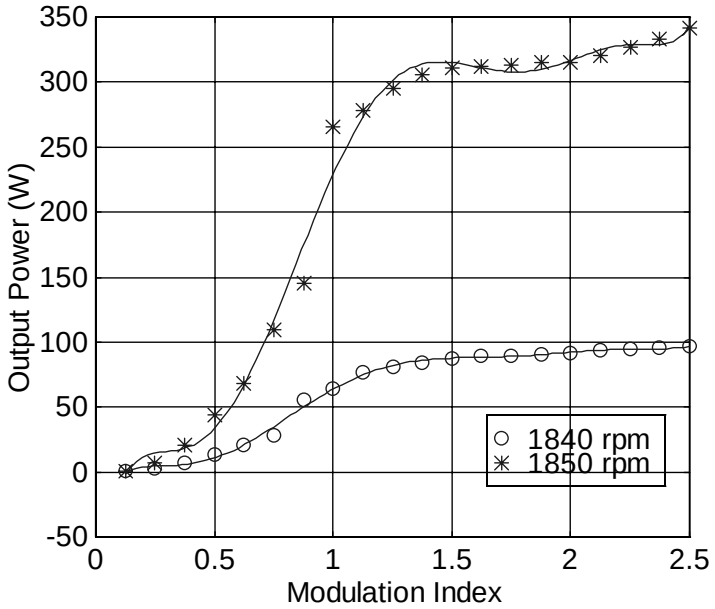

Figure 4.30: Measured Output Power as a function of modulation index. Constant load impedance = 20.8 ohms.

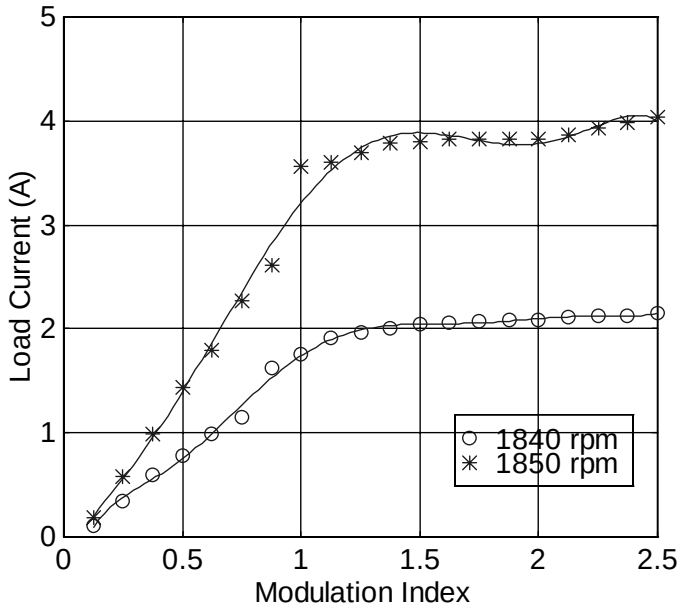

Figure 4.31: Measured Load Current as a function of modulation index. Constant load impedance = 20.8 ohms.

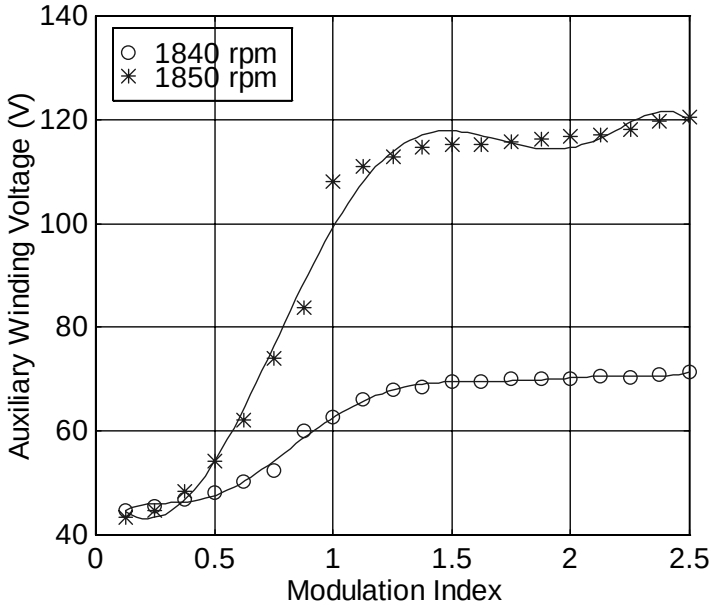

Figure 4.32: Measured auxiliary winding voltage as a function of modulation index. Constant load impedance = 20.8 ohms.

The single-phase induction generator auxiliary winding current as a function of the modulation index is shown in Figure 4.33. Due to the presence of higher harmonic in the auxiliary winding current, as shown in the dynamic waveforms in Figures 4.7 and 4.12, the current increases relatively over the range of modulation index.

Figure 4.34 shows the generator system battery current as a function of modulation index. It is observed that the figure shows the two modes of operation of the generator system (when the battery absorbs power and when the battery provides power). At generator rotor speed of 1850 rpm battery current is negative. This is due to the fact that the battery absorbs the excess power not required by the load produced by the single-phase induction generator. On the other hand, when the generator rotor speed is 1840 rpm, the battery current is positive. Under this condition the single-phase induction

generator gives lower power required by the load hence the battery augments the power of the induction generator by providing extra power.

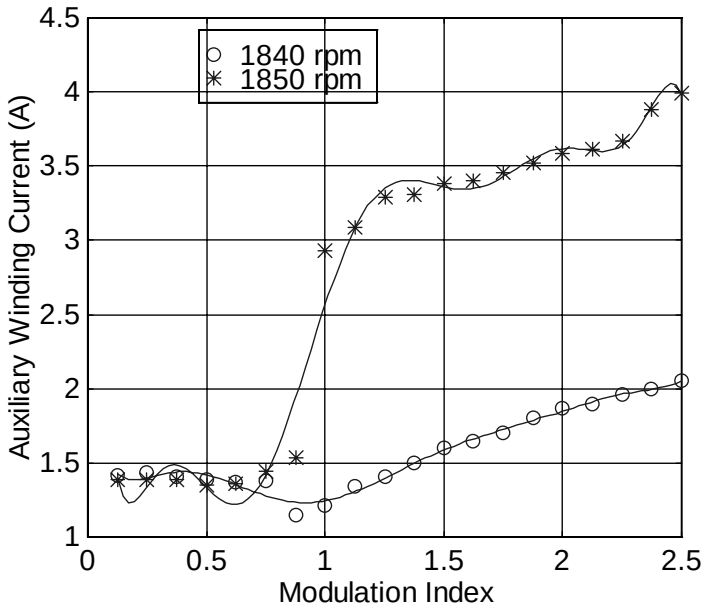

Figure 4.33: Measured auxiliary winding current as a function of modulation index. Constant load impedance = 20.8 ohms.

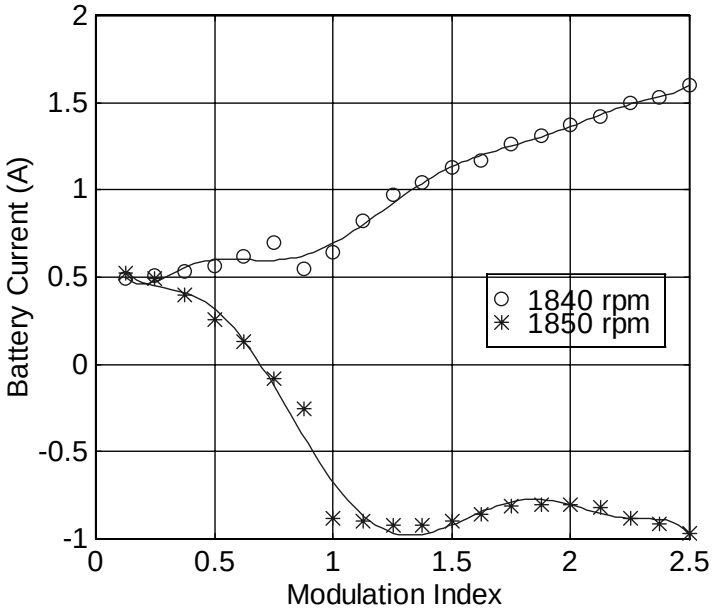

Figure 4.34: Measured battery current as a function of modulation index. Constant load impedance = 20.8 ohms.

4.4.4 Experiment Performance Results for Regulated Load Voltage

This section discusses the measured steady state performance of the battery inverter generator system feeding a resistive load. The modulation index of the PWM inverter is adjusted appropriately to ensure a constant load voltage. The experiment is carried out with load resistance of 41.1 ohms; the triangular wave signal frequency (carrier frequency) was set at 2 kHz and sinusoidal wave signal frequency (modulating frequency) was set at 60 Hz. The battery voltage and load capacitor are 144 V and 180 μF, respectively. The parameters of the test generator are given in the appendix A.

Figure 4.35 shows the auxiliary winding voltage of the induction generator as a function of generator slip. The figure indicates that maximum auxiliary winding voltage is obtained at about -0.05 slip under the regulated voltages considered. With a higher regulated load voltage there is higher auxiliary winding voltage.

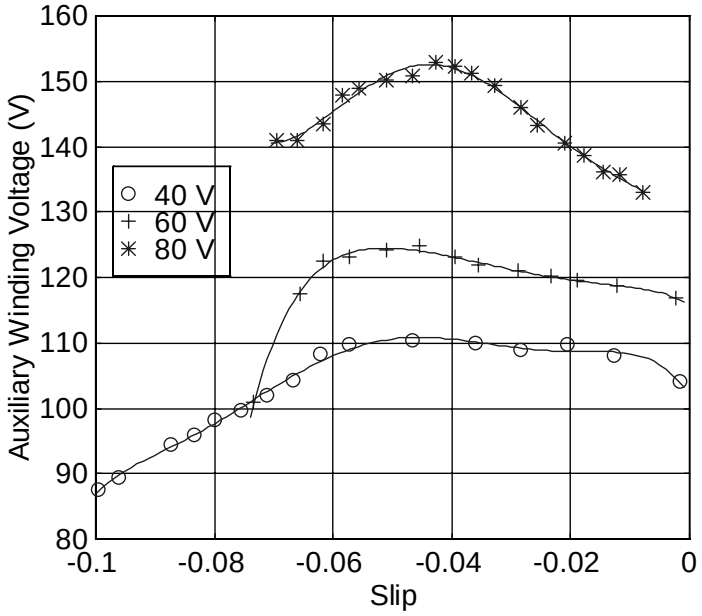

Figure 4.35: Measured auxiliary winding voltage as a function of slip. Constant load impedance = 41.1 ohms.

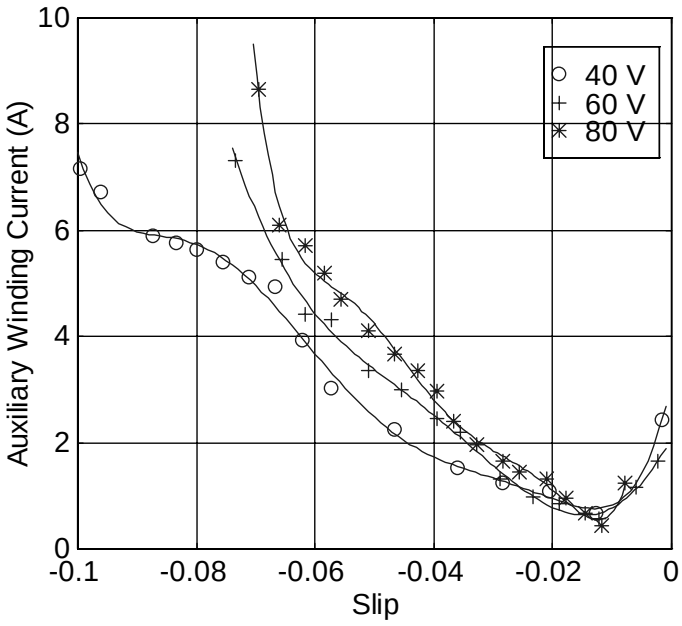

Figure 4.36: Measured auxiliary winding current as a function of slip. Constant load impedance = 41.1 ohms.

The auxiliary winding current of the generator as a function of generator slip is shown in Figure 4.36. The auxiliary winding current of the generator increases at decreasing values of generator slip. The graph also indicates that at higher values of induction generator slip the auxiliary winding currents at the given regulated voltage are generally the same.

Figure 4.37 shows the variation of the modulation index as a function of the generator slip. As the generator slip increases the modulation index also increases. The graph also indicates a higher regulated output voltage can be obtained by increasing the modulation index.

Figure 4.38 shows the measured battery current as a function of generator slip. The generator system takes power from the battery for a range of the rotor speeds, especially at high load voltage.

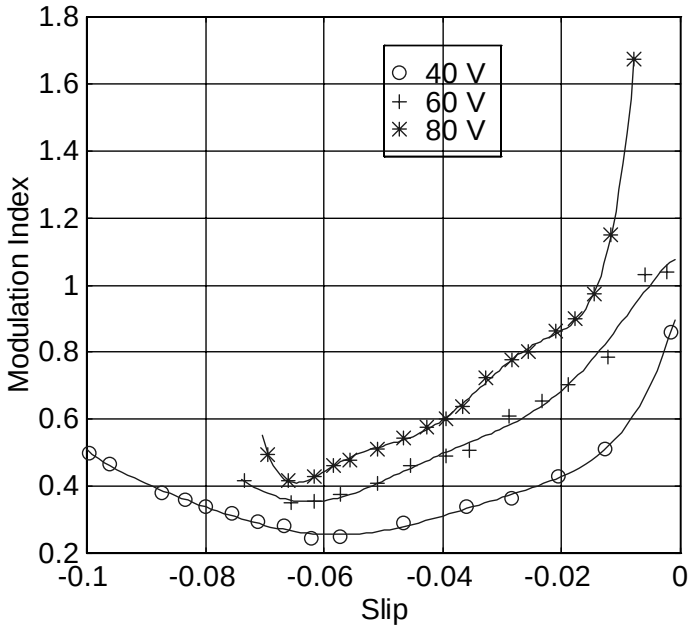

Figure 4.37: Measured modulation index as a function of slip. Constant load impedance = 41.1 ohms.

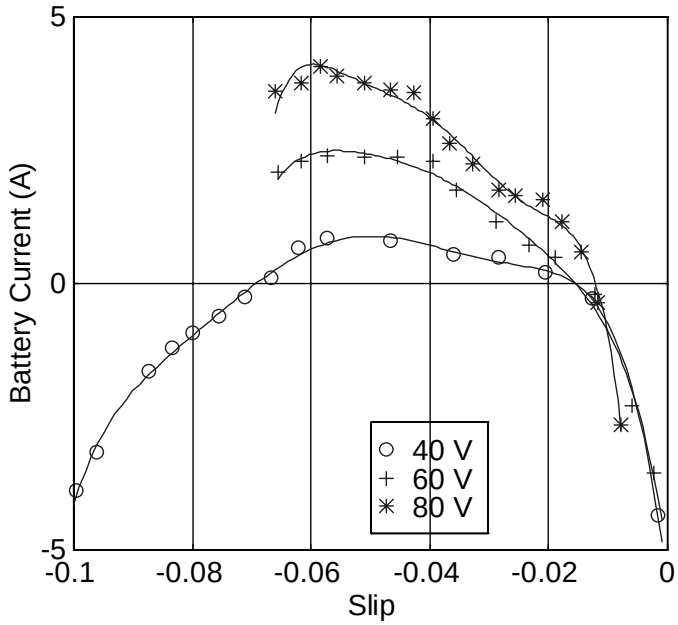

Figure 4.38: Measured battery current as a function of slip. Constant load impedance = 41.1 ohms.

4.5 Parametric Studies for the Battery Inverter Single-Phase Induction Generator with Impedance Load

This section gives a description of the influences of the generator system parameter on the generator system performance. In the study that follows, two different PWM inverter switching scheme are considered - the unipolar voltage switching and modified bipolar voltage switching.

A proper selection of the compensating capacitor, C_q, and the generator rotor speed can ensure that the generator system with impedance load operates in optimum condition. It can be seen from the steady state results in section 4.4, that the generator system has to operate in the overmodulation range to obtain higher a load voltage. The selection of the load capacitor, C_q and the generator rotor speed should be carefully done to ensure overall generator system efficiency and maximum power. This will be useful in applications such as heating where load voltage frequency is not important consideration. The generator system steady state was studied by keeping the load impedance and the load frequency constant.

In Figure 4.39 - 4.46 the modulation index is kept constant at a value of one, the load impedance of 50 ohms, and load frequency of 60Hz. Method A shows the PWM with unipolar voltage switching and Method B shows the PWM with bipolar voltage switching.

Figure 4.39 shows the contour plots of the load voltage with variation of the generator rotor speed and load capacitor, C_q with the two PWM methods. The graph shows that generally method B gives a higher input voltage than method A under the

same condition. From the graph, if maximum load voltage is desired, a higher value of C_q has to be selected and a generator rotor speed of about 1.08 p.u. is required.

A family of main winding currents as a variation of the generator rotor speed and load capacitor, C_q with the two PWM methods is shown in Figure 4.40. The graph shows that as the load capacitor increases the main winding current also increases. The

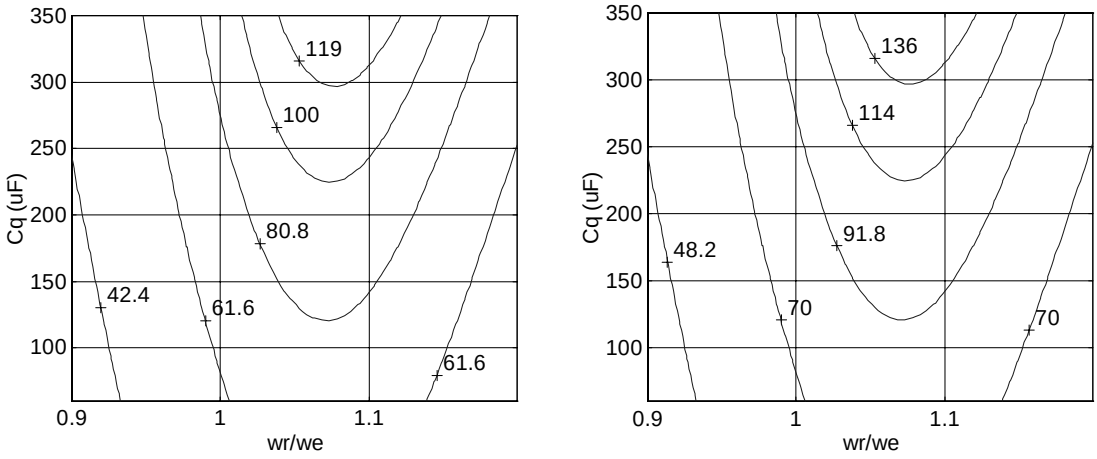

Method A Method B

Figure 4.39: Contour plot of load voltage, [V] as a variation of generator rotor speed (per unit) and load capacitor C_q.

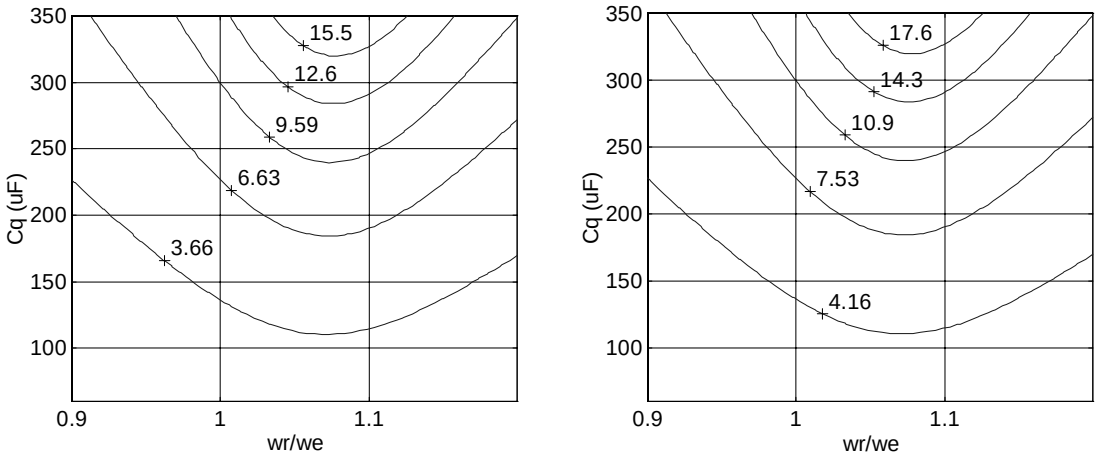

Method A Method B

Figure 4.40: Contour plot of main winding current, [A] as a variation of generator rotor speed (per unit) and load capacitor C_q.

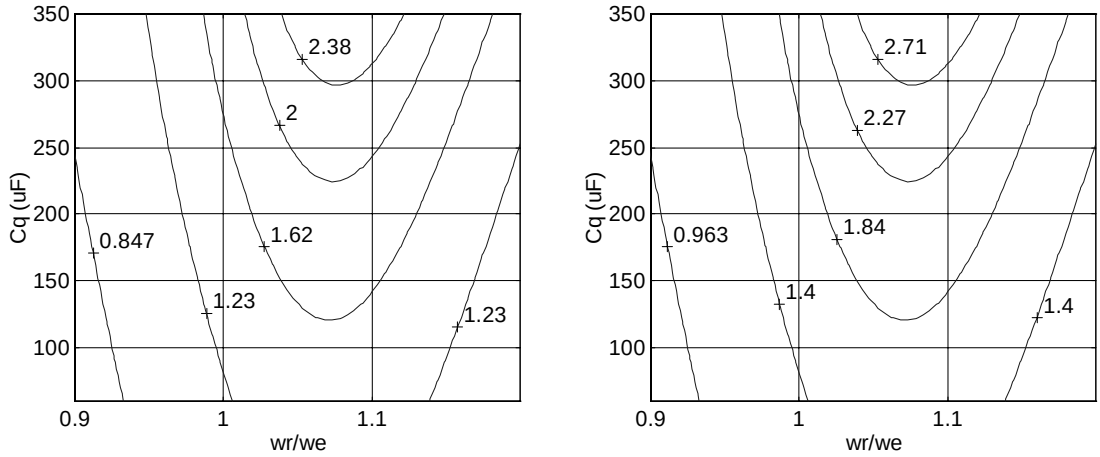

Method A Method B

Figure 4.41: Contour plot of load current, [A] as a variation of generator rotor speed (per unit) and load capacitor C_q.

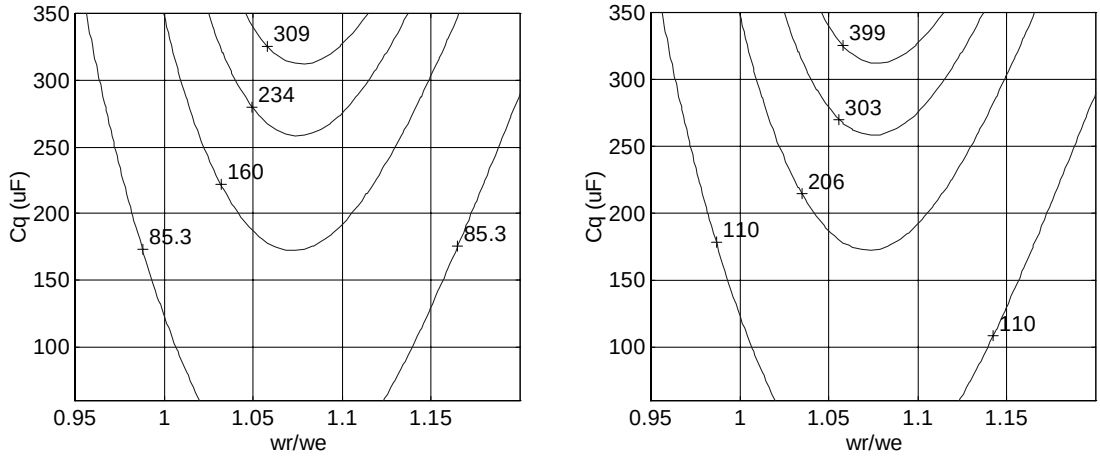

Method A Method B

Figure 4.42: Contour plot of load power, [W] as a variation of generator rotor speed (per unit) and load capacitor C_q.

maximum main winding current is obtained at a generator rotor speed of about 1.08p.u. Method B gives more main winding current than Method A.

Figure 4.41 gives the load current contour plots as a variation of the generator speed and load capacitor, C_q with the two PWM methods. Both methods A and B indicate that the load current decreases as the load capacitor decreases. The maximum load current can be obtained at a generator rotor speed of about 1.08p.u.

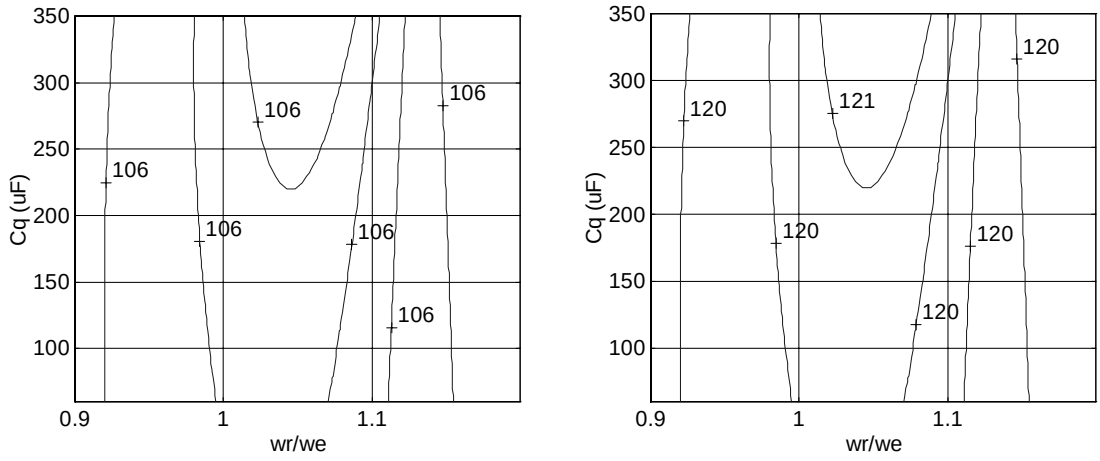

Figure 4.43: Contour plot of auxiliary winding voltage, [V] as a variation of generator rotor speed (per unit) and load capacitor C_q.

Figure 4.42 shows the load power contour as variation of the generator speed and load capacitor, C_q with the two PWM methods. The graph clearly indicates that for maximum power application of the generator system, the generator system must be operated at higher value of load capacitor, at about 1.075 p.u generator rotor speed. This will be useful for heating applications when optimum power is desired.

The family of auxiliary winding voltage and current as variation of the generator speed and load capacitor, C_q with the two PWM methods are shown in Figures 4.43 and 4.44. The auxiliary winding voltage is generally constant for both PWM methods. The auxiliary winding current, on the other hand, is fairly constant as the load capacitor changes for constant generator rotor speed. The minimum auxiliary winding current is obtained at generator rotor speed of about 1.0 p.u.

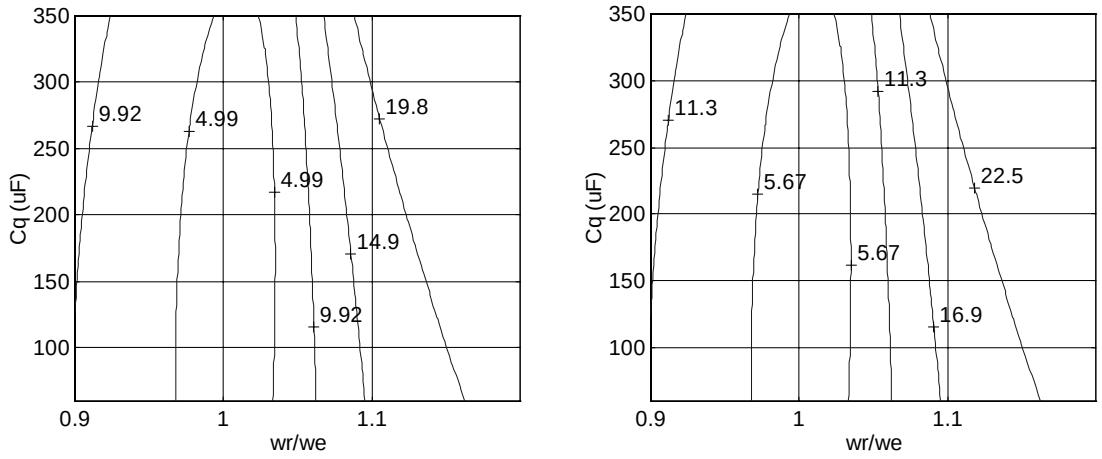

Method A Method B

Figure 4.44: Contour plot of auxiliary winding current, [A] as a variation of generator rotor speed (per unit) and load capacitor C_q.

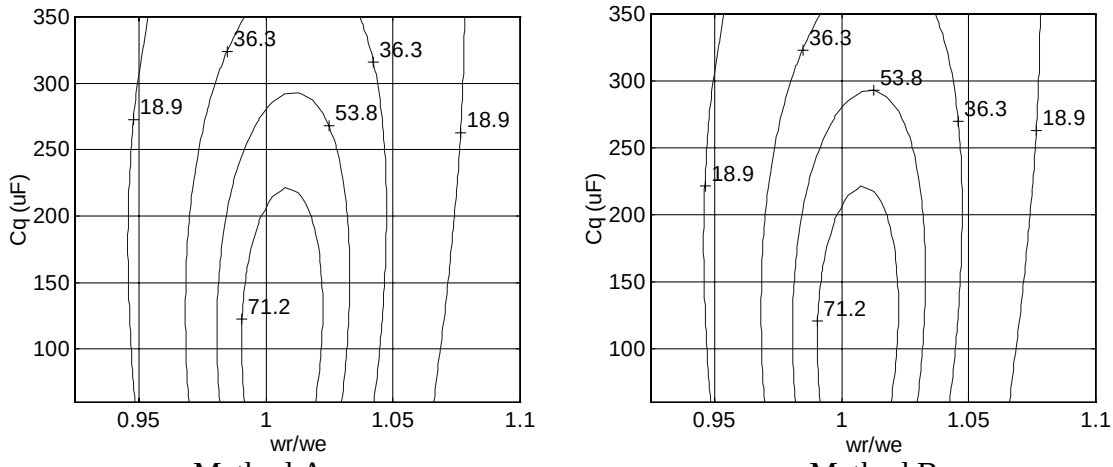

Method A Method B

Figure 4.45: Contour plot of efficiency as a variation of generator rotor speed (per unit) and load capacitor C_q.

Figure 4.45 shows the generator system efficiency contour as a function of the generator speed and load capacitor, C_q with the two PWM methods. The graph shows that generator system efficiency is better at lower values of load capacitor and at a generator rotor speed between 0.99 to 1.01 p.u.

The family of battery current curves as variation of the generator speed and load capacitor, C_q with the two PWM methods is shown in Figure 4.46. Generally the plots indicate that when the generator rotor speed is greater than 1.0 p.u. the battery current is negative (absorbs real power from the load) and when it is lesser than 1.0 p.u. the battery current is positive (supplies real power to the load) under different values of load capacitor.

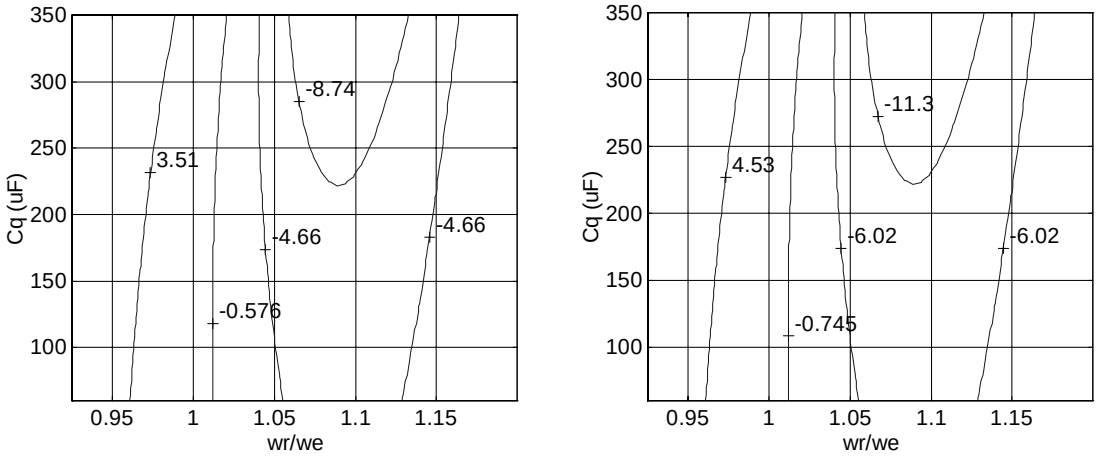

Method A Method B

Figure 4.46: Contour plot of battery current, [A] as a variation of generator rotor speed (per unit) and load capacitor C_q.

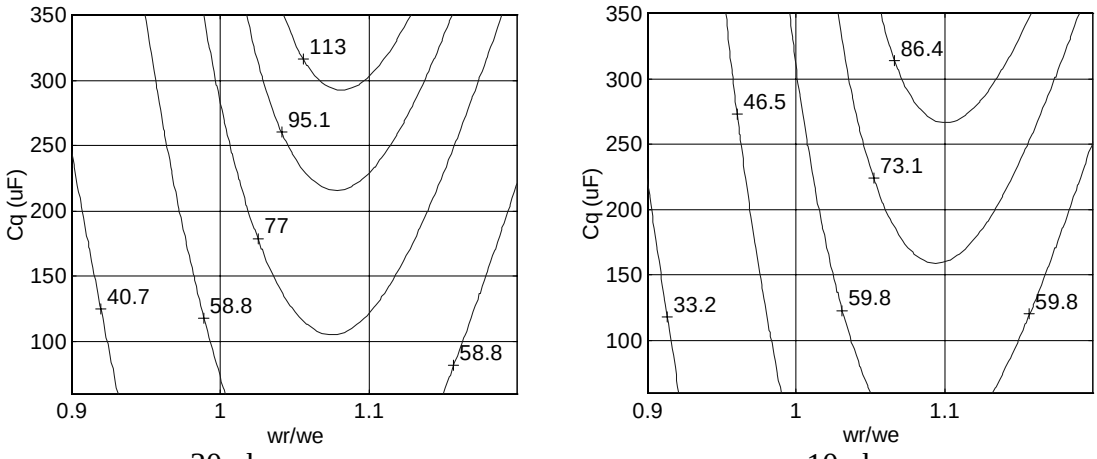

30 ohms 10 ohms

Figure 4.47: Contour plot of load voltage, [V] as a variation of generator rotor speed (per unit) and load capacitor C_q.

In Figures 4.47 - 4.49 the modulation index is kept constant at a value of one and load frequency of 60Hz with the PWM with unipolar voltage switching (Method B) and at load impedance of 30 and 10 ohms.

Figure 4.47 shows the contour plots of the load voltage with variation of the generator rotor speed and load capacitor, C_q with the two load impedance. The graphs generally have similar contours but differ simply in the load voltage magnitudes. As the load impedance increases the load voltage increases. In addition, to obtain maximum load voltage (also in Figure 4.39 method A) a higher value of C_q has to be selected and a generator rotor speed of about 1.08 p.u.

Figure 4.48 shows the contour plots of the generator system efficiency as a function of the generator rotor speed and load capacitor, C_q with two load impedance. Examining Figure 4.45 (Method A) and Figure 4.48; the generator system efficiency is seen to be better at lower value of load impedance at fixed value of load capacitor and generator rotor speed. The graphs also indicate that the generator system efficiency is higher at about (0.99 to 1.01 p.u.) generator rotor speed for different values of load capacitor.

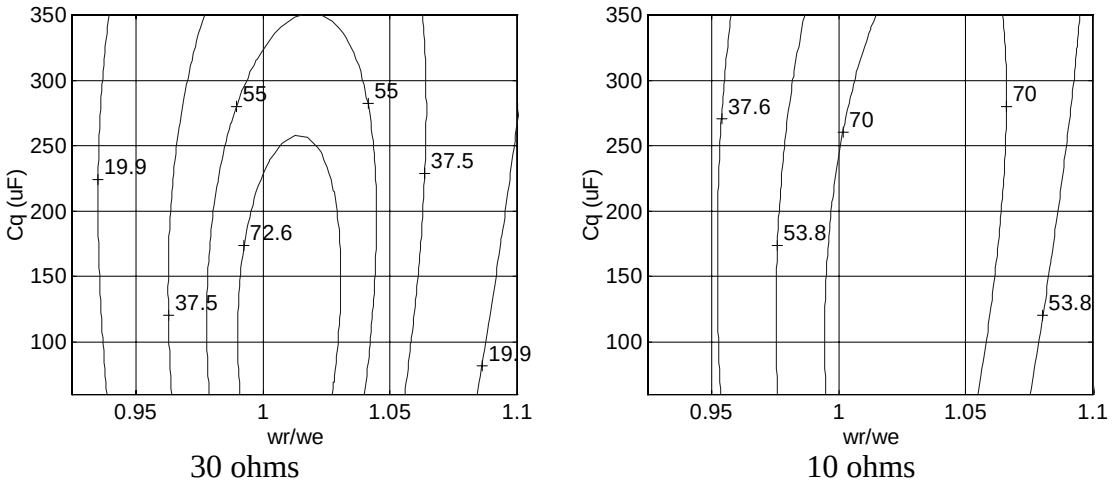

30 ohms 10 ohms

Figure 4.48: Contour plot of efficiency as a variation of generator rotor speed (per unit) and load capacitor C_q.

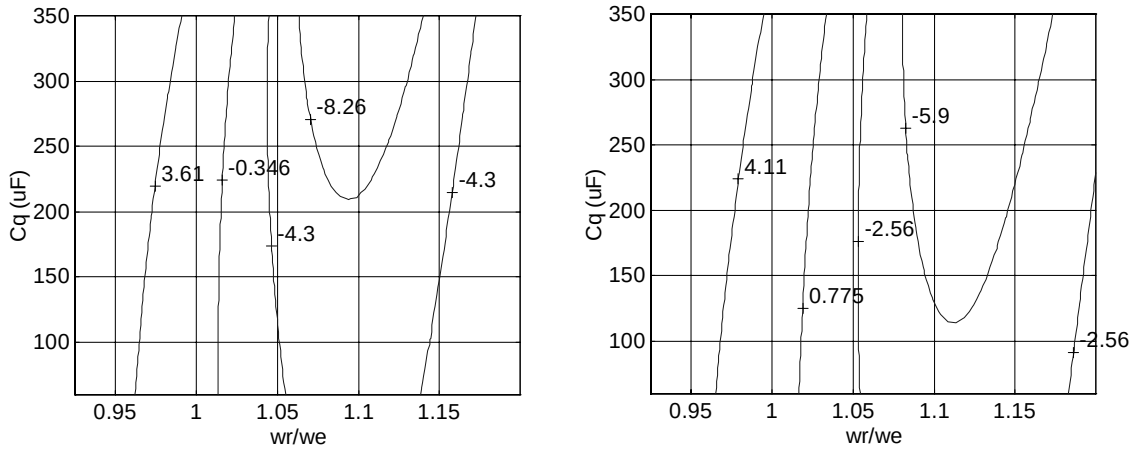

Figure 4.49: Contour plot of battery current, [A] as a variation of generator rotor speed (per unit) and load capacitor C_q.

Figure 4.49 shows the battery current contour curves as variation of the generator rotor speed and load capacitor, C_q under different load condition. Considering Figure 4.46 (Method A) with Figure 4.49, the battery current is observed to be more positive (or higher) as the load impedance decreases at constant load capacitor and generator rotor speed. When the battery current is negative it indicates that real power is being absorbed by the battery and when the battery current is positive it shows that the battery supplies real power to the load.

4.6 Transient and Dynamic Performance for the System Feeding an Impedance Load

This section examines the transient and dynamic performance of the battery inverter single-phase induction generator feeding a resistive load. The transient and dynamic studied gives a better understanding of the operation of the generator system and also shows how the generator system can perform with either variation in load or speed.

The generator system start-up process is simulated and the response of the generator system to changes in load is examined. Next the system dynamic performance with the generator rotor speed change is discussed.

4.6.1 Start-up Process

This section examines the start-up process for the battery inverter generator system feeding a resistive load. The simulation was carried out with generator rotor speed of 1860 rpm and a load of resistance of 20 ohms. The modulation index was set a value of 0.80 with a carrier frequency of 2 kHz and modulating frequency of 60 Hz.

The system load voltage build-up is shown in Figure 4.50. The load voltage waveform increases quickly until it reaches a steady-state peak value of about 80 volts. Figure 4.51 shows the start-up process of the system main winding current. The main winding current increases rapidly until it reaches a steady state value.

The auxiliary winding current waveform build-up is shown in Figure 4.52. The current decreases fast to a steady state peak value of about 4.0A. The transient waveform of the battery current is shown in Figure 4.53 during start up. The battery current is initially high then decreases to a steady state value. Initially the battery current is positive indicating that the battery supplies real power to meet the load requirement, then at steady state the battery current is negative indicating that the battery is absorbing real power.

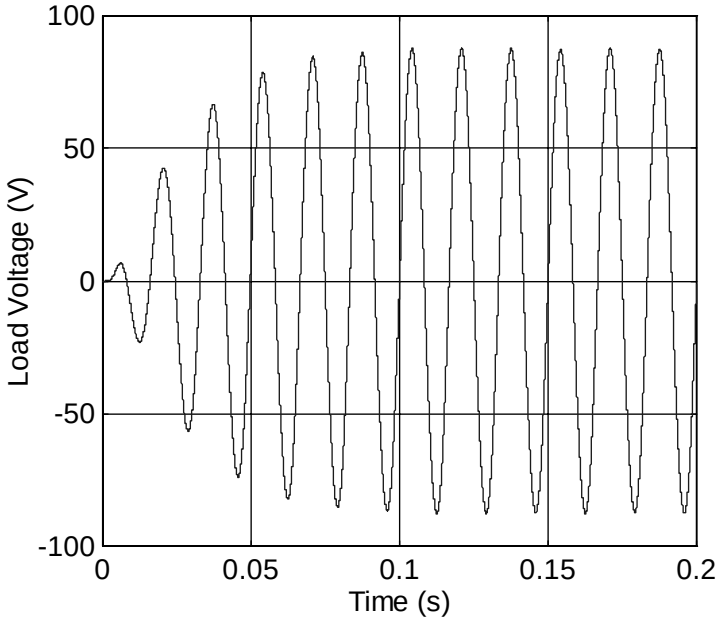

Figure 4.50 Load voltage start-up waveform. Modulation index = 0.8, load impedance = 20 ohms, rotor speed = 1860 rpm.

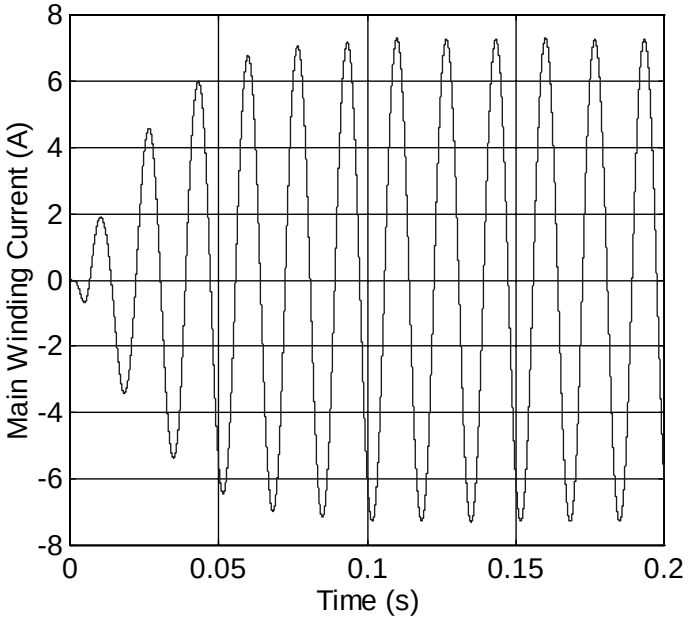

Figure 4.51 Main winding current start-up waveform. Modulation index = 0.8, load impedance = 20 ohms, rotor speed = 1860 rpm.

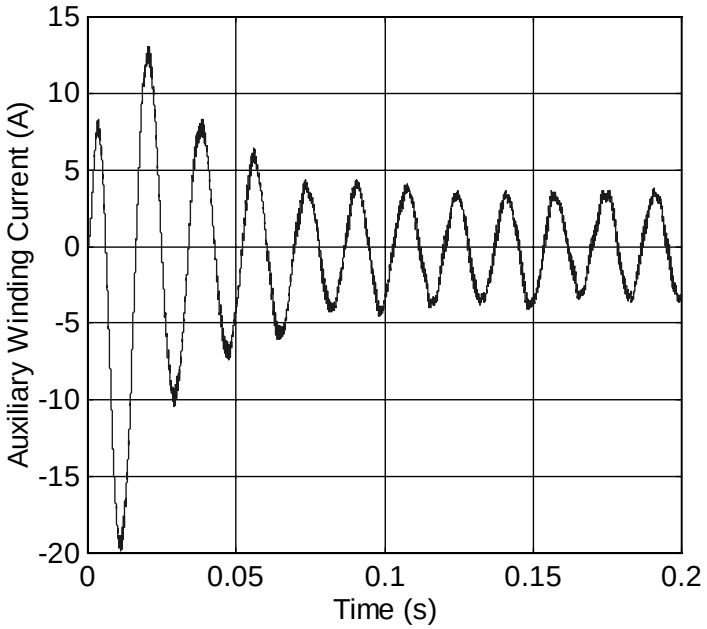

Figure 4.52 Auxiliary winding current start-up waveform. Modulation index = 0.8, load impedance = 20 ohms, rotor speed = 1860 rpm.

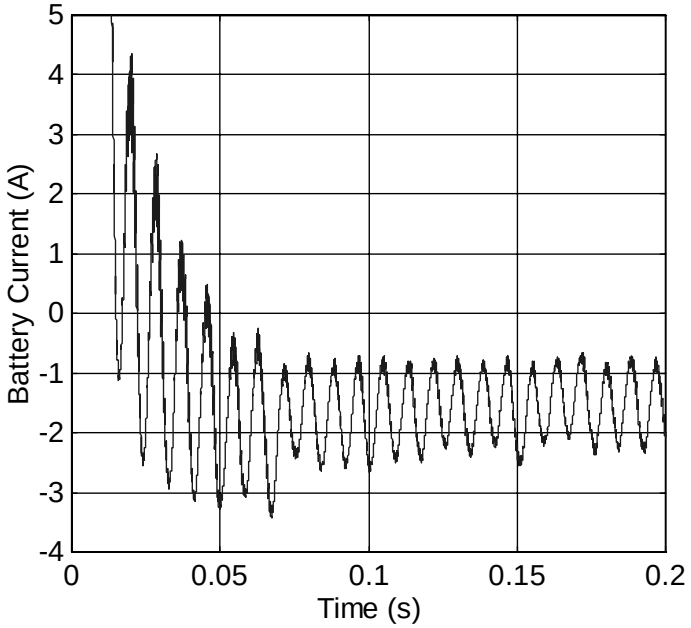

Figure 4.53 Battery current start-up waveform. Modulation index = 0.8, load impedance = 20 ohms, rotor speed = 1860 rpm.

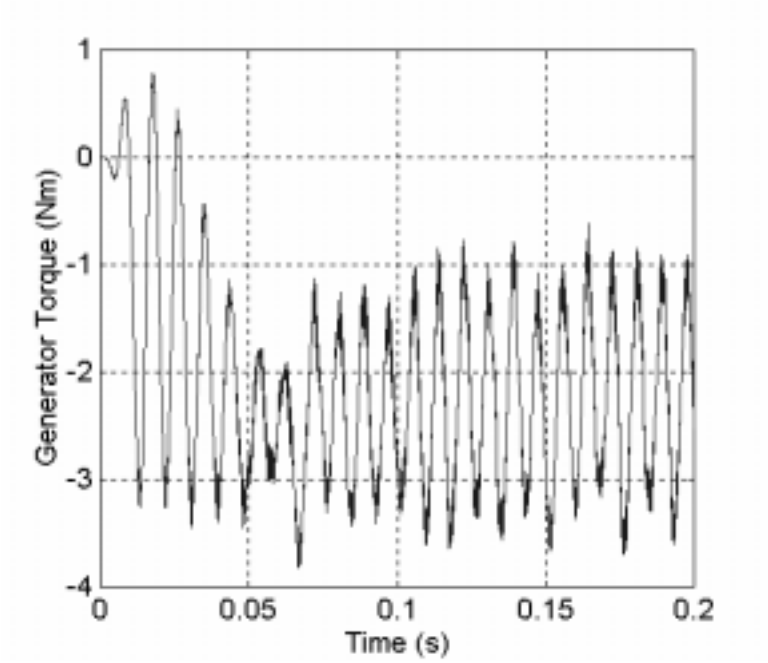

Figure 4.54 Generator torque start-up waveform. Modulation index = 0.8, load impedance = 20 ohms, rotor speed = 1860 rpm.

The single-phase induction generator torque waveform is shown in Figure 4.54. The graph shows how the generator torque falls quickly to a steady state value.

4.6.2 System Dynamics due to Changes in Load

This section examines the dynamics for the battery inverter generator system feeding a resistive load for changes in the load impedance. The simulation was carried out with generator rotor speed of 1840 rpm, the modulation index of 0.80, a carrier frequency of 2 kHz, and modulating frequency of 60 Hz.

The load impedance is initial is set at a value of 30 ohms and when the system reaches its steady state operating condition it is changed from 30 ohms to 50 ohms and afterward it is change to 10 ohms. The change in load impedance is illustrated in Figure 4.55.

The system load voltage waveform is shown in Figure 4.56. It can be seen that the generator responded quickly to the change in the load impedance to operate in steady-state condition. Figure 4.57 shows the main winding current waveform. The main winding current increases as the load impedance is changed from 50 ohms to 10 ohms.

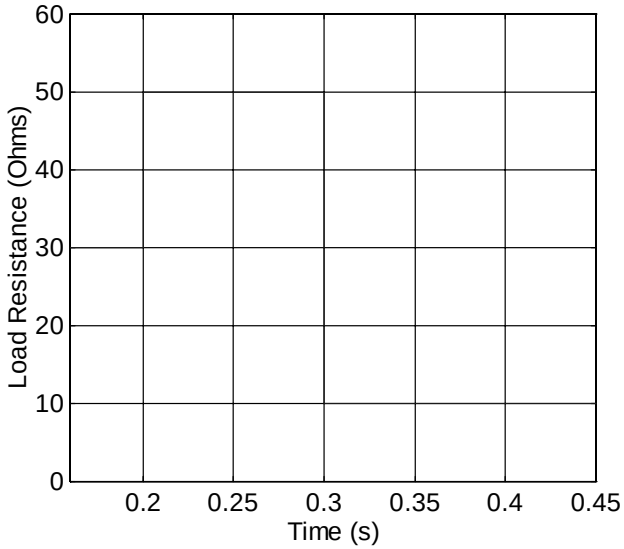

Figure 4.55. Changes in the values of the load impedance. Modulation index = 0.8, and rotor speed = 1840 rpm.

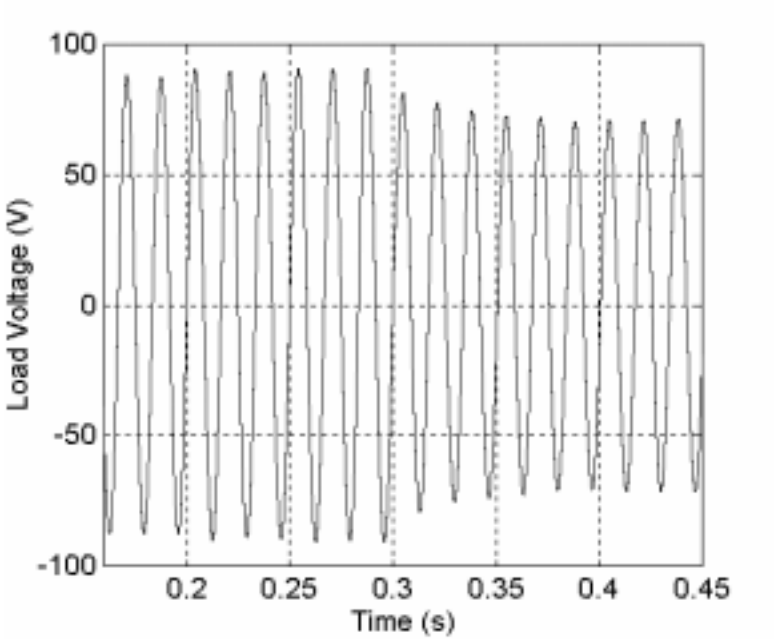

Figure 4.56. Load voltage waveform response to changes in load. Modulation index = 0.8, and rotor speed = 1840 rpm.

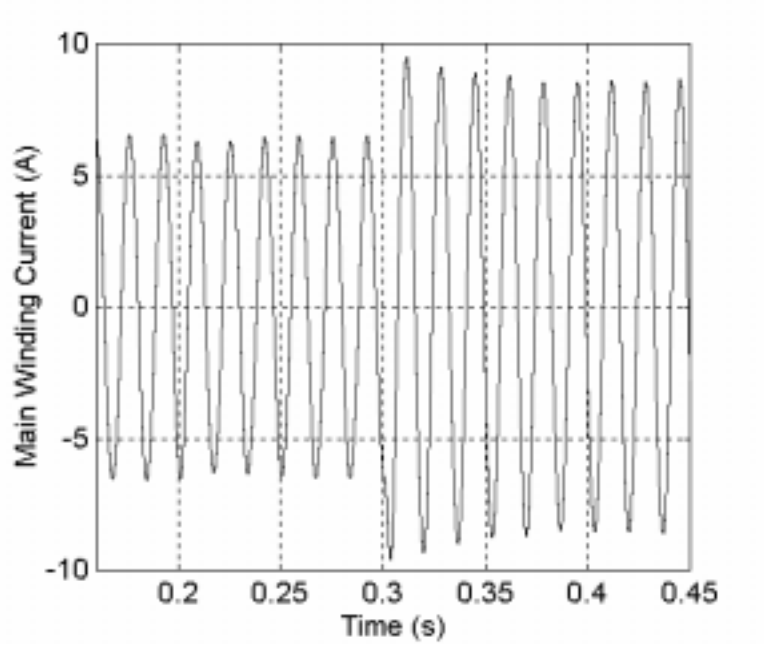

Figure 4.57. Main winding current waveform response to changes in load. Modulation index = 0.8, and rotor speed = 1840 rpm.

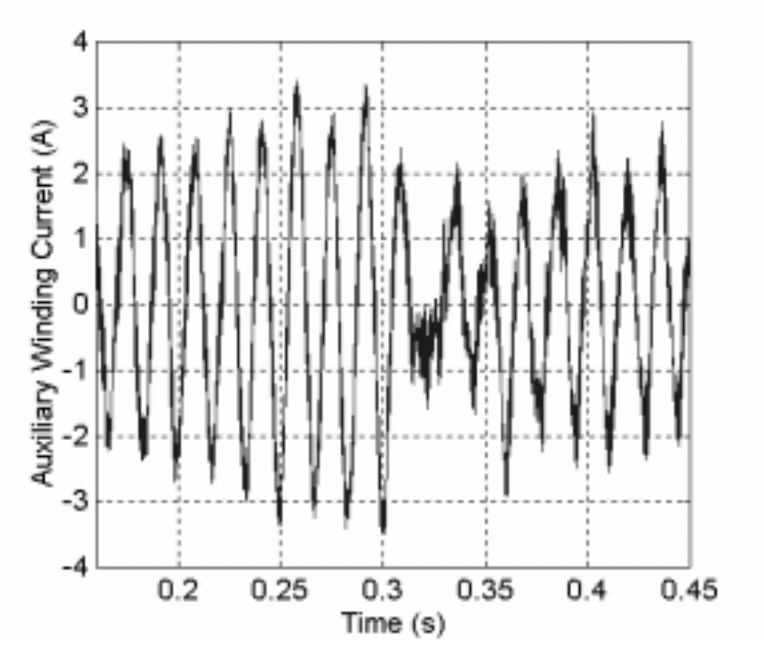

Figure 4.58. Auxiliary winding current waveform response to changes in load. Modulation index = 0.8, and rotor speed = 1840 rpm.

The auxiliary winding current waveform response due to changes in load is shown in Figure 4.58. As the load impedance is changed from 50 ohms to 10 ohms, the auxiliary winding current decreases. The battery current waveform is shown in Figure 4.59. The battery current is initially negative when the load impedance is at 30 and 50 ohms. The battery current becomes positive as the battery supplies real power to augment the real power provided by the generator to the load when the load impedance is changed from 50 ohms to 10 ohms. This clearly indicates the reliability of the system to a sudden change in power requirement by the load.

The single-phase induction generator torque waveform is shown in Figure 4.60. The generator torque increase when the load impedance changes from a light load (50 ohms) to a heavy load (10 ohms).

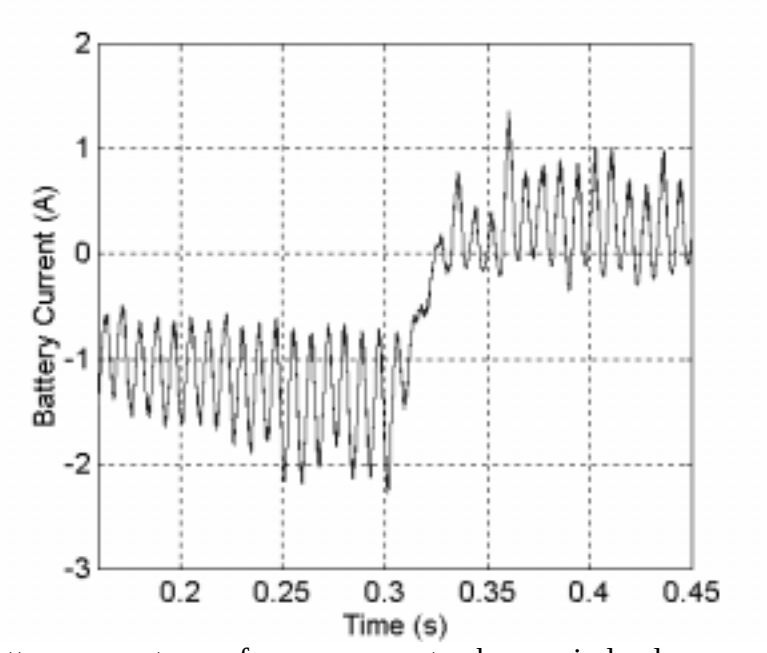

Figure 4.59. Battery current waveform response to changes in load.
Modulation index = 0.8, and rotor speed = 1840 rpm.

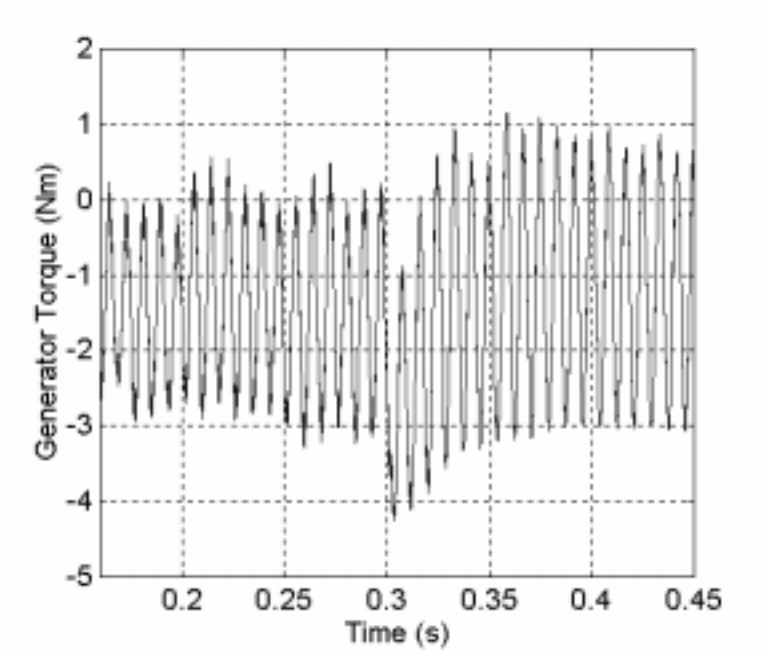

Figure 4.60 Generator torque waveform response to changes in load. Modulation index = 0.8, and rotor speed = 1840 rpm.

4.6.3 System Dynamics due to Changes in Generator Rotor Speed

This section examines the dynamics for the battery inverter generator system feeding a resistive load for changes in generator rotor speed. The simulation was carried out with a load resistance of 40 ohms, modulation index of 0.80, a carrier frequency of 2 kHz, and modulating frequency of 60 Hz.

The generator rotor speed is initially is set at a value of 1840 rpm when the system reaches its steady state operating condition it is changed from 1840 rpm to 1900 rpm and then to 1740 rpm as shown in Figure 4.61.

Figure 4.62 shows load voltage waveform response to changes in the generator rotor speed. The load voltage is maintained while the generator rotor speed is less than the 1800 rpm (synchronous speed) as the battery supplies the needed real power required

by the load. Figure 4.63 shows the main winding current waveform. The main winding current decrease as the generator rotor speed changes from 1900 rpm to 1740 rpm.

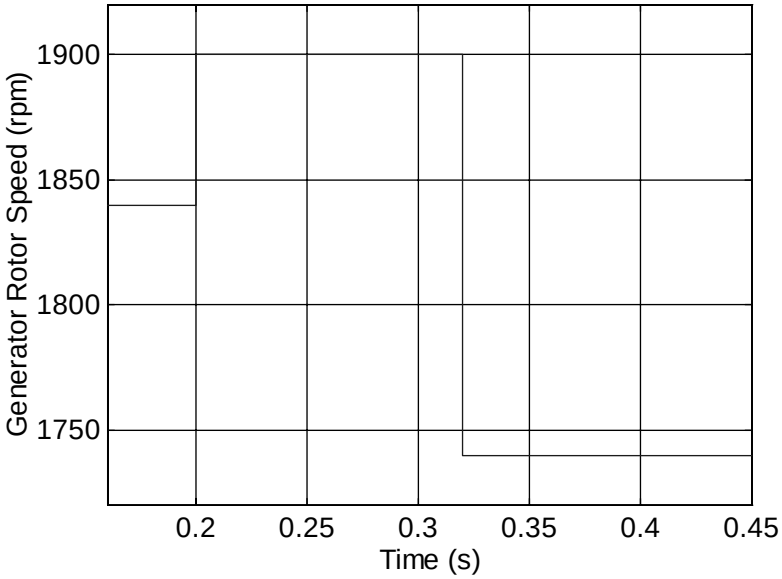

Figure 4.61. Changes in the values of generator rotor speeds. Modulation index = 0.8, and load resistance = 40 ohms.

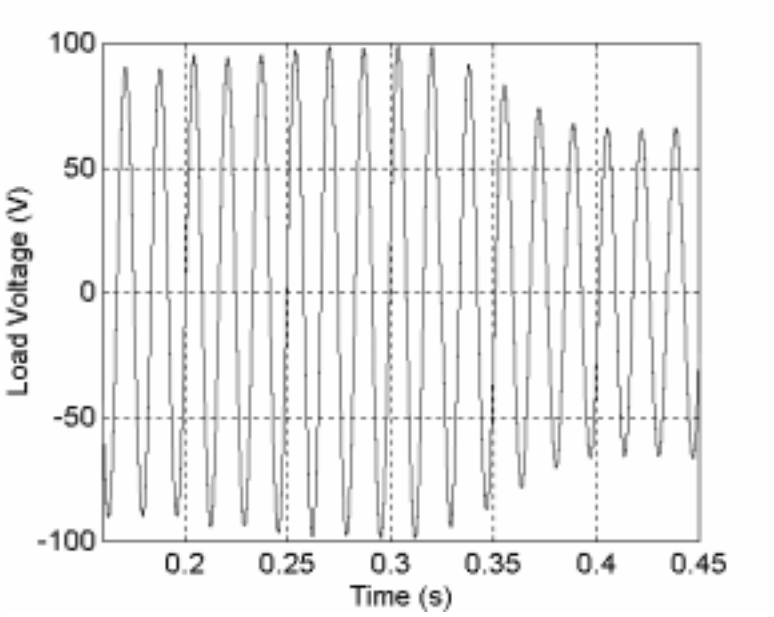

Figure 4.62. Load voltage waveform response to changes in generator rotor speed. Modulation index = 0.8, and load resistance = 40 ohms.

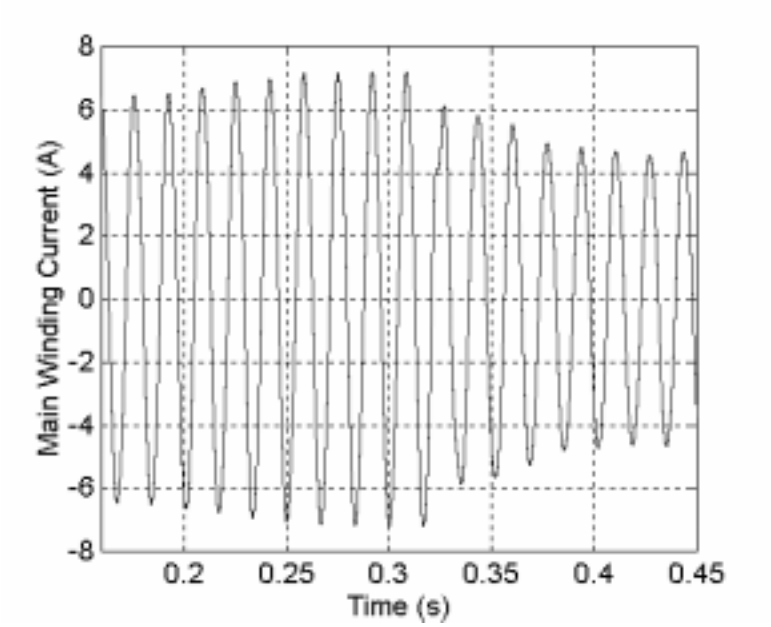

Figure 4.63. Main winding current waveform response to changes in generator rotor speed. Modulation index = 0.8, and load resistance = 40 ohms.

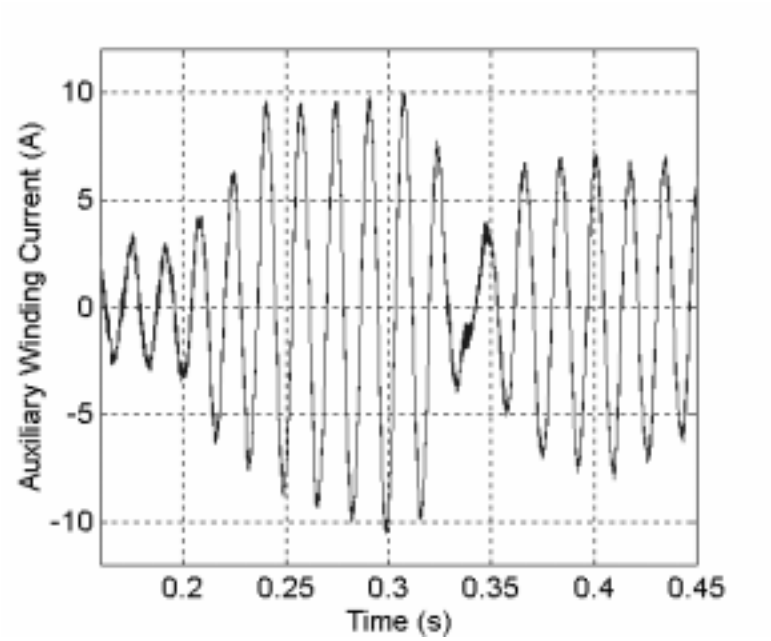

Figure 4.64. Auxiliary winding current waveform response to changes in generator rotor speed. Modulation index = 0.8, and load resistance = 40 ohms.

The auxiliary winding current waveform response due to changes in generator rotor speed is shown in Figure 4.64. The auxiliary winding current decreases in response

to change in the generator rotor speed as the speed changes from 1900 rpm to 1740 rpm. The battery current waveform response to changes in the generator rotor speed is shown in Figure 4.65. Initially the battery absorb real power (negative current) afterwards when the generator rotor speed changes to 1740 rpm from 1900 rpm the battery now provides real power (positive current) to the load. This result shows an advantage of the battery-inverter system over the conventional single-phase induction generator that will operate as a motor if the generator rotor speed is less than the synchronous speed.

The single-phase induction generator torque waveform is shown in Figure 4.66. The generator torque is negative when the speed is at 1840 and 1900 rpm and becomes positive when the generator rotor speed is 1740 rpm.

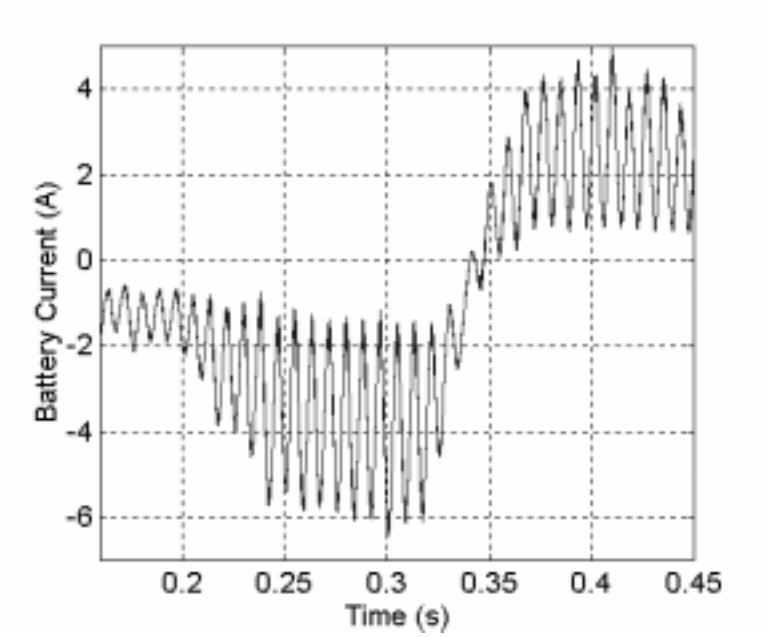

Figure 4.65. Battery current waveform response to changes in generator rotor speed. Modulation index = 0.8, and load resistance = 40 ohms.

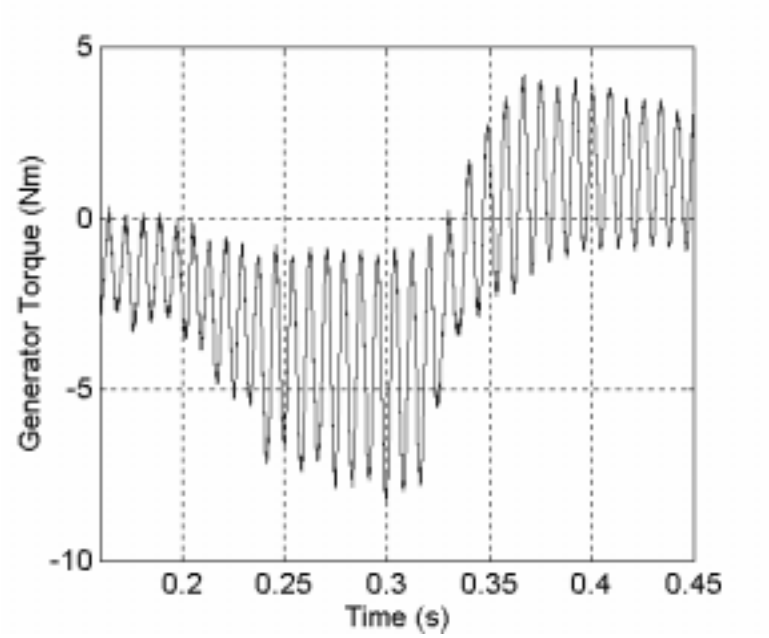

Figure 4.66. Generator torque waveform response to changes in generator rotor speed. Modulation index = 0.8, and load resistance = 40 ohms.

CHAPTER 5

ANALYSIS OF BATTERY INVERTER SINGLE-PHASE INDUCTION GENERATOR SYSTEM WITH SINGLE-PHASE INDUCTION MOTOR LOAD

5.1 Introduction

Most industrial and household applications involve the uses of single-phase induction motor in appliances such as in fans, washing machines, dryers, refrigerator, etc. In view of the various application of the single-phase induction motor, it will be worthwhile to analyze and study the performance of the battery inverter single-phase induction generator system feeding a single-phase induction load.

In this chapter, the analysis of the battery inverter single-phase induction generator system (SPIG) feeding a single-phase induction motor (SPIM) load will be studied. This system can be applied as a source of power in a remote location where there is no conventional utility power supply. Some of the system applications include milling, cold store, stone crushing, wood processing, etc.

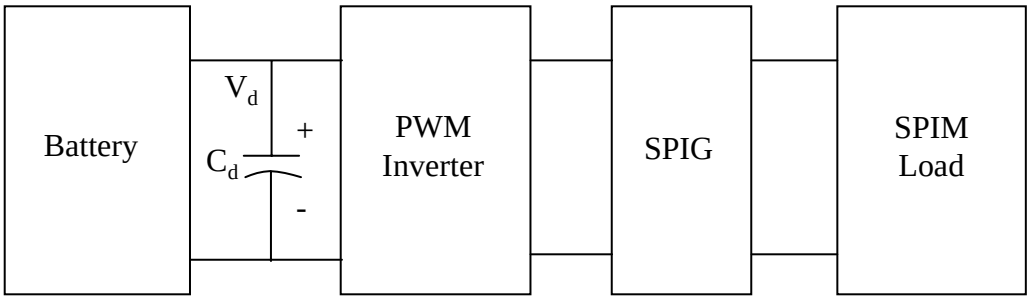

Figure 5.1. Block diagram of the system.

The block diagram describing the battery inverter SPIG feeding SPIM is shown in Figure 5.1.

The first part of this chapter looks into the system operation and the mathematical model of the battery inverter system with SPIM load. The dynamic mathematical model of the generator system developed is used in the simulation. The simulation results are compared with the measured waveform. The steady-state equation is further developed from the dynamic mathematical model. The resulting steady-state equation is used to predict the system steady-state performance characteristics. Finally the predicted performance is compared with measured steady-state characteristics.

5.2 Mathematical Model of System

The generator system comprises of a battery, a PWM inverter, a single-phase induction generator, and the load (single-phase induction motor). The schematic is shown in Figure 5.2.

The system operation is similar to the system description in section 4.2. With the generator connected in the fashion shown in Figure 5.2, the H bridge transistors are switched using the bipolar voltage switching scheme. The input to PWM inverter is obtained from a bank of battery fed through a capacitor. The capacitor, C_d ensures that the input voltage to the inverter is kept constant. The induction generator is connected in a manner that ensures that minimum induced inverter harmonics. The generator topology is configured in such away that the output from the inverter is connected to the auxiliary

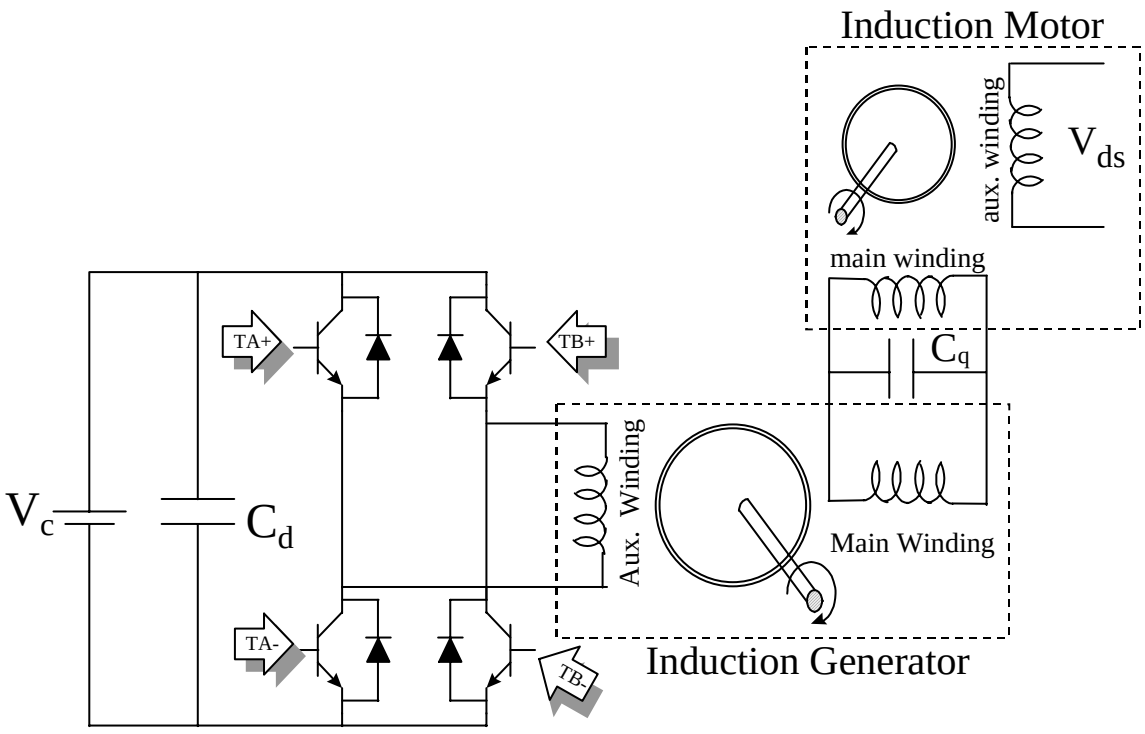

Figure 5.2. Schematic diagram of the system with induction motor load.

winding (the d-axis) and the main winding is connected to the single-phase induction motor load. The advantage of this scheme is that it ensures that the output voltage into the inverter is free from the inverter induced harmonics.

The frequency of the input voltage of SPIM motor load is determined by the modulating signal (sine waveform) of the PWM. Hence simply adjusting the modulating signal appropriately the motor load changes speed. The power requirement by the motor load is supplied from the battery or SPIG, depending on the speed of the SPIG. Also the reactive power needed by the motor load is supplied by the inverter [13,16]. The advantage of this isolated system is its ability to meet the motor load power demand. When the SPIG supplies more power than required by the motor the excess power is used

to charge the battery and when the power provided by the generator is less than the requirement by the motor the battery provides the balance.

The equivalent circuit of the battery, PWM inverter, generator and motor is shown in Figure 5.3. Equations 4.1 - 4.9 representing the model of the battery, inverter, and generator dynamic equations are repeated here as

$$C_{bp}\,pV_{bp} = I_s - \frac{V_{bp}}{r_{bp}} \tag{5.1}$$

$$C_{b1}\,pV_{b1} = I_s - \frac{V_{b1}}{r_{b1}} \tag{5.2}$$

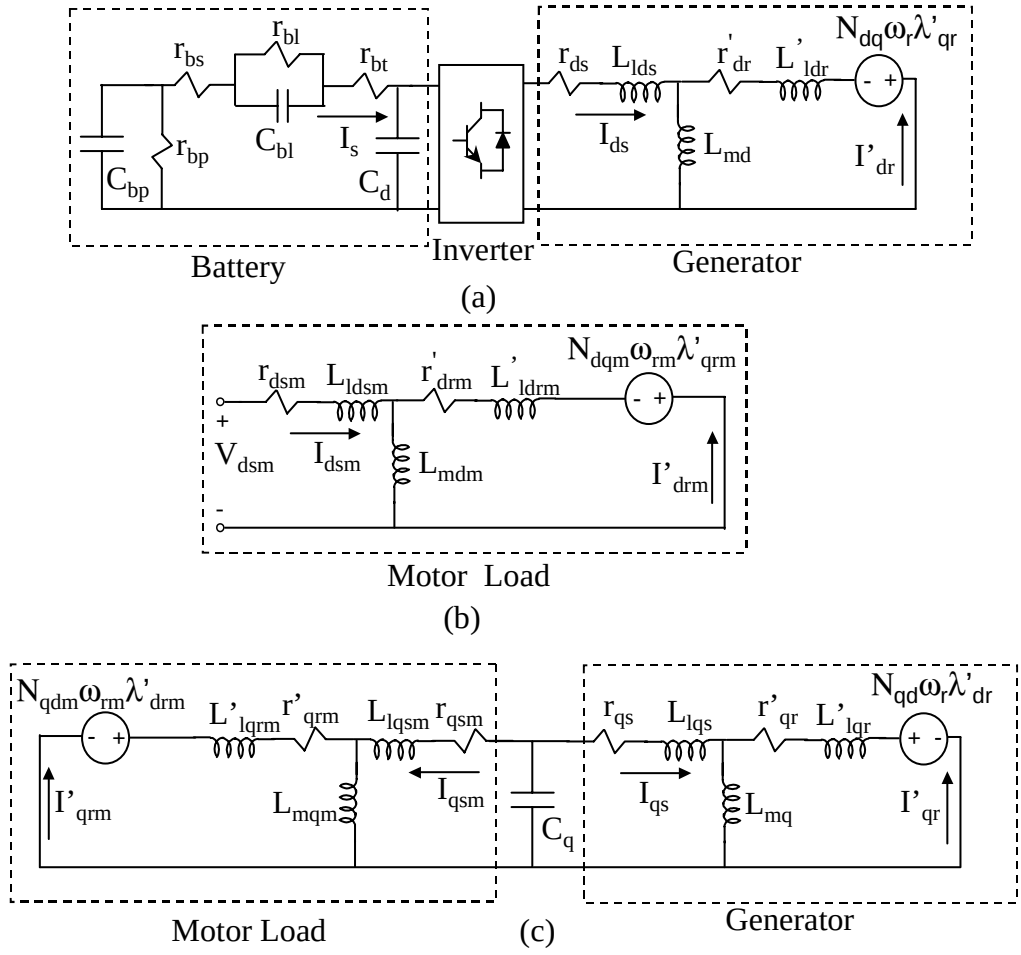

Figure 5.3. The q-d equivalent circuit of the battery-PWM inverter generator system with single-phase induction motor load. (a-b) d-axis circuit, (c) q-axis circuit.

$$V_c = V_{bp} - V_{b1} - I_s\left(r_{bs} + r_{bt}\right) \tag{5.3}$$

$$pV_c = \frac{1}{C_d}\left(I_s - I_{ds}S_a\right) \tag{5.4}$$

$$V_{ds} = S_a V_c \tag{5.5}$$

$$p\lambda_{ds} = V_{ds} - r_{ds} I_{ds} \tag{5.6}$$

$$p\lambda_{qs} = V_{qs} - r_{qs} I_{qs} \tag{5.7}$$

$$p\lambda'_{qr} = N_{qd}\omega_r\lambda'_{dr} - r'_{qr}I'_{qr} \tag{5.8}$$

$$p\lambda'_{dr} = -N_{dq}\omega_r\lambda'_{qr} - r'_{dr}I'_{dr}\,. \tag{5.9}$$

The dynamic equation for the SPIM are given as

$$pV_{qsm} = -\frac{1}{C_q}\left(I_{qs} + I_{qsm}\right) \tag{5.10}$$

$$p\lambda_{qsm} = V_{qsm} - r_{qsm} I_{qsm} \tag{5.11}$$

$$p\lambda_{dsm} = V_{dsm} - r_{dsm} I_{dsm} \tag{5.12}$$

$$p\lambda'_{qrm} = N_{qdm}\omega_{rm}\lambda'_{drm} - r'_{qrm}I'_{qrm} \tag{5.13}$$

$$p\lambda'_{drm} = -N_{dqm}\omega_{rm}\lambda'_{qrm} - r'_{drm}I'_{drm} \tag{5.14}$$

where the motor main winding and auxiliary winding voltage are denoted as V_{qsm} and V_{dsm}, respectively. The ratio of the number of turns of the motor q-axis winding and the d-axis winding is denoted as N_{qdm}. The inverse of is N_{qdm} is denoted as N_{dqm}. The motor stator q and d axes currents are I_{qsm} and I_{dsm}, respectively, while those of the rotor referred circuits are I'_{qrm} and I'_{drm}, respectively. The motor stator q and d axes flux linkages are λ_{qsm} and λ_{dsm}, respectively, while those of the rotor referred circuits are λ'_{qrm} and λ'_{drm}, respectively.

Equations 4.12 - 4.15 representing the q-d flux linkages of the generator are given as

$$\lambda_{qs} = L_{qs} I_{qs} + L_{mq} I'_{qr} \tag{5.15}$$

$$\lambda_{ds} = L_{ds} I_{ds} + L_{md} I'_{dr} \tag{5.16}$$

$$\lambda'_{qr} = L'_{qr} I'_{qr} + L_{mq} I_{qs} \tag{5.17}$$

$$\lambda'_{dr} = L'_{dr} I'_{dr} + L_{md} I_{ds} \ . \tag{5.18}$$

The q-d flux linkages of the motor load are given as

$$\lambda_{qsm} = L_{qsm} I_{qsm} + L_{mqm} I'_{qrm} \tag{5.19}$$

$$\lambda_{dsm} = L_{dsm} I_{dsm} + L_{mdm} I'_{drm} \tag{5.20}$$

$$\lambda'_{qrm} = L'_{qrm} I'_{qrm} + L_{mqm} I_{qsm} \tag{5.21}$$

$$\lambda'_{drm} = L'_{drm} I'_{drm} + L_{mdm} I_{dsm} \tag{5.22}$$

where $L_{qsm} = L_{lqsm} + L_{mqm}$, $L_{dsm} = L_{ldsm} + L_{mdm}$, $L_{qrm} = L'_{lqrm} + L_{mqm}$, and $L_{drm} = L'_{ldrm} + L_{mdm}$. The referred motor rotor q-d leakage inductances are L'_{lqrm} and L'_{ldrm}, respectively. The referred motor rotor q-d resistance are r'_{qrm} and r'_{drm}, respectively. The motor stator q-d leakage inductances are L'_{lqsm} and L'_{ldsm}, respectively, with the q-d magnetizing inductances given, respectively, as L_{mqm} and L_{mdm}. The motor stator per-phase resistance for the q-winding and the corresponding value for the d-axis winding are r_{qsm} and r_{dsm}, respectively. The motor electrical angular speed is ω_{rm}.

The dynamics of the generator turbine is given in Equations 4.16 and 4.17 and are given as

$$p\omega_r = \frac{P}{2J}\left(T_o - T_e\right) \tag{5.23}$$

$$T_e = \frac{P}{2}\left(N_{dq}\lambda'_{qr} I'_{dr} - N_{qd}\lambda'_{dr} I'_{qr}\right) . \tag{5.24}$$

The dynamics of the SPIM turbine are expressed as

$$p\omega_{rm} = \frac{P_m}{2J_m}\left(T_{em} - T_{om}\right) \tag{5.25}$$

$$T_{em} = \frac{P_m}{2}\left(N_{dqm}\lambda'_{qrm}I'_{drm} - N_{qdm}\lambda'_{drm}I'_{qrm}\right). \tag{5.26}$$

The moment of inertia and the number of poles of the generator are J_m and P_m, respectively. The driving and generated electromagnetic torques are respected as T_{om} and T_{em}, respectively.

5.3. Comparison of Simulation and Experiment Waveforms for the System Feeding SPIM Load

This section contains the comparison between simulation and measured waveforms of the battery inverter SPIG system feeding SPIM load. The conditions examined include when the modulation index of the PWM inverter is in the linear modulation region and also when the modulation index is in the overmodulation region.

The simulation of the system Equations 5.1 to 5.26 is implemented using MATLAB/Simulink.

5.3.1 Battery Inverter SPIG System Feeding SPIM Load (Linear Region)

This section looks at the measured and simulated waveforms when the battery inverter SPIG is feeding a SPIM when the modulation index of PWM inverter is in the linear region. The experiment and simulation were carried out with generator rotor speed of 1840 rpm. The modulation index was set a value of 0.875 with a carrier frequency of

2 kHz and modulating frequency of 60 Hz. The battery voltage and load capacitor are 144 V and 180 μF, respectively. The parameter of the SPIM is shown in appendix B.

Figure 5.4 shows the input voltage into the single-phase induction motor under no load consideration. Simulation and experiment waveforms are observed to have the same characteristics.

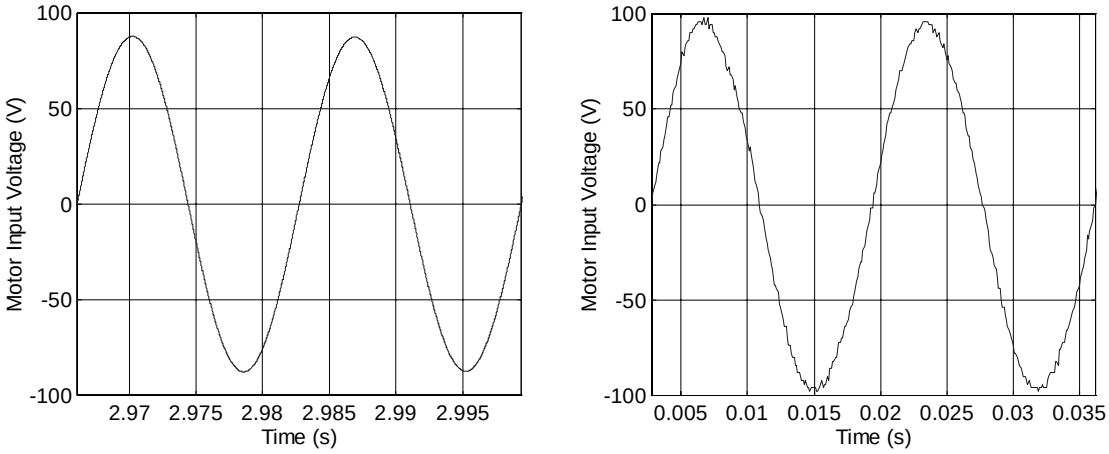

I. Simulation II. Experiment

Figure 5.4. Induction motor input voltage steady-state waveforms. Modulation index = 0.875, rotor speed = 1840 rpm

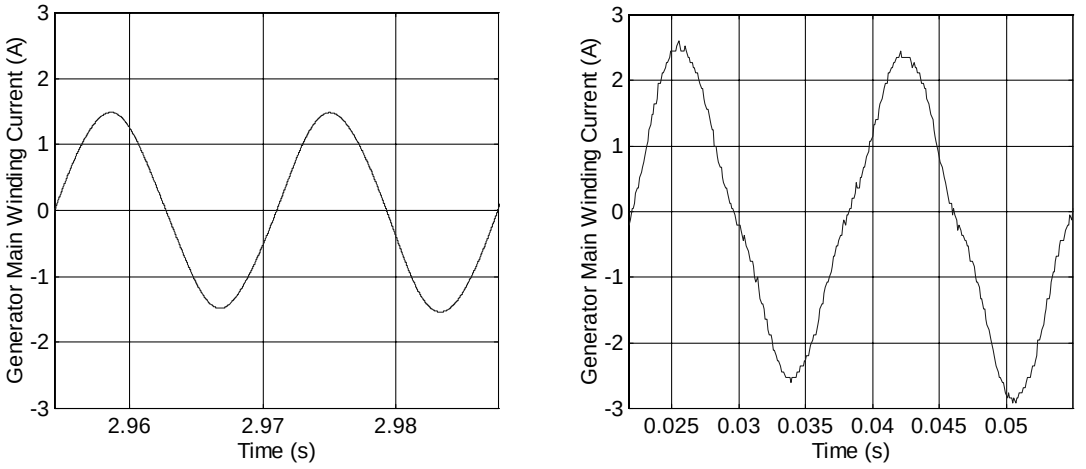

I. Simulation II. Experiment

Figure 5.5. Induction generator main winding current steady-state waveforms. Modulation index = 0.875, rotor speed = 1840 rpm.

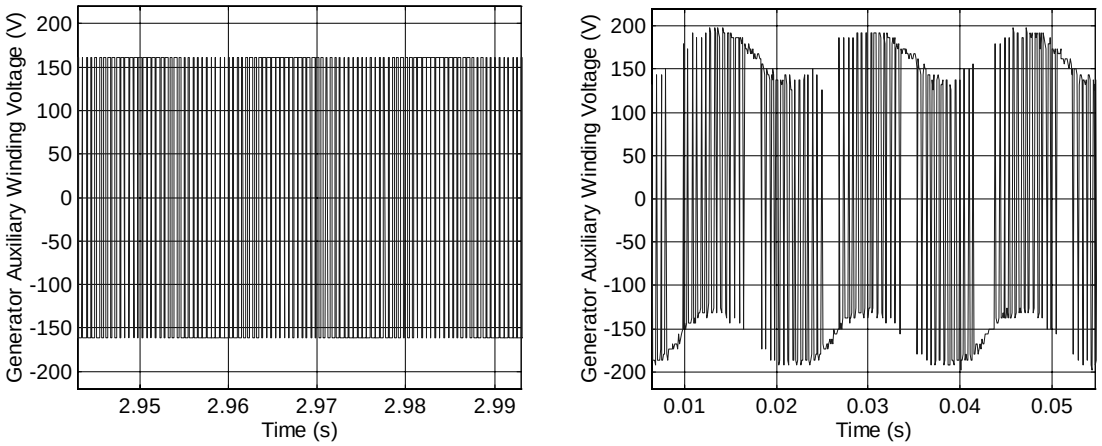

I. Simulation II. Experiment

Figure 5.6. Generator auxiliary winding voltage steady-state waveforms. Modulation index = 0.875, rotor speed = 1840 rpm.

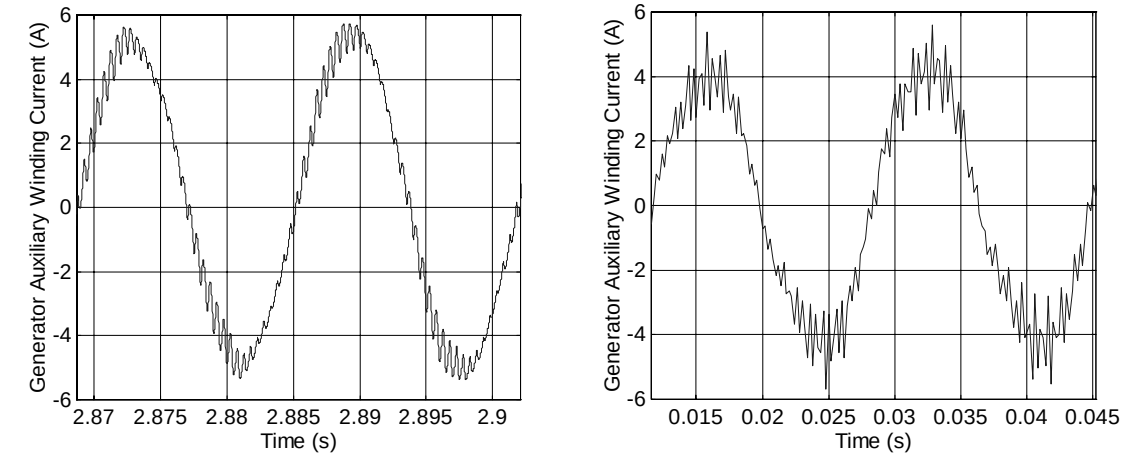

I. Simulation II. Experiment

Figure 5.7. Generator auxiliary winding current steady-state waveforms. Modulation index = 0.875, rotor speed = 1840 rpm.

Figure 5.5 shows the simulated and measured steady-state generator main winding current. The current waveform harmonic is insignificant because of circuit topology used for the system.

The simulated and experimental steady-state waveforms of the auxiliary winding voltage of the generator are shown in Figure 5.6. The experimental waveform is different from the simulate waveform due to the harmonic content in the battery current.

The simulated and experimental steady-state waveforms for the generator auxiliary winding current are shown in Figure 5.7. The inverter induced harmonic is shown on the simulated and experimental current waveforms.

Figure 5.8 shows the input current or the main winding current steady-state waveform of the single-phase induction motor. The results show that the frequency of the current is same as the modulating frequency, which in this case is 60 Hz. The results from the experiment compare favorably.

The simulated and experimental battery current steady-state waveform is shown in Figure 5.9. The battery current waveform is negative indicating that the battery is being charged. The experimental waveform shows the inverter induced harmonics riding on the battery current.

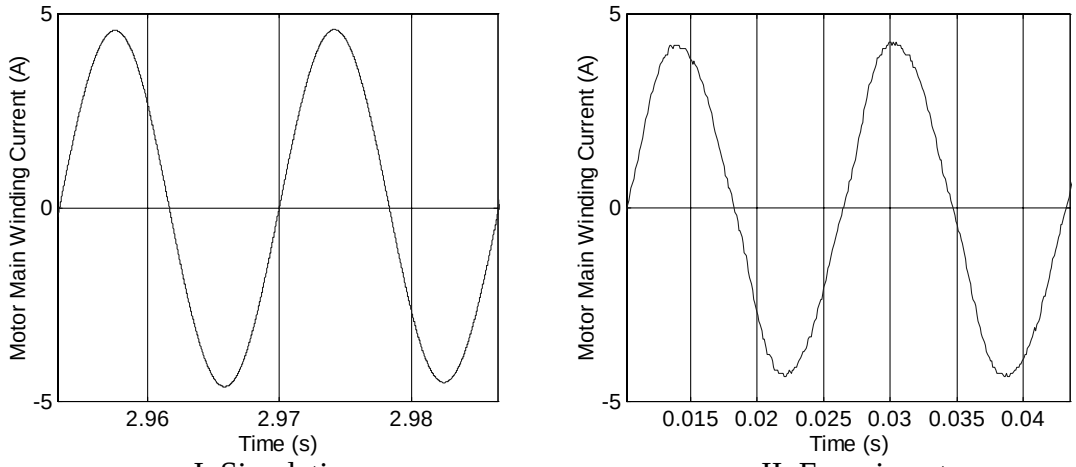

I. Simulation II. Experiment

Figure 5.8. Induction motor main winding current steady-state waveforms.
Modulation index = 0.875, rotor speed = 1840 rpm.

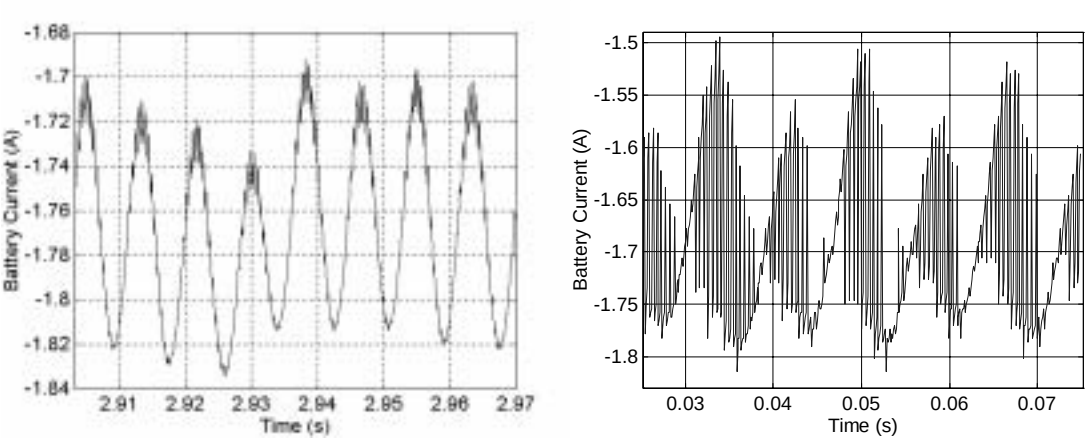

I. Simulation II. Experiment

Figure 5.9. System battery current steady-state waveforms. Modulation index = 0.875, rotor speed = 1840 rpm.

5.3.2 Battery Inverter SPIG System Feeding SPIM Load (Overmodulation Region)

This section looks at the measured and simulated waveforms when the battery inverter SPIG is feeding a SPIM when the modulation index of PWM inverter is in the overmodulation region. The experiment and simulation were carried out with generator rotor speed of 1840 rpm. The modulation index was set a value of 1.375 with a carrier frequency of 2 kHz and modulating frequency of 60 Hz. The battery voltage and load capacitor are 144 V and 180 μF, respectively. The parameter of the SPIM is shown in appendix B.

Figure 5.10 shows the simulated and experimental motor input steady-state voltage waveform. The waveform shows that its frequency is the same as the modulating signal of the inverter and it is also free from the inverter induced harmonics.

The simulated and experimental steady-state waveform of the induction generator main winding current is shown in Figure 5.11. The simulated and experimental waveforms have similar characteristics as indicated in the figure.

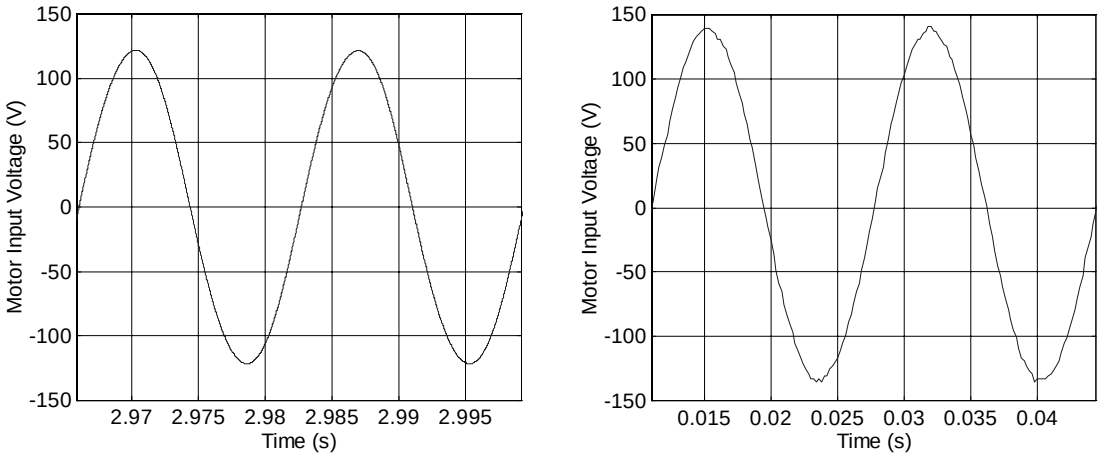

I. Simulation II. Experiment

Figure 5.10. Induction motor input voltage steady-state waveforms.
Modulation index = 1.375, rotor speed = 1840 rpm

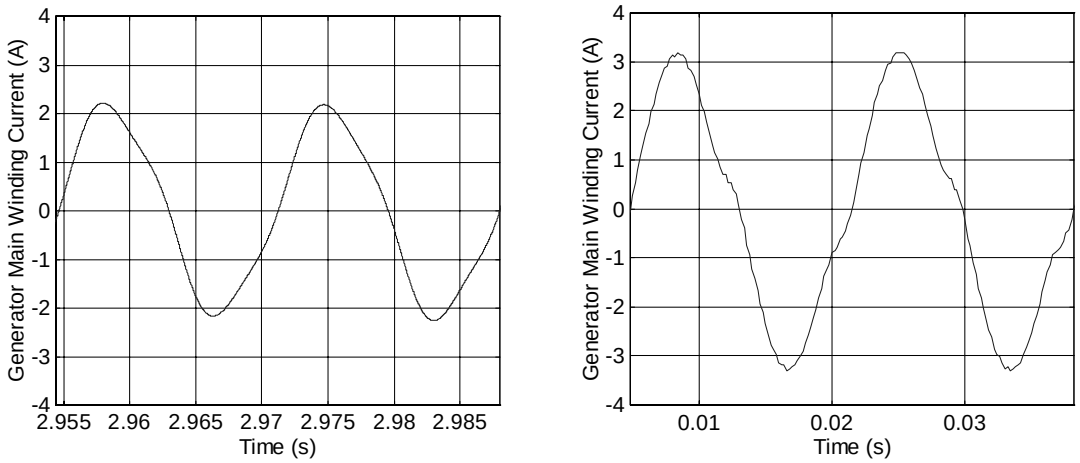

I. Simulation II. Experiment

Figure 5.11. Induction generator main winding current steady-state waveforms.
Modulation index = 1.375, rotor speed = 1840 rpm.

Figure 5.12 shows the simulated and experimental waveforms of the induction generator steady-state auxiliary winding voltage. The experimental results show that the auxiliary winding voltage is influence by the charging of the battery (that is battery is absorbing power) as shown in Figure 5.12.

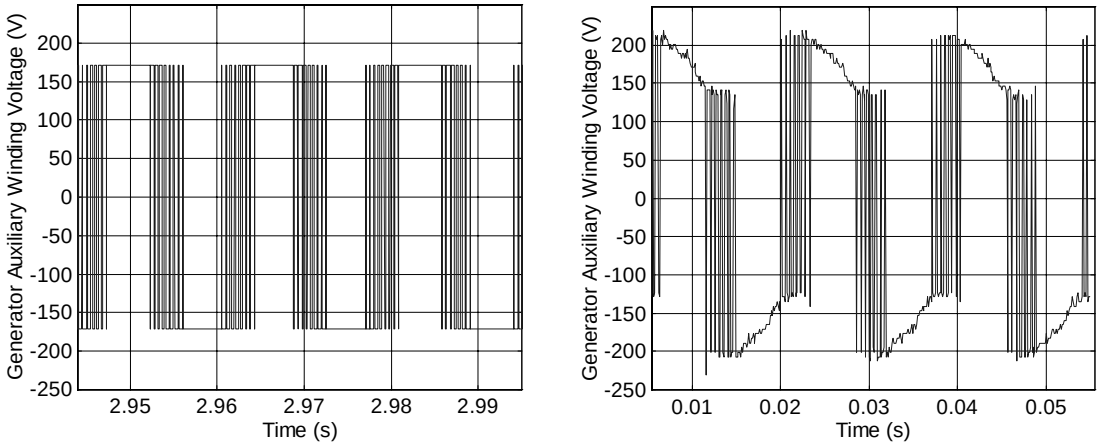

I. Simulation II. Experiment

Figure 5.12. Generator auxiliary winding voltage steady-state waveforms. Modulation index = 1.375, rotor speed = 1840 rpm.

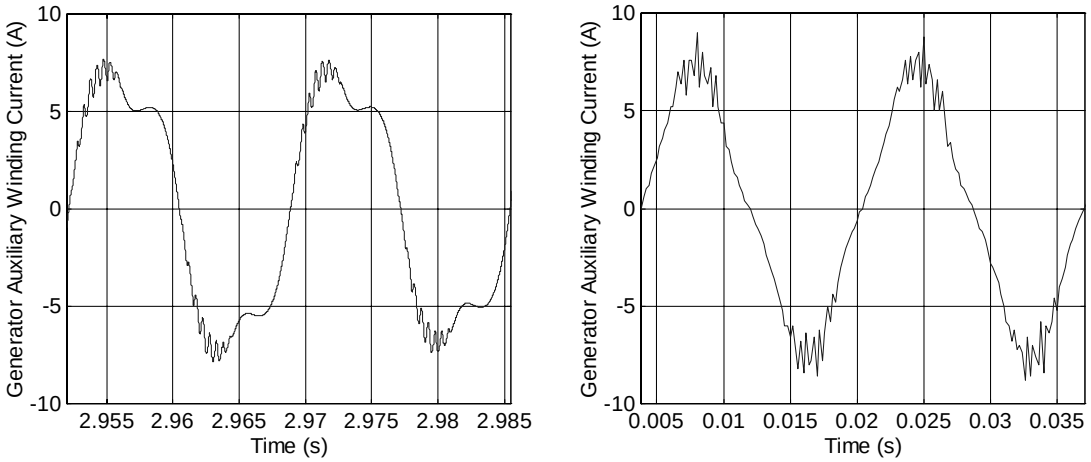

I. Simulation II. Experiment

Figure 5.13. Generator auxiliary winding current steady-state waveforms. Modulation index = 1.375, rotor speed = 1840 rpm.

The simulation and experimental steady-state waveforms of the auxiliary winding current of the induction generator is shown in Figure 5.13. The inverter-induced harmonics is observed on the auxiliary winding current.

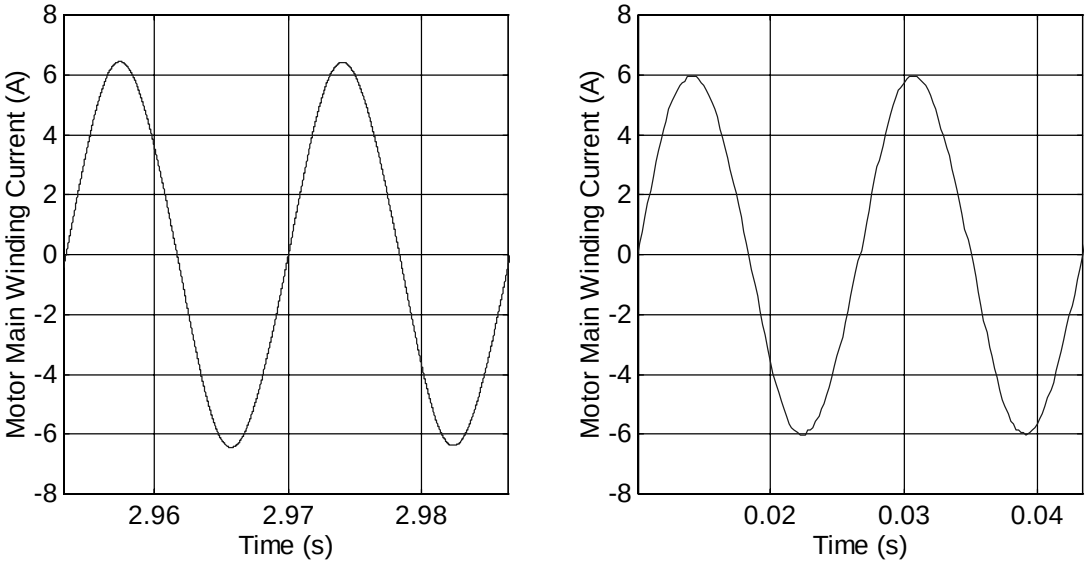

I. Simulation II. Experiment

Figure 5.14. Induction motor main winding current steady-state waveforms. Modulation index = 1.375, rotor speed = 1840 rpm.

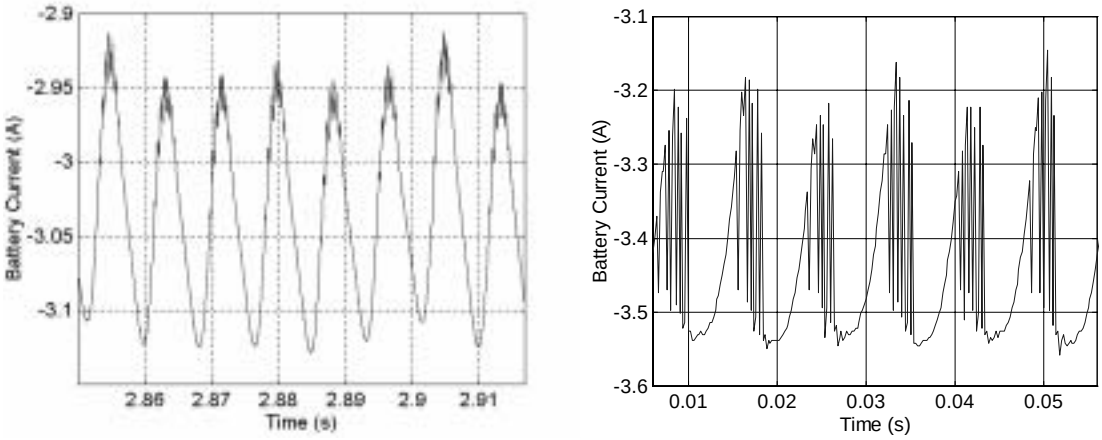

I. Simulation II. Experiment

Figure 5.15. System battery current steady-state waveforms. Modulation index = 1.375, rotor speed = 1840 rpm.

Figure 5.14 shows the single-phase induction motor main winding current waveform. The current waveform is observed to be free inverter induced harmonics.

The system steady-state battery current is shown in Figure 5.15. The simulated and experimental waveform clearly shows that the battery is being charged (that is the

battery is absorbing power). The experimental current waveform in Figure 5.15 also shows the inverter switching frequency component on the battery current.

5.4 Steady State Calculation and Experiment

The steady-state equation for the battery, inverter, single-phase induction generator using harmonic balance have been discussed in Chapter 4. Equations 4.52 - 4.55, 4.61 will be repeated here for continuity.

$$MV_{do} + \frac{M^2 R_d I_{dss}}{4(1 - j2\omega_e C_d R_d)} - r_{ds} I_{dss} - j\omega_e \left(L_{ds} I_{dss} + L_{md} I'_{drr}\right) = 0 \tag{5.27}$$

$$V_{qss} - r_{qs} I_{qss} - j\omega_e \left(L_{qs} I_{qss} + L_{mq} I'_{qrr}\right) = 0 \tag{5.28}$$

$$N_{qd}\omega_r \left(L'_{dr} I'_{drr} + L_{md} I_{dss}\right) - r'_{qr} I'_{qrr} - j\omega_e \left(L'_{qr} I'_{qrr} + L_{mq} I_{qss}\right) = 0 \tag{5.29}$$

$$-N_{dq}\omega_r \left(L'_{qr} I'_{qrr} + L_{mq} I_{qss}\right) - r'_{dr} I'_{drr} - j\omega_e \left(L'_{dr} I'_{drr} + L_{md} I_{dss}\right) = 0 \tag{5.30}$$

$$T_{e1} = \frac{P}{4}\left(N_{dq}\lambda'_{qrr} I'^{*}_{drr} - N_{qd}\lambda'_{drr} I'^{*}_{qrr}\right) \tag{5.31}$$

The steady-state equation of the single-phase induction motor is given as

$$\frac{1}{C_q}\left(I_{qss} + I_{qssm}\right) + j\omega_e V_{qss} = 0 \tag{5.32}$$

$$V_{qssm} - r_{qsm} I_{qssm} - j\omega_e \left(L_{qsm} I_{qssm} + L_{mqm} I'_{qrrm}\right) = 0 \tag{5.33}$$

$$N_{qdm}\omega_r \left(L'_{drm} I'_{drrm} + L_{mdm} I_{dssm}\right) - r'_{qrm} I'_{qrrm} - j\omega_e \left(L'_{qrm} I'_{qrrm} + L_{mqm} I_{qssm}\right) = 0 \tag{5.34}$$

$$-N_{dqm}\omega_r \left(L'_{qrm} I'_{qrrm} + L_{mqm} I_{qssm}\right) - r'_{drm} I'_{drrm} - j\omega_e \left(L'_{drm} I'_{drrm} + L_{mdm} I_{dssm}\right) = 0 \tag{5.35}$$

$$T_{em} = \frac{P_m}{4}\left(N_{dqm}\lambda'_{qrrm} I'^{*}_{drrm} - N_{qdm}\lambda'_{drrm} I'^{*}_{qrrm}\right). \tag{5.36}$$

The steady-state equations (5.27 - 5.36) are used to solved for the state variables using MATLAB.

5.4.1 Experiment and Predicted Performance Results

In this section, the measured steady state performance of the battery inverter SPIG system feeding a SPIM will be compared with the predicted performance of the system. The steady state performance was carried at different values of modulation indexes. The experimental measurement and calculation was carried out with generator rotor speed of 1840 rpm, a carrier frequency of 2 kHz, and modulating frequency of 60 Hz. The battery voltage and load capacitor are 144 V and 180 μF respectively. The constant parameters used for the steady-state experiment and calculation are shown in appendix B.

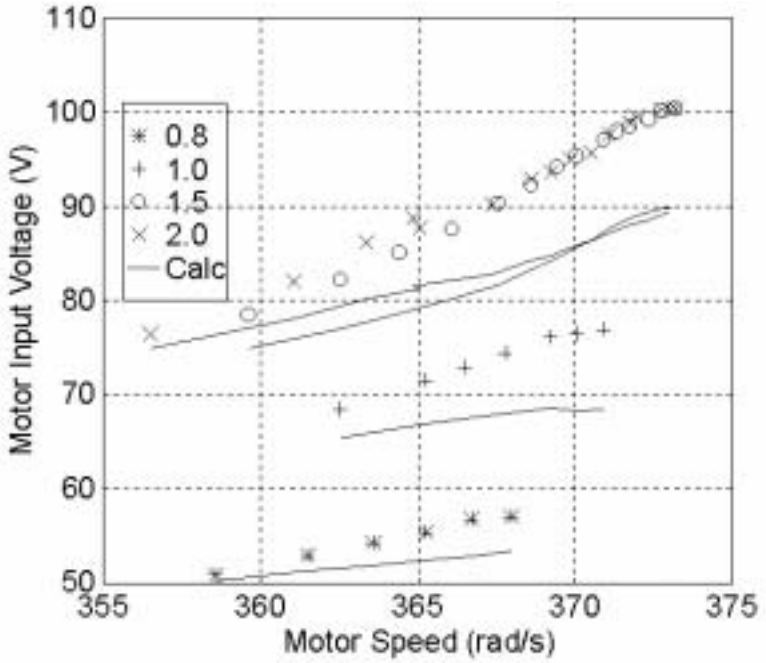

Figure 5.16: Measured and calculated motor input voltage as a function of motor speed. Constant generator rotor speed = 1840 rpm.

The measured and calculated steady-state input voltage into the single-phase induction motor as a function of the motor speed is shown in Figure 5.16. Figure 5.16 shows the motor input voltages are higher with the higher modulation index. In addition as the motor speed increases the input voltage also increases.

Figure 5.17 shows the measured and calculated steady-state torque of the single-phase induction motor as a function of motor speed. The motor torque decreases with increase in the motor speed. The figure also indicates that the higher the modulation index the higher the torque of the induction motor.

Figure 5.18 shows how measured and calculated steady-state input power to the induction motor varies as a function of the motor speed. It can be observed that the predicted performance curves show the trend of the actual measured points, but there is fairly substantial magnitude difference in output power between the predicted and measured curves.

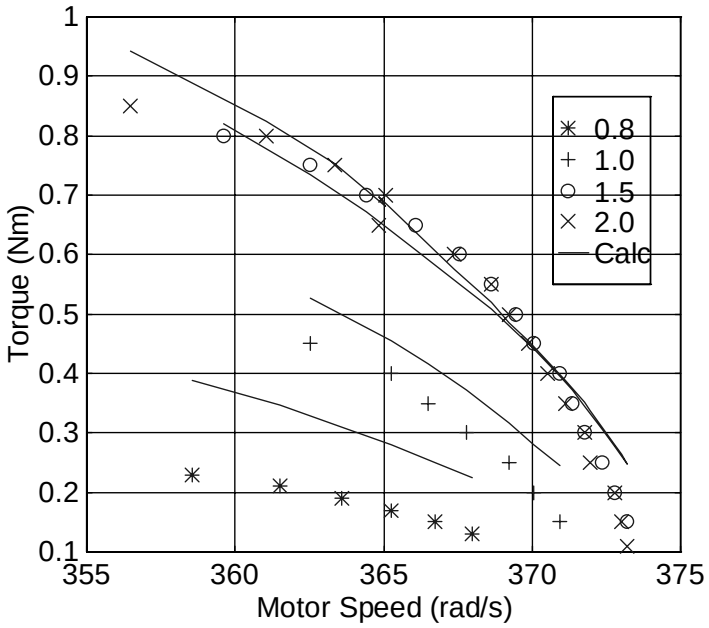

Figure 5.17: Measured and calculated motor torque as a function of motor speed. Constant generator rotor speed = 1840 rpm.

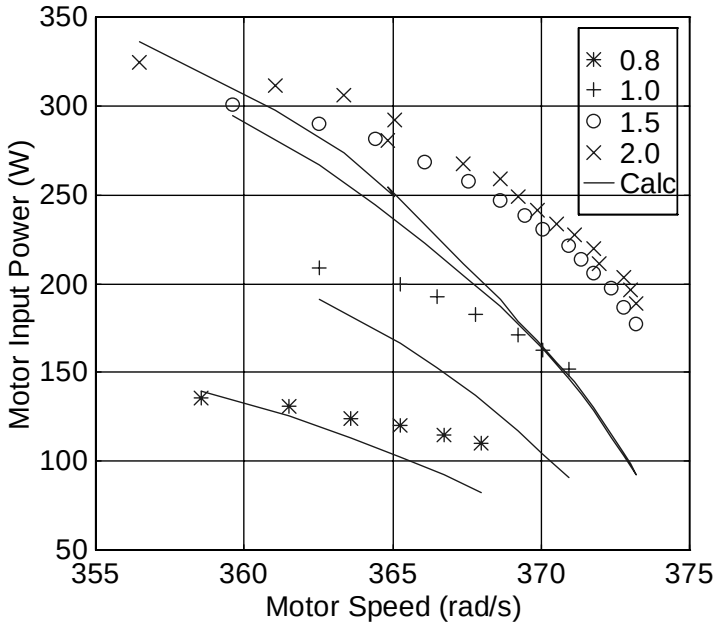

Figure 5.18: Measured and calculated motor input voltage as a function of motor speed. Constant generator rotor speed = 1840 rpm.

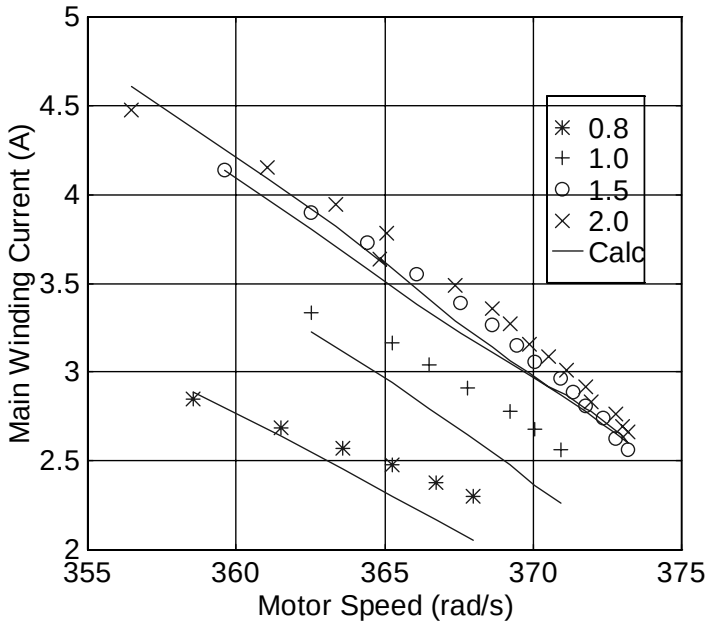

Figure 5.19: Measured and calculated generator winding current as a function of motor speed. Constant generator rotor speed = 1840 rpm.

The steady-state measurement and calculated generator winding current as a function of motor speed is shown in Figure 5.19. The main winding current increases with increase in the modulation index and decreases almost linearly with increases in

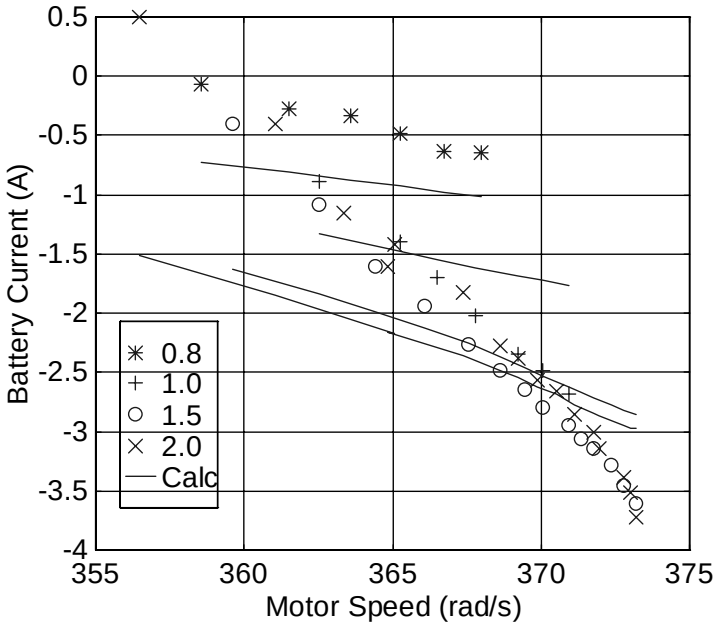

Figure 5.20: Measured and calculated battery current as a function of motor speed. Constant generator rotor speed = 1840 rpm.

motor speed. The predicted curves are similar to the measurement though they are different in magnitude.

The graph shown Figure 5.20 displays the measured and calculated battery steady-state current as a function of the motor speed. The battery currents are negative showing that the battery is absorbing real power.

5.4.2 Predicted Performance Results

In this section, the predicted steady state performance of the battery inverter SPIG system feeding a SPIM load will be discussed. The steady state performance was carried at different values of modulation indexes. The experimental measurement and calculation were carried out with generator rotor speed of 1840 rpm, a carrier frequency of 2 kHz and modulating frequency of 60 Hz. The battery voltage and load capacitor are 144 V and

210 μF, respectively. The constant parameters used for the steady-state experiment and calculation are shown in appendix B.

Figure 5.21 shows the motor voltage as a function of the motor torque at different modulation index. The motor voltage and torque increases as the modulation index increases. For a fixed value of modulation index the motor voltage decreases as the motor torque increases to its peak value.

Figure 5.22 shows the motor voltage as a function of the motor input power at different modulation index. The motor voltage and input power increases as the modulation index increases. For a fixed value of modulation index the motor voltage decreases as the motor input power increases to its peak value.

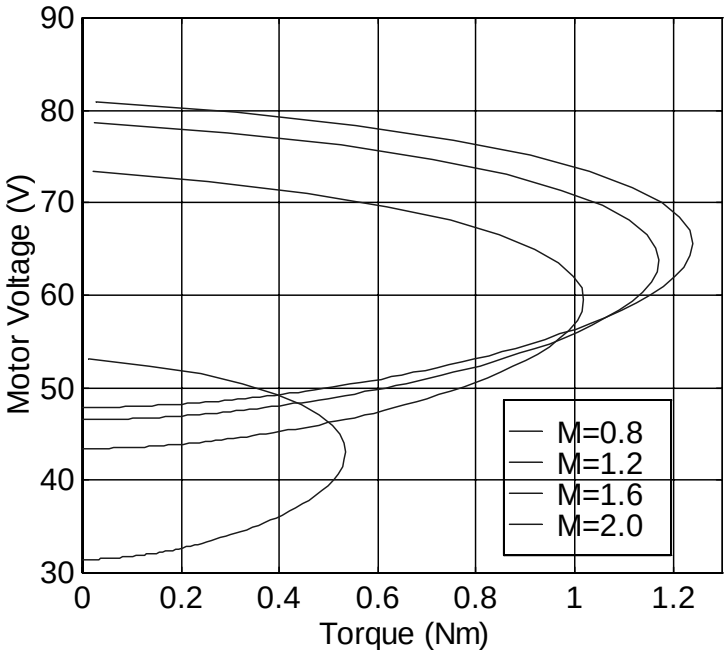

Figure 5.21: Predicted motor voltage as a function of motor torque. Constant generator rotor speed = 1840 rpm.

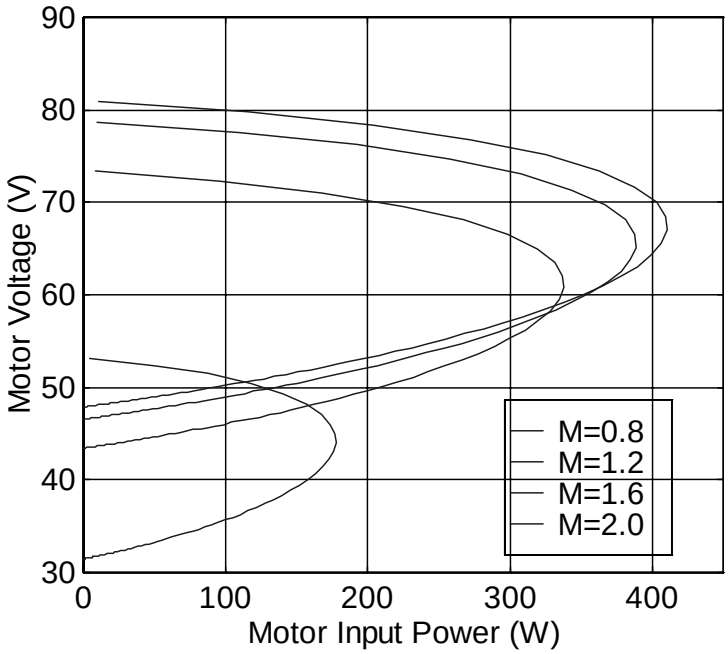

Figure 5.22: Predicted motor voltage as a function of motor input power. Constant generator rotor speed = 1840 rpm.

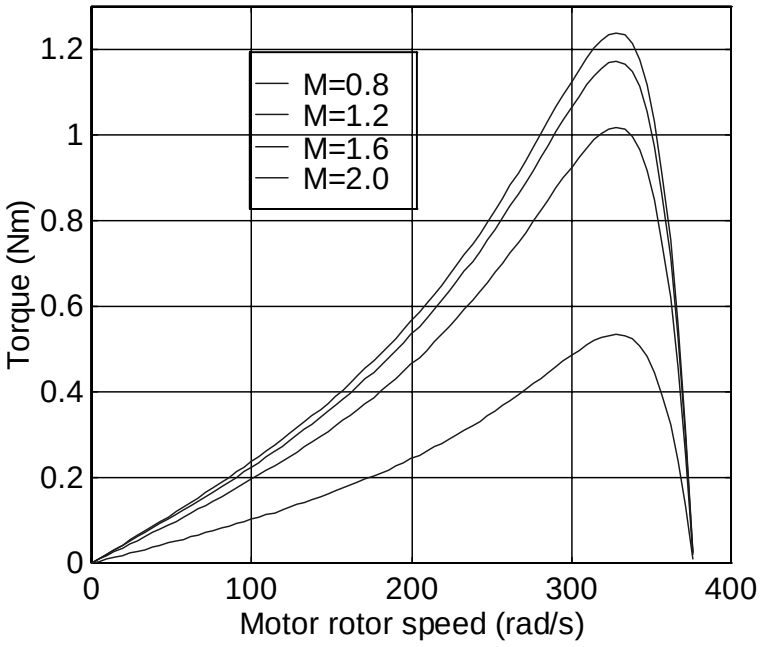

Figure 5.23: Predicted motor torque as a function of motor rotor speed. Constant generator rotor speed = 1840 rpm.

Figure 5.23 shows the motor torque as a function of the motor rotor speed at different modulation index. As the modulation index increases the motor torque increases. In addition as the motor torque increases as the motor rotor speed increases the maximum torque is obtained at about 330 rad/s of the motor rotor speed then the torque start falling as the motor rotor speed is increased further. If maximum torque is desired, it could be obtained by operating the system in the overmodulation region and at a motor rotor speed of 330 rad/s.

5.5 Parametric Studies for the Battery Inverter Single-Phase Induction Generator with SPIM Load

This section gives a description of the influences of the system parameter on the system performance. A proper selection of the motor rotor speed and the generator rotor speed can ensure that the system with induction motor operates in optimum condition. The selection of the motor load rotor speed and the generator rotor speed can be carefully done to ensure overall system efficiency, maximum torque and maximum power. For instance, if maximum torque is desired for driving a pump, the appropriate generator and motor rotor speed could be selected to achieve this.

In the study that follows three load frequencies are selected - 30Hz, 45Hz and 60Hz. The modulation index is fixed at a value of one and the load capacitor, C_q is set equal to 180 μF.

Figure 5.24 shows the contour plot of the motor torque as a function of the generator rotor speed and the motor rotor speed for different load frequency. As the load

frequencies increase the motor torque decrease for constant values of generator rotor speed and motor rotor speed. In particular at a specific load frequency (45 Hz) maximum torque can be obtained at high value of motor rotor speed and at about 1.1 p.u. of the generator rotor speed. The graph will be an excellent tool in selecting generator rotor speed and motor rotor speed for maximum torque operation such as in pump application.

The contour curves for the motor voltage as a function of the generator rotor speed and the motor rotor speed for different load frequencies is shown in Figure 5.25. In general at a constant load frequency the motor voltage is increases at a higher motor rotor speed and constant generator speed. The graph also indicates that maximum motor voltage is obtained at generator rotor speed of about 1.12p.u. The graph shows that as the frequency decreases the motor voltage is relatively constant at constant generator rotor speed and motor rotor speed.

Figure 5.26 shows the contour plot of generator output power as a funnction of the generator rotor and the motor rotor speeds for different load frequencies. Considering a load frequency of 30 Hz for instance the maximum power is obtained at a higher motor rotor speed and at a generator rotor speed of about 1.18p.u. The graph also indicates that the choice of operating load frequency generally affects the output power. If the frequency increases the output power generally decreases.

The family of contour curves of the battery current as a function of the generator rotor and the motor rotor speeds for different load frequencies is given in Figure 5.27. At a constant generator rotor speed the graph shows that the battery current is fairly constant at different values of motor rotor speed. The graph also indicates that the battery current generally decreases as load frequency increases. The negative battery current indicates

the condition when the battery absorbs real power while positive battery current shows that battery provides real power.

5.6 Transient and Dynamic Performance for the System Feeding a SPIM Load

This section examines the transient and dynamic performance of the battery inverter single-phase induction generator feeding a single-phase induction motor. The transient and dynamic studies give us better understanding of the operation of the system and also show how the system can perform with either change in load torque or generator rotor speed. The system start-up process is initially set forth. The response of the system to changes in load torque is discussed next. The system dynamic performance with the generator rotor speed changed is discussed and afterward the system performance to a high load is presented.

5.6.1 Start-up Process

This section examines the start-up process for the battery inverter generator system feeding a single-phase induction motor. The simulation was carried out with a generator rotor speed of 1840 rpm under no load condition. The modulation index was set a value of 0.80 with a carrier frequency of 2 kHz and modulating frequency of 60 Hz.

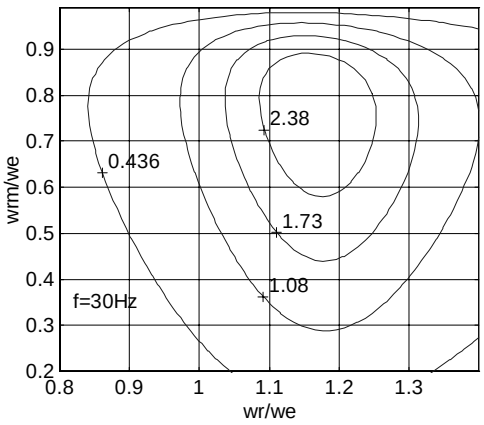

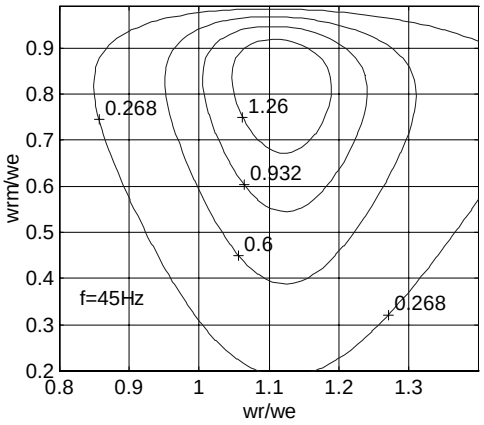

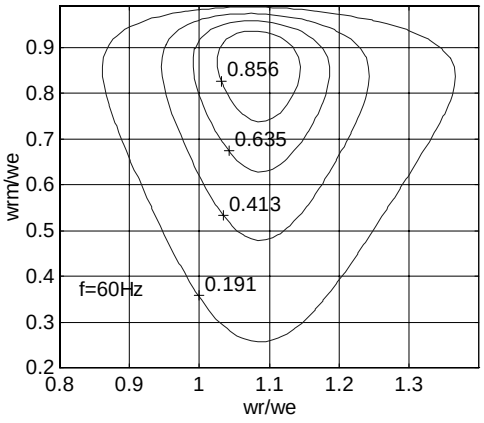

Load Frequency, f = 30Hz Load Frequency, f = 45Hz Load Frequency, f = 60Hz

Figure 5.24: Contour plot of torque, [Nm] as a variation of generator rotor speed (per unit) and motor rotor speed (per unit).

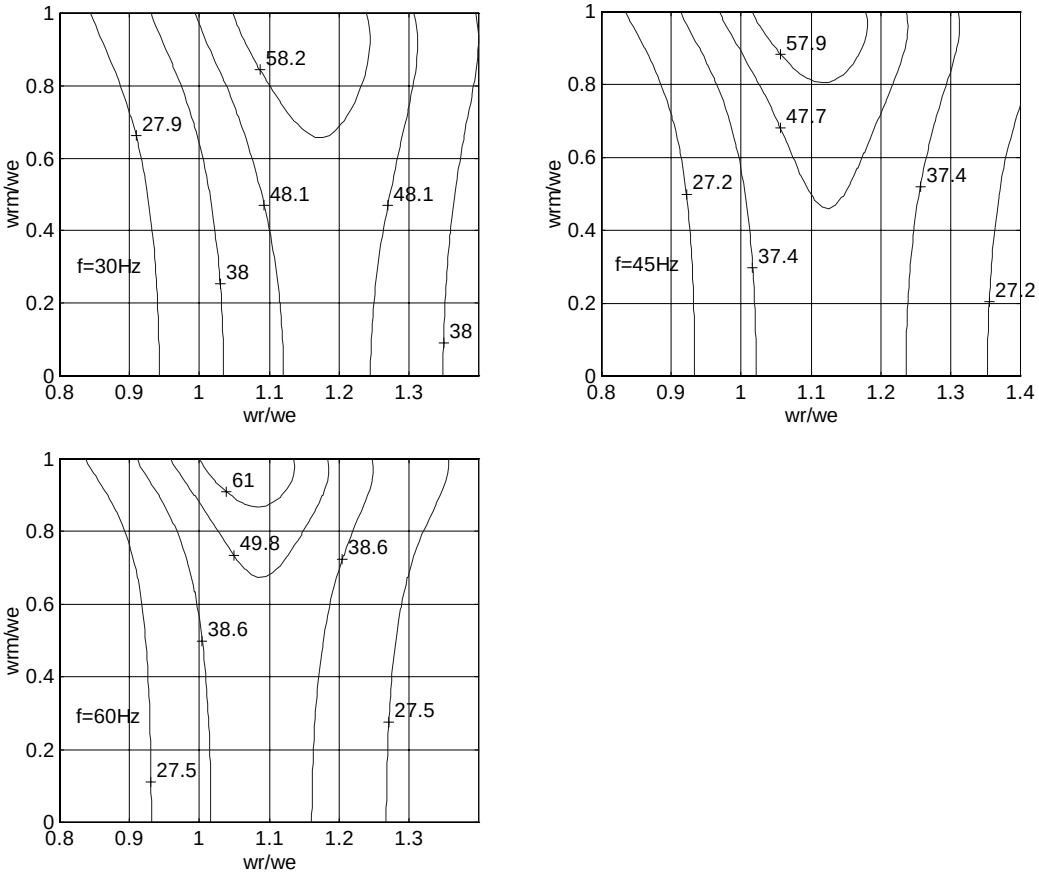

Load Frequency, f = 30Hz Load Frequency, f = 45Hz Load Frequency, f = 60Hz

Figure 5.25: Contour plot of motor voltage, [V] as a variation of generator rotor speed (per unit) and motor rotor speed (per unit).

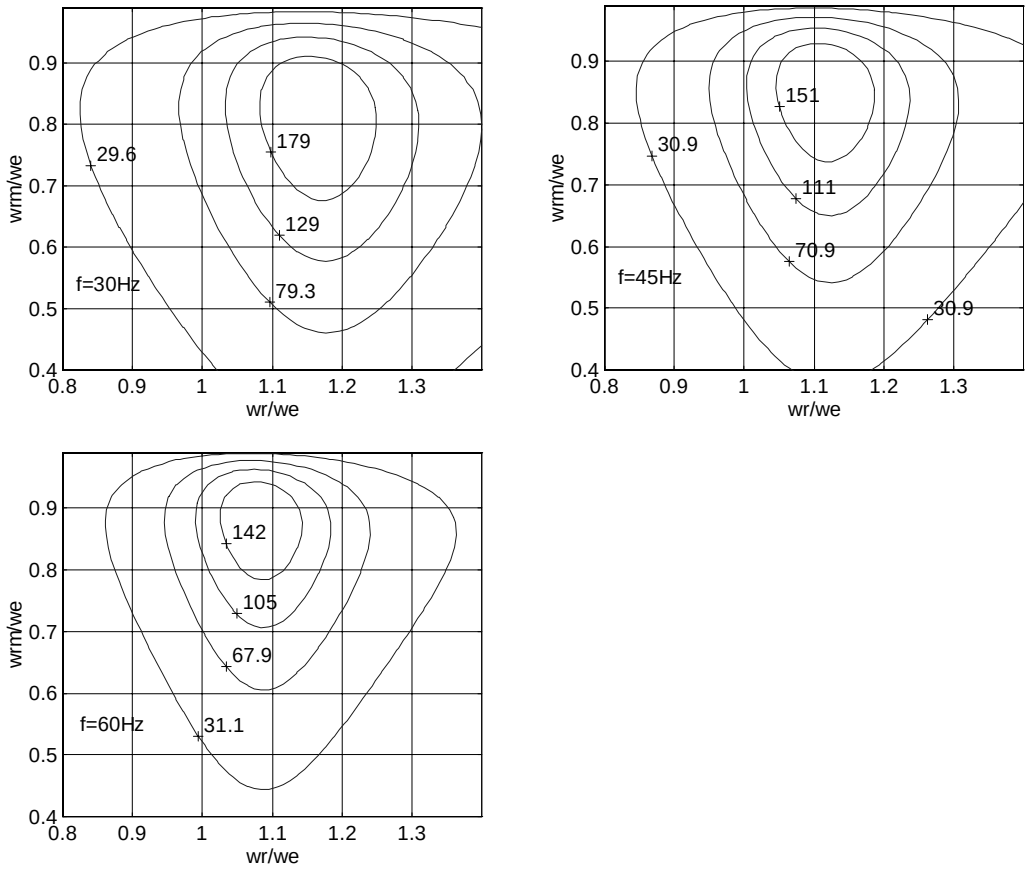

Load Frequency, f = 30Hz Load Frequency, f = 45Hz Load Frequency, f = 60Hz

Figure 5.26: Contour plot of output power, [W] as a variation of generator rotor speed (per unit) and motor rotor speed (per unit).

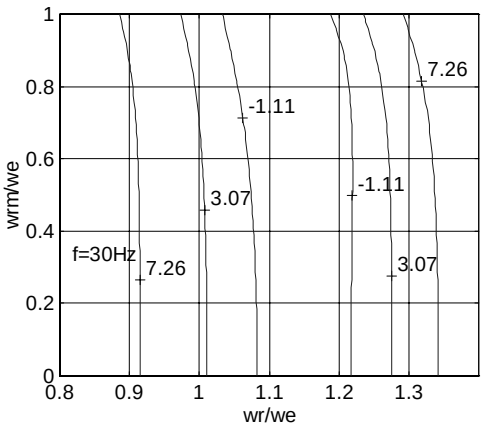

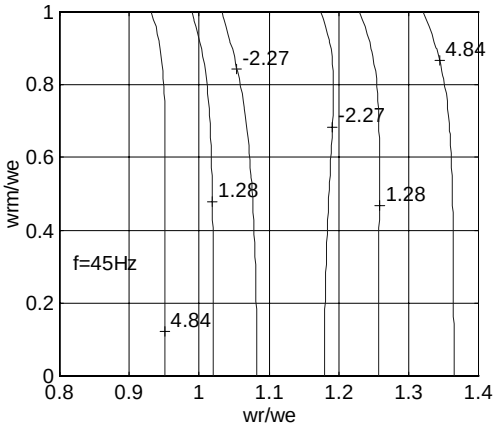

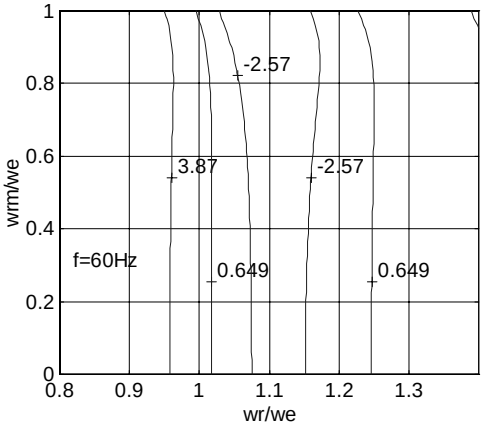

Load Frequency, f = 30Hz Load Frequency, f = 45Hz

Load Frequency, f = 60Hz

Figure 5.27: Contour plot of battery current, [A] as a variation of generator rotor speed (per unit) and motor rotor speed (per unit).

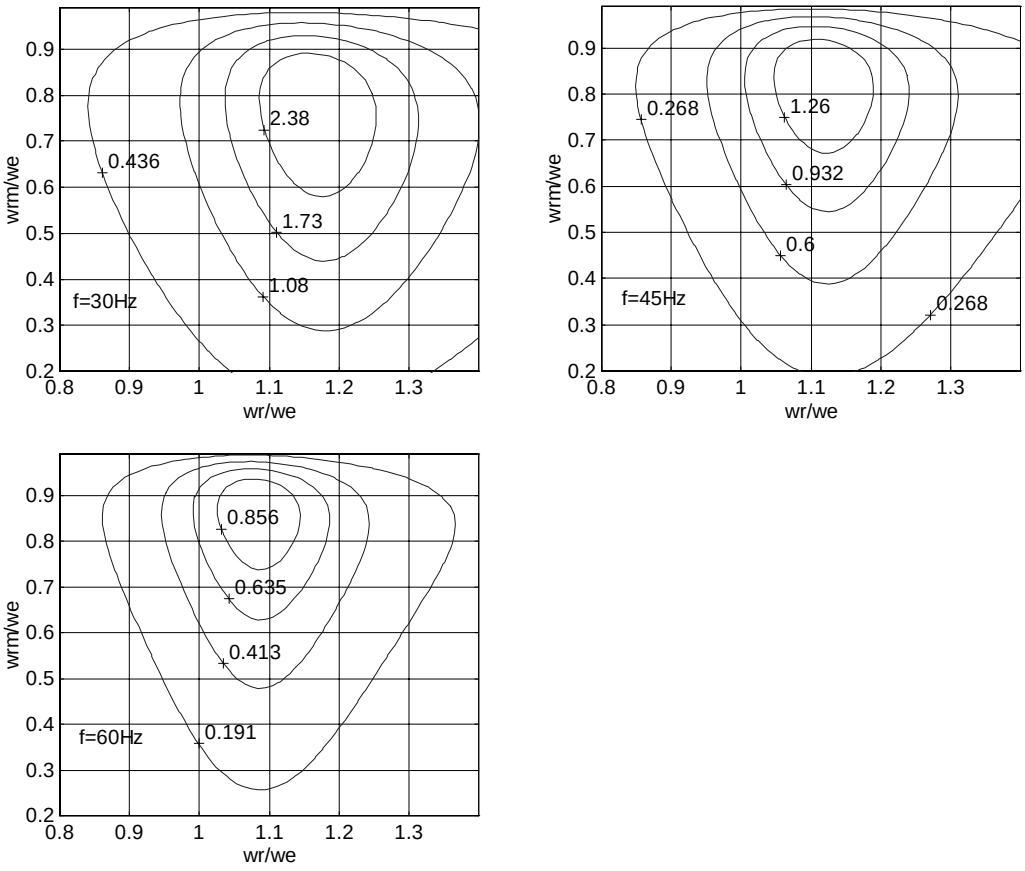

Load Frequency, f = 30Hz Load Frequency, f = 45Hz Load Frequency, f = 60Hz

Figure 5.24: Contour plot of torque, [Nm] as a variation of generator rotor speed (per unit) and motor rotor speed (per unit).

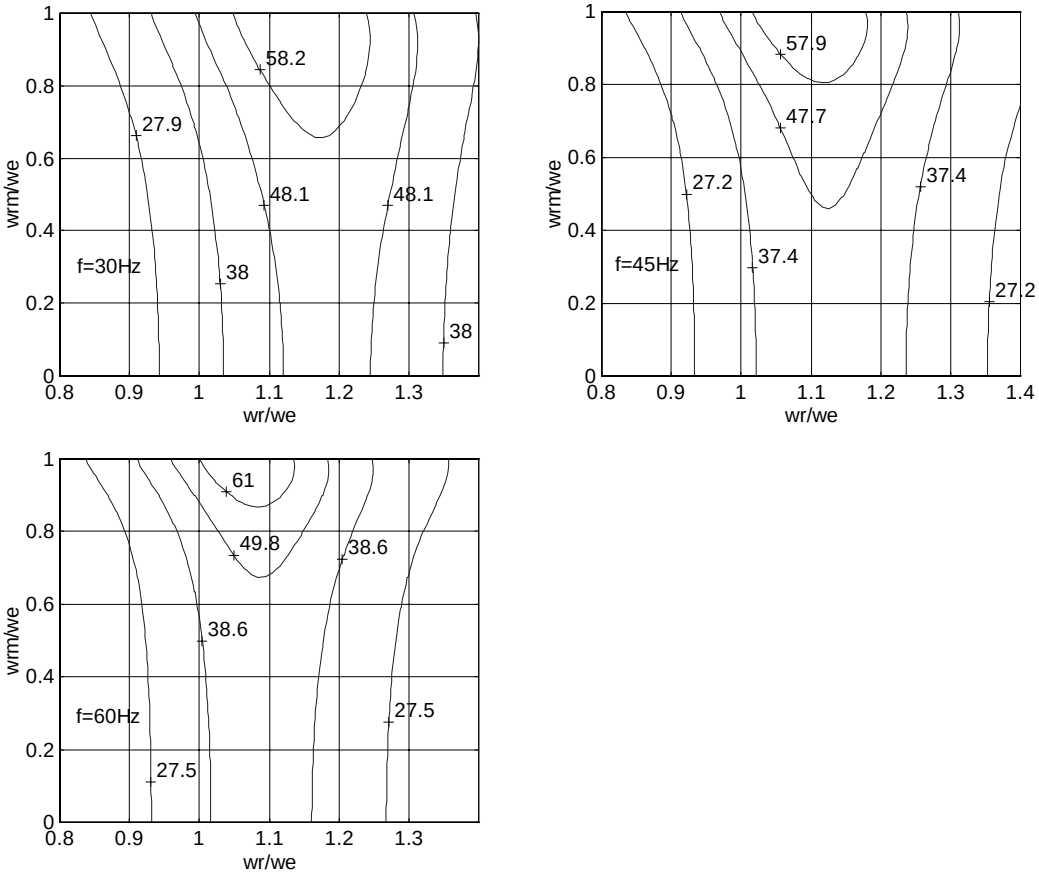

Load Frequency, f = 30Hz Load Frequency, f = 45Hz Load Frequency, f = 60Hz

Figure 5.25: Contour plot of motor voltage, [V] as a variation of generator rotor speed (per unit) and motor rotor speed (per unit).

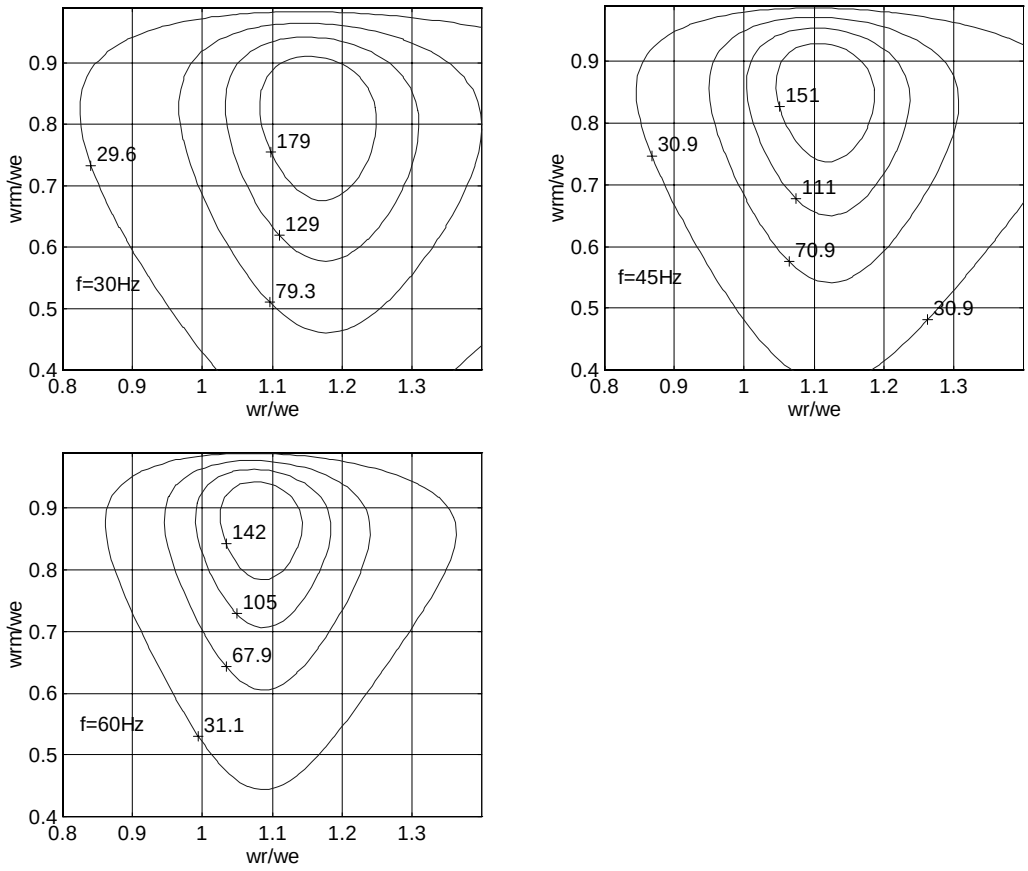

Load Frequency, f = 30Hz Load Frequency, f = 45Hz Load Frequency, f = 60Hz

Figure 5.26: Contour plot of output power, [W] as a variation of generator rotor speed (per unit) and motor rotor speed (per unit).

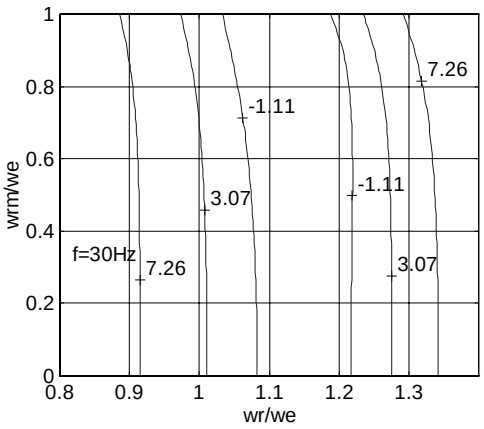

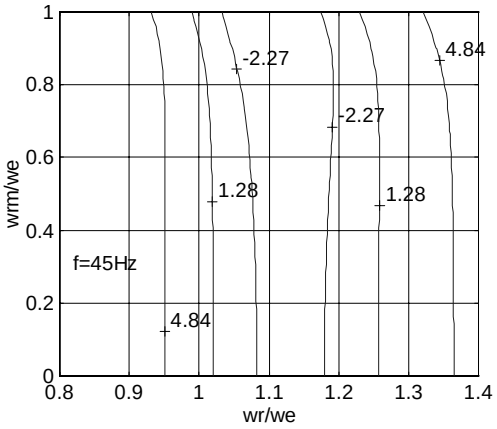

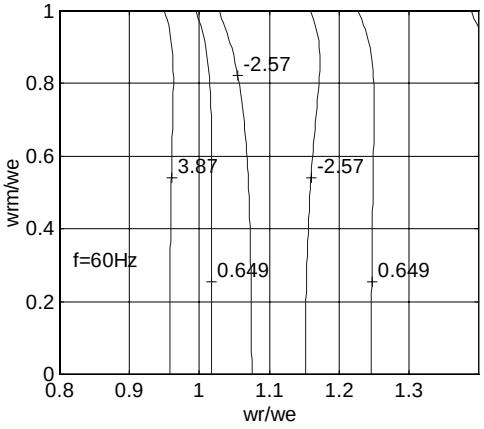

Load Frequency, f = 30Hz Load Frequency, f = 45Hz

Load Frequency, f = 60Hz

Figure 5.27: Contour plot of battery current, [A] as a variation of generator rotor speed (per unit) and motor rotor speed (per unit).

Figure 5.28 shows the motor input voltage waveform during startup. The motor input voltage waveform increases quickly until it reaches a steady-state peak value of about 46 volts. Figure 5.29 shows the generator main winding current. The main winding current increases rapidly until it reaches a steady state value.

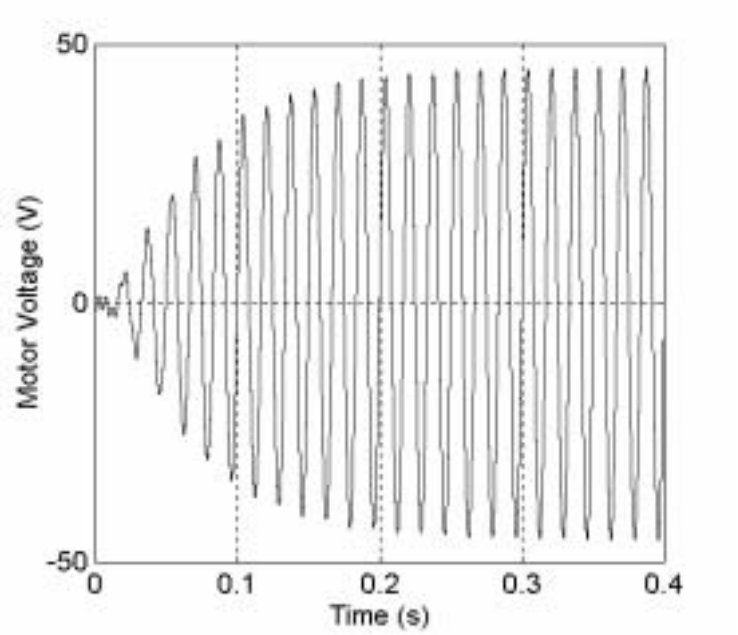

Figure 5.28 Motor voltage start-up waveform. Modulation index = 0.8, and generator rotor speed = 1840 rpm.

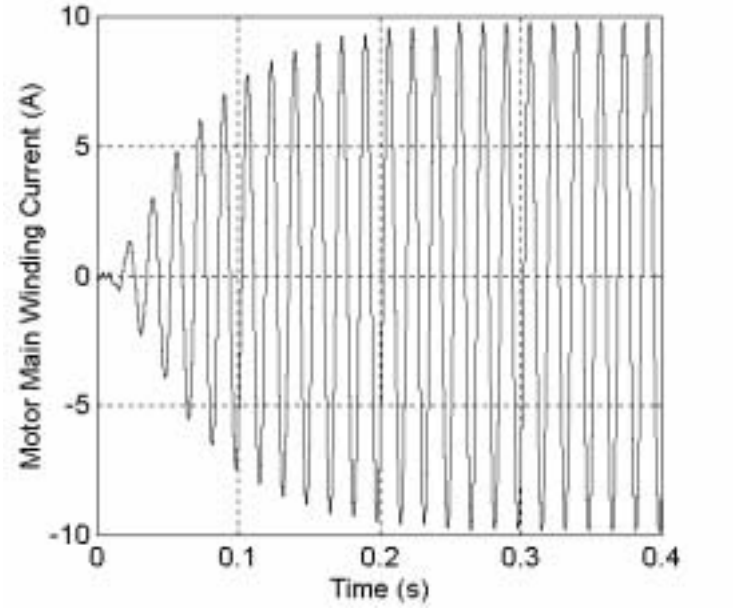

Figure 5.29 Motor main winding current start-up waveform. Modulation index = 0.8, and generator rotor speed = 1840 rpm.

Figure 5.30 shows the motor rotor speed transient waveform. The motor rotor speed ramps gradually and then to a steady state value. The motor speed graph is observed to change sharply about 4.5 seconds when the auxiliary winding of the motor in series with starting capacitor is switched out of circuit.

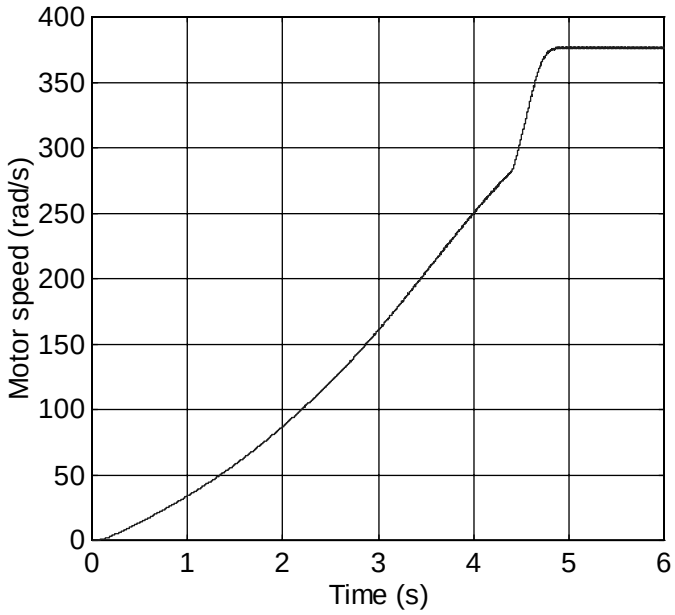

Figure 5.30 Motor rotor speed start-up waveform. Modulation index = 0.8, and generator rotor speed = 1840 rpm.

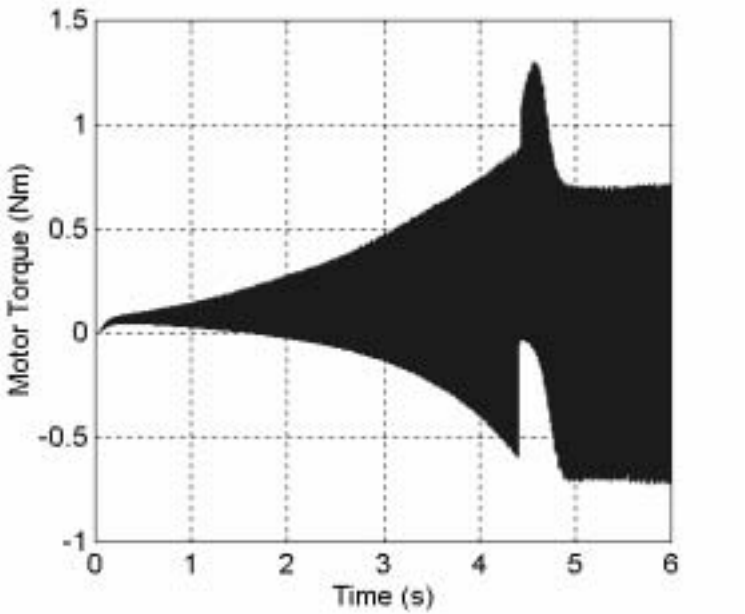

Figure 5.31 Motor torque start-up waveform. Modulation index = 0.8, and generator rotor speed = 1840 rpm.

The no load motor torque start-up waveform is shown in Figure 5.31. The motor torque gradually grows and gets to a steady-state in about 5 seconds.

The generator winding current waveform build-up is shown in Figure 5.32. The current increases rapidly to a steady state peak value of about 8.0A. Figure 5.33 gives the transient waveform of the auxiliary winding current. The auxiliary winding current increases quickly to a steady state value.

The transient waveform of the battery current is shown in Figure 5.34 during start up. The battery current is initially high then decreases to a steady state value. The battery current is positive indicating that the battery supplies real power to meet the load requirement. The single-phase induction generator torque waveform is shown in Figure 5.35. The graph shows how the generator torque grows quickly to a steady state value.

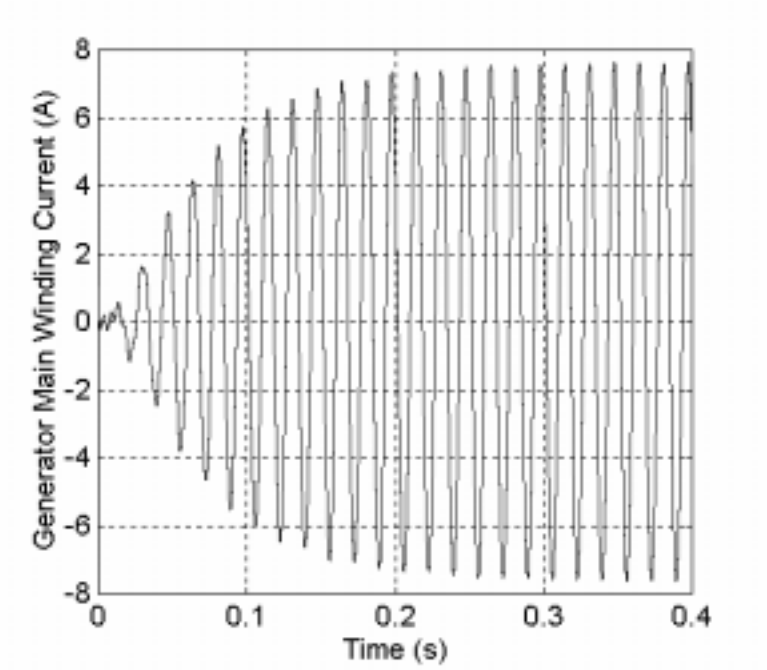

Figure 5.32 Generator main winding current start-up waveform. Modulation index = 0.8, and generator rotor speed = 1840 rpm.

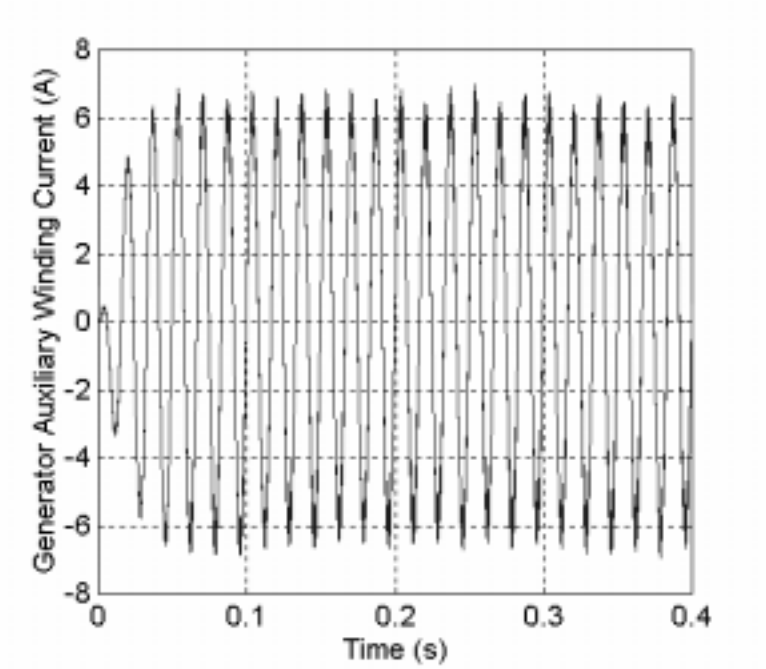

Figure 5.33 Generator auxiliary winding current start-up waveform. Modulation index = 0.8, and generator rotor speed = 1840 rpm.

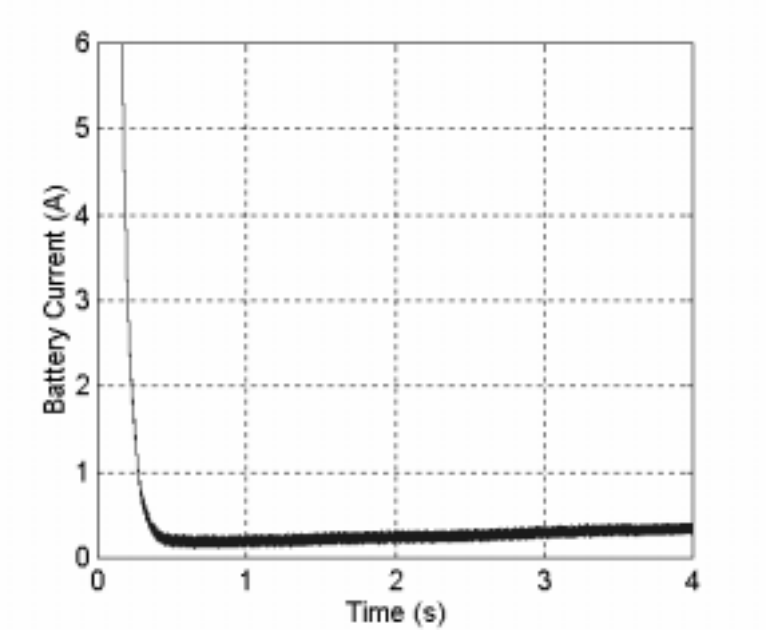

Figure 5.34 Battery current start-up waveform. Modulation index = 0.8, and generator rotor speed = 1840 rpm.

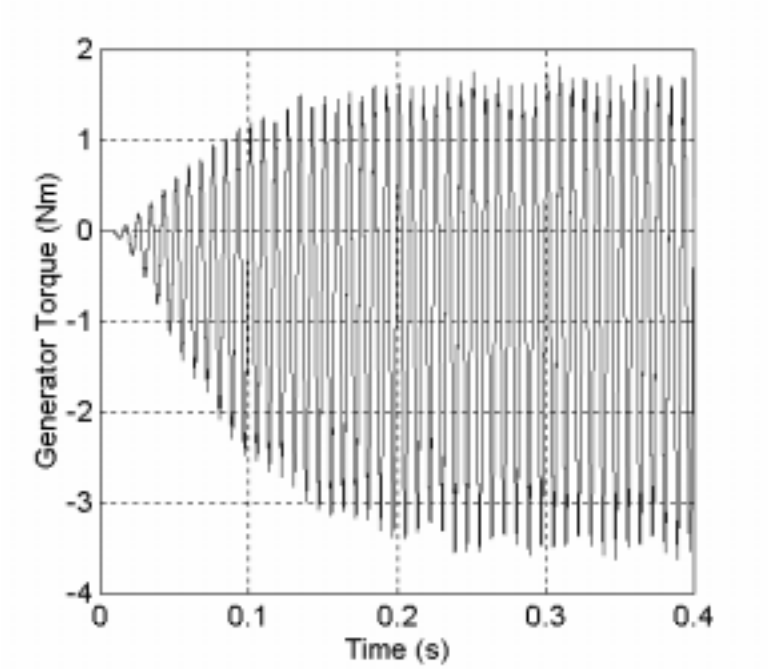

Figure 5.35 Generator torque start-up waveform. Modulation index = 0.8, and generator rotor speed = 1840 rpm.

5.6.2 System Dynamics due to Changes in Load Torque

This section examines the dynamics for the battery inverter generator system feeding a SPIM for changes in the load torque. The simulation was carried out with generator rotor speed of 1840 rpm and the modulation index was set a value of 2.0 with a carrier frequency of 2 kHz and modulating frequency of 60 Hz.

The load torque is initial set at a value of 0 Nm. When the system reaches its steady state operating condition it is changed from 0 Nm to 1.2 Nm afterward it is changed to 0.2 Nm. The changes in the load torque are illustrated in Figure 5.36.

Figure 5.37 shows the motor input voltage waveform. The graph shows how the system responded to a change in load torque. The motor input voltage decreases as the load torque is increased from 0 Nm to 1.2 Nm. The response of the motor rotor speed to changes in the load torque is shown in Figure 5.38. The motor rotor speed decreases as a

load torque of 1.2 Nm is applied to the motor. When the load torque is reduced to 0.2 Nm the motor speed increases.

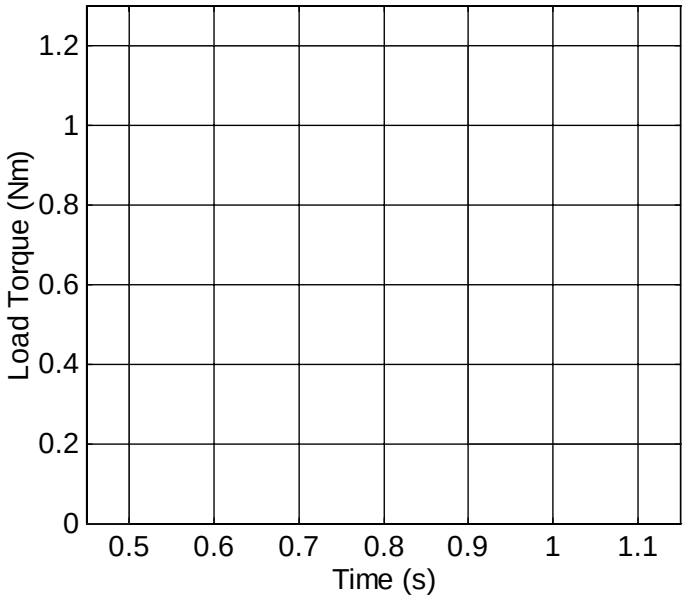

Figure 5.36. Changes in the values of the load torque. Modulation index = 2.0 and rotor generator speed = 1840 rpm.

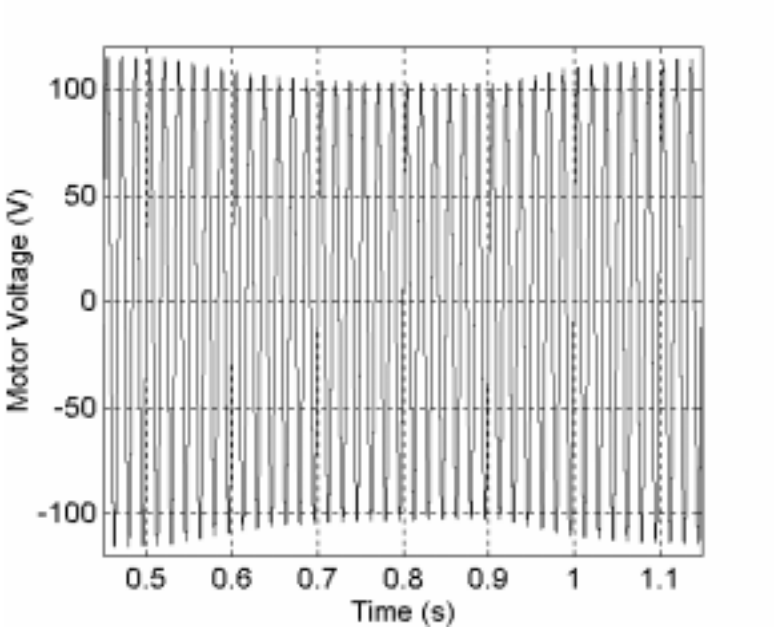

Figure 5.37. Motor input voltage waveform response to changes in load torque. Modulation index = 2.0 and rotor generator speed = 1840 rpm.

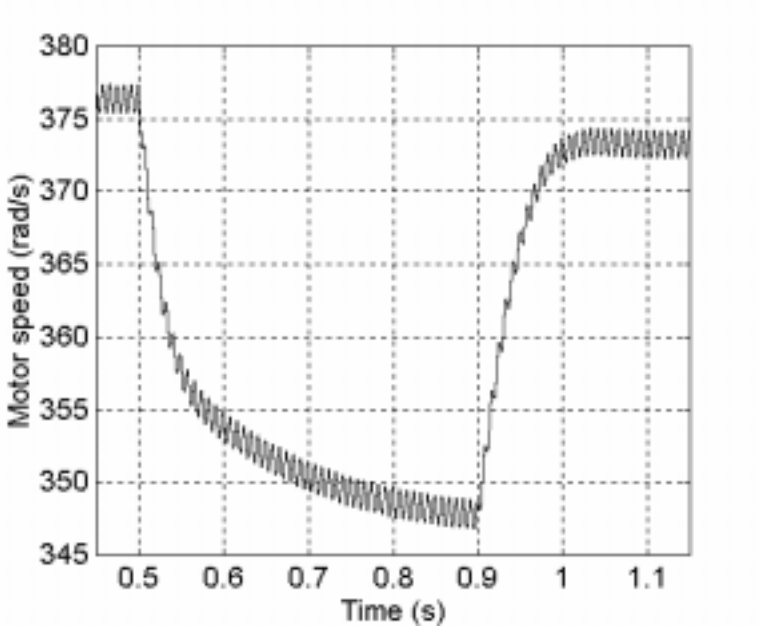

Figure 5.38. Motor rotor speed waveform response to changes in load torque. Modulation index = 2.0 and rotor generator speed = 1840 rpm.

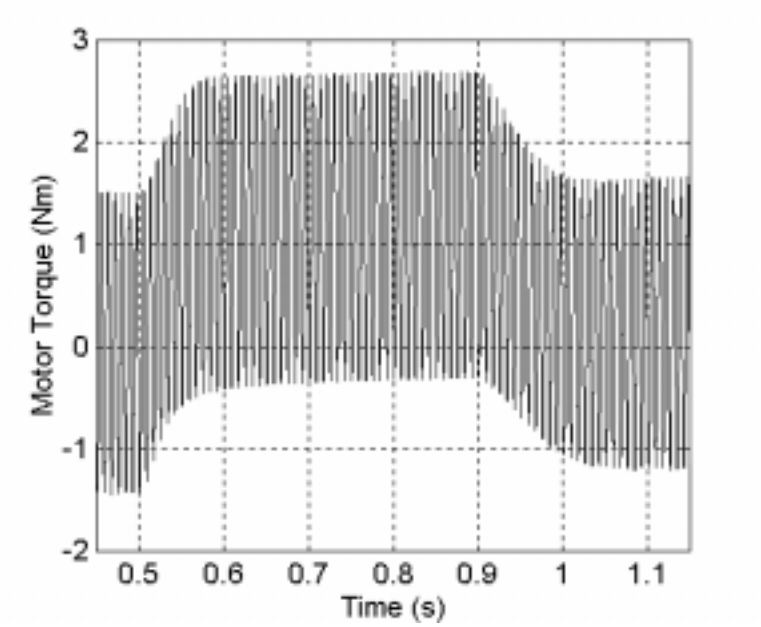

Figure 5.39. Motor torque waveform response to changes in load torque. Modulation index = 2.0 and rotor generator speed = 1840 rpm.

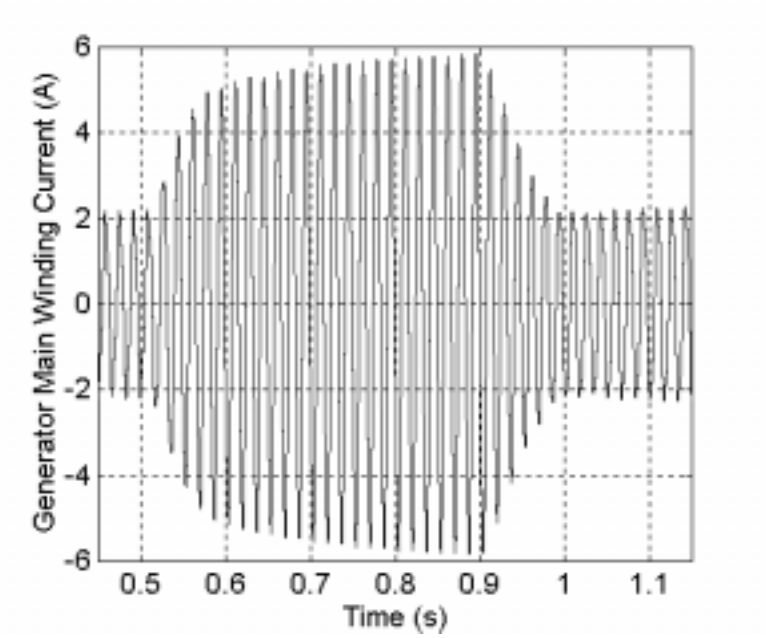

Figure 5.40. Generator main winding current waveform response to changes in load torque. Modulation index = 2.0 and rotor generator speed = 1840 rpm.

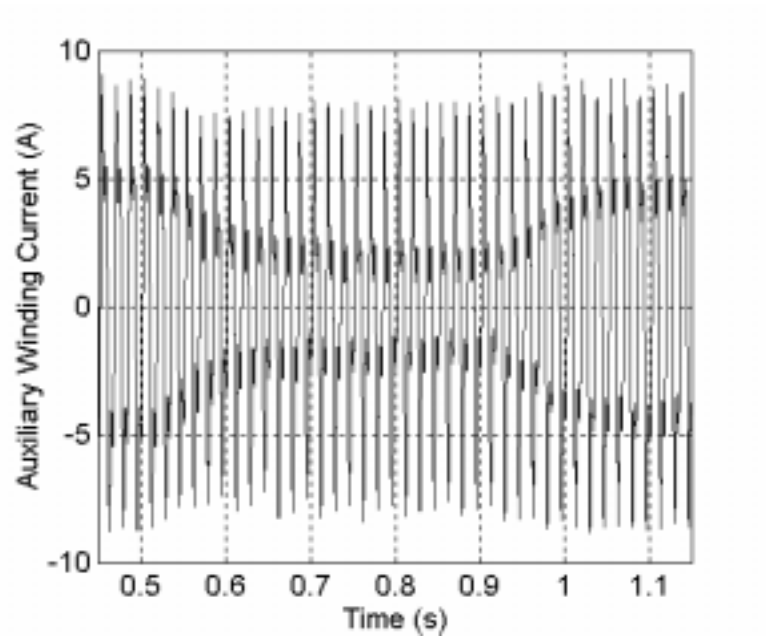

Figure 5.41. Generator auxiliary winding current waveform response to changes in load torque. Modulation index = 2.0 and rotor generator speed = 1840 rpm.

The response of the motor torque waveform to a change in load torque is shown in Figure 5.39. The motor torque initially increases and then decreases in response to a change in load torque. Figure 5.40 shows the main winding current waveform response to

a change in load torque. The main winding current waveform increases and decreases in response to change in load torque.

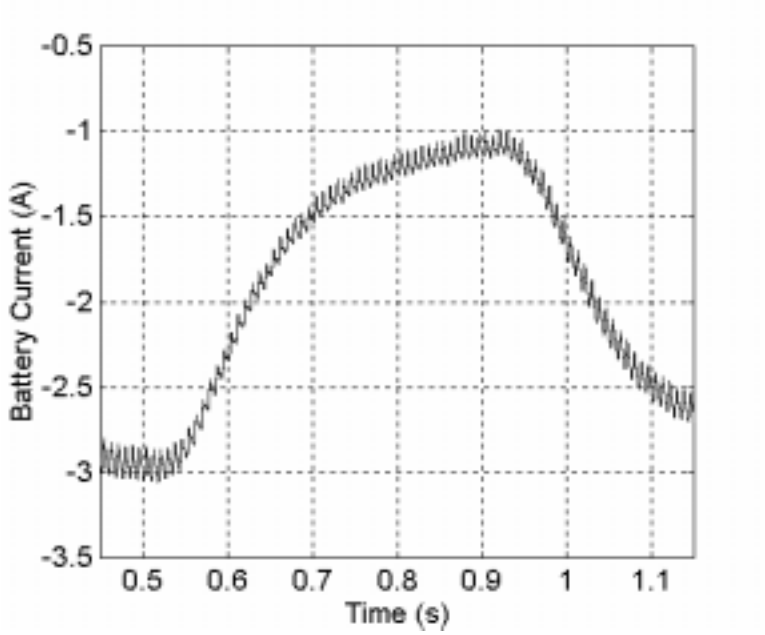

Figure 5.42. Battery current waveform response to changes in load torque. Modulation index = 2.0 and rotor generator speed = 1840 rpm.

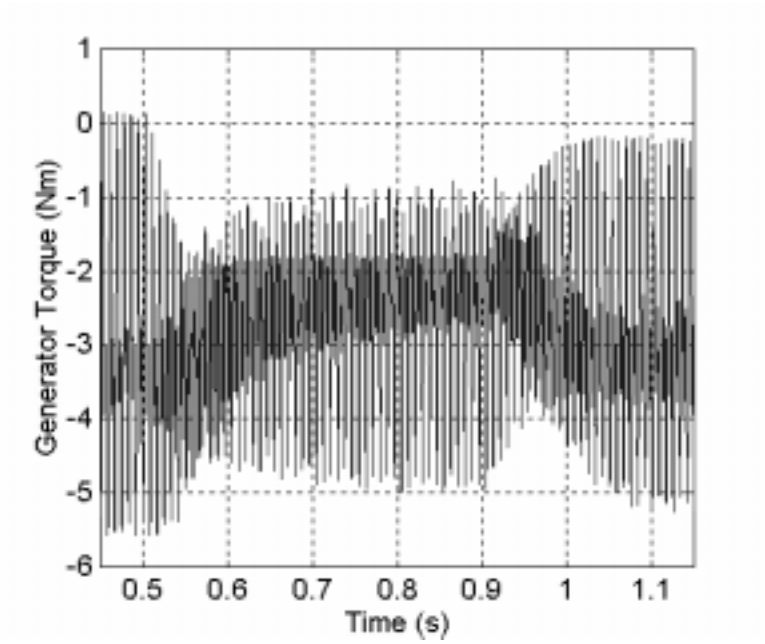

Figure 5.43. Generator torque waveform response to changes in load torque. Modulation index = 2.0 and rotor generator speed = 1840 rpm.

Figure 5.41 shows the auxiliary winding current waveform response to changes in load torque. The main winding current waveform decreases and increases in response to changes in load torque. The battery current waveform in response to changes in load torque is shown in Figure 5.42. The battery current increases and decreases in response to changes in load torque. The battery current is negative showing that the battery is absorbing real power from the load. Figure 5.43 shows the generator torque waveform response to changes in load torque. The generator speed decreases and increases in response to changes in load.

5.6.3 System Dynamics due to Changes in Generator Rotor Speed

This section examines the dynamics for the battery inverter generator system feeding a SPIM load for changes in the generator rotor speed. The simulation was carried out with load torque of 0.25Nm. The modulation index was set a value of 2.0 with a carrier frequency of 2 kHz and modulating frequency of 60 Hz.

The generator rotor speed is initial is set at a value of 1840 rpm when the system reaches its steady state operating condition it is changed from 1840 rpm to 1900 rpm then to 1740 rpm as shown in Figure 5.44.

Figure 5.45 shows motor input voltage waveform response to changes in the generator rotor speed. It is observed that the motor voltage is still maintained while the generator rotor speed is less than the 1800 rpm (synchronous speed) as the battery supplies the needed real power required by the load. Figure 5.46 shows the main winding

current waveform. The main winding current decrease as the generator rotor speed changes from 1900 rpm to 1740 rpm.

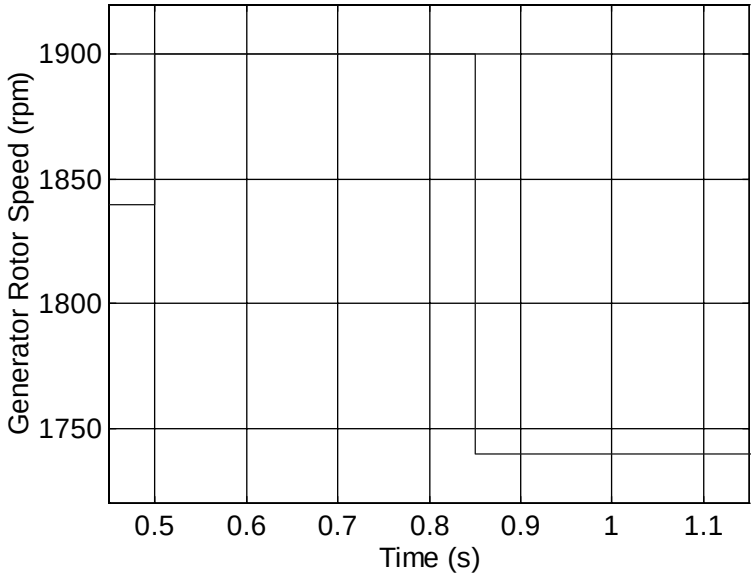

Figure 5.44. Changes in the values of generator rotor speeds. Modulation index = 2.0 and Load Torque = 0.25 Nm.

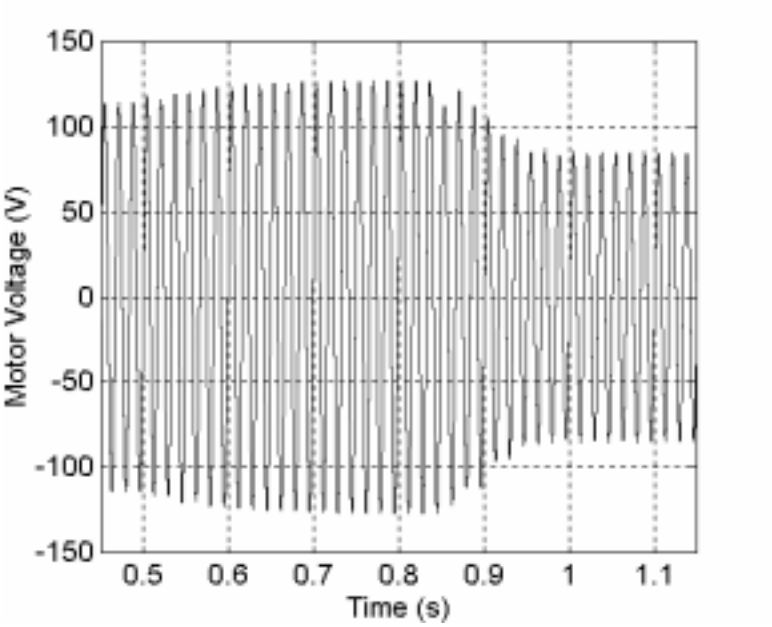

Figure 5.45 Motor input voltage waveform response to changes in generator rotor speed. Modulation index = 2.0 and Load Torque = 0.25 Nm.

Figure 5.47 shows motor rotor speed waveform in response to changes in the generator rotor speed. The motor speed decreases slightly in response to changes in generator rotor speed from 1900 rpm to 1740 rpm. Figure 5.48 shows the motor torque waveform in response to changes in generator rotor speed. The motor torque increases and then decreases in response to changes in generator rotor speed.

Figure 5.49 shows the generator main winding current response to changes in generator rotor speed. The generator main winding current decreases as the generator rotor speed changes from 1900 rpm to 1740 rpm. The auxiliary winding current waveform response to changes in the generator rotor speed is shown in Figure 5.50. The auxiliary winding current initially increases then decreases in response to changes in the generator rotor speed.

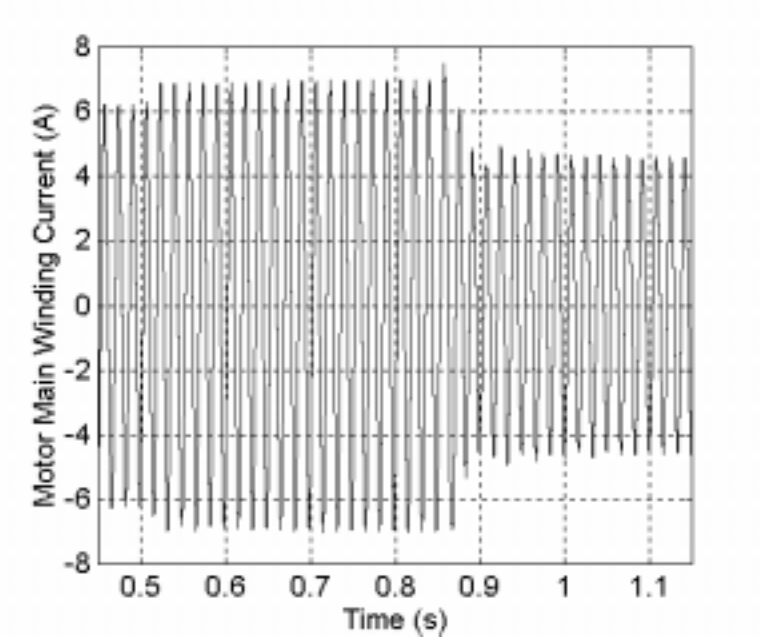

Figure 5.46 Motor main winding current waveform response to changes in generator rotor speed. Modulation index = 2.0 and Load Torque = 0.25 Nm.

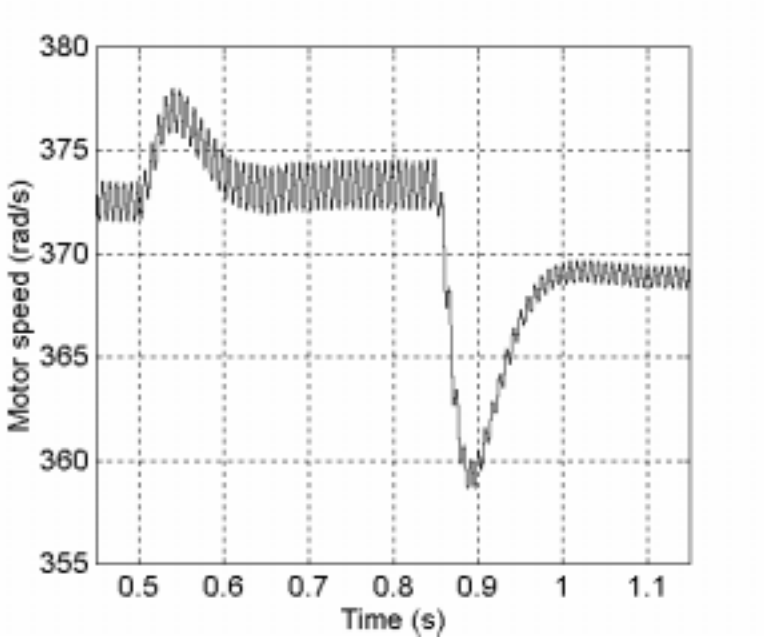

Figure 5.47 Motor rotor speed waveform response to changes in generator rotor speed. Modulation index = 2.0 and Load Torque = 0.25 Nm.

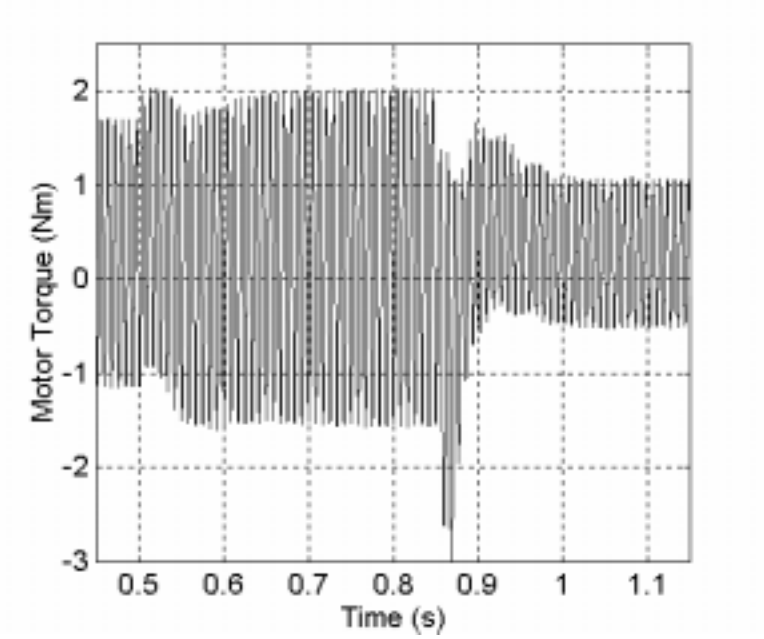

Figure 5.48 Motor torque waveform response to changes in generator rotor speed. Modulation index = 2.0 and Load Torque = 0.25 Nm.

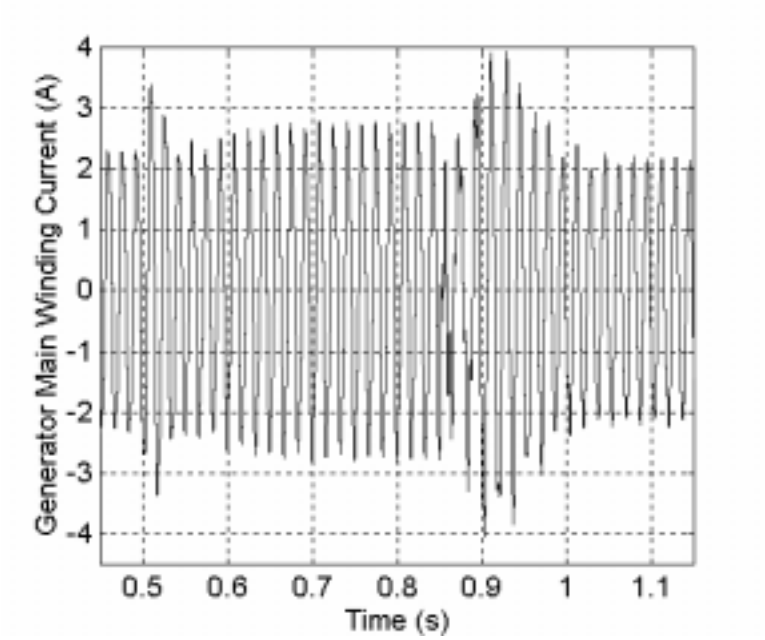

Figure 5.49 Generator main winding current waveform response to changes in generator rotor speed. Modulation index = 2.0 and Load Torque = 0.25 Nm.

Figure 5.51 shows the battery current response to changes in generator rotor speed. The battery current increases as the generator rotor speed changes from 1900 rpm to 1740 rpm. The graph also shows that the system is able to sustain its operation even when the generator rotor speed (1740 rpm) is less than the synchronous speed (1800 rpm) as the battery provides real power requirement for the motor load.

The generator torque waveform response to changes in the generator rotor speed is shown in Figure 5.52. The generator torque increases in response to changes in the generator rotor speed from 1900 rpm to 1740 rpm. It can be observed that the generator torque is positive indicating that the machine is now operating as a motor.

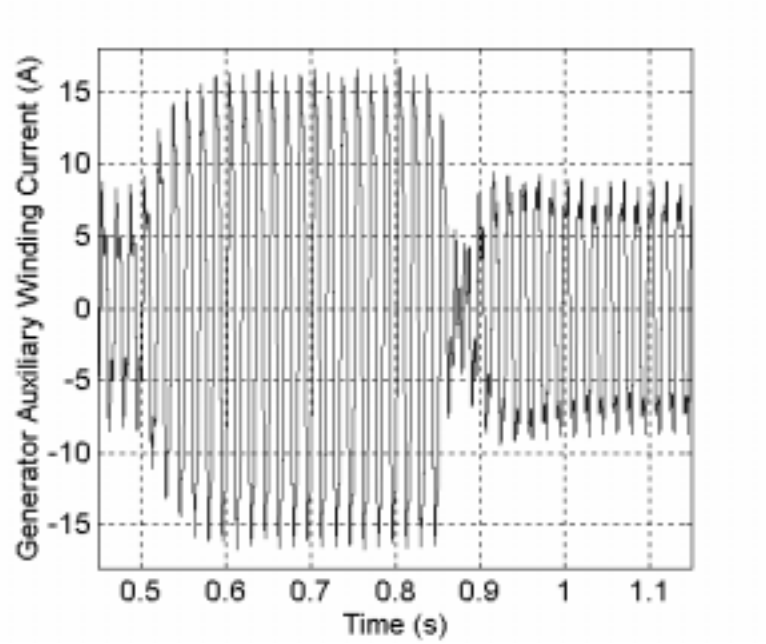

Figure 5.50 Generator auxiliary winding current waveform response to changes in generator rotor speed. Modulation index = 2.0 and Load Torque = 0.25 Nm.

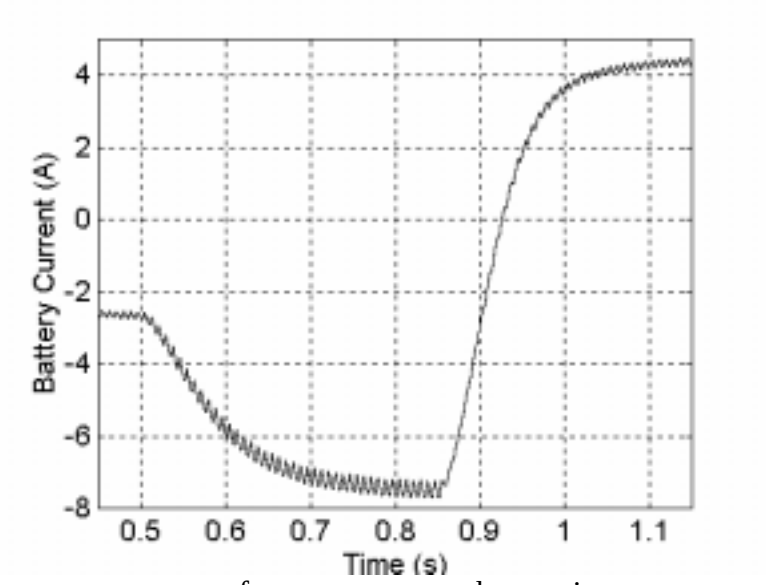

Figure 5.51. Battery current waveform response to changes in generator rotor speed. Modulation index = 2.0 and Load Torque = 0.25 Nm.

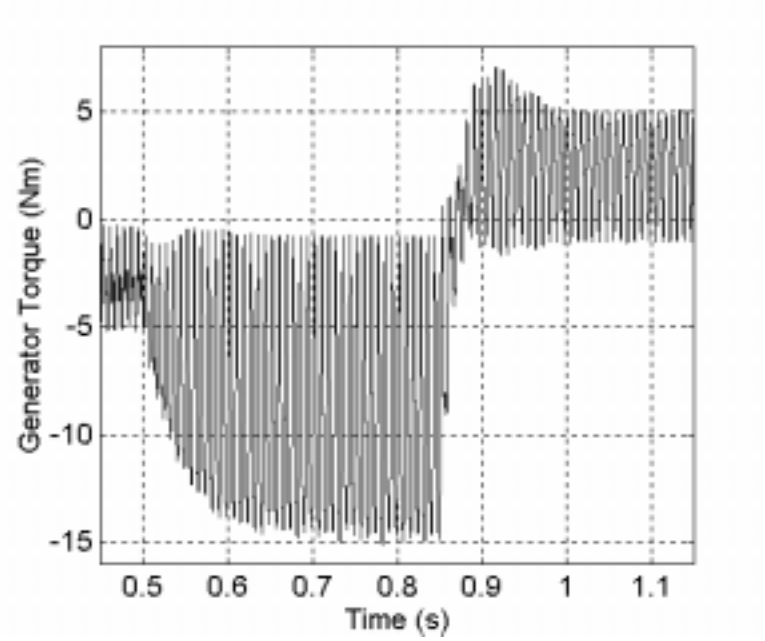

Figure 5.52 Generator torque waveform response to changes in generator rotor speed. Modulation index = 2.0 and Load Torque = 0.25 Nm.

5.6.4 System Voltage Collapse

This section examines the dynamics of the battery inverter generator system feeding a SPIM when heavily loaded. The simulation was carried out with generator rotor speed of 1840 rpm. The modulation index was set a value of 1.2 with a carrier frequency of 2 kHz and modulating frequency of 60 Hz.

The load torque is initial set at a value of 0 Nm when the system reaches its steady state operating condition it is changed from 0 Nm to 4.0 Nm. The changes in load torque are illustrated in Figure 5.53.

Figure 5.54 shows the motor input voltage waveform. The graph shows how the system response to a change in load torque. The motor input voltage collapses to a lower peak value as it is loaded with a torque of 4 Nm. The response of the motor main winding

current to a change in the load torque is shown in Figure 5.55. The motor main winding current increases in response to the high load.

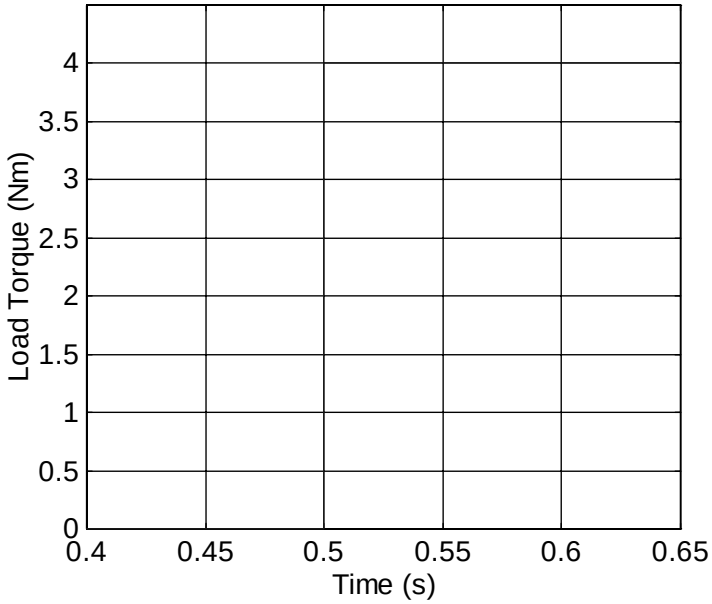

Figure 5.53. Changes in the values of the load torque. Modulation index = 1.2 and rotor generator speed = 1840 rpm.

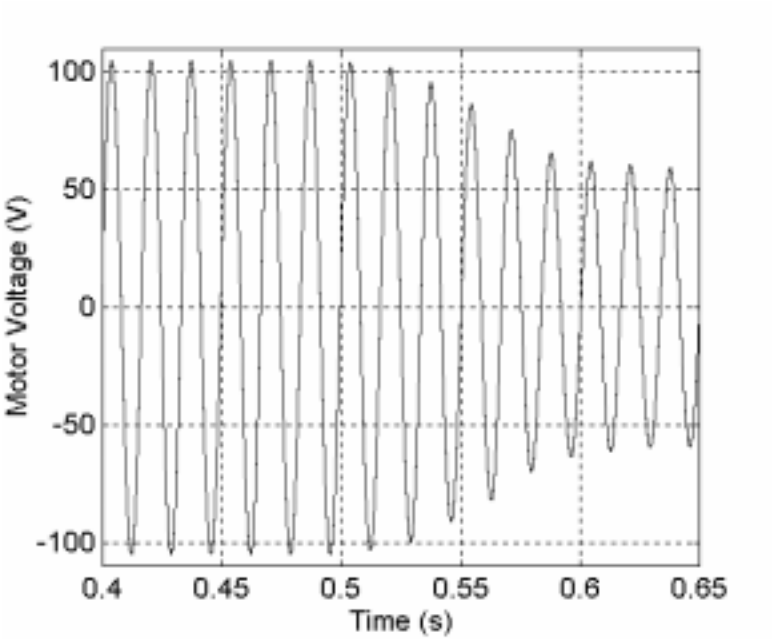

Figure 5.54. Motor input voltage waveform. Modulation index = 1.2 and rotor generator speed = 1840 rpm.

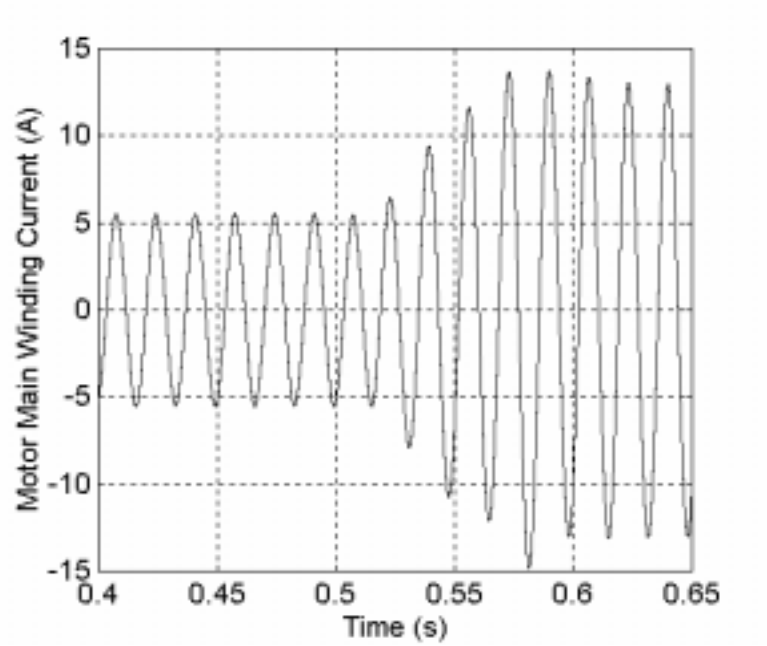

Figure 5.55. Motor main winding current waveform. Modulation index = 1.2 and rotor generator speed = 1840 rpm.

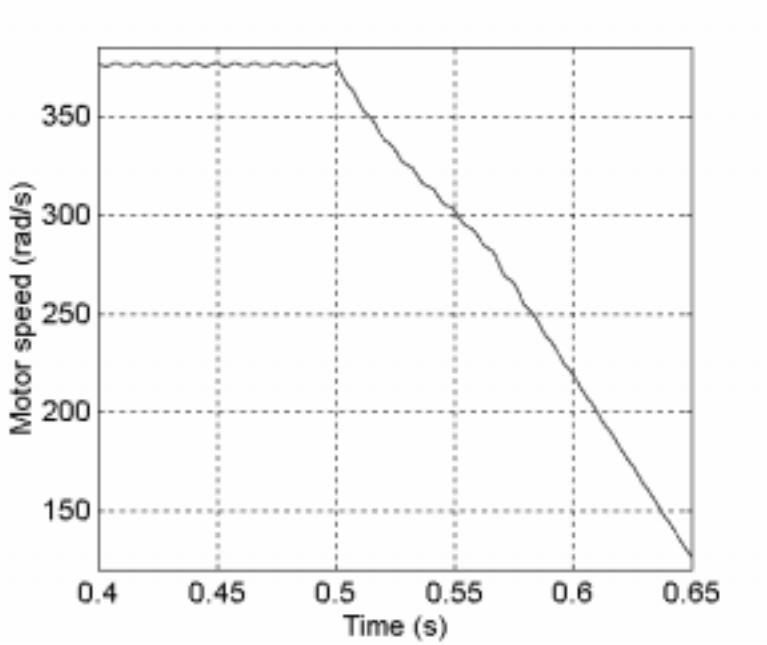

Figure 5.56. Motor speed waveform. Modulation index = 1.2 and rotor generator speed = 1840 rpm.

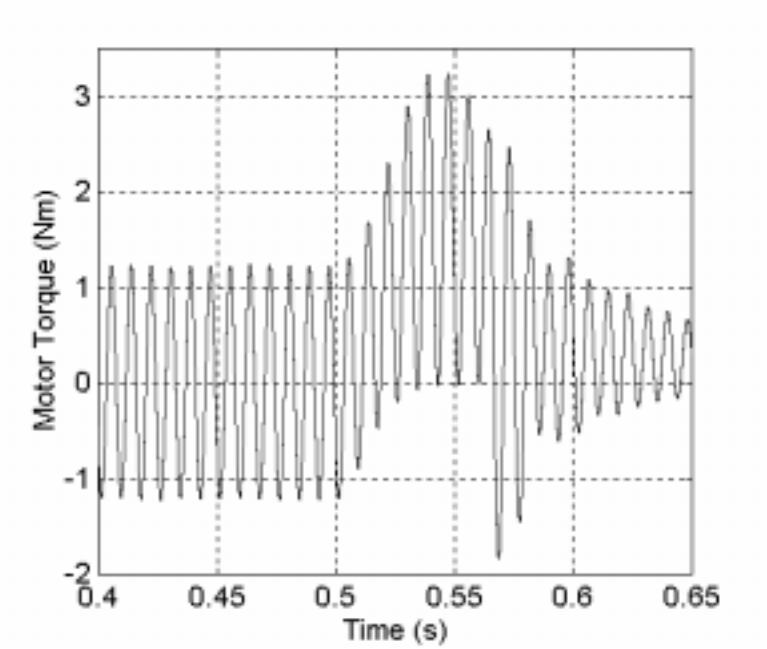

Figure 5.57. Motor torque waveform. Modulation index = 1.2 and rotor generator speed = 1840 rpm.

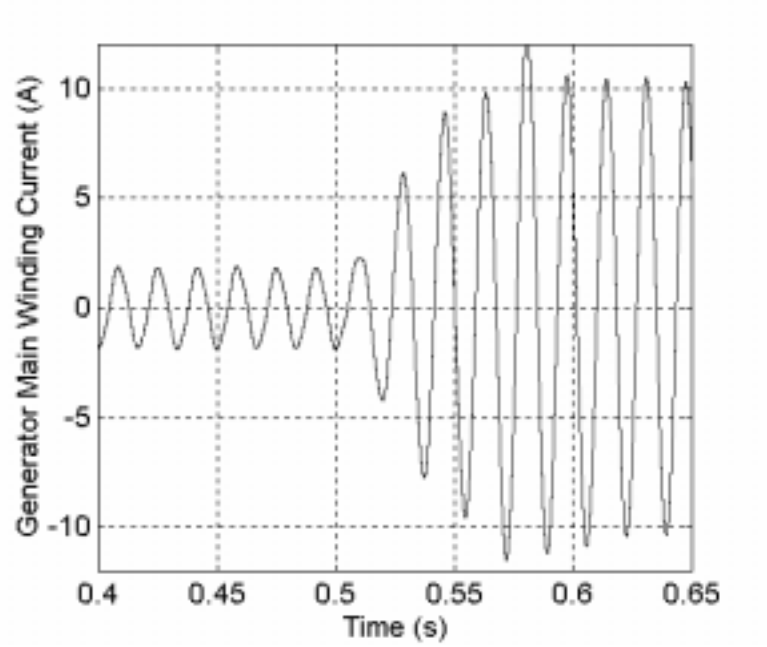

Figure 5.58. Generator main winding current waveform. Modulation index = 1.2 and rotor generator speed = 1840 rpm.

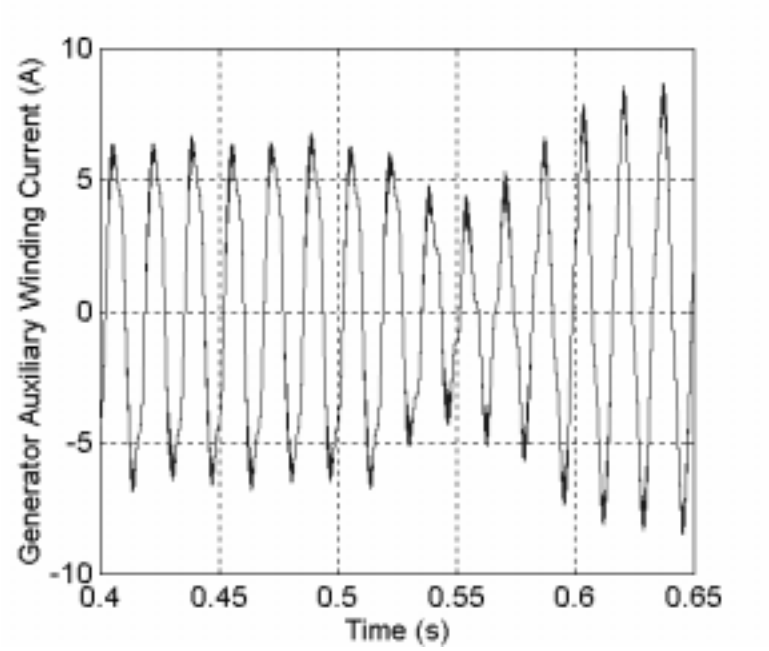

Figure 5.59. Generator auxiliary winding current waveform. Modulation index = 1.2 and rotor generator speed = 1840 rpm.

The response of the motor rotor speed to a change in the load torque is shown in Figure 5.56. The graph shows that the motor rotor speed falling rapidly as it is loaded with a load of 4 Nm. Figure 5.57 shows the motor torque waveform. As the system is loaded with 4 Nm the motor stalls as show in the waveform (torque reduces).

The generator main winding current is shown in Figure 5.58. The graphs shows that the current grows quickly as it is loaded. Figure 5.59 shows the waveform of the generator auxiliary winding current. The auxiliary winding current grows rapidly as the system is loaded.

The battery current waveform response to a change in load torque is shown in Figure 5.60. The graph indicates that initial the battery absorbs real power (negative current), when it is loaded afterwards the current increases to meet the power requirement of the motor. Figure 5.61 shows the system generator torque waveform response to a change in load torque. The waveform grows quickly as the system is loaded.

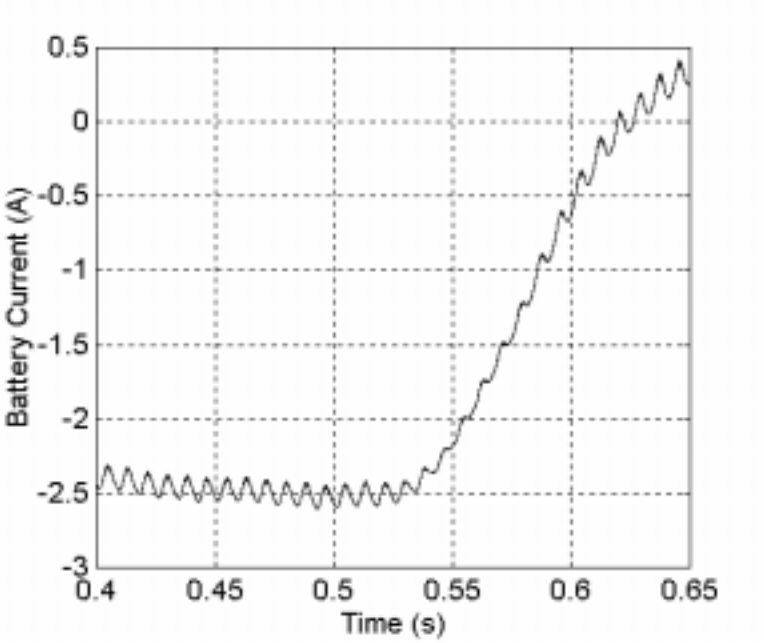

Figure 5.60. Battery current waveform. Modulation index = 1.2 and rotor generator speed = 1840 rpm.

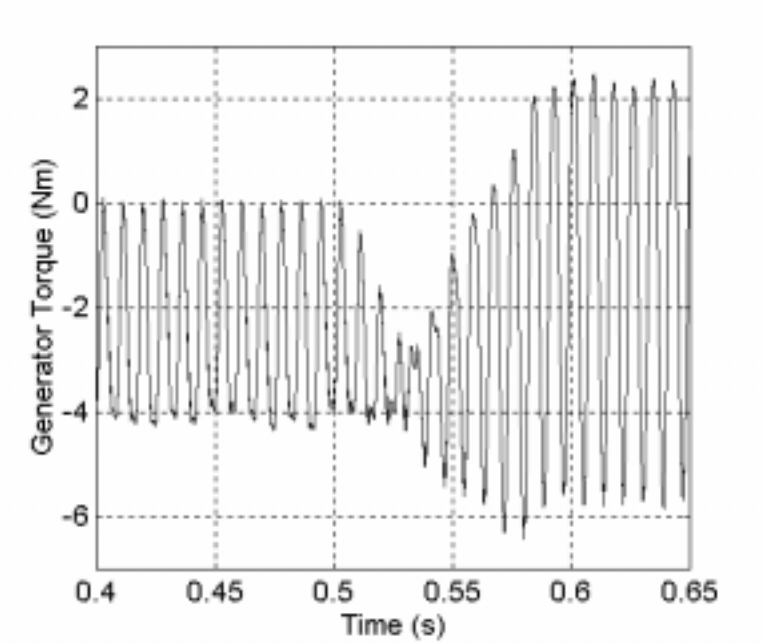

Figure 5.61. Generator torque waveform. Modulation index = 1.2 and rotor generator speed = 1840 rpm.

CHAPTER 6

ANALYSIS OF CAPACITOR INVERTER SINGLE-PHASE INDUCTION GENERATOR SYSTEM WITH IMPEDANCE LOAD

6.1 Introduction

In this chapter, the analysis of the capacitor inverter single-phase induction generator system feeding an impedance load will be presented. The block diagram of the single-phase generator system without battery and impedance load is shown in Figure 6.1. This generator system is similar to the system in Figure 4.1. The only difference is that the battery is not connected. The operation of the capacitor inverter SPIG system is also similar to the generator system in chapter 4.

The first part of this chapter deals with the development of the steady state mathematical model for the generator system feeding an impedance load using harmonic balance technique. Next the condition for self-excitation for the generator system without battery is discussed. The minimum requirements for system parameters for fixed impedance load results are shown.

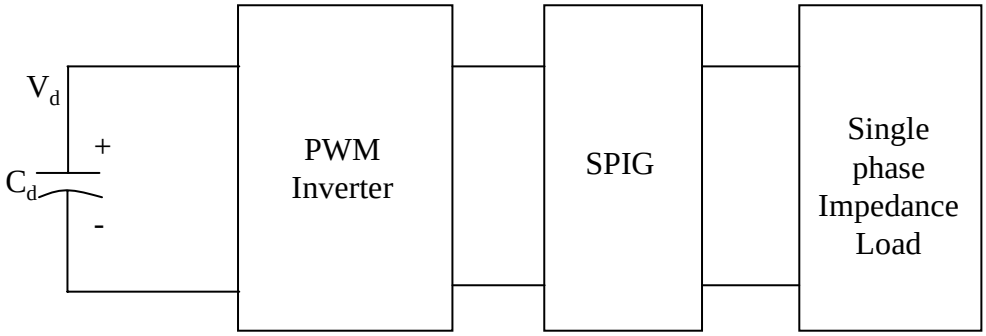

Figure 6.1. Block diagram of the system.

6.2 Mathematical Model of System

The PWM inverter, the single-phase induction generator, and the impedance load makes up the generator system. The schematic diagram of the generator system is shown in Figure 6.2.

The capacitor inverter SPIG system operation is similar to the generator system description in section 4.2. The main difference is that capacitor inverter SPIG system under consideration is without the battery. The full charged capacitor is connected into the input of the PWM inverter. The inverter is switched using the bipolar voltage switching scheme. The output of the inverter is fed to the auxiliary winding of the single-phase generator. The output from the main winding is fed to the impedance load. The system has the same features as the system discussed in chapter four. When the SPIG is supplied more than enough power required by the motor load the excess power is used to charge the capacitor and when the power provided by the generator is less than the

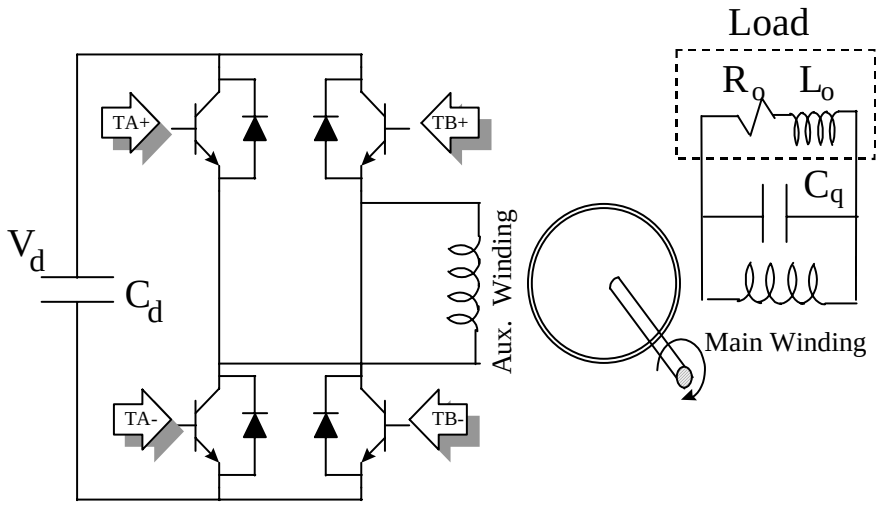

Figure 6.2. Schematic diagram of the system.

requirement by the impedance load the capacitor discharges to provide the balance. A regulated output voltage can be achieved by appropriately choice of the modulation index.

The equivalent circuit of the system that is the capacitor, PWM inverter, single-phase induction generator, and impedance load is shown in Figure 6.3.

The dynamic equation for the capacitor-PWM inverter generator system is given as

$$pV_d = \frac{1}{C_d}\left(-I_{ds}S_a\right) \tag{6.1}$$

$$V_{ds} = S_a V_d \tag{6.2}$$

$$p\lambda_{ds} = V_{ds} - r_{ds} I_{ds} \tag{6.3}$$

$$p\lambda_{qs} = V_{qs} - r_{qs} I_{qs} \tag{6.4}$$

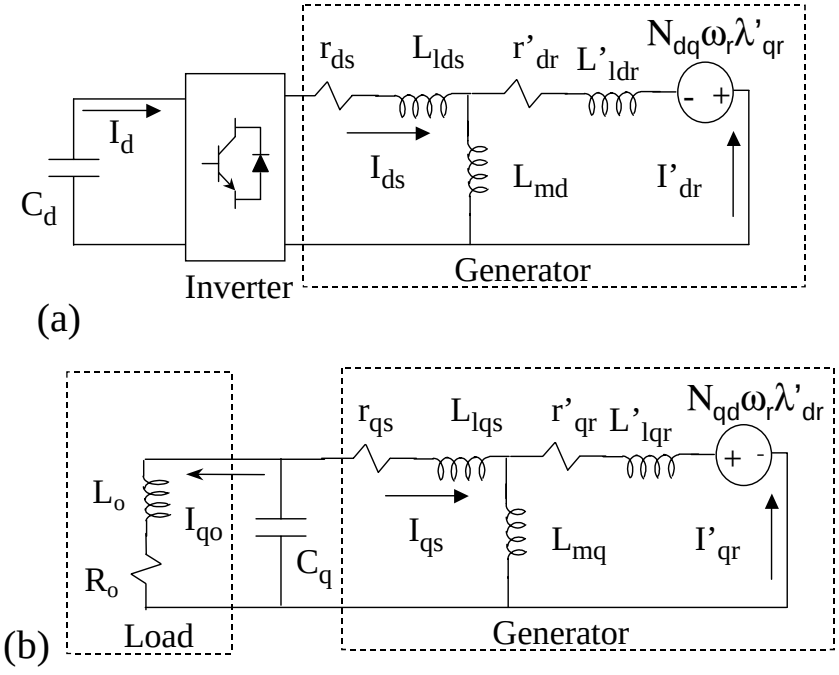

Figure 6.3. The q-d equivalent circuit of the capacitor-PWM inverter generator system with impedance load. (a) d-axis, (b) q-axis circuit.

$$p\lambda'_{qr} = N_{qd}\omega_r\lambda'_{dr} - r'_{qr}I'_{qr} \tag{6.5}$$

$$p\lambda'_{dr} = -N_{dq}\omega_r\lambda'_{qr} - r'_{dr}I'_{dr} \ . \tag{6.6}$$

$$pV_{qs} = -\frac{1}{C_q}\left(I_{qs} + \frac{V_{qs}}{Z_o}\right) \tag{6.7}$$

where the capacitor voltage and current are denoted V_d and I_d. The other state variable and parameter are as defined in chapter 4.

Equations 4.12 - 4.15 representing the q-d flux linkages of the generator are given as

$$\lambda_{qs} = L_{qs}I_{qs} + L_{mq}I'_{qr} \tag{6.8}$$

$$\lambda_{ds} = L_{ds}I_{ds} + L_{md}I'_{dr} \tag{6.9}$$

$$\lambda'_{qr} = L'_{qr}I'_{qr} + L_{mq}I_{qs} \tag{6.10}$$

$$\lambda'_{dr} = L'_{dr}I'_{dr} + L_{md}I_{ds} \ . \tag{6.11}$$

The dynamics of the generator turbine is given in Equations (4.16 and 4.17) and are given as

$$p\omega_r = \frac{P}{2J}(T_o - T_e) \tag{6.12}$$

$$T_e = \frac{P}{2}\left(N_{dq}\lambda'_{qr}I'_{dr} - N_{qd}\lambda'_{dr}I'_{qr}\right) \tag{6.13}$$

with the parameter and other state variables represented in chapter 4.

6.3. Condition for Self Excitation

The capacitor inverter generator system in Figure 6.2 does not have any battery source; for excitation to occur the system need to be carefully studied. If a close examination of the generator system equation is carried out the necessary parameter for self-excitation can be determined. In the analysis that follows harmonic balance technique was used in determine the condition for self-excitation. The steady state equation can be obtained from the dynamic Equation 6.1 to 6.13. S_a, I_{ds} and V_d are defined as

$$S_a = M_q \cos(\theta) + M_{dq} \sin(\theta)$$

$$I_{ds} = I_{ds1} \cos(\theta) + I_{ds2} \sin(\theta)$$

$$V_d = V_{do} + V_{d1} \cos(2\theta) + V_{d2} \sin(2\theta).$$

Applying harmonic balance technique on Equation 6.1

$$pV_d = \frac{1}{C_d}\left(M_q \cos(\theta) + M_{dq} \sin(\theta)\right) * \left(I_{ds1} \cos(\theta) + I_{ds2} \sin(\theta)\right); \tag{6.14}$$

the differential of V_d above results in

$$pV_d = pV_{do} + \left(pV_{d1} + 2\omega_e V_{d2}\right)\cos(\theta) + \left(pV_{d2} - 2\omega_e V_{d1}\right)\sin(\theta). \tag{6.15}$$

Since Equations 6.13 and 6.14 are equal, terms must also be equal. Comparing terms in Equation 6.13 and 6.14

$$pV_{do} = -\frac{1}{2C_d}\left(M_q I_{ds1} + M_d I_{ds2}\right) \tag{6.16}$$

$$pV_{d1} + 2\omega_e V_{d2} = -\frac{1}{2C_d}\left(M_q I_{ds1} - M_d I_{ds2}\right) \tag{6.17}$$

$$pV_{d2} - 2\omega_e V_{d1} = -\frac{1}{2C_d}\left(M_q I_{ds2} + M_d I_{ds1}\right). \tag{6.18}$$

Substituting S_a and V_d in Equation 6.2, V_{ds} becomes

$$V_{ds} = \left(M_q V_{do} + \frac{1}{2}M_q V_{d1} + \frac{1}{2}M_d V_{d2}\right)cos(\theta) + \left(M_d V_{do} + \frac{1}{2}M_q V_{d2} - \frac{1}{2}M_d V_{d1}\right)sin(\theta); \tag{6.19}$$

also Equation 6.3 can be expressed as

$$V_{ds} = \left(r_{ds} I_{ds1} + \omega_e \lambda_{ds2} + p\lambda_{ds1}\right)cos(\theta) + \left(r_{ds} I_{ds2} - \omega_e \lambda_{ds1} + p\lambda_{ds2}\right)sin(\theta). \tag{6.20}$$

Since Equations 6.19 and 6.20 are equal, the terms are also equal. Hence

$$r_{ds} I_{ds1} + \omega_e \lambda_{ds2} + p\lambda_{ds1} = M_q V_{do} + \frac{1}{2}M_q V_{d1} + \frac{1}{2}M_d V_{d2} \tag{6.21}$$

$$r_{ds} I_{ds2} - \omega_e \lambda_{ds1} + p\lambda_{ds2} = M_d V_{do} + \frac{1}{2}M_q V_{d2} - \frac{1}{2}M_d V_{d1}. \tag{6.22}$$

With harmonic balance technique applied to Equations (6.4 - 6.7) the following equation results

$$V_{qs1} = r_{qs} I_{qs1} + \omega_e \lambda_{qs2} + p\lambda_{qs1} \tag{6.23}$$

$$V_{qs2} = r_{qs} I_{qs2} - \omega_e \lambda_{qs1} + p\lambda_{qs2} \tag{6.24}$$

$$p\lambda'_{qr1} + \omega_e \lambda'_{qr2} = N_{qd}\omega_r \lambda'_{dr1} - r'_{qr} I'_{qr1} \tag{6.25}$$

$$p\lambda'_{qr2} - \omega_e \lambda'_{qr1} = N_{qd}\omega_r \lambda'_{dr2} - r'_{qr} I'_{qr2} \tag{6.26}$$

$$p\lambda'_{dr1} + \omega_e \lambda'_{dr2} = -N_{dq}\omega_r \lambda'_{qr1} - r'_{dr} I'_{dr1} \tag{6.27}$$

$$p\lambda'_{dr2} - \omega_e \lambda'_{dr1} = -N_{dq}\omega_r \lambda'_{qr2} - r'_{dr} I'_{dr2} \tag{6.28}$$

$$pV_{qs1} + \omega_e V_{qs2} = -\frac{1}{C_q}\left(I_{qs1} + \frac{V_{qs1}}{Z_o}\right) \tag{6.29}$$

$$pV_{qs2} - \omega_e V_{qs1} = -\frac{1}{C_q}\left(I_{qs2} + \frac{V_{qs2}}{Z_o} \right) . \tag{6.30}$$

At steady state, peak of the state variables are constant making derivatives in Equations 6.13 - 6.30 to be equal to zero.

The system equation in terms of flux is then obtained by substituting for current using Equations 6.8 - 6.11. The system equation in matrix form is given in Equation 6.31.

$$\begin{bmatrix} 0 \\ 0 \\ 0 \\ 0 \\ 0 \\ 0 \\ 0 \\ 0 \\ 0 \\ 0 \\ 0 \\ 0 \end{bmatrix} = \begin{bmatrix} 0 & 0 & 0 & Cdd\,Mq\,U2 & Cdd\,Md\,U2 & 0 & 0 & 0 & 0 & -Cdd\,Mq\,U1 & -Cdd\,Md\,U1 & 0 & 0 \\ 0 & 0 & -2\,we & Cdd\,Mq\,U2 & -Cdd\,Md\,U2 & 0 & 0 & 0 & 0 & -Cdd\,Mq\,U1 & Cdd\,Md\,U1 & 0 & 0 \\ 0 & 2\,we & 0 & Cdd\,Md\,U2 & Cdd\,Mq\,U2 & 0 & 0 & 0 & 0 & -Cdd\,Md\,U1 & -Cdd\,Mq\,U1 & 0 & 0 \\ Mq & \frac{Mq}{2} & \frac{Md}{2} & U4 & -we & 0 & 0 & 0 & 0 & -U3 & 0 & 0 & 0 \\ Md & -\frac{Md}{2} & \frac{Mq}{2} & we & U4 & 0 & 0 & 0 & 0 & 0 & -U3 & 0 & 0 \\ 0 & 0 & 0 & 0 & 0 & -U6 & -we & U5 & 0 & 0 & 0 & 1 & 0 \\ 0 & 0 & 0 & 0 & 0 & we & -U6 & 0 & -U5 & 0 & 0 & 0 & 1 \\ 0 & 0 & 0 & 0 & 0 & U7 & 0 & -U8 & -we & Nqd\,wr & 0 & 0 & 0 \\ 0 & 0 & 0 & 0 & 0 & 0 & U7 & we & -U8 & 0 & Nqd\,wr & 0 & 0 \\ 0 & 0 & 0 & -U9 & 0 & 0 & 0 & -\frac{wr}{Nqd} & 0 & T1 & -we & 0 & 0 \\ 0 & 0 & 0 & 0 & -U9 & 0 & 0 & 0 & -\frac{wr}{Nqd} & we & T1 & 0 & 0 \\ 0 & 0 & 0 & 0 & 0 & -Cqq\,T3 & 0 & Cqq\,T2 & 0 & 0 & 0 & -Cqq\,Zoo & -we \\ 0 & 0 & 0 & 0 & 0 & 0 & -Cqq\,T3 & 0 & Cqq\,T2 & 0 & 0 & we & -Cqq\,Zoo \end{bmatrix} \begin{bmatrix} Vdo \\ Vd1 \\ Vd2 \\ I\,ds1 \\ I\,ds2 \\ I\,qs1 \\ I\,qs2 \\ I\,qr1 \\ I\,qr2 \\ I\,dr1 \\ I\,dr2 \\ I\,qs1 \\ Vqs2 \end{bmatrix}$$

(6.31)

where $U_1 = \frac{L_{md}}{2\Delta_2}$, $C_{dd} = \frac{1}{C}$, $U_2 = \frac{L_{dr}}{2\Delta_2}$, $U_3 = \frac{r_{ds}L_{md}}{\Delta_2}$, $U_4 = \frac{r_{ds}L_{dr}}{\Delta_2}$, $U_5 = \frac{r_{qs}L_{mq}}{\Delta_1}$, $U_6 = \frac{r_{qs}L_{qr}}{\Delta_1}$, $U_7 = \frac{r_{qr}L_{mq}}{\Delta_1}$, $U_8 = \frac{r_{qr}L_{qs}}{\Delta_1}$,

$U_9 = \frac{r_{dr}L_{md}}{\Delta_2}$, $T_1 = \frac{r_{dr}L_{ds}}{\Delta_2}$, $T_2 = \frac{L_{mq}}{\Delta_1}$, $T_3 = \frac{L_{qr}}{\Delta_1}$, $C_{qq} = \frac{1}{C_q}$, $Z_{oo} = \frac{1}{Z_o}$, $\Delta_1 = \left(L_{qs}L_{qr} - L_{mq}^2\right)$ and $\Delta_2 = \left(L_{md}^2 - L_{ds}L_{dr}\right)$.

Equation 6.31 is of the form $[0] = [A][X]$ where [X] is the state variables. The solution to this equation is relatively straight forward, it is either that [A] = 0 or [X] = 0, since the state cannot be zero hence the solution is therefore [A] = 0. With this, the [A] matrice can be solved for the condition for self-excitation. The condition for self-excitation is found by evaluating the determinant of the A matrice set to zero.

6.4. Results

The evaluating [A] matrix determinant clearly shows that for self-excitation to occur it is independent of the input capacitor, C_d. The effect of change in parameter is a secondary effect [16] in self-excitation of the generator system hence constant parameters were used in the results that follows.

The results that follows are obtained by assuming that M_d is zero that is modulation index is real in other words the angle is zero. The determinant of A matrices when M_d=0 shows that the generator system is independent of the modulation index, M_q. Figure

6.4 shows the required value of load resistance to choose at a corresponding rotor speed. The load frequency and capacitor, C_q are kept constant.

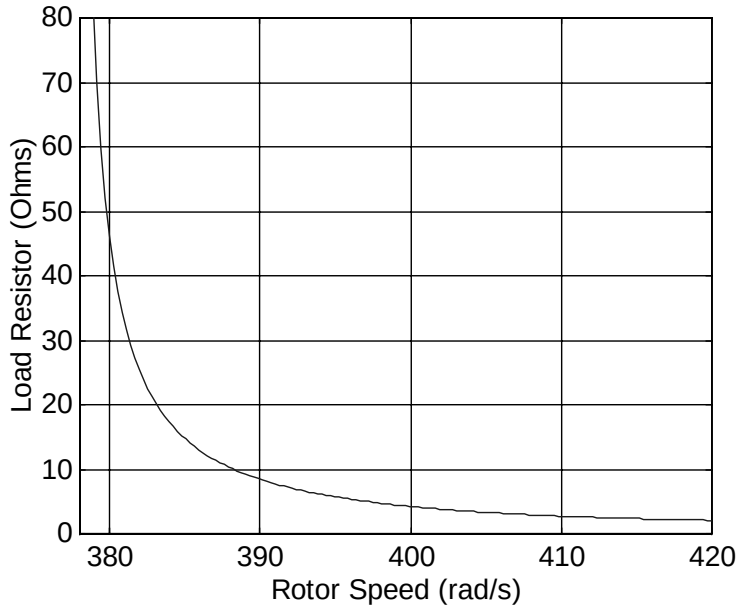

Figure 6.4. Self-excitation for the system without battery. Calculated load resistance vs generator rotor speed.

In order to achieve a self-excitation at a load capacitor, C_q of 180 μF and load frequency of 60Hz, and generator rotor speed ωr of 385 rad/s will require a minimum load impedance of 14.72 Ohms as show in Figure 6.4.

Figure 6.5 shows the contour plot at various value of load resistance. From Figure 6.5 given specific load impedance, the corresponding load capacitor and generator rotor speed for self-excitation of the system could be obtained. Under this condition load frequency is kept constant.

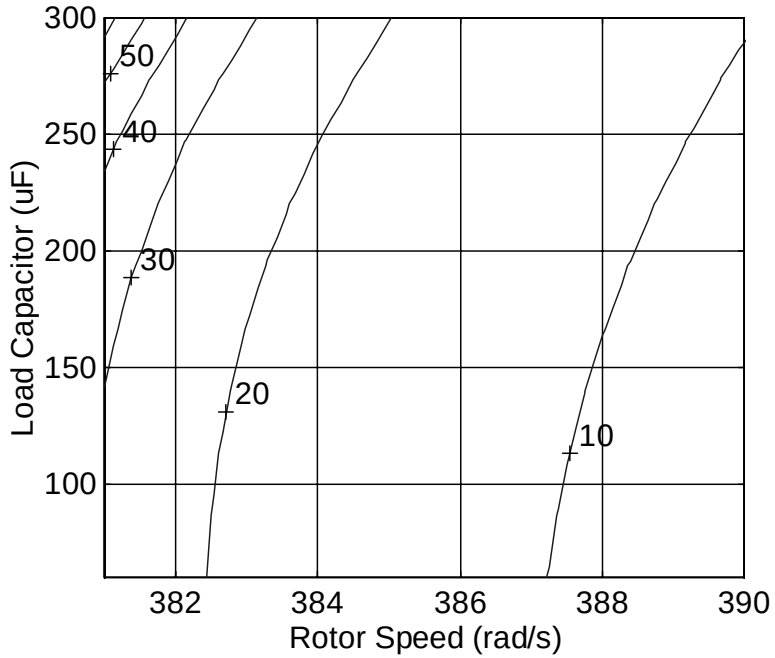

Figure 6.5. Self-excitation for the system without battery. Contour plot of load resistance, [Ω] as a variation of generator rotor speed and load capacitor.

The minimum load impedance to obtain self-excitation with variation of M_d and M_q was also computed. Figure 6.6 shows the required value of load resistance to choose at a corresponding value of M_d and M_q. The load frequency, generator rotor speed, and capacitor, C_q are kept constant. The constant parameter value are the load frequency, f = 60Hz, generator rotor speed, ω_r = 1840 rpm, and capacitor, C_q = 180 μF.

Figure 6.6 shows the contour plot at various value of load resistance. From Figure 6.6 given specific load impedance, the corresponding modulation M_d and M_q for self-excitation of the system could be obtained with other system parameter kept constant.

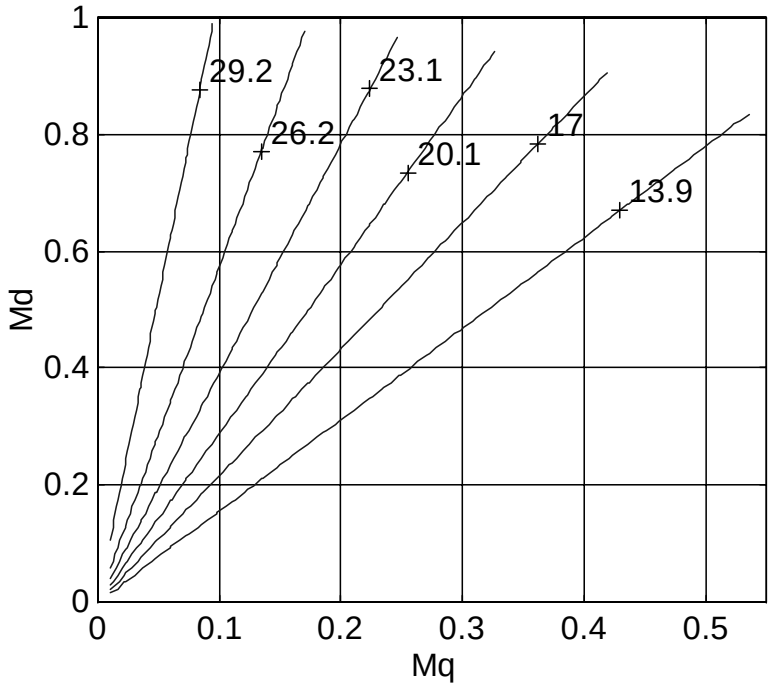

Figure 6.6. Self-excitation for the system without battery. Contour plot of load resistance, [Ω] as a variation of M_d and M_q .

$$\begin{bmatrix} 0 \\ 0 \\ 0 \\ 0 \\ 0 \\ 0 \\ 0 \\ 0 \\ 0 \\ 0 \end{bmatrix} = \begin{bmatrix} 0 & 0 & 0 & Cdd\,Mq\,U2 & Cdd\,Md\,U2 & 0 & 0 & 0 & 0 & -Cdd\,Mq\,U1 & -Cdd\,Md\,U1 & 0 & 0 \\ 0 & 0 & -2\,we & Cdd\,Mq\,U2 & -Cdd\,Md\,U2 & 0 & 0 & 0 & 0 & -Cdd\,Mq\,U1 & Cdd\,Md\,U1 & 0 & 0 \\ 0 & 2\,we & 0 & Cdd\,Md\,U2 & Cdd\,Mq\,U2 & 0 & 0 & 0 & 0 & -Cdd\,Md\,U1 & -Cdd\,Mq\,U1 & 0 & 0 \\ Mq & \frac{Mq}{2} & \frac{Md}{2} & U4 & -we & 0 & 0 & 0 & 0 & -U3 & 0 & 0 & 0 \\ Md & -\frac{Md}{2} & \frac{Mq}{2} & we & U4 & 0 & 0 & 0 & 0 & 0 & -U3 & 0 & 0 \\ 0 & 0 & 0 & 0 & 0 & -U6 & -we & U5 & 0 & 0 & 0 & 1 & 0 \\ 0 & 0 & 0 & 0 & 0 & we & -U6 & 0 & -U5 & 0 & 0 & 0 & 1 \\ 0 & 0 & 0 & 0 & 0 & U7 & 0 & -U8 & -we & Nqd\,wr & 0 & 0 & 0 \\ 0 & 0 & 0 & 0 & 0 & 0 & U7 & we & -U8 & 0 & Nqd\,wr & 0 & 0 \\ 0 & 0 & 0 & -U9 & 0 & 0 & 0 & -\frac{wr}{Nqd} & 0 & T1 & -we & 0 & 0 \\ 0 & 0 & 0 & 0 & -U9 & 0 & 0 & 0 & -\frac{wr}{Nqd} & we & T1 & 0 & 0 \\ 0 & 0 & 0 & 0 & 0 & -Cqq\,T3 & 0 & Cqq\,T2 & 0 & 0 & 0 & -Cqq\,Zoo & -we \\ 0 & 0 & 0 & 0 & 0 & 0 & -Cqq\,T3 & 0 & Cqq\,T2 & 0 & 0 & we & -Cqq\,Zoo \end{bmatrix} \begin{bmatrix} Vdo \\ Vd1 \\ Vd2 \\ I\,ds1 \\ I\,ds2 \\ I\,qs1 \\ I\,qs2 \\ I\,qr1 \\ I\,qr2 \\ I\,dr1 \\ I\,dr2 \\ I\,qr1 \\ I\,qr2 \end{bmatrix}$$

(6.31)

CHAPTER 7

CONCLUSIONS AND SUGGESTION FOR FURTHER WORK

7.1 Conclusions

The operation of a single-phase induction generator with a PWM inverter as a source of excitation was tested and analyzed. The battery included in the system was found to be an excellent configuration for a source or sink of real power depending on the given load of the single-phase induction generator. The system modeling was done considering the effect of saturation of magnetizing inductance. Experimental results were recorded for different impedance and motor loads for a one horse power single-phase induction generator.

The steady-state model for the system was developed for impedance and motor loads using the harmonic balance technique. Experimental results for different impedance and motor loads compare favorably with the steady-state model calculation.

The simulation of the single-phase induction generator, battery, and PWM inverter was done using device model. Matlab/Simulink was found to be an excellent tool in modeling model the PWM inverter and the single-phase induction generator. Simulation results of different impedance and motor loads compare favorably with experimental waveforms of the single-phase induction generator system.

7.2 Suggestion for Further Work

Proper design of the induction machine as a generator will greatly improve its performance; for instance designing the induction machine to have appropriate turns for the main and auxiliary winding.

Photovoltaic cells could be added in parallel to the battery in the single-phase induction generator scheme with PWM inverter. This configuration will greatly improve overall system performance since the solar cell will provide additional source of real power.

A control design using proportional integral (PI) or linear quadratic gaussian / loop transfer recovery (LQG/LTR) to minimize the effect of disturbance as well as to ensure controlled load voltage and frequency can be further provided for the system. A digital signal processing (DSP) implementation of the control scheme will ensure system reliability and accuracy.

APPENDIX

APPENDIX A

The constant parameters of the 1 hp single-phase generator and a banks of batteries are:

r_{qs} = 0.62575 Ohm	r_{qr} = 0.5292 Ohm
r_{ds} = 2.80 Ohms	r_{dr} = 1.3940 Ohms
L_{lqs} = 0.00258 H	L_{lqr} = 0.0025 H
L_{lds} = 0.00679 H	L_{ldr} = 0.00658 H
L_{md} = 0.18 H	L_{mq} = 0.083 H
C_d = 37000μF	C_{bp} = 54,000F
C_{b1} = 1F	r_{bp} = 10,000 Ohms
r_{b1} = 0.001 Ohms	r_{bs} = 0.013 Ohms
r_{bt} = 0.0167 Ohms	N_{dq} (turns ratio) = 1.6227
ω_e = 377 rad/s;	

APPENDIX B

The constant parameters of the 1/2 hp single-phase motor:

r_{qsm} = 1.1 Ohm	r_{qrm} = 2.0229 Ohm
r_{dsm} = 4.30 Ohms	r_{drm} = 3.9454 Ohms
L_{lqsm} = 0.005512 H	L_{lqrm} = 0.005512 H
L_{ldsm} = 0.011463 H	L_{ldrm} = 0.011463 H
L_{mdm} = 0.182 H	L_{mqm} = 0.0841 H
N_{dq} (turns ratio) = 1.4421	w_e = 377rad/s

APPENDIX C

Derivation of Output Voltage Equation.

The following derivation explains the steps in arriving at Equation 2.37.
For n = 0 and k =1,

$$f(x)=\sum_{-k}^{k} c_k e^{jkx} \tag{C.1}$$

From Equation 2.36,

$$c_k = jV_d\left(\frac{1}{\pi}+\frac{m_a}{4}\right) \tag{C.2}$$

But

$$c_k = c_k^* = c_{-k} \tag{C.3}$$

Since f(x) is real conjugate from Equation C.3

$$\overline{c_k} = c_{-k} = c_k^* = -jV_d\left(\frac{1}{\pi}+\frac{m_a}{4}\right) \tag{C.4}$$

Equation C.4 is a complex Fourier series. If the Fourier series of f(x) is expressed in real variable form and n = 0, k =1, then

$$f(x)=b_k \cos kx + b_k \sin kx \tag{C.5}$$

But

$$c_k = \frac{a_k - jb_k}{2},\ c_{-k} = \frac{a_k + jb_k}{2} \tag{C.6}$$

rearranging Equation C.6 result in

$$a_k - jb_k = 2c_k \tag{C.7}$$

$$a_k + jb_k = 2c_{-k} \tag{C.8}$$

Solving Equations C.7 and C.8 gives

$$a_k = c_k + c_{-k} \tag{C.9}$$

$$b_k = \frac{1}{j}(c_{-k} - c_k). \tag{C.10}$$

In this case k=1

$$a_1 = jV_d\left(\frac{1}{\pi}+\frac{m_a}{4}\right) - jV_d\left(\frac{1}{\pi}+\frac{m_a}{4}\right) = 0 \tag{C.11}$$

$$b_1 = \frac{1}{j}\left(-jV_d\left(\frac{1}{\pi}+\frac{m_a}{4}\right) - jV_d\left(\frac{1}{\pi}+\frac{m_a}{4}\right)\right) = -2V_d\left(\frac{1}{\pi}+\frac{m_a}{4}\right) \tag{C.12}$$

$$M = 2\left(\frac{1}{\pi}+\frac{m_a}{4}\right) = \left(\frac{2}{\pi}+\frac{m_a}{2}\right) \tag{C.13}$$

The real Fourier expansion can also be applied to other conditions of k and n.

REFERENCES

1. F. P. de Mello, J. W. Feltes, L. N. Hannett and J. C. White, “Application of induction generators in power systems,” IEEE Transactions on Power Apparatus and Systems, Vol. PAS-101, no. 9, pp. 3385-3393, September 1982.

2. G. Raina and O. P. Malik, “Wind energy conversion using a self-excited induction generator,” IEEE Transactions on Power Apparatus and Systems, Vol. PAS-102, no. 12, pp. 3933-3936, December 1983.

3. D. B. Watson, J. Arrillaga and T. Densem, "Controllable d.c. power supply from wind-driven self-excited induction machines," Proc. IEE, vol. 126, no. 12, pp. 1245-1248, December 1979.

4. S. S. Murthy, O. P. Malik and A. K. Tandon, “Analysis of self-excited induction generators,” IEE Proc. Vol. 129, Pt. C, No. 6, pp. 260-265, November 1982.

5. N. H. Malik and A. A. Mazi, “Capacitance requirement for isolated self excited induction generators,” IEEE Trans. on Energy Conversion, vol. EC-2, no. 1, pp. 62-68, March 1987.

6. Y. H. A. Rahim, A. I. Alolah and R. I. Al-Mudaiheem, "Performance of a single-phase induction generators," IEEE Trans. on Energy Conversion, vol. 8, no. 3, pp. 389-395, September 1993.

7. S. S. Murthy, “A novel self-excited self-regulated single phase induction generator Part 1, Basic System and Theory,” IEEE Transactions on Energy Conversion, vol. 8, no. 3, pp. 377-382, September 1993.

8. S. S. Murthy, O. P. Malik and A. K. Tandon, “A novel self-excited self-regulated single phase induction generator Part 11, Experimental Investigation,” IEEE Transactions on Energy Conversion, vol. 8, no. 3, pp. 383-388, September 1993.

9. O. Ojo and I. Bhat, “An analysis of single-phase self-excited induction generators: Model development and steady state calculations,” IEEE Trans. on Energy Conversion, vol. 10, no. 2, pp. 254-260, June 1995.

10. T. F. Chan, “Analysis of a single-phase self-excited induction generator,” Electric Machines and Power Systems, vol. 23, pp. 149-162, 1995.

11. O. Ojo, “The transient and qualitative performance of a self-excited single-phase induction generator,” IEEE Trans. on Energy Conversion, vol. 10, no. 3, pp. 493-501, September 1995.

12. O. Ojo, “Performance of a self-excited single-phase induction generators with shunt, short-shunt and long-shunt excitation connections,” IEEE Trans. on Energy Conversion, vol. 11, no. 3, pp. 477-482, September 1996.

13. D. W. Novotny, D. J. Gritter and G. H. Studtmann, “Self-excitation in inverter driven induction machines,” IEEE Transactions on Power Apparatus and Systems, Vol. PAS-96, no. 4, pp. 1117-1125, July/August 1977.

14. M. B. Brennen and A. Abbondanti, "Static Exciters for Induction Generator," *IEEE* Trans. on Industry Applications, vol. IA-13, no. 5, pp. 422-428, September/October 1977.

15. J. Arrillaga and D. B. Watson, "Static power conversion from self-excited induction generators," Proc. IEE, vol. 125, no. 8, pp. 743-746, August 1978.

16. J. A. A. Melkebeek and D. W. Novotny, “Steady State Modelling of Regeneration and Self-excitation in Induction Machines,” IEEE Trans. on Power Apparatus and Systems, Vol. PAS-102, no. 8, pp. 2725-2733, August 1983.

17. E. Muljadi and T. A. Lipo, “Series compensated PWM inverter with battery supply applied to an isolated induction generator,” IEEE Trans. on Industry Applications, vol. 30, no. 4, pp. 1073-1082, July/August 1994.

18. MATLAB, “The Math Works, Inc.", Natick, MA, 1994.

19. Leon O. Chua, Charles A. Desoer and Ernest S. Kuh, “Linear and Nonlinear Circuits", McGraw-Hill Book Company, 1987.

20. Mathcad User's Guide, “MathSoft, Inc.", 101 Main Street, Cambridge, MA 02142-1521, 1995.

21. Mathematical for Student, “Wolfram Research, Inc.", 100 Trade Center Drive Champaign, IL 61820, USA, 1994.

22. Ray Holland, “Appropriate technology - rural electrification in developing countries,” IEE Review, Vol. 35, no. 7, pp. 251-254, July/August 1989.

23. N. Mohan, T. M. Undeland and W. P. Robbins, Power Electronics: Converters, Applications and Design, John Wiley and Sons, Inc, New York, 1989.

24. B. K. Bose, Modern Power Electronics Evolution, Technology, and Applications, IEEE Press, 1991.

25. B. K. Bose, Power Electronics and Variable Frequency Drives, Technology and Applications, IEEE Press, New York, 1997.

26. Semikron International, “SEMIKRON Semidriver Medium power six IGBT and MOSFET driver SKHI60, SKHI60H4 Preliminary data,” Semikron International, Sigmundstr. 200, Postfach 82 02 51, D-90253 Nurnberg Germany.

27. International Rectifier, “Designer's Manual Insulated Gate Bipolar Transistor,” International Rectifier, 233 Kansas St., El Segundo, California 90245, 1996.

28. O. Ojo, Class notes on ECE662 (Advance Electric Machinery), Tennessee Tech. Uni., Cookeville, TN, 1996.

29. P. C. Krause, O. Wasynczuk, and S. D. Sudhoff, Analysis of Electric Machinery, IEEE Press, 1995.

30. S. D. Sudhoff, “Multiple Reference Frame Analysis of an Unsymmetrical Induction Machine,” IEEE Transactions on Energy Conversion, vol. 8, no. 3, pp. 425-432, September 1993.

31. C. F. Lu, C. C. Liu and C. J. Wu, “Dynamic modelling of battery energy storage system and application to power system stability,” IEE Proceedings—Generation, Transmission and Distribution, vol. 142, no. 4, July 1995, pp. 429-435.

32. E. Muljadi, “Series compensated PWM inverter with battery supply applied to an isolated operation of induction generator,” Ph.D. thesis, University of Wisconsin, Madison, 1987.

33. T. Nakae, Y. Kanamaru and Y. Amemiya, “A method of single-phase PWM for an independeant power supply in photovoltaic power generation systems,” Electrical Engineering in Japan, vol. 122, no. 4, 1998, pp. 55-61.

34. Erwin Kreyszig, Advanced Engineering Mathematics, John Wiley and Sons, Inc, New York, 1979.